Cryptic Carbon: Improving Wetland Representation and Soil Carbon Characterization across Forested Landscapes

Anthony Stewart

A dissertation

submitted in partial fulfillment of the

requirements for the degree of

Doctor of Philosophy

University of Washington

2025

Reading Committee:

L. Monika Moskal, Chair

David Butman, Chair

David D'Amore

Meghan Halabisky

Program Authorized to Offer Degree:

Environmental and Forest Sciences

University of Washington

Abstract

Cryptic Carbon: Improving Wetland Representation and Soil Carbon Characterization across Forested Landscapes

Anthony Stewart

Chairs of the Supervisory Committee:

L. Monika Moskal

David Butman

Environmental and Forest Sciences

Inland freshwater wetlands disproportionately contain soil organic carbon (SOC), storing greater than 30% of the total global pool but only cover 6% of the land surface. However, many of these wetlands, especially in the Pacific Northwest, are hidden under forest canopy and excluded from maps of wetland extent, estimates of landscape SOC stock, and under-evaluated in broader soil science. Chapter 1 shows that implementing a new wetland mapping tool, the wetland intrinsic potential (WIP) tool, to identify hidden "cryptic" wetlands can improve estimates of landscape SOC stocks and identifies approximately 5-fold wetland SOC stock than previous estimates. Chapter 2 describes how the WIP wetland identification can be applied in models across regional scales, producing consistently higher landscape and wetland SOC measurements. This shows that the patterns of landscape soil moisture regimes with WIP is significant driver of SOC stock but not mineral soil SOC% across regional scales with climatic variation. Chapter 3 further investigates the

mineral associations with soil organic matter (MAOM) and evaluates the SOC stability in forested wetlands and uplands finding that forested wetlands have lower MAOM SOC content (MAOM-C) compared to dry uplands but the radiocarbon dating of the MAOM-C (MAOM-$\Delta^{14}C$) in forested wetlands was much older. The results suggest that landscape class, Fe, pH and SOC% are drivers of the MAOM-C and MAOM-$\Delta^{14}C$. Overall this dissertation reveals new insights into the spatial distribution of inland freshwater wetlands and wetland SOC as well as how well this SOC is preserved.

Table of Contents

List of Figures

List of Tables

Acknowledgements

There are too many people to thank for their support throughout the work in this dissertation but everyone I am extremely thankful for everyone I interacted with during my PhD. Sometimes even the smallest moments can be profound. First, I want to thank my advisors and my committee who have given me guidance and support from the very first day. Thank you, Monika Moskal, for letting me join the Teal Carbon team, the RSGAL group, and the PFC. You took a chance on someone without remote sensing experience and gave them the tools needed to complete a PhD using these tools. I cannot imagine doing a PhD in any other lab that would have this much support whether that is remote field work deep in the pandemic to conference travel to expand my network. I would not have made as much progress in both research and professional development without your encouragement and support. I'm looking forward to continuing our work on Teal Carbon in the future. I want to give thanks to David Butman. Our meeting in 2016(?) in Juneau, AK set me on the path to achieve research goals I could only have dreamed of, and I am grateful for you extending the opportunity to me. Although it isn't lateral fluxes in Southeast Alaska, I am grateful and happy to be in the carbon world, working on wetlands, and thinking about terrestrial-aquatic links. I have greatly appreciated your mentorship and our science conversations over the years which have always revealed new exciting questions. You've always encouraged and supported me to pursue my interests and I'm excited to continue developing new research and pursue future collaborations. Many thanks also to Meghan Halabisky. I do not think there could be a person in the world I would rather talk to more about wetlands than you. Your enthusiasm for these ecosystems sparked a never-ending curiosity and changed my perspective forever. There's no going back now and I'm excited to see how we take this work into the future. I hope to model your tenacity as a scientist and push myself to make it in the world of science. I'm thankful as well for Dave D'Amore, who shares an unparalleled passion for soils and soil science. If I had one recommendation for any soil scientist, it would be spending a day in the field with Dave digging soil pits, preferably Spodosols or the Typic Humicryods. You helped me achieve one of my life goals of conducting research in Southeast Alaska and I'm ever grateful for that experience. Gordon Holtgrieve for guiding my early PhD career with thoughtful questions and opening my mind to the fundamentals of aquatic ecology. David Shean for teaching the best data science course at UW and showing me the powers of SAR.. Maureen Walczak for stepping in as a GSR just in time!

Several others along my journey have given me guidance and mentorship that I cannot thank enough. Katerina Georgiou for giving me the opportunity to expand my dissertation at LLNL into the cutting edge of soil science and facilitating connections to so many other amazing scientists. Diogo Spinola for inspiring more broad soil science research, getting me excited about lithology and geology, and being one of the best partners in the field for sampling soils. Chad Babcock for demystifying Bayesian statistics and guiding the Teal Carbon analysis no matter what questions I might have. Dan Miller, for developing the WIP tool and opening the possibilities for terrain and topographical modeling. Joe Rocchio for sharing your wetland wisdom and showing me the unique characteristics of any wetlands, we cross. Tynan Ramm-Granberg for consistent support on the wetland climate project during some hectic times (Also a bit of skiing). Amy Yahnke for supporting our Teal Carbon research and giving depth and insight into the diversity of wetland projects across the state. Ailene Ettinger, thank you so much for letting me work with you and the TNC and for giving thoughtful and supportive feedback on this work. Becca Neumann for providing helpful advice on several aspects of my research and sharing some of the most interesting personal highs and lows in lab meetings. Sheel Bansal for sharing insight into wetland biogeochemistry and giving me confidence in working in this field. Alix Contosta, I'm glad we were able to reconnect through

Sheel with annual AGU meet ups and thank you for sharing your experience which has inspired me to continue research work. Amanda Nahlik, for inspiring the "Teal Carbon" term and eventually "Cryptic Carbon" with your seminal work with the NWCA and EPA that I am always looking up to. Jennifer Pett-Ridge, Enrica Balboni, Karis McFarlane, Keith Morrison, Brooke Creager, Katie Grant, and Abrar Shahir, thank you for making LLNL a wonderful place to work and learn. All the folks at the NASA Wet Carbon team, thank you for letting me contribute to a diverse team of amazing remote sensing scientists.

I want to thank several undergraduate research assistants that worked with me in the field and lab: Claire Johnson, Hazel Sanders, Abby Nesper, Megan Sayasemawong, Thomas Kakatsakis, Lindsey Skidmore, Sheridan Stanner, Clem Taylor-Roth, Alana Margerum; thank you for putting up with the tireless work of soil sampling in the field and processing in the lab. My dissertation was also supported with several knowledgeable experts from geography with Frances Biles; wetland expertise with Joe Rocchio, Amy Yahnke, Nate Hough-Snee, and Amanda Nahlik; project management with Maureen Duane; and the wonderful support staff at SEFS that helped navigate proposals and the administration: Jack Lockhart, Liz Collier, Wanjiku Gitahi, Matt Gray, and Jennifer Weiss. We especially thank Dongsen Xue for soil analysis at the former University of Washington Analytical Service Center.

I also thank my many past and present lab mates and SEFS students who have made pursuing a PhD a smoother journey with conversations, adventures, and just hanging around – Caden Chamberlain, Don Radcliff, Ray Deininger, Deborah Nemens, Keenan Ganz, Jonathan Batchelor, Yelyzaveta Ismatullayeva, Casey Ducan, Hannah Conroy, Helen Miller, Joel Eklof, Hannah Redford, Sage Fox, Pratima KC, Astrid Sana, Bryce Bartl-Geller, Rachel Buchler, Gina Cova, Yu Li, and many others.

This work could also not have been done without those outside of UW academia. Thanks to my oldest friends from Juneau, AK I feel like we've grown up so much and I've always been thankful for having you in my life: Dylan, Jamie, Keath, Cole, Alex, Peter, Aaron, Andrew, and Jonathan. To the Seattle friends Kevin, Jake, Hutto, Will, Brandon (including NH too), Noah, Meike, and Katherine thanks for skiing and letting me join your adventures.

My PhD is especially not possible without my family. To my Mom and Dad, you've supported me since the day I was born and always let me continue to pursue my passions. I am eternally grateful for your love and support. I don't think many kids from Juneau, AK get to grow up to be scientists, but you gave me everything I needed to succeed. To my brother Nick, in some ways I'm following your footsteps and I'm super proud to have you as my brother.

Most of all, I could not have done this PhD nor gone through a pandemic in a 1 bedroom apartment without my wife and partner Karen Naomi Barnard. Watching you do your PhD inspired me to pursue my own and you've provided more support than you know throughout this entire time. I could not be happier coming home to you after a long day or a long trip in the field and I can also not be prouder of us for getting married during the PhD! You continue to inspire me to be my best and I'll continue to support you as well. I also promise to help take care of the best dog in the world: Yukon. I think we both agree that both of our degrees transfer to him and two PhDs, back to back, is pretty good for him! Looking forward to building on our love for long after this.

This Dissertation was supported by funding from the National Aeronautics and Space Administration Grant Number 80NSSC20K0427 P00003 and 80NSSC20K0427, USDA Forest Service Joint Venture Agreement 20-JV-11261933-058 AM003, Washington Department of Natural Resources and the Washington Cooperative Fish and Wildlife Research Unit, U.S. Department of Energy SCGSR fellowship, the Precision Forestry Cooperative and The Nature Conservancy. We also acknowledge this work takes place on the traditional lands of the many tribes across the Pacific Northwest from the Lingít Aaní, to the Hoh, Quileute, Spuyaləpabš, and Colville lands.

Introduction

Anthropogenic activity has altered and shaped the earth's terrestrial system through modification of the land surface with agriculture, urbanization, and emission of greenhouse gases (GHGs) with fossil fuel use. These modifications have dramatically altered the Earth's carbon (C) cycle by introducing continuous inputs of C, mostly from fossil fuel sources since the industrial revolution (Friedlingstein et al., 2024). The overall amount of C throughout the Earth's C cycle has increased, with large amounts entering the atmosphere resulting in large irreversible changes to the earth's climate (Foley et al., 2005; Solomon et al., 2009; Intergovernmental Panel On Climate Change, 2022; Friedlingstein et al., 2024). The terrestrial environment has also seen increased C and continues to act as a C sink with a rate that has increased as CO2 concentrations in the atmosphere enhance photosynthesis (Ruehr et al., 2023). The CO2 fertilization is only one aspect of the potential for the terrestrial environment to act as a C sink and mitigate atmospheric C increases. Conducting mitigation pathways such as ecosystem restoration, reducing deforestation, and reducing land use conversion would improve the C sequestration in the terrestrial environment (Shukla et al., 2022). However, some pathways, such as forest management which have a larger ceiling for C sequestration also have risk associated with being a shorter-term sink, with forest management, current lifespans, and disturbances on the decadal time scale (Pugh et al., 2019; Anderegg et al., 2020). Instead, the soil carbon pool may offer a more permanent and resilient pathway for terrestrial C sequestration (Bossio et al., 2020).

Soil organic carbon (SOC) is the largest of the actively cycling terrestrial C pools, containing approximately 1,500-1,700 Petagrams C (PgC) at a 1 m depth, nearly twice the amount in the atmosphere and terrestrial biomass combined (Scharlemann et al., 2014; Jackson et al., 2017; Friedlingstein et al., 2024). The magnitude of the SOC pool represents both opportunity and risk in

the face of climate change. In opportunity, it has been presented that there is large capacity to add more C to the SOC pool through management and conservation (Minasny et al., 2017; Bossio et al., 2020). However, in risk, as global atmospheric CO2 emissions and temperatures rise, there is increased risk of C released from equivalent to nearly 30% of current global fossil fuel emissions in response to warming temperatures (Hicks Pries et al., 2017). Land use conversion also represents pathways for C loss in soils with an already well known large reduction of the global SOC stock from agriculture (Sanderman et al., 2017). Given both the uncertainties and potential advantages, a comprehensive understanding of SOC and quantification of carbon pools in soils are essential to determine their function in the global carbon cycle.

SOC is contained within soil organic matter (SOM) which is comprised of a dynamic amalgamation of inorganic minerals and inputs from organic material from plants and organisms which undergo continual microbial processing to smaller molecular sizes (Lehmann & Kleber, 2015). The microbial decomposition which converts large particulate SOM to microbial biomass, CO2, CH4, or other carbon gases depends on abiotic and biotic factors such temperature, soil moisture, mineral composition, and plant inputs (von Lützow & Kögel-Knabner, 2009). The interactions and dynamics with different abiotic and biotic factors influencing soil development, SOM, and SOC has been conceptualized by Jenny, 1941 in the soil formation equation, CLORPT: climate (CL), organisms/biology (O), relief/topography (R), and time (T). This equation can be applied to understand the variation of many soil properties including SOM and SOC stocks and changes across terrestrial spatial extents and serves as a framework to model at landscape to regional scales (Jenny, 1994; McBratney et al., 2003). Global SOC maps and surveys reveal that large amounts of SOC are contained in organic soils within wet and cool climates which develop peatlands and wetlands (Jobbágy & Jackson, 2000; Lal, 2008; Scharlemann et al., 2014; Köchy et al., 2015).

Nearly 30% of the global SOC pool is stored in inland freshwater wetlands, which accumulate organic matter and SOC much more rapidly than non-wetland soils due to the anoxic conditions generated by consistent water saturation (Poulter et al., 2021). Consequently, inland freshwater wetlands disproportionately store SOC in relation to their surface area extent, which is approximately 6-8% of the global land surface (Reis et al., 2017; Poulter et al., 2021; Zhang et al., 2021; Campbell et al., 2022). The substantial contribution of inland freshwater wetlands to the global SOC pool highlights them as potential natural climate solutions (Thorslund et al., 2017) but also as potential hot spots for C loss and transfer due to land use change and disturbance (Ma et al., 2022). However, there are deficiencies for mapping particular wetland types despite the substantial effort used to produce these maps. According to the National Wetland Inventory (NWI), inland freshwater forested wetlands, which are classified as palustrine forested wetlands in the NWI, are the most abundant wetland type in the CONUS (Dahl, 2011). Yet, evidence has shown that these forested wetlands often missing from maps and inventories (Matthews et al., 2016; Maxwell et al., 2016; Halabisky et al., 2023). Forested wetlands can be too small to detect, often occluded by their canopy, and many are seasonally saturated or rarely inundated which hinders their detection by manual mapping, passive or active remote sensing (Adeli et al., 2020; Halabisky et al., 2023).

Forested wetlands comprise the majority of wetlands within the CONUS, which suggests even minor percentage adjustments in the total estimated extent would result in outsized effects on the total estimate wetland area and aggregated wetland functions. Land use conversion of wetlands can reduce or remove the disproportionate SOC storage of many inland freshwater wetlands which underscores a change to a prominent wetland function with global implications (Nahlik & Fennessy, 2016; Fluet-Chouinard et al., 2023). Neglecting forested wetlands also occurs in soil science research where much of the contemporary literature has yet to apply recent paradigm shifts in SOC storage and persistence to wetland soils. This compromises the conceptualization and quantification of

terrestrial carbon cycling due to their role as a disproportionate pool of SOC (Davidson et al., 2022). However, it is uncertain as to the magnitude of this compromise without new empirical evidence that focuses on the forested wetland knowledge gap in both contemporary spatial and soil science. Therefore, we pose the critical overarching question**: To what extent are forested wetlands excluded from current wetland land cover and SOC stock maps and can we apply contemporary soil science frameworks to reveal new SOC insights?**

Dissertation overview

This dissertation consists of three chapters investigating the missing spatial extent and SOC storage of forested wetlands and its impact on contemporary SOC research. The impact of this knowledge gap spans not only the spatial research realm, where estimates of wetland SOC require considerable improvement towards accurate representations, but also into intrinsic soil properties where forested wetland soils are also underrepresented. Therefore, the research in these chapters covers a range of scales including both spatially-explicit and non-spatial research.

Chapter 1. How much wetland area is unidentified or misclassified in a forested watershed and how much SOC do these wetlands hold?

Chapter 2. How does wetland presence perform as a spatial predictor of SOC stock and SOC% in combination with other bioclimatic and edaphic factors across Pacific Northwest climate zones?

Chapter 3. What mechanisms drive soc persistence in wetlands versus uplands and how do environmental factors explain these differences?

Chapter 1: Revealing the hidden carbon in forested wetland soils

Author List

Anthony J Stewart*[1]
Meghan Halabisky[1]
Chad Babcock[2]
David E. Butman[1]
David V. D'Amore[3]
L. Monika Moskal[1]

Affiliations

[1]School of Environmental and Forest Sciences, University of Washington, Seattle
[2]Department of Forest Resources, University of Minnesota, St Paul
[3]Pacific Northwest Research Station, U.S. Department of Agriculture Forest Service

Abstract

Inland wetlands are critical carbon reservoirs storing 30% of global soil organic carbon (SOC) within 6% of the land surface. However, forested regions contain SOC-rich wetlands that are not included in current maps, which we refer to as 'cryptic carbon'. Here, to demonstrate the magnitude and distribution of cryptic carbon, we measure and map SOC stocks as a function of a continuous, upland-to-wetland gradient across the Hoh River Watershed (HRW) in the Pacific Northwest of the U.S., comprising 68,145 ha. Total catchment SOC at 30 cm depth (5.0 TgC) is between estimates from global SOC maps (GSOC: 3.9 TgC; SoilGrids: 7.8 TgC). For wetland SOC, our 1 m stock estimates are substantially higher (Mean: 259 MgC ha^{-1}; Total: 1.7 TgC) compared to current wetland-specific SOC maps derived from a combination of U.S. national datasets (Mean: 184 MgC ha^{-1}; Total: 0.3 TgC). We show that total unmapped or cryptic carbon is 1.5 TgC and when added to current estimates, increases the estimated wetland SOC stock to 1.8 TgC or by 482%, which highlights the vast stores of SOC that are not mapped and contained in unprotected and vulnerable wetlands.

Introduction

Conserving Earth's carbon-rich ecosystems is critical to meet the goals of balancing carbon sources and sinks for the Paris Climate Agreement (Griscom et al., 2017). Among ecosystems with high carbon stocks, inland freshwater wetlands and peatlands contain greater than 30% of the global total soil organic carbon (SOC) stock of 1,500-2,400 PgC but only cover approximately 6% of the land surface (Jackson et al., 2017; Poulter et al., 2021; Zhang et al., 2021). However, below the global scale, wetland SOC mapping is considerably more uncertain due to poor spatial representation. Estimates of wetland SOC stocks often rely on coarse resolution mapping and broad scale inventories that omit many wetlands outside of large homogenous wetland complexes such as peatland plateaus in the high latitude northern hemisphere (>60°) (Hugelius, 2012; Poggio et al., 2021). In the more heterogenous, complex terrain of mid-latitude temperate forested regions (30°-60°), wetlands still disproportionately contribute towards terrestrial carbon storage compared to upland areas but are difficult to map and can occur subtly within a forested landscape and remain hidden under the canopy (Bridgham et al., 2006). This temperate wetland area has been a frequent target of land use conversion to agriculture and urban land uses contributing to the recently estimated loss of 21% of the original global wetland area since 1700 AD (Fluet-Chouinard et al., 2023). The recent ruling by the U.S. Supreme Court potentially enables more wetland loss (U.S. Supreme Court, 2023). Estimating SOC lost from anthropogenic disturbance requires comprehensive SOC mapping that accounts for high SOC in forested wetlands and wet areas which are not contained in contemporary inventories. Omitting these high SOC stocks propagates a potential underestimation of the terrestrial carbon stock in forested regions which contain SOC stores that have accumulated over centuries making them invaluable but irrecoverable if lost within the timeframe to reach net-zero emissions (Noon et al., 2022).

Freshwater inland wetlands make up 95% of the wetland area in the United States and contain a total SOC stock 8-10-fold higher than the total SOC stock in tidal wetlands (Nahlik & Fennessy, 2016; Uhran et al., 2021). Within the inland wetland population, forested wetlands cover the largest extent but represent the most difficult wetland mapping category to detect, especially in satellite and aerial imagery, due to the canopy coverage, small surface area, and isolation from surface waters (Dahl, 2011). Despite the limited appearance, forested wetlands have interconnective roles within terrestrial carbon cycle in addition to SOC storage, including but not limited to: accumulating carbon in aboveground biomass(Davidson et al., 2022); transporting of labile dissolved organic matter to streams(D'Amore et al., 2015a); supplying dissolved CO_2 to surface waters leading to significant outgassing(Abril et al., 2014); and potentially acting as the highest non-ebullitive CH_4 flux from groundwater through tree stems(Pangala et al., 2017). This diverse array of carbon functions highlights forested wetlands role as a hotspot or ecosystem control point within a landscape (Bernhardt et al., 2017). Indeed, seemingly isolated wetlands can connect to surface waters through groundwater links throughout a catchment (Laudon et al., 2011; Leibowitz et al., 2018) and integrating previously unidentified 'cryptic' forested wetlands can better explain catchment scale surface water chemistry patterns (Creed et al., 2003). Cryptic wetlands can also act as the transition between terrestrial and aquatic environments where rapid biogeochemical cycling can occur in spaces only a few meters wide (McClain et al., 2003). Mapping SOC along the terrestrial-aquatic gradient containing forested wetlands can reveal hidden SOC spatial patterns that help balance carbon budgets in heterogenous landscapes (Buffam et al., 2011). However, mapping the distribution of SOC stocks within forested landscapes is challenging, especially with small forested wet areas that do not exhibit conspicuous wetland indicators such as signs of water saturation affecting the aboveground vegetation (Lidberg et al., 2020).

Maps of SOC stocks are commonly generated with digital soil mapping (DSM) using geospatial land cover maps and remote sensing metrics relating to the spatial variation of soil forming factors (Minasny & McBratney, 2016). Wetlands integrated into DSM are often inconsistently defined with insufficiently measured wetland extent that promotes underestimation and inaccurate spatial distributions of SOC stocks (Köchy et al., 2015). Yet generally wetland mapping continues to improve with machine learning models utilizing geospatial wetland and peatland soil properties, but there is still substantial variation and underestimates in forested wetlands and wet areas (Minasny et al., 2019). In areas where forest canopy obscures wet areas, data driven machine learning approaches utilizing topography focused metrics can identify previously hidden forested wetlands and wet areas by capturing patterns of surface and groundwater flow that facilitate water accumulation within a landscape (Maxwell et al., 2016). Utilizing continuous probabilities simulated from presence/absence data (Poggio et al., 2020), probabilistic wetland mapping can capture the spatial representation of the terrestrial to aquatic gradient, with wetlands as one end of a water saturation continuum (Delancey et al., 2019; Goldman et al., 2020). SOC is expected to increase with the higher probability of a wetland where soil saturation that inhibits microbial respiration and facilitates organic matter accumulation and potential wetland extent can be estimated above a chosen probability threshold (Deluca & Boisvenue, 2012; Bailey et al., 2014). We have yet to note SOC maps informed by potential wetland presence which: 1) identifies new unmapped SOC in potential wetland area; 2) compares potential wetland SOC with maps of existing wetland SOC estimates; and 3) compares overall SOC distributions with available SOC mapping products. Therefore, we conduct a new DSM SOC mapping approach in the Hoh River Watershed (HRW), a densely forested, geomorphologically complex watershed using a continuous probabilistic wetland identification metric to reveal significant amounts of unmapped SOC contained in potential forested wetlands and wet areas. We adapt the term 'cryptic wetland' from Creed et al. (2003) as

'cryptic carbon' to distinguish hidden SOC stocks within potential forested wetlands that have not been mapped or estimated previously, with the caveat that we are not mapping jurisdictional wetland boundaries. Our approach represents an adaptable and flexible way for natural resource managers and conservationists to identify cryptic carbon stocks and it reveals an immense SOC stock that has not been associated with potential forested wetlands.

Results

Field collected pedon SOC stocks

We investigated the distribution of SOC stock across the field collected pedon sample depth profile where the overall mean pedon depth was 95 ± 4.4 cm (standard error of the mean ($\frac{\hat{\sigma}^2}{\sqrt{n}}$)) with 94 ± 5.4 cm for uplands and 99 ± 6.5 cm for wetlands. Within wetland pedons, 38% of the entire SOC stock was in 0-30 cm, 31% in 30-60 cm, 27% in the 60-100 cm, and 4% in 100-120 cm (Table 1.1). Within upland pedons, 49% of the SOC stock was in 0-30 cm, 32% in 30-60 cm, 16% in 60-100 cm, and 3% in the top 120 cm. Overall, 96% and 97% of the entire soil carbon stock was contained in the top 1 m of the soil profile for wetlands and uplands, respectively, which we used as a standardized depth for spatial predictions across the HRW. Mean 1 m depth SOC stocks within our field pedon dataset was 221 ± 27.0 MgC ha^{-1} standard error of the mean ($\frac{\hat{\sigma}^2}{\sqrt{n}}$). Wetlands in our field pedon dataset contained a higher mean 1 m SOC stock of 346 ± 89.1 MgC ha^{-1} which was also much higher compared to 185 ± 20.2 MgC ha^{-1} in uplands (Table 1.1.). Within wetlands, we classified riverine and palustrine wetlands due to differences in soil parent material leading to significant differences in SOC. Palustrine wetlands defined here are similar to the Cowardin classification adapted by the NWI (Dahl, 2011) of any freshwater (or less than 0.5 ppt salt concentration), non-tidal, non-riverine, or non-lacustrine wetland, inclusive of forested and non-forested vegetation. Palustrine contained a mean 1 m SOC stock of 447 ± 81.6 MgC ha^{-1} compared to a mean of 43.3 ± 11.7 MgC ha^{-1} in riverine wetlands. Palustrine wetland SOC stock distribution in the soil profile was 37% in the top 30 cm, 31% in 30-60 cm, and 28% in the 60 cm-100 cm. Riverine wetland SOC stock distribution was mostly contained in the top 30 cm (96%). We noted in field observations that pedon locations with WIP probabilities between 25-50% that appeared to maintain a mesic soil moisture environment between wetland and upland ends of the WIP probability range.

Pedons within the mesic zone contained a 1 m mean SOC stock of 241 ± 36.5 MgC ha^{-1} SOC stock which is elevated above uplands in our dataset and within the standard error range of the overall WIP wetland class. Pedons with WIP probabilities below 25% contained a mean of 149 ± 19.8 MgC ha^{-1}.

Table 1.1 SOC stocks, sample depths, and sample numbers collected in the HRW. ± indicates standard error. * Indicates landscape class subsets from WIP wetlands.

Landscape Class	30cm SOC Stock	60cm SOC Stock	1m SOC Stock	120cm SOC Stock	Sample Depth	n
WIP Wetland	138 ± 22.9	250 ± 53.4	346 ± 89.1	362 ± 96.9	99 ± 6.5	8
Riverine Wetland*	41.7 ± 12	42.8 ± 11.6	43.3 ± 11.7	43.3 ± 11.7	81 ± 4.0	2
Palustrine Wetland*	171 ± 11.8	320 ± 38.7	447 ± 81.6	468 ± 92.3	110 ± 6.9	6
WIP Upland	93.6 ± 7.65	153 ± 15.1	185 ± 20.2	190 ± 21.2	94 ± 5.4	28
All Landscapes	104 ± 8.27	175 ± 17.7	221 ± 27.0	228 ± 28.8	95 ± 4.4	36

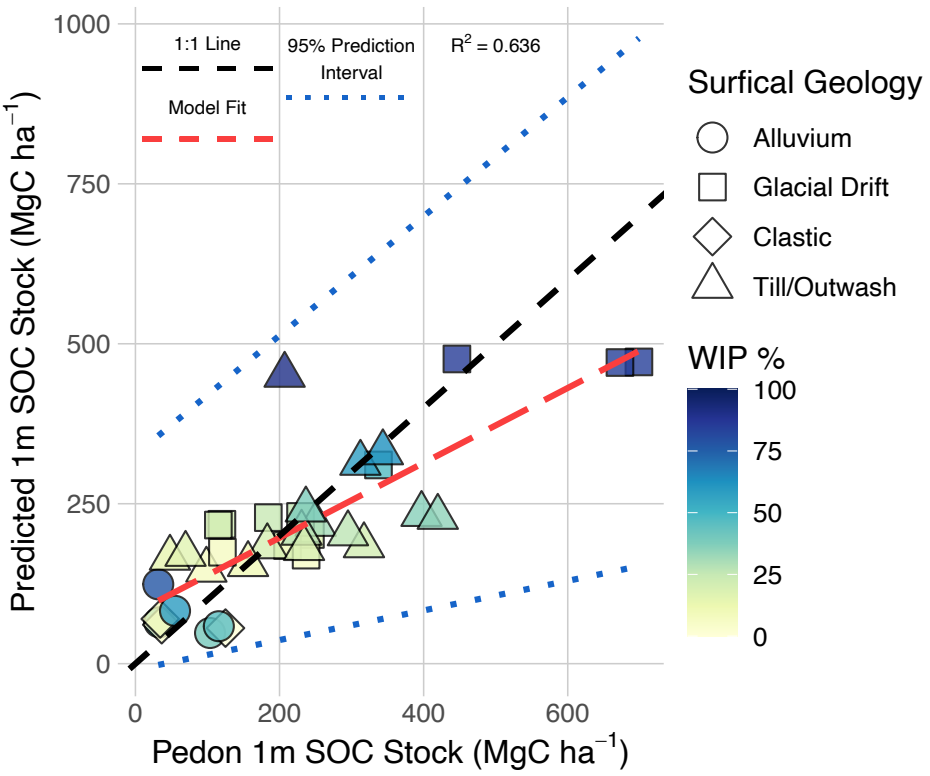

Figure 1.1 Model predicted SOC stock compared to field sampled pedon soil organic carbon (SOC) stock. Modeled SOC stocks were back transformed from square root values in the original linear mixed effects model with the fixed effect of wetland intrinsic potential (WIP) probability and random effect of surficial geology. Shading represents WIP probability. Shapes represent different surficial geology categories. Prediction intervals are based on bootstrapped 95% confidence intervals.

Model predictions and mapping of SOC stocks

We used the model shown in Equation 2 and graphed in Figure 1.1 to predict SOC stocks across the HRW (Figure 1.2). From these predicted maps, we calculated a mean 1 m SOC stock of 127 ± 26.0 (87-178) MgC ha^{-1} (± standard deviation, parentheses contain 95% confidence interval from the bootstrapped mapped predictions) and a mean 30 cm SOC stock of 72.9 ± 12.5 (55.1-103) MgC ha^{-1} (See Methods for model fit evaluation, Table 1.2. for tabulated 1 m and 30 cm SOC stocks, Supplementary Figure 1.4 for mapped 1 m SOC stock standard deviation and Supplementary Figure 1.5 & 1.6 for mapped mean and standard deviation of 30 cm SOC stocks and Supplementary Figure 1.7. for 30 cm model prediction vs. actual scatterplot). The overall total 1 m and 30 cm SOC stocks of the HRW were 8.6 ± 1.8 (5.9-12.1) TgC and 5.0 ± 0.9 (3.8-7.0) TgC, respectively. We focus on

the 1 m SOC stocks for mapped predictions with wetlands. Comparisons where wetlands defined by the WIP probability ≥ 50% covered 6,115 ha of the HRW and contained a mean 1 m SOC stock of 277 ± 49.7 (197-383) MgC ha^{-1} which was more than twice as high as the overall HRW concentration and the mean upland SOC concentration of 112 ± 23.6 (75.7-157) MgC ha^{-1}. Wetlands in our study also contained disproportionately more SOC for a total of 1.7 ± 0.3 (1.2-2.3) TgC SOC stock or 20% of the overall HRW SOC stock in 9.0% of the total landscape surface area for an SOC:Extent ratio of 2.2. Comparatively, uplands contained 6.9 ± 1.5 (4.7-9.8) TgC or 80% of the HRW SOC stock in 91% of the HRW surface area for a SOC:Extent ratio of 0.9. Within overall wetlands, we identified 4,935 ha of forested wetlands with canopy coverage ≥ 50% that contained higher mean SOC stocks of 292 ± 50.5 (210-399) MgC ha^{-1} for a total of 1.4 ± 0.2 (1.0-2.0) TgC SOC stock. These forested wetlands composed 81% of the overall wetland extent and 85% of the overall WIP wetland SOC stock for an SOC:Extent ratio of 2.3. Of the two wetland types delineated by surficial geology, riverine wetlands covered 1,726 ha and lower mean SOC stocks of 101 ± 34.7 (50.4-181) MgC ha^{-1} and a total SOC stock of 0.2 ± 0.1 (0.1-0.3) TgC and 0.8 SOC:Extent ratio. Conversely, palustrine wetlands contained a significantly higher 347 ± 55.7 (255-463) MgC ha^{-1} SOC stock and totaled 1.5 ± 0.2 (1.1-2.0) TgC or 18% of the total landscape SOC within 6% of the surface area of the HRW for a 2.7 SOC:Extent ratio.

Table 1.2 Metrics from mapping 1 m and 30 cm depth SOC stocks across the HRW. The ± indicates the standard deviation of the bootstrapped model predictions for the WIP derived estimates and published standard deviations from the NWCA-SSURGO datasets in Uhran et al. (Uhran et al., 2021) Landscape class metrics were determined by masking the map of 1 m SOC stocks with surficial geology, canopy cover ≥ 50%, or WIP ≥ 50%. * indicates the landscape class subsets from overall wetlands in both WIP & NWCA-SSURGO maps. We only show ± standard deviations for combined metrics.

Source	Landscape Class	Surface Area	30cm Depth		1m Depth	
			Mean SOC Stock	Total SOC Stock	Mean SOC Stock	Total SOC Stock
		(ha)	(MgC ha^{-1})	(TgC)	(MgC ha^{-1})	(TgC)
WIP	Wetland	6,115	122 ± 14.0 (101-153)	0.7 ± 0.1 (0.6-0.9)	277 ± 49.7 (197-383)	1.7 ± 0.3 (1.2-2.3)
	Riverine*	*1,726*	59.6 ± 18.4 (35.1-101)	0.1 ± 0.0 (0.1-0.2)	101 ± 34.7 (50.4-181)	0.2 ± 0.1 (0.1-0.3)
	Palustrine*	*4,390*	146 ± 12.2 (126-174)	0.6 ± 0.1 (0.6-0.8)	347 ± 55.7 (255-463)	1.5 ± 0.2 (1.1-2.0)
	Forested*	*4,935*	127 ± 13.4 (106-157)	0.6 ± 0.1 (0.5-0.8)	292 ± 50.5 (210-399)	1.4 ± 0.2 (1.0-2.0)
	Upland	62,030	68.1 ± 12.4 (50.6-97.9)	4.2 ± 0.8 (3.1-6.1)	112 ± 23.6 (75.7-157)	6.9 ± 1.5 (4.7-9.8)
	Total HRW	68,145	72.9 ± 12.5 (55.1-103)	5.0 ± 0.9 (3.8-7)	127 ± 26.0 (86.6-178)	8.6 ± 1.8 (5.9-12)
NWCA-SSURGO	Wetland	1,640	89.2 ± 51.8	0.1 ± 0.08	184 ± 108	0.3 ± 0.2
	Forested*	*1,442*	90.6 ± 51.8	0.1 ± 0.08	188 ± 110	0.3 ± 0.2
WIP – (NWCA-SSURGO)	Wetland	5,308	121 ± 13.9 (99.9-152)	0.6 ± 0.1 (0.5-0.8)	275 ± 49.2 (196-379)	1.5 ± 0.3 (1.0-2.0)
	Forested*	*4,236*	127 ± 13.3 (106-157)	0.5 ± 0.1 (0.4-0.7)	290 ± 50.0 (209-396)	1.2 ± 0.2 (0.9-1.7)
Combined: WIP + (NWCA-SSURGO)	Wetland	6,948	114 ± 22.9	0.8 ± 0.2	253 ± 63.0	1.8 ± 0.4
	Forested*	*5,678*	117 ± 23.3	0.7 ± 0.1	264 ± 65.3	1.5 ± 0.4

Wetland SOC stocks measured from the National Wetland Condition Assessment (NWCA) and U.S. Department of Agriculture's National Cooperative Soil Survey (NCSS) Soil Survey Geographic Database (SSURGO) datasets were upscaled with wetland extent from the National Land Cover Database (NLCD) in Uhran et al. (2021) and termed NWCA-SSURGO for reference. Wetlands in NWCA-SSURGO contained a mean stock of 184 ± 108 MgC ha^{-1} (standard deviation only, Uhran et al. (2021) did not report 95% confidence intervals; Figure 1.3 inset and Figure 1.4c). Using the 1,640 ha wetland extent measured within the HRW for the NWCA-SSURGO dataset, we calculated a total of 0.3 ± 0.2 TgC across the HRW for a SOC:Extent ratio of 1.4 (Table 1.2.). Within the total NWCA-SSURGO wetlands, forested wetlands, defined by the canopy coverage ≥ 50%, comprised 90% of the wetland SOC and 88% of the wetland extent. Compared to our WIP-

derived wetland SOC estimates, the mean concentration NWCA-SSURGO wetland SOC stock was approximately two-thirds or 66% of the mean WIP wetland SOC stock. Due to the large differences in wetland extent, the total wetland SOC of the WIP-derived estimates (1.7 TgC) was 462% higher than the total wetland SOC stock in NWCA-SSURGO (0.3 TgC) showing that only 18% of the total potential wetland SOC stock is currently mapped. By removing overlapping wetland areas covered by the NWCA-SSURGO datasets within our WIP dataset we estimated 5,308 ha of unmapped potential wetlands which we designate as cryptic carbon. This cryptic carbon contained a mean SOC stock of 275 ± 49.2 (196-379) MgC ha^{-1} and a total SOC stock of 1.5 ± 0.3 (1.0-2.0) TgC for an SOC:Extent ratio of 2.2 (Table 1.2.). The total SOC stock of cryptic carbon is 382% higher than the currently mapped total wetland SOC in NWCA-SSURGO estimates and approximately 17% of the total HRW SOC stock from our model. Within cryptic carbon, 80% is considered forested with canopy cover ≥ 50% and contains 84% of the total cryptic carbon SOC. Adding the overall new wetland SOC of 1.5 ± 0.3 TgC to the 0.3 ± 0.2 TgC in the NWCA-SSURGO increases total wetland SOC stock in the HRW by 482% to 1.8 ± 0.2 TgC (note, 95% confidence intervals removed from combined total, see Supplementary Table 1.2 for details) and more than quadruples the estimated SOC stored in wetlands.

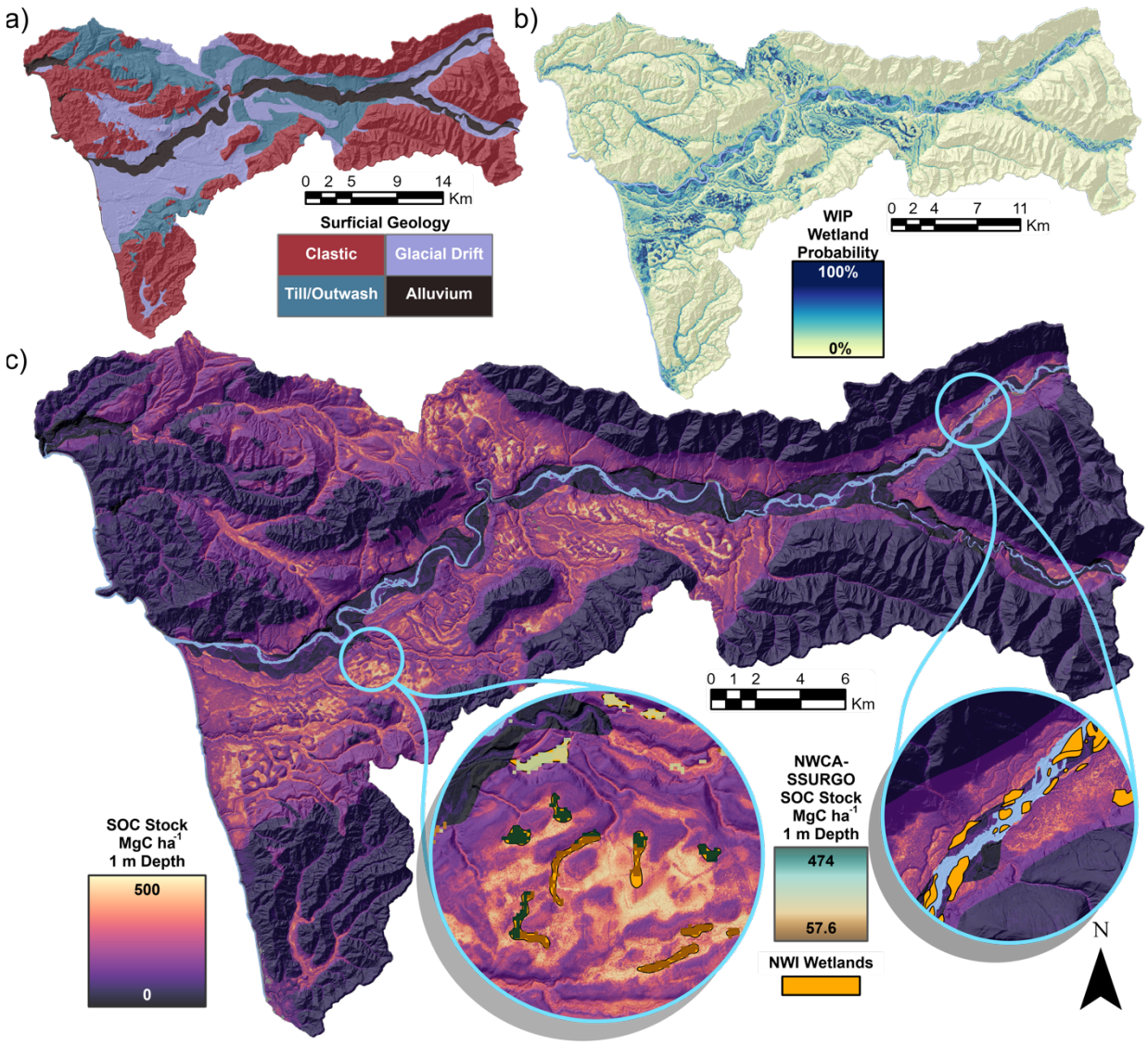

Figure 1.2 Maps of parameters and soil organic carbon (SOC) model output in the Hoh River Watershed (HRW). a) Shows the surficial geology categories of the HRW by color classes in surficial geology legend, b) shows the wetland intrinsic potential (WIP) wetland probability gradient shown by yellow-blue shading indicated in WIP legend, c) shows the predicted 1 m SOC stock across the HRW with purple-to-yellow shading that continues in inset maps showing fine scale SOC patterns overlain by estimated SOC shown by brown-teal shading from the harmonized National Wetland Condition Assessment and Soil Survey Geographic Database dataset (NWCA-SSURGO) in Uhran et al. (2021) and additional current wetland extent from the National Wetland Inventory (NWI). We added a semi-transparent hill shade layer to highlight terrain and removed the river surface water shown in light blue for the final prediction map.

In our analysis of the wetland extent distribution from the WIP model (Figure 1.3b), our minimum wetland extent ranged from 64 m^2 or 0.0064 ha to the largest wetland with 400 ha. In total, we found 31,981 individual wetlands of which approximately 96% were smaller than the minimum mapping unit of 1 acre (0.40 ha) used by the NWI (Supplementary Table 1.3.). After extracting SOC stocks from our earlier WIP-based model prediction, the SOC distribution across WIP wetlands sizes showed that a majority of wetland surface area (86%) and SOC stock (87%) was contained in wetlands greater than 1 acre (0.40 ha). Indeed, the extent of each of the largest 5 wetlands were all greater than 100 ha, the largest of which was a 400 ha wetland containing 0.15 TgC or 18% of the total wetland SOC stock (1.7 TgC). The relationship between SOC stock and individual wetland extent was shown to be linear in a log-log plot indicating that there is a non-linear increase in total SOC stock with increasing wetland extent (Supplementary Figure 1.8). Mean stock SOC density across the size distribution was consistent around 250 ± 40.8 (185-335) MgC ha^{-1} to 252 ± 42.0 (185-340) MgC ha^{-1} with slight increase with surface area with the smaller wetlands containing 251 ± 40.5 (187-336) Mg ha^{-1} compared to the largest wetlands containing 264 ± 47.8 (188-367) Mg ha^{-1} (Supplementary Table 1.3.).

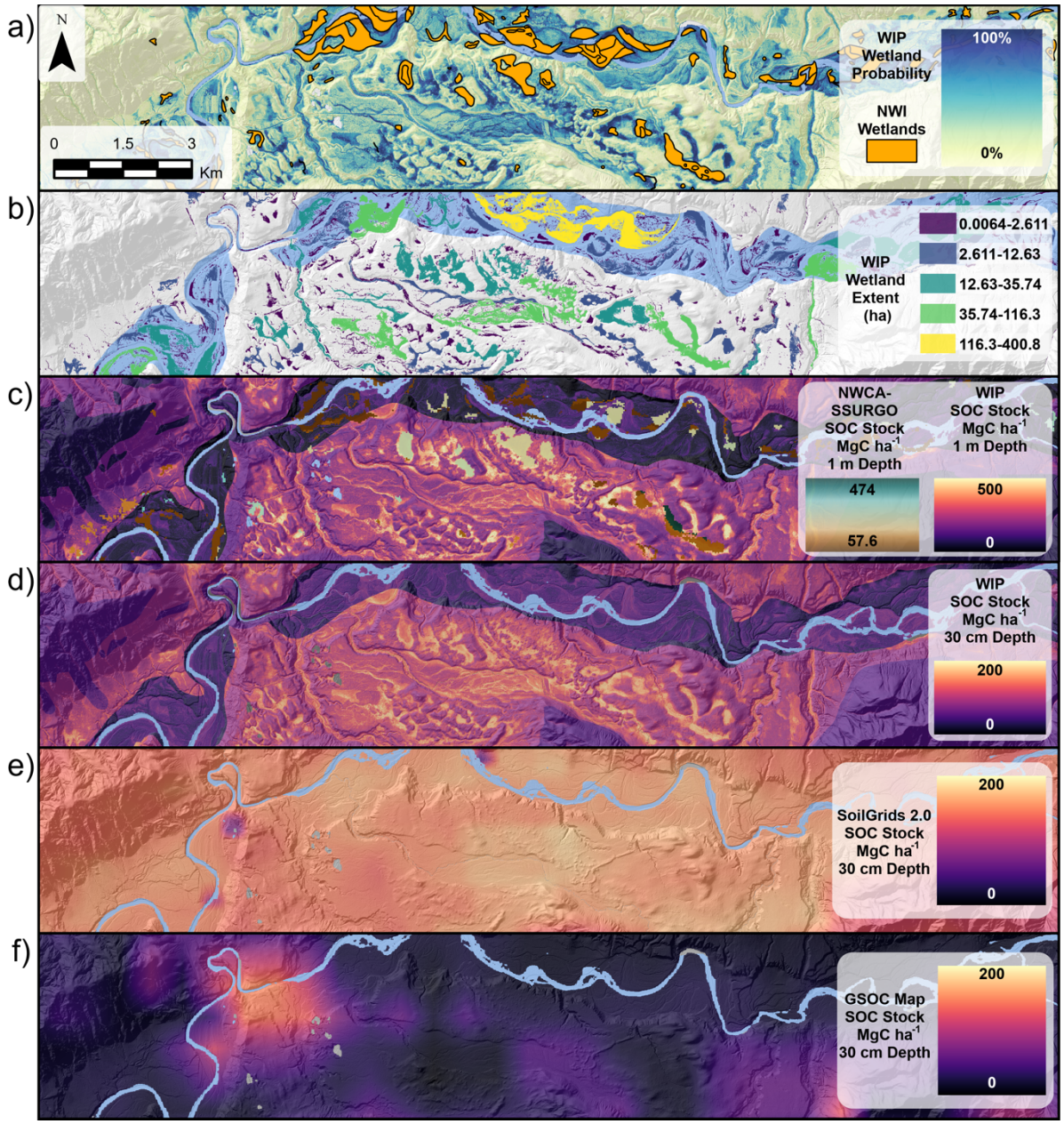

Figure 1.3 Hoh River Watershed (HRW) section maps showing the wetland areas mapped by the Wetland Intrinsic Potential (WIP) tool and the National Wetland Inventory (NWI), WIP wetland extents, WIP-based soil organic carbon (SOC) distribution with currently estimated SOC from the harmonized National Wetland Condition Assessment and Soil Survey Geographic Database dataset (NWCA-SSURGO) in Uhran et al. (2021), and WIP-based SOC compared to global SOC map products. a) shows the WIP wetland probability gradient shown by yellow-blue shading overlain by orange NWI wetlands; b) shows classes of wetland extent colored by size ranges where wetlands are defined WIP ≥ 50%; c) shows the 1 m WIP modeled SOC stock distribution with purple-to-yellow shading overlain by SOC estimates from NWCA-SSURGO shown by brown-teal shading; d) shows the 30 cm WIP modeled SOC stock distribution with purple-to-yellow shading; e) shows the 30 cm SoilGrids 2.0 (Poggio et al., 2021) modeled SOC stock distribution with purple-to-yellow shading; and f) shows the 30 cm SOC stocks from the Global Soil Organic Carbon (GSOC) Map (FAO, 2018) with purple-to-yellow shading. All maps have an added a semi-transparent hill shade layer to highlight terrain and removed the river surface water shown in light blue.

Discussion

Our results show continuous representation of potential wetlands and that wet areas integrated into DSM SOC mapping approach greatly improves the spatial representation of SOC. The results explicitly show high SOC stocks in potential wetland areas along with gradients between wetland and upland areas corresponding to the terrestrial to aquatic gradient. Overall, the spatially continuous WIP probability metric was a significant covariate for SOC when combined with surficial geology corresponding to soil parent material and enabled wall-to-wall mapping across the large heterogenous and geomorphologically complex HRW catchment. Probabilistic modeling of wetland presence has become increasingly relevant in wetland mapping research instead of more discrete land cover classification (Delancey et al., 2019) and the WIP probability model generated with fine resolution topography metrics, identified cryptic wetland features beneath a forest canopy (Halabisky et al., 2023).

The statistical model we developed to predict SOC stocks from the WIP probability is simple and conservative, appearing to underestimate large wetland SOC stocks shown by the underprediction of the upper range of SOC values in Figure 1.1. The treatment of surficial geology as a random effect which shrinks overall estimates towards an overall mean driven by the WIP. Finer scale surficial geology and other drivers of SOC, such as primary productivity are present but not accounted for in the model, but we explain substantial variation with our prediction (R^2=0.63). We found that cryptic carbon defined as the WIP-defined wetland SOC outside of currently mapped areas contains the majority of the modeled wetland SOC stock with approximately 86% of the wetland SOC. Consequently, cryptic carbon added to current NWCA-SSURGO estimates increased the total wetland SOC stock in the HRW from 0.3 TgC to 1.8 TgC or by 482%. Most of the cryptic carbon stock is due to the 273% increase in potential wetland extent from the WIP ≥ 50%, However, identification of previously omitted wetland extent using the WIP tool contained wetlands

with a higher mean SOC stock of 259 ± 72 (187-331) MgC ha^{-1} compared to the mean SOC stock in NWCA-SSURGO wetlands (184 ± 108 MgC ha^{-1}) showing a new inclusion of wetlands with high SOC stocks. The wetland SOC measured in this study was predominantly contained in the first 1 m of soil depth and within large wetland extents although there are potentially numerous small wetlands within the HRW. We note, however, that wetlands identified within our study do not represent jurisdictional wetlands or delineate wetland boundaries, nor do they represent the greater population of wetlands outside our study area. But the framework of our study begins to address the critical gap in omitting wetlands and wet areas in SOC mapping showing significant SOC underestimates when upscaling current wetland SOC data (NWCA) with optical imagery based landcover datasets (NLCD). This study provides an initial step towards improving wetland carbon monitoring systems.

While our study focused on potential wetland SOC, upland SOC is the largest fraction of the total HRW SOC stock. Two global models that provide readily accessible gridded 30 cm SOC maps are SoilGrids 2.0(Poggio et al., 2021) and the Global Soil Organic Carbon (GSOC) (FAO, 2018) Map. Our estimates of mean 30 cm SOC stock are lower than those of SoilGrids 2.0 but higher than GSOC (Supplementary Table 1.4.) indicating appropriately estimated SOC stock magnitude at the lower end of the WIP probability which may represent soil moisture regimes and their control on SOC in non-wetland areas. Compared to GSOC and our results, SoilGrids 2.0 potentially overestimates SOC stocks in the HRW but is also within the range of other studies using data from the National Forest Inventory (Cao et al., 2019). Soils are typically carbon dense in the Pacific Northwest region due to the humid temperate climate of the region and tends to be higher than SOC measurements in other systems for both wetlands and uplands (DellaSala et al., 2011). The region our study takes place in, is the southern portion of the North Pacific Coastal Temperate Rainforest, a region that expands north to central Alaska. For this same region McNicol et al. (2019)

(McNicol et al., 2019) measured a median SOC stock of 168.4 MgC ha^{-1} and mapped mean SOC stock of 228 ± 111 MgC ha^{-1}, much higher than our overall mapped SOC of 127 ± 26 (87-178) MgC ha^{-1} in the HRW. This discrepancy is likely due to the presence of numerous northern peatland SOC stocks >500 MgC ha^{-1} in the region. Peat formation is more frequent farther north in cooler and wetter climates and can accumulate organic material in deposits as deep as 3-5 m (Minasny et al., 2019). Our estimates in the HRW are potentially missing these high SOC stocks due to lack of peat samples in the sampling scheme and limiting the model prediction to 1 m depth. Similarities to the remote-sensing driven peatland probability model developed by Delancey et al. (2019) show our approach could apply towards landscape areas containing peatlands but additional classification may be needed since peatlands store significantly more SOC than mineral soil wetlands per unit area (Kolka et al., 2018).

For wetland-specific SOC stocks across different climatic zones in CONUS, Uhran et al (2021) measured 114.8-398.5 MgC ha^{-1} wetland SOC stocks with higher SOC stocks in the Eastern Mountain region due to presence of peatlands and lower SOC stocks in the arid West and Coastal Plains. Lower wetland SOC stocks are prevalent in more arid regions shown by Tangen and Bansal (2020) (Tangen & Bansal, 2020) who measured 81.97 MgC ha^{-1} wetland SOC in the semi-arid prairie pothole region. The forested wetlands in our study can be compared to findings from Davidson et al. (2022) who measured mean forested wetland SOC concentrations across the Eastern-to-Midwest U.S. and Canada ranging from 165 ± 12 MgC ha^{-1} to 264 ± 46 MgC ha^{-1} noting the highest amounts in broad-leaved and shrub/thicket wetland types and lowest in needle-leaved forests. However, it is not uncommon for SOC to be higher in needle-leaved forests which can accumulate significant amounts of carbon in colder and wetter climates (Byun et al., 2018).

Although SOC stocks vary between wetlands, SOC stocks can also vary within individual wetlands (Pearse et al., 2018). Tangen and Bansal (2020) showed significant differences in SOC stocks between different landscape positions within individual wetlands and landscape position factored heavily into restored wetland SOC stock. Stewart et al. (2023) showed that although there was considerable variability of SOC stocks within wetlands, terrain metrics related to hydrology explained a significant amount of the variation and further pointed towards topography enhancing large-scale analyses. This inference on topography informing larger scale analysis corresponded well to our use of the WIP tool in this current study which relies on topographic metrics calculated at different scales (Halabisky et al., 2023). Because of the continuous gradient produced by the WIP, we speculate that some intra-wetland variability may be accounted for in the SOC stock map. However, more explicit intra-wetland sampling would be necessary to support this notion.

Applying the framework of SOC modeling based on wetland probability in and across larger regional and continental scales would require adjusting the wetland probability with additional covariates corresponding to climatic controls on SOC in order to accurately represent changes in SOC accumulation in different wetland types in different locations. The HRW as a single watershed does not represent most of the forested watersheds in CONUS which inhibits extrapolating SOC stock numbers across larger extents, particularly in non-temperate regions. However, we have shown that the large increase in wetland extent corresponds to substantial shift in the landscape spatial pattern of SOC stocks. Moreover, these results support a critical need to evaluate the wetland SOC stocks in forested regions, particularly the large central and eastern temperate hardwood forests which contained large wetland SOC stocks shown in NWCA data from Nahlik and Fennessey (2016) and NWCA-SSURGO data from Uhran et al. (2021). Additional improvements to mapping SOC would also include modeling the probability of different wetland classes, especially peat-

forming wetlands, by using classification data available from open sources such as the NWI and NLCD (Jin et al., 2019).

The wetlands we identified with the WIP and not included in the NLCD maps used to upscale the NWCA-SSURGO wetland SOC estimates contained 1.5 TgC or 86% of the 1.7 TgC total HRW wetland SOC, constituting a substantial cryptic carbon stock. The HRW wetlands estimated by the WIP are dominated by forested wetlands which we estimate conservatively with tree cover >50% compared to 30% tree cover in the Cowardin classification system (Dahl, 2011). Although the climate, forest species composition, and landform distribution in the HRW are not fully representative of forested regions in the rest of CONUS, we believe cryptic carbon can be a significant proportion of the forested wetland inventory of CONUS. Forested wetlands are the most extensive wetland type in CONUS according to the inventory of freshwater forested wetlands in the NLCD (Uhran et al., 2021) and in the NWI (Dahl, 2011) and approaching the estimation of SOC stocks across CONUS would require a more extensive analysis with additional bioclimatic, physical, and anthropogenic parameters. For example, the Eastern CONUS features extensive deciduous forests with contrasting leaf phenology compared to the coniferous forests of the HRW which contributes to differences in forested wetland SOC stocks for each forest type (Davidson et al., 2022). Further, other CONUS regions may have more subtle landforms and topography compared to the HRW which can affect the rate of forested wetland carbon sequestration (Bernal & Mitsch, 2012). Notwithstanding, many forested wetlands remain mis-classified as upland forest due to difficulty in confirming soil moisture conditions due to dense canopies that obscure surface features from remote imagery. We suggest that there is significant potential to improve on the wetland SOC upscaling by replacing the NLCD wetland mapping from Uhran et al. (2021) which leveraged the publicly available SOC data from NWCA and Nahlik and Fennessey (2016). The NWCA dataset in Nahlik and Fennessey (2016) was sampled to represent 38.4 x 10^6 ha total wetlands in CONUS

measured as different wetland types by the U.S. Fish and Wildlife Service Status and Trends of Wetlands in the NWI program (Dahl, 2011). Forested wetlands in Nahlik and Fennessey (2016) NWCA SOC data contained mean concentrations of 283 ± 35.4 MgC ha^{-1} and extrapolation to the 20.1 x 10^6 ha in forested wetlands of CONUS inventory resulted in a total forested wetland SOC stock of 5.92 PgC. Uhran et al. (2021) updated wetland SOC estimates from Nahlik and Fennessey (2016) by revising the NWCA SOC dataset, harmonizing it with the hydric soil data in the Soil Survey Geographic Database (SSURGO), and extrapolated using wetland extent maps from the NLCD. Uhran et al. (2021) reported 191± 103 MgC ha^{-1} mean SOC stock density over 33.9 x 10^6 ha of woody wetland extent for a total stock of 6.49 PgC in woody wetlands. We emphasize any extrapolation is highly uncertain but using our example of missing extent in the HRW, a more than 3-fold increase in wetland extent (1,640 ha in NWCA-SSURGO to 6,949 ha in WIP + NWCA-SSURGO) could substantially drive a similar increase in cryptic carbon within forested areas of CONUS which we estimate to be up to 20 ± 13 PgC or 31% ± 11% (standard deviation) of the current 65 PgC total CONUS 1 m SOC stock(Soil Survey Staff & Loecke, 2016; Lajtha et al., 2018) calculated by extrapolating the mean and uncertainty from Uhran et al. (2021) and Nahlik and Fennessey (2016) by the 324% increase in wetland extent observed in this study (6,949 ha in WIP + NWCA-SSURGO area compared to 1640 ha in NWCA-SSURGO only). The underestimation of wetland SOC stocks due to wetland omission has been proposed in previous research using currently available large scale maps of land cover (Tifafi et al., 2018) and is clearly shown here using products like the NLCD. Publicly available datasets such as the NWI, NWCA, and SSURGO will continue to add data and improve in the future and represent opportunities to improve upscaling wetland SOC estimates at larger regional scales with more comprehensive and accurate wetland extent maps. Our analysis supports improving SOC distribution estimates with new approaches

using topography-based probabilistic models that better reflect the spatial distribution of soil moisture conditions and provide a continuous, spatially-explicit upscaling metric.

Due to the forested overstory, cryptic carbon is likely to experience deforestation as a disturbance, but its detection and frequency is unknown due to its omission from current wetland maps and inventories (Dahl, 2011). The SOC stored as cryptic carbon depends on consistently wet soil conditions and forest harvest practices negatively affect SOC stocks by utilizing intensive site preparation through draining wet areas for tree extraction (Mayer et al., 2020). Cryptic carbon in headwaters may be especially sensitive to hydrologic disturbance from forestry activities due to more intimate connections to groundwater (Janisch et al., 2011). Removal of forest canopy in forested wetlands and exposing soil to warmer temperatures can lead to higher rates of SOC decomposition (Trettin et al., 1996). But long periods of recovery post-harvesting can allow SOC and soil nutrients to return to pre-harvest levels ameliorating impacts on forest wetland function (Trettin et al., 2011). The effects of deforestation on forested wetlands will also vary by ecosystem type and region. Significant SOC stock destabilization and export of fluvial organic carbon was found in tropical forested wetlands and peatlands that experience deforestation and drainage (Moore et al., 2013). More work is needed to improve wetland mapping under forest canopy in tropical regions which are one of the largest sources of uncertainty in the global carbon cycle (Sjögersten et al., 2014). While deforestation itself may not lead to complete wetland drainage, land use conversion to agriculture is another persistent threat to wetlands that more effectively drains wetlands and produces substantial carbon release as greenhouse gases (Smith et al., 2016).

Globally since 1700, the main driver of wetland loss has been drainage and conversion to agriculture with regional hotspots in the United States, Europe, Central and Southeast Asia, and Japan (Fluet-Chouinard et al., 2023). Land use conversion is a top contributor to carbon emissions

after fossil fuels and is driven mostly by deforestation (Friedlingstein et al., 2022). Carbon emissions and losses of SOC from disturbed soils are more uncertain than forest biomass carbon loss in the global carbon budget (Todd-Brown et al., 2013) but as much as 133 PgC of SOC has been lost from soils over the course of 12,000 years of human agriculture (Sanderman et al., 2017). There is yet to be a consensus estimate of total global SOC losses due to wetland conversion, but there is consistent evidence of increased carbon emissions and SOC loss when wetlands, and in particular peatlands, are drained and converted to agriculture (Joosten, 2010; Houghton et al., 2012; Qiu et al., 2021; Ma et al., 2022). Utilizing the newest global wetland maps which model inundation frequency could help improve spatial estimates of SOC with large global soil pedon databases (Poggio et al., 2021; Zhang et al., 2021). At the continental or national scale, research with moderate resolution remote sensing from Landsat has been used to map wetland extent with SOC stock declines showing significant reductions in the last half century (Lu et al., 2021). Similar approaches can be applied at the large catchment scale, such as our current study in the HRW which could potentially provide contemporary insight to wetland SOC changes since the lidar acquisition in 2012 and 2013. The wetland types examined here and in other regions also experience SOC stock destabilization and emit previously stored carbon as CO_2 due to conversion to cropland (Nahlik & Fennessy, 2016; Tangen & Bansal, 2020). It is uncertain how the inclusion of cryptic carbon stocks will affect the total estimates of wetland SOC stock affected by disturbance and the magnitude of potential SOC release as CO_2. But more accurate mapping of forested wetland extent and SOC stock will improve conservation of a valuable carbon sink that is underestimated with currently mapped wetland extents.

Our study provides an adaptable approach that is informed by a continuous wetland identification metric which maps and reveals high SOC stocks driven by wetland potential on the landscape. This mapping revealed the vast stores of unmapped forested wetland SOC stocks or

cryptic carbon compared to currently available wetland SOC maps. We show cryptic carbon contained a higher mean SOC stock than both currently mapped wetlands and uplands. When added to the currently available estimates of wetland SOC stock in the HRW, cryptic carbon increased the total SOC stock from 0.3 TgC to 1.8 TgC or by 482%. The majority of this cryptic carbon was contained in wetlands greater than 1-acre or 0.4 ha, a common minimum mapping unit. There are still considerable uncertainties in extrapolating SOC increase results to the greater population of forested wetlands in the U.S., but the potential magnitude of cryptic carbon supports the need for more wetland identification in forested regions in ways that can inform SOC spatial patterns. We provide one approach which integrates potential wetlands into a SOC prediction model, but future research should explore variations of this type of modeling. Metrics that represent the landscape as a gradient of wetlands to uplands can better represent the terrestrial to aquatic gradient that includes potential wetlands and, therefore, areas of SOC accumulation. Land and natural resource managers will be able to use this framework to improve future estimates of SOC spatial patterns as well as wetland SOC vulnerability to land use change.

Methods

Study area

This study takes place in the Hoh River Watershed (HRW) within the Pacific Northwest of the Conterminous United States (Figure 1.4.) which contains some of the highest aboveground carbon and SOC stocks in the world reaching 375 MgC ha-1 and 709 MgC ha-1, respectively (Bidlack et al., 2021). In the HRW, mean annual air temperature is 7.2oC and mean annual precipitation is 274 cm and can exceed 300 cm with most of the precipitation in winter which mainly falls as rain, but snowfall is more common in the upper elevations (NOAA National Centers for Environmental Information, 2023). The mountains of the HRW were created 17-20 million years ago during the Miocene to Eocene periods with the uplifting of marine sedimentary rock over the denser ocean crust. The uplifted marine sedimentary rock also formed hills and terraces in the lower HRW. During the end of the Pleistocene and the period of deglaciation, large floods from glacial melt deposited material over the lower elevation so the HRW creating large floodplains. Rivers continued to incise this deposited glacial material over the Holocene and into the present depositing alluvium near the present main channel of the Hoh river that bisects the HRW (Gavin et al., 2013). Current topography varies from mountains with steep slopes (>40%) in the eastern portion of the HRW to rolling hills and flat areas in the lower floodplain that drains eastward to the Pacific Ocean. Soils of the HRW reflect this geologic history and topography with dominant soils containing loamy to sandy-clay coarse textures although there is a moderate presence of volcanic ash, which promotes Andisol soil development(Edmonds et al., 1998). The HRW has a mix of both private and public forestlands dominated by Sitka Spruce (Picea sitchensis) and Western Hemlock (Tsuga heterophylla) in the lower elevations that is actively managed for timber harvest although areas along the coast and in the upper watershed are part of the Olympic National Park with protected old-growth forest containing trees up to 4 m in diameter and 80 m in height(McKee et al., 1982). The mapped

wetlands within the HRW are diverse, from precipitation-driven bogs to riparian wetlands (Figure 1.4. insets).

Many of the wetlands are under dense forest overstory but in some forested areas with high levels of inundation trees are stunted in size and have a lower overall height and biomass. The most prominent Hydrogeomorphic wetland classes are Riverine, Mineral Flats, Organic Flats, and Depressional (Brinson, 1993). There is a notable difference between Riverine wetlands and the other wetland classes for SOC and we mark this distinction with grouping all wetland hydrogeomorphic classes into two classes for our soil pedon dataset: Riverine and Palustrine (non-riverine). Palustrine wetlands are similar to the Cowardin classification as any freshwater (or less than 0.5 ppt salt concentration), non-tidal non-riverine, or non-lacustrine wetland, inclusive of forested and non-forested vegetation (Dahl, 2011).

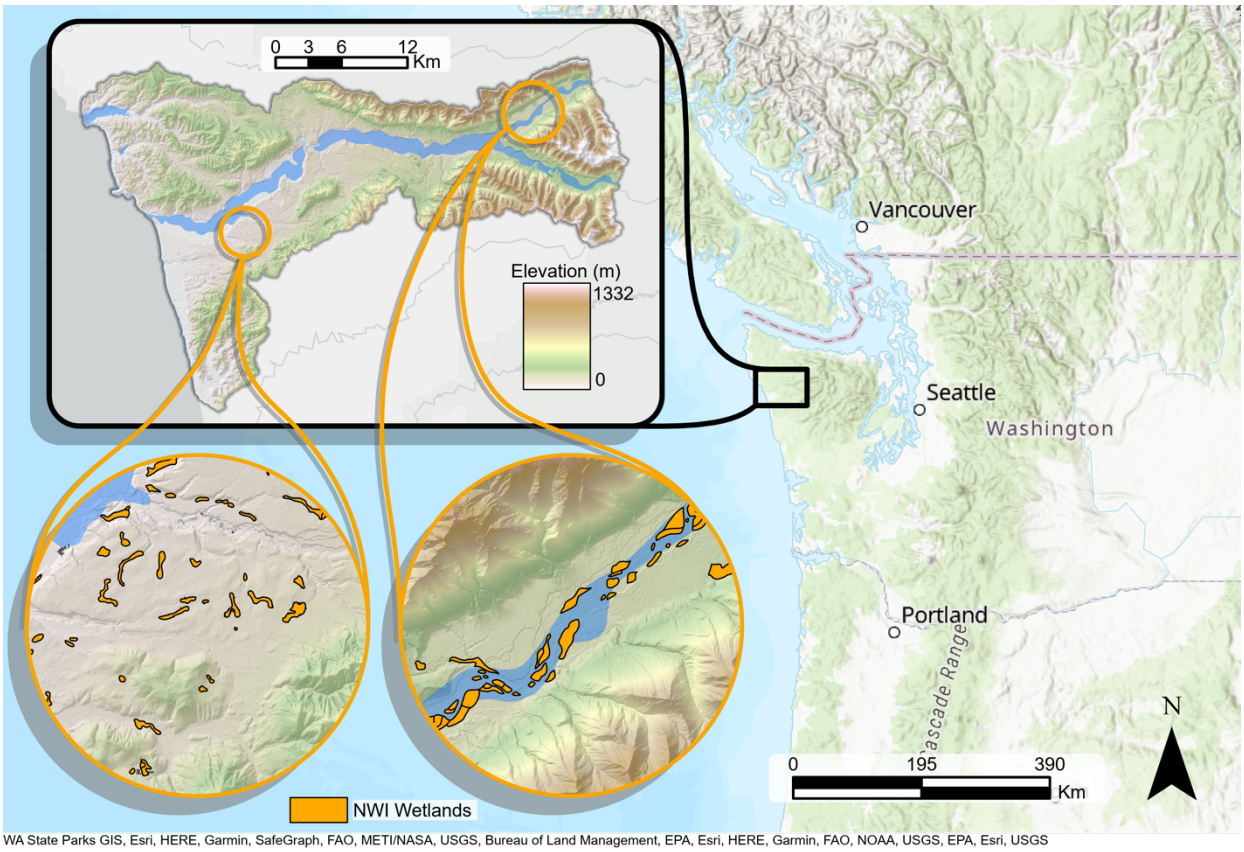

Figure 1.4 The region of the United States with the location of the Hoh River Watershed (HRW) with National Wetland Inventory (NWI). The HRW is located in the Pacific Northwest of the United States on the coast of Washington State. The eastern portion of the HRW is mountainous and drains westward to the ocean, which is highlighted by the shaded elevation and topography. Circle inset maps show the eastern and western portions of the lower watershed with wetlands from the NWI colored in orange. We color the river basin area with light blue for the HRW. Basemap image credits are listed below the map figure.

Mapping wetlands with the Wetland Intrinsic Potential Tool (WIP)

We mapped wetlands using the Wetland Intrinsic Potential (WIP) tool, a multi-scale terrain-based wetland identification and mapping tool developed by Halabisky et al. (2023). The WIP tool models wetland presence in a spatially explicit, continuous pixel approach using input parameters related to hydrophytic vegetation, hydrology, and hydric soils. The topographic and terrain input data layers are derived from discrete point aerial lidar which was processed to create a digital elevation model at a 4 m cell size resolution of the terrain surface (Lidar source: 2012-2013 Puget Sound LiDAR Consortium (PSLC) Topographic LiDAR: Hoh River Watershed, Washington (Deliveries 1 and 2), vertical absolute accuracy RMSE: 0.043 m; vertical relative accuracy RMSE:

0.082 m). Unlike aerial or satellite imagery, lidar can detect small topographic features under tree canopy and terrain metrics were integrated into a random forest model that was trained on wetland presence/absence point datasets derived from the National Wetland Inventory (NWI) and validated with additional field collected ground-truthed datasets. The WIP tool was specifically developed to identify wet areas missing in most wetland inventories because they do not have standing water or are hidden under tree or vegetation canopy making them difficult to detect in satellite or aerial imagery. We refer the readers to Supplementary material and Halabisky et al. (2023) for the full summary of how the WIP tool was implemented in the HRW. The output produces a wetland probability score based on the proportion of classification trees in the random forest model of how likely a pixel is a wetland (0%-100%) which is the estimated likelihood that the wetland class label is correct for a given input of terrain, hydrology, and vegetation parameters. For example, a pixel that has a wetland probability of 80% will contain a combination of landscape features that generate a wetland within 80% of the dataset. Wetlands, therefore, represent the high end of continuum corresponding to landscape soil moisture and inundation and the other end is an absence of these conditions. Because the wetland probability is continuous across the entire landscape, it enables SOC stock to be modeled continuously across the entire HRW. However, setting a threshold probability also allows estimates of wetland extent. In order to determine potential wetland extent, we chose the threshold value of 50%, above which classifies a pixel as a wetland and below which classifies pixels as non-wetland or upland. WIP model accuracy for the HRW in Washington State using wetland probability ≥ 50% to create a binary class of wetland (>50%) vs. upland (<50%) was 93.0%. Readers should consider that wetlands defined by the WIP tool do not have jurisdictional boundaries which require field delineation and verification to determine their exact extent based on hydrology, hydric soil, and hydrophytic vegetation at a much smaller scale.

Field sampling

We developed a stratified random sampling approach across the HRW WIP probability distribution. Our strategy was to sample at a consistent interval in the distribution to evenly obtain samples and address potential areas of uncertainty. We divided the WIP distribution into 30 probability bins and sampled 1 pedon at a random location per bin then added 6 additional pedons split between the highest and lowest probabilities as time allowed. Once sampling locations were selected, we used Garmin Handheld Global Positioning System (GPS) to navigate to each point. After designating the pedon sampling location, we then used a JAVAD GNSS Triumph-2 for more precise georeferencing. While we strove to remain unbiased in our selection of sample sites, we faced difficulty accessing the precise location of randomly selected, 4 m resolution pixels due to limited precision in GPS navigation equipment which was approximately 4-10 m in ideal open sky conditions and degraded further under canopy. Therefore, the final distribution of WIP probability values for our sampled pedons was not evenly split between wetlands and uplands. We note that uplands compose the majority of the HRW as shown by the histogram of the entire HRW WIP (Supplementary Figure 1.3a). Our sampling results somewhat reflect this overall distribution (Supplementary Figure 1.3b) and help prevent wetland-bias in our model. In total, we sampled pedons in 8 wetlands and 28 uplands according to the WIP probability ≥ 50% cutoff for the wetland class from the mapped model. Within the wetland class defined by the WIP ≥ 50%, we classified two distinctive wetland types: riverine (n=2) and palustrine (n=6), which differed in their parent material and organic matter content. Riverine wetlands consisted of recently deposited alluvial material and exhibited very little soil development. We classified these observations in the field and later used a surficial geology map to delineate riverine areas with lower predicted SOC described below.

At each pedon site, a pit was excavated to at least 100 cm depth or to a restricting layer to characterize soil horizons, color, texture, structure, and redoximorphic features (Soil Science Division Staff, 2017). Samples were collected by each soil horizon for bulk density and total carbon analysis. Bulk density was carefully extracted from the pedon face for each horizon using a fixed volume metal cylinder with a volume of 98.175 cm^3 for mineral soils or a beveled polyvinylchloride (PVC) cylinder with a volume of 132.536 cm^3 for organic soils. Bulk soil samples were taken from each horizon for total carbon analysis. All samples were transported in coolers and stored in refrigerated spaces between 4-6° C until laboratory preparation and analysis. Laboratory sample preparation included drying all soil samples for at least 48 hours or to a constant weight in drying ovens at 75 °C. Soil samples were then sieved to extract the fraction less than 2 mm and remove coarse fragments. Bulk density was calculated as the mass of the less than 2 mm fraction divided by the volume of the fixed volume soil core sampler. SOC was also measured with the <2 mm fraction. Samples were prepared by ball milling a subsample for 2 minutes at 1/30 second frequency. Then a 20 mg subsample was run on a Perkin Elmer Co. 2400 model Total Carbon, Hydrogen, and Nitrogen (CHN) Analyzer. SOC stocks for each horizon were calculated from the total carbon percentage from the CHN analyzer (C) multiplied by the bulk density (BD) and the soil horizon thickness (D) (Equation 1.1).

$$1.1)\ SOC\ Stock = \sum C_i * BD_i * D_i * (1 - CF_i)$$

Where C denotes the carbon percentage, BD represents bulk density, D (g cm-3) represents the horizon thickness (cm), and CF represents the coarse fragment fraction of the soil sample i. For the purpose of this analysis, we do not spatially predict SOC deeper than 1 m soil depth although we collected data beyond 1 m. Soil pedon landscape classes were defined as wetlands for pedons with WIP ≥ 50%, as uplands for WIP < 50%, and as riverine wetland or palustrine wetlands when the

sample location was inside or outside the Hoh River floodplain defined by the surficial geology, respectively.

SOC stock modeling and covariates

To generate a prediction model for SOC, we used a linear mixed effects modeling approach using the 'lme4' (Bates et al., 2015) R package with fixed and random effects to conduct our SOC carbon stock spatial prediction. Linear mixed effect models were used to specify the fixed effect as the WIP probability metric for our primary covariate for SOC. We also investigated multiple remote sensing metrics such as Normalized Difference Vegetation Index (NDVI), Enhanced Vegetation Index (EVI), and the Modified Normalized Difference Water Index (MNDWI), as well as single band reflectance from Landsat imagery as additional fixed effects in the model. We used surficial geology of the HRW to the map riverine quaternary sediments which represent river floodplains that are strongly predicted as wetland areas in the WIP tool but do not develop soil or accumulate organic matter due to recent river water scouring. Surficial geology data were downloaded as 1:100,000 scale polygons from the Washington State Department of Natural Resources geologic information portal. Four broad classes of lithological material and geologic age were extracted from the surficial geology data to provide grouping for SOC samples: Clastic, Glacial Drift, Till/Outwash, and Alluvium. Surficial geology was designated as a random effect due to the uneven sample sizes in each surficial geology group and to account for variation by adjusting the intercept based on surficial geology categories within the model. Surficial geology could be designated as a fixed effect due to fewer than 5 levels (4) which is a common cutoff for random effects, but this has been shown to not affect model performance especially when another parameter is of interest. Choosing between fixed and random effect designation is not straightforward but designating random effects can be helpful to improve parameter estimation such as the WIP in this study (Harrison et al., 2018).

Stepwise variable selection using Akaike information criterion (AIC) was used to determine fixed effect covariates in addition to the WIP tool probability metric and surficial geology random effect. However, there were no significant effects from adding remote sensing metrics to the WIP and surficial geology. Further, the heterogeneity of the forested landscape due to forest harvest was prohibitive for using spectral remote sensing metrics or lidar metrics of forest structure to predict SOC which could weight clearings or reflective surfaces inappropriately in SOC predictive modeling. Additional terrain metrics were also excluded to avoid intercorrelations with the WIP probability covariate which already incorporates terrain information and surficial geology. Overall, the best model according to AIC was also simplest using just the WIP probability with surficial geology classes (Eq. 1.2).

$$1.2)\ \sqrt{(SOC\ Stock)}_{ij} = \boldsymbol{X}\beta_{WIP_i} + \boldsymbol{Z}\alpha_{Surfical\ Geology_j} + \in_{ij}$$

Where $\boldsymbol{X}$ is the fixed effects design matrix for the β_{WIP_i} in pedon i, $\boldsymbol{Z}$ is the random effects design matrix for the random effects $\alpha_{Surfical\ Geology_j}$ for an geology type j, and $\in_{ij}$ is our model error described as $\in_{ij} \sim N(0, \sigma_{\in}^2)$. Pedons sampled from the random effect $\alpha_{Surfical\ Geology_j}$, described as $\alpha_{Surfical\ Geology_j} \sim N(0, \sigma_{\alpha}^2)$ are considered a random sample from a separate normal distribution for each surficial geology type j.

SOC Stock Prediction

The Eq. 1.2 model was used to predict SOC stock at a 1 m and 30 cm depth with a R^2 of 0.63 and 0.61 respectively between observed (Pedon SOC stocks) and predicted SOC stock values**.** The WIP variable as a strongly significant predictor with an estimated non-transformed coefficient for 1 m SOC stock of 391 (95% Conf. Interval: 241-516 MgC ha^{-1}, see Supplementary Table 1.1 for full model parameter estimates and details). This was much higher than the surficial geology random

effect (Supplementary Table 1.1.) showing that the finer scale WIP parameter was driving SOC more than the coarser scale patterns of surficial geology. The Root Mean Square Error (RMSE) for the 1 m model was 96.8 MgC ha^{-1} and 31.0 MgC ha^{-1} for the 30 cm model. A leave one out cross validation computed a cross-validation RMSE of 22.8 MgC ha^{-1} for 1 m SOC stocks and 11.7 MgC ha^{-1} for 30 cm SOC stocks. Bootstrapped model predictions for the 1 m model showed 95% confidence intervals (2.5% to 97.5%) around the mean based on 1000 simulations were 216 to 511 MgC ha^{-1} for the WIP, 3.67 to 129 MgC ha^{-1} for the intercept, 77.0 to 131 MgC ha^{-1} for the variance, and 49.5 to 145 MgC ha^{-1} for the surficial geology random effect intercept. Bootstrapped model predictions for the 30 cm model, were 51.8 to 147 MgC ha^{-1} for the WIP, 36.7 to 76.1 MgC ha^{-1} for the intercept, 24.4 to 41.4 MgC ha^{-1} for the variance, and 24.3 to 55.8 MgC ha^{-1} for the surficial geology random effect intercept. We note these bootstrapped confidence intervals were computed on the non-transformed model which potentially widens the confidence intervals but allows for better interpretation with results in SOC response variable units of MgC ha^{-1}.

Rasters data layers for the WIP probability and surficial geology were projected to the NAD83 UTM Zone 10 (EPSG:26910) and resampled to match the WIP original 4 m pixel resolution of the digital elevation model. SOC stocks at 30 cm and 1 m depths were predicted across the HRW using the two raster data layers and the model from Equation 2 which resulted a spatially continuous map of the square root SOC that was then back transformed with squaring to result in SOC stocks in MgC ha^{-1}. We masked surface water presence by using the median modified normalized difference water index (MNDWI) across a five-year period from 2016 to 2021. We examined the riverine classification and classified all MNDWI values above 0.30 as river surface water to be masked out. The masking process also removed a small lake located in the mountains on the eastern portion of the watershed and small gravel pits in the center of the watershed. The resulting SOC prediction map was used to calculate the total HRW SOC stock, wetland SOC stock,

forested wetland SOC stock, riverine wetland SOC stock, palustrine wetland SOC stock, and non-wetland/upland SOC stock. Wetland SOC stock was estimated by classifying pixels as wetlands with WIP probability ≥ 50% and we refer back to Halabisky et al. (2023) for the discussion of error with this threshold. We note that this WIP-based classification reflects potential wetland extent but is not meant to confer jurisdictional wetland extent which requires ground truth delineations. Surficial geology delineation of the Hoh River main channel and floodplain was used to classify riverine wetland and palustrine wetland SOC stocks. Forested wetland SOC stocks were estimated from a forest/non-forest mask of wetland SOC stocks derived from tree cover ≥ 50% in the Global Tree Cover product in Sexton et al. (2013). Non-wetlands were delineated as the total area outside of the WIP probability ≥ 50% and we classify this area and SOC stock as uplands.

We quantified uncertainty using several methods. First, we examined the R^2 value of the fit vs. the predicted values in the final model output to judge the overall fit of the model on the actual SOC values in the current dataset. Next, we calculated confidence intervals using the 'confint.merMod' function in the lme4 R package(Bates et al., 2015). Next, we generated a prediction interval for the model using the 'predictInterval' function in the 'merTools'(Knowles & Frederick, 2023) R package. This function computes a simulated distribution for all parameters in the model. For the random effect simulation, the distribution is simulated by sampling from a multivariate normal distribution defined by the best linear unbiased prediction estimate and the variance-covariance matrix for each level of the grouping terms. The result is a matrix of simulated values for the linear mixed effects model and each random effect grouping term has a matrix for each observation. The 5^{th} and 95^{th} percentiles of the final simulated distribution were used to define the uncertainty in the prediction and root mean square error was calculated from the difference in the fit vs. the predicted values. Finally, we calculated the mapped SOC prediction uncertainty with a bootstrapping approach. Bootstrapped datasets were constructed by sampling the pedon SOC

values from the current dataset with replacement, then integrating that dataset into the prediction model in Eq. 1 which was used to further predict SOC across the HRW. In total we used 300 bootstrapped SOC prediction maps where each pixel contained 300 predictions to simulate a distribution from which we extracted the standard deviation to represent the prediction interval uncertainty. We then compared the WIP wetland SOC stocks with 1 m SOC stocks derived from Uhran et al. (2021) which harmonized the National Wetland Condition Assessment (NWCA) and U.S. Department of Agriculture's National Cooperative Soil Survey (NCSS) Soil Survey Geographic Database (SSURGO) datasets then upscaled the harmonized dataset to spatially explicit inland wetland extent measured by the Landsat-derived National Land Cover Database (NLCD). We term the spatially explicit maps of wetland SOC from Uhran et al (2021) as NWCA-SSURGO which provides the latest mapped wetland SOC stocks at 30 cm and 1 m depths for the continental U.S. at a 30 m resolution. To identify differences between our pedon collection upscaled with WIP and currently mapped estimates, which we term 'cryptic carbon', NWCA-SSURGO SOC stocks were subtracted from the WIP wetland SOC stocks. Standard deviations are reported from Uhran et al. (2021) for the mapped NWCA-SSURGO SOC estimates and we provide those in Table 1.2. While NWCA-SSURGO dataset contains NLCD-defined forested wetlands, we instead relied on the >50% forest cover from the Global Tree Cover in Sexton et al. (2013) for consistency with our estimates of dense canopy forested wetlands within the WIP.

Wetland size distribution

Wetland size and extent was derived defining wetlands from the WIP tool probability greater than 50%. All wetland pixels greater than 50% were classified as wetland and converted to polygons using the 'terra'(Hijmans, 2023) and 'sf'(Pebesma, 2018) R packages. The wetland polygons were filtered to remove all wetlands below 64 m2 which is the area equivalent to 2x2 pixels in order to conservatively estimate wetland size classes. Examination of the wetlands below 64 m2 did not

reveal significant cumulative proportions of SOC or extent. Wetlands above 64 m2 were used to extract SOC values in MgC ha-1 from the prediction raster. Size classes were defined as quantiles: 1%, 25%, 50%, 75%, 96.4% and 100% and cumulative sums for SOC and areal extent were calculated. The 96.4% quantile marks the 1-acre or 0.40 ha extent that is the minimum mapping unit of the National Wetland Inventory (NWI), separate from the NLCD, and is used as a threshold for small wetlands in this study. The NWI defines 0.40 ha as the minimum mapping unit due to constraints with manual aerial photo interpretation, but wetlands can still be mapped at smaller extents with less consistently (Dahl, 2011).

Supplementary Material for Chapter 1. Revealing the hidden carbon in forested wetland soils

Methods: The Wetland Intrinsic Potential Tool

We rely on the Wetland Intrinsic Potential (WIP) tool to generate the continuous wetland-to-upland gradient across the Hoh River Watershed (HRW). The details of building, training, and executing the model are described in Halabisky et al. (2023) and we refer readers to there for further and more detailed information. However, to provide more insight into our use of the tool, we describe the WIP model briefly here.

The WIP model is a geospatial wetland mapping model using multiple metrics corresponding to topography, hydrology, soil characteristics, and vegetation in a random forest algorithm (Supplementary Figure 1.1). There is an emphasis on topographic metrics within the WIP due to the thick forest canopy in the HRW that obscures potential wetlands. Additionally, these topography metrics are calculated at multiple scales, enabling cross-scale variables to inform the wetland prediction model whereas many other studies only utilize single scale variables(Maxwell et al., 2016). The total number of variables used in the model was 19.

Training data for the model were initially developed using first with 1000/2000 wetland/non-wetland locations based on maps from the National Wetland Inventory (NWI). Using the random forest with the 19 predictors, this generated a preliminary model of wetland probability across the HRW with pixel values on a scale from 0.0-1.0, with 1.0 being the maximum probability of being a wetland which we translate to a percentage (0%-100% wetland) from this point onward. We note that presence and absence based on the NWI can contain many misclassified points due to the assumption that there were many missing wetlands. Therefore, another training dataset was developed from a stratification of the NWI-derived preliminary model and sampling points in bins

of the probability range (0%-25%, 25%-50%, 50%-75%, and 75%-100%). This provided a way to identify areas where there is high model uncertainty (i.e., probability near 50%). A total of 598 sample points were equally split among bins and validated using site visits and aerial photo interpretation (two points were removed due to unclear wetland/non-wetland boundary). The final random forest algorithm was run with these 600 points and the 19 predictors. A validation dataset of 100 wetland points and 200 upland points were sampled from the output of the random forest model mapped onto the HRW and were also validated with site visits and aerial photos. With wetland and non-wetland defined as above and below 50%, respectively overall accuracy of the WIP according to validation data was 91.77%.

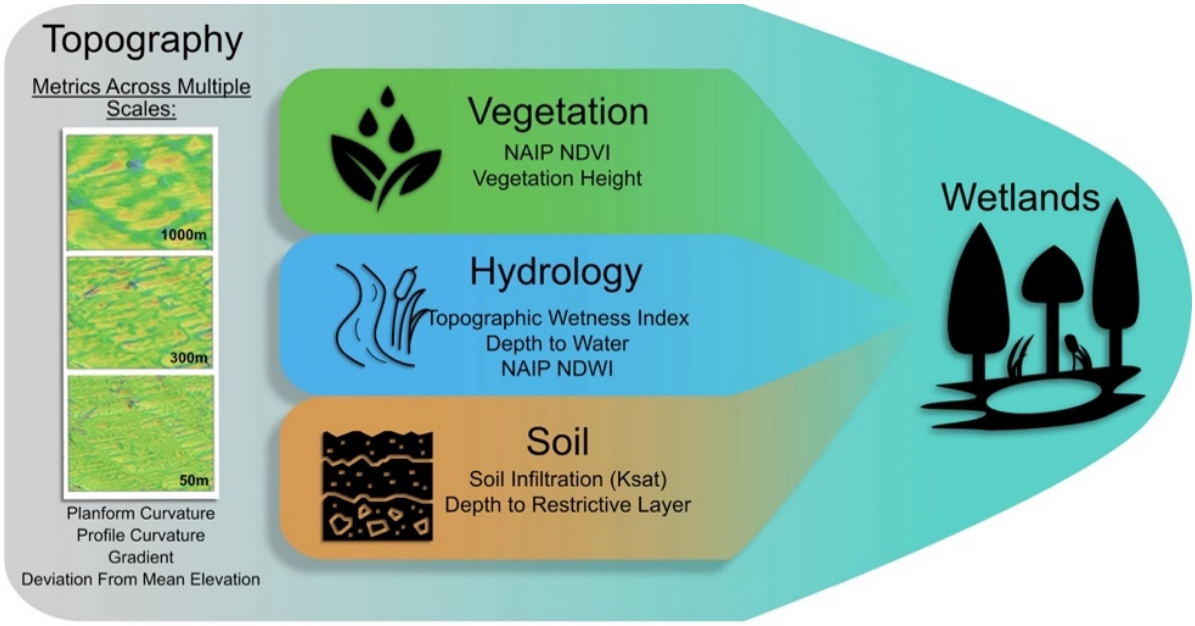

Supplementary Figure 1.1 Conceptual model of the Wetland Intrinsic Potential (WIP) Tool The National Agriculture Imagery Program (NAIP) provided fine resolution imagery for normalized difference vegetation index (NDVI) and normalized difference water index (NDWI). The conceptual model is unaltered and was originally published as Figure 2 in Halabisky et al. (2023) under the Creative Commons Attribution 4.0 License (https://creativecommons.org/licenses/by/4.0/).

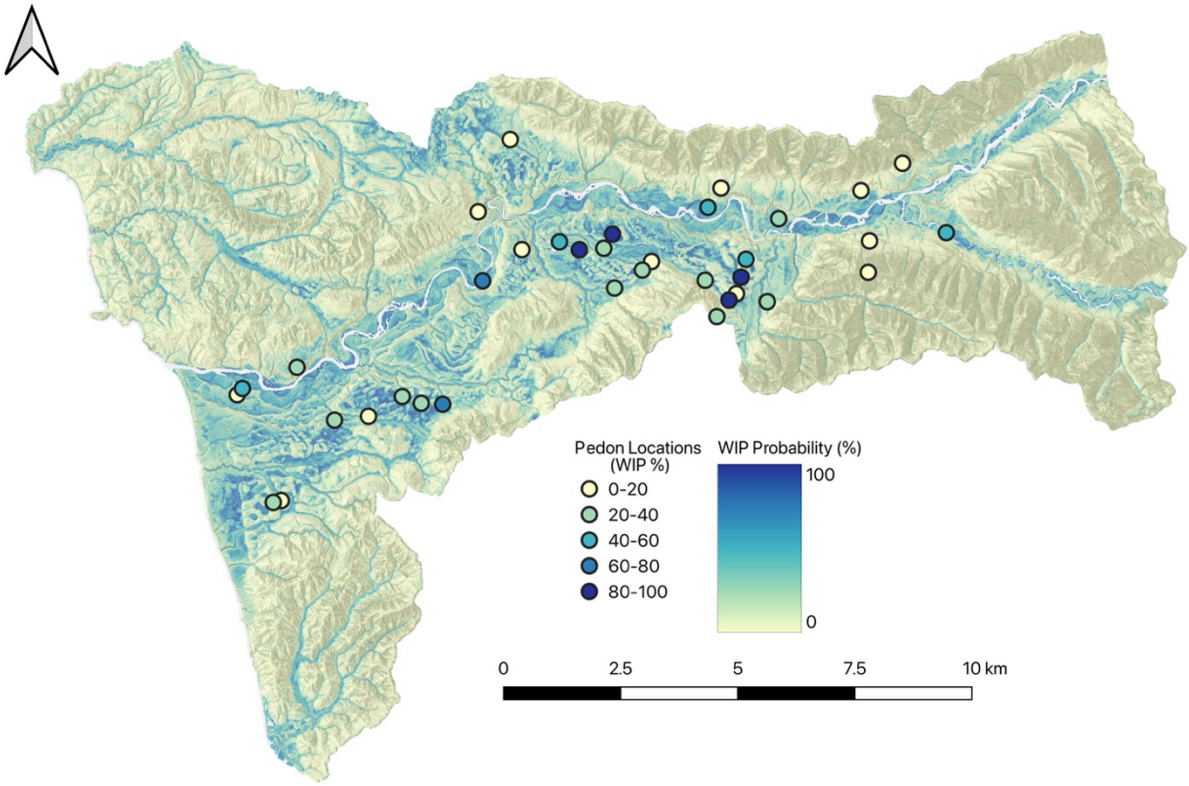

Supplementary Figure 1.2 Locations for pedon soil sample collections on a map of the wetland probability from the Wetland Intrinsic Potential (WIP) tool. WIP probability values are mapped continuously across the HRW according to the shading for probability (%). A corresponding WIP value was extracted for each location and shown in the icon. We added a semi-transparent hill shade layer to highlight terrain.

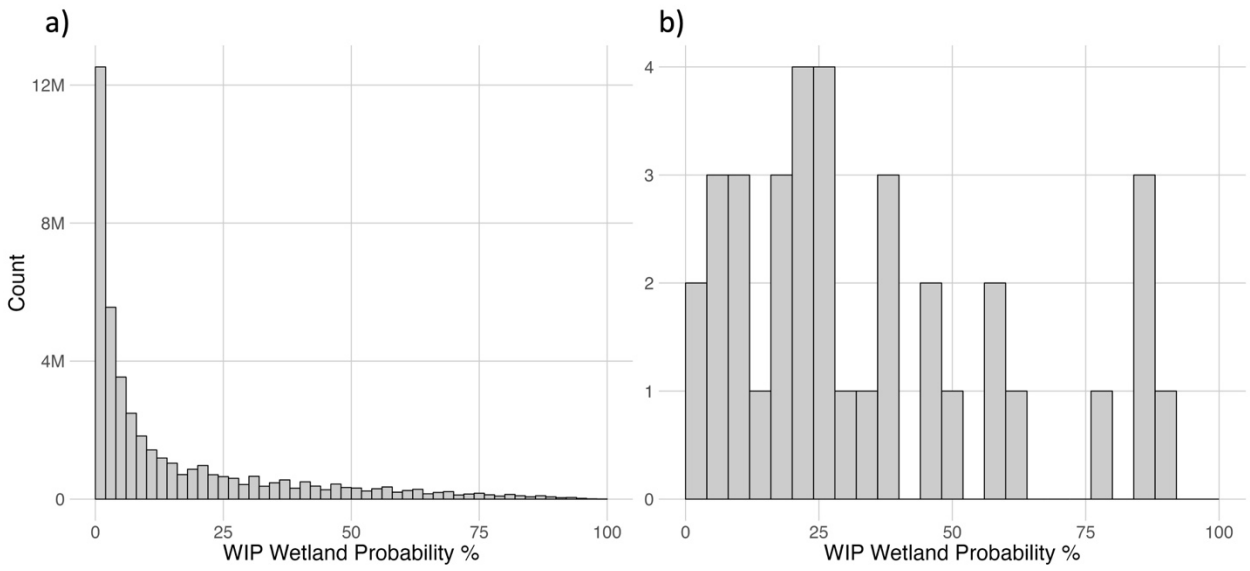

Supplementary Figure 1.3 Histograms of the Wetland Intrinsic Potential (WIP) tool probability values from maps and pedons a) Histogram distribution of the WIP map shown with the mapped area in Supplementary Figure 1.2; b) Histogram distribution of pedon locations also shown with points in Supplementary Figure 1.2.

Supplementary Table 1.1 Confidence intervals of the transformed and untransformed models of the 1 m soil organic carbon (SOC) stock. The random effect refers to the surficial geology. Sigma refers to the overall model error. The Wetland Intrinsic Potential (WIP) is the fixed effect.

	Square Root Transformed			Non-Transformed		
Parameter	**2.5%**	**Mean**	**97.5%**	**2.5%**	**Mean**	**97.5%**
Random Effect Standard Deviation	2.77	4.65	6.01	46.7	108	141
Sigma	2.56	3.39	4.23	75.9	102	126
Model Intercept	6.71	8.42	10.7	-0.39	48.6	123
WIP	6.28	11.0	15.5	241	391	516

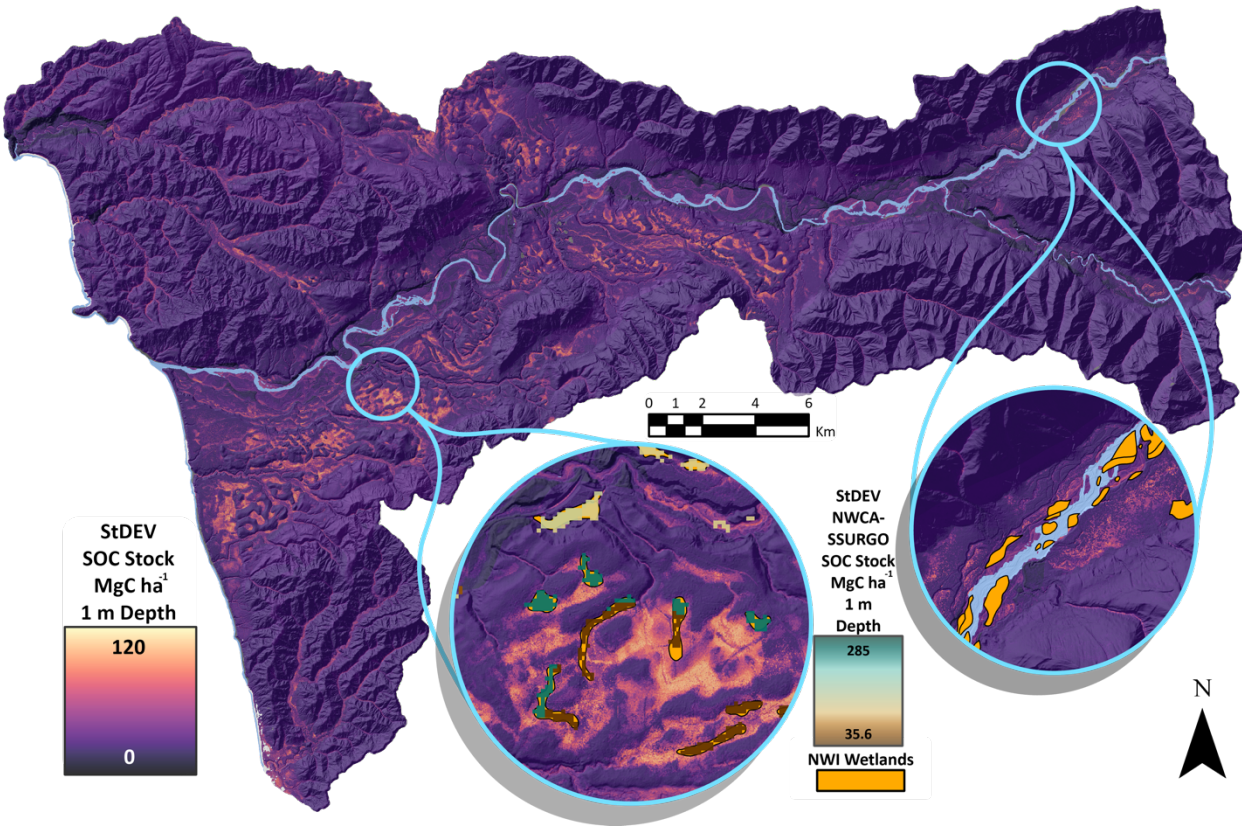

Supplemental Figure 1.4 Standard deviation of modeled 1 m soil organic carbon (SOC) stocks from bootstrapping in the Hoh River Watershed (HRW). Insets show both National Wetland Inventory (NWI) wetland locations and wetland SOC stocks from National Wetland Condition Assessment and Soil Survey Geographic Database dataset (NWCA-SSURGO) from Uhran et al. (2021). NWCA-SSURGO wetlands with SOC values are derived from the standard deviation in Uhran et al. (2021). We added a hill shade layer to highlight terrain and removed the river surface water shown in light blue for the final prediction map.

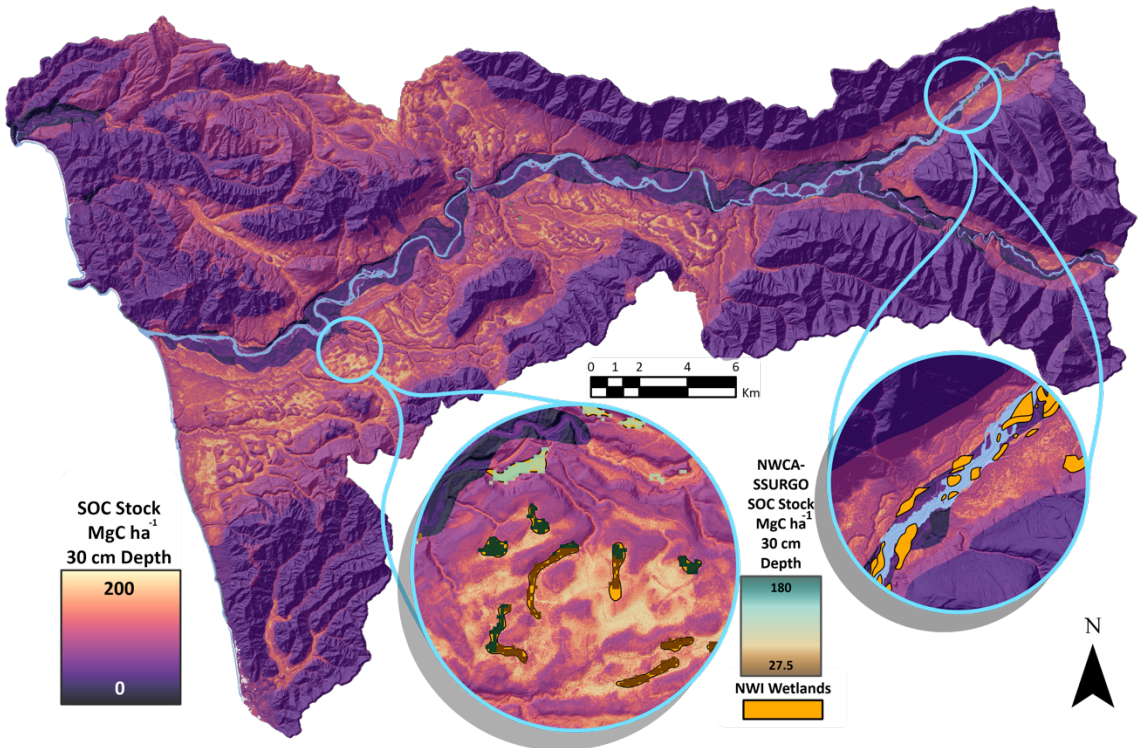

Supplemental Figure 1.5 Predicted mean 30 cm soil organic carbon (SOC) stocks across the Hoh River Watershed (HRW.) Insets show both National Wetland Inventory (NWI) wetland locations and SOC stocks from National Wetland Condition Assessment and Soil Survey Geographic Database dataset (NWCA-SSURGO) from Uhran et al. (2021). We added a hill shade layer to highlight terrain and removed the river surface water shown in light blue for the final prediction map.

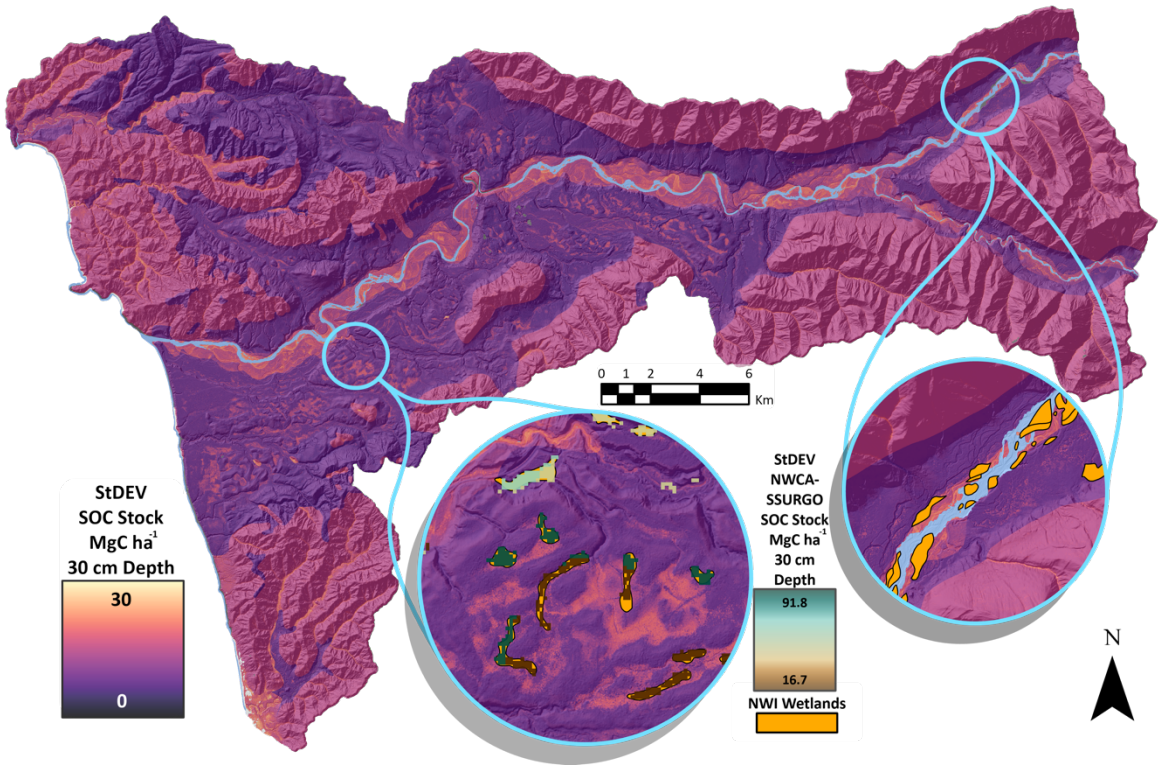

Supplemental Figure 1.6. Standard deviation of modeled 30 cm soil organic carbon (SOC) stocks from bootstrapping in the Hoh River Watershed (HRW). Insets show both National Wetland Inventory (NWI) wetland locations and wetland SOC stocks from National Wetland Condition Assessment and Soil Survey Geographic Database dataset (NWCA-SSURGO) from Uhran et al. (2021). NWCA-SSURGO wetlands with SOC values are derived from the standard deviation in Uhran et al. (2021). We added a hill shade layer to highlight terrain and removed the river surface water shown in light blue for the final prediction map.

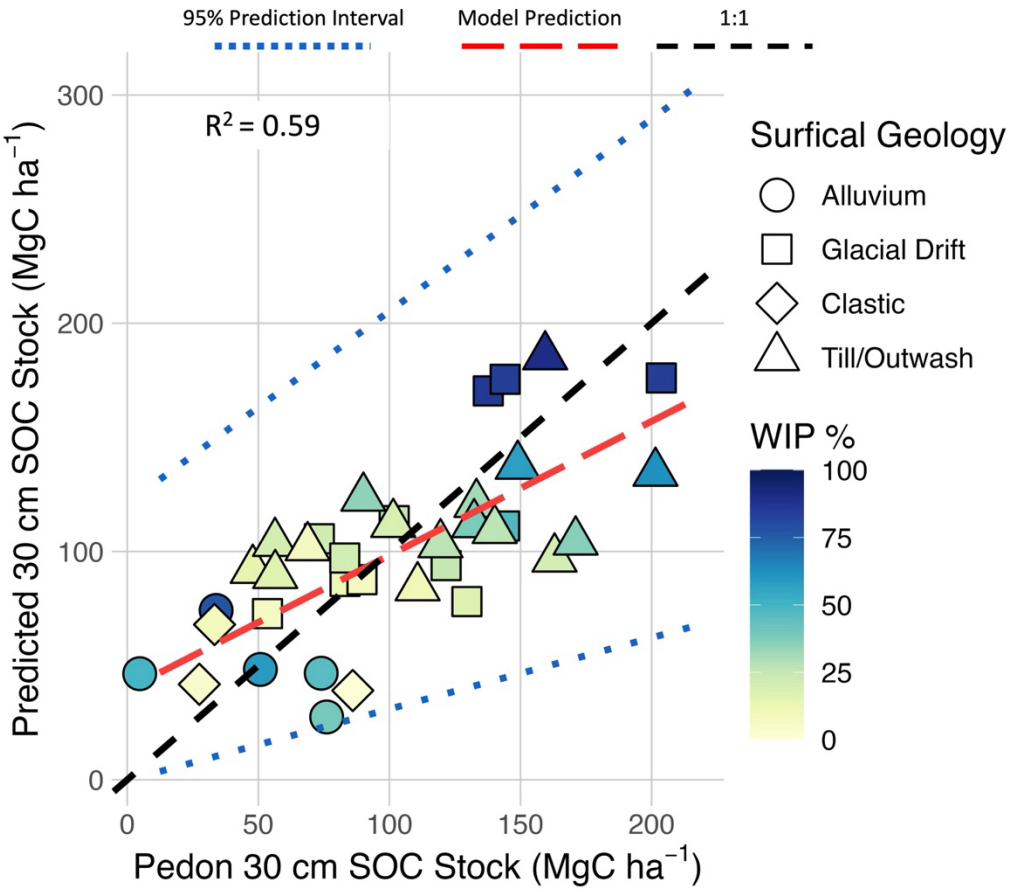

Supplementary Figure 1.7 Model predicted soil organic carbon (SOC) stock compared to field sampled pedon SOC stock with a gradient of probability from the Wetland Intrinsic Potential (WIP) tool for the 30 cm depth. Modeled SOC stocks were back transformed from square root values in the original linear mixed effects model with the fixed effect of WIP probability and random effect of surficial geology. Prediction intervals are based on bootstrapped 95% confidence intervals.

Supplementary Table 1.2 Combined WIP and NWCA-SSURGO wetland SOC metrics for 1 m and 30 cm depth SOC stocks across the HRW. The ± indicates the standard deviation and the values in parentheses indicate 95% confidence intervals of the bootstrapped model predictions for the WIP derived estimates and published standard deviations for the NWCA-SSURGO datasets in Uhran et al. (2021). Combined mean SOC stocks were calculated on a weighted area basis shown by the percentages. Forested wetlands were determined by masking maps of wetland SOC stocks canopy cover ≥ 50%

	Surface Area			30cm		1m	
Landscape Class	Combined Surface (ha)	WIP (% of Total) (ha)	NWCA-SSURGO Surface Area (% of Total) (ha)	Area Weighted Mean SOC Stock (MgC ha^{-1})	Sum Total SOC Stock (TgC)	Area Weighted Mean SOC Stock (MgC ha^{-1})	Sum Total SOC Stock (TgC)
Wetland	6949	5308 (76%)	1640 (24%)	114 ± 22.9	0.8 ± 0.1	253 ± 63.1	1.8 ± 0.2
Forested Wetland	5678	4236 (75%)	1442 (25%)	117 ± 23.3	0.7 ± 0.1	264 ± 65.3	1.5 ± 0.2

Supplementary Table 1.3 Wetland surface area size class distribution using individual wetland surface area quantiles. The Size Classes group shows metrics for each individual percentile size class. The Cumulative Sum group shows the increasing sum over each quantile approaching 100% of all wetlands. Soil organic carbon (SOC) stock and Area within the Size Classes group were calculated as the sum within the wetland surface area size class for all wetlands above 0.0064 ha. Mean SOC stock was calculated as the mean SOC stock within each wetland and across all wetlands within the quantile size class.

	Size Classes				Cumulative Sum		
Quantiles of Wetland Area (ha)	SOC Stock (Tg)	Mean SOC Stock (Mg ha^{-1})	Count	Area (ha)	SOC Stock (Tg)	Area (ha)	Count
0-5% (0.006 ha)	0.0101	254	6216	40	0.0101	39.8	6216
5-25% (0.006-0.008)	0.00878	252	4375	35	0.0189	74.5	10591
25-50% (0.008-0.011)	0.0142	254	5467	56	0.0331	130	16058
50-75% (0.011-0.026)	0.0348	254	7973	137	0.0678	267	24031
75-96.4% (0.026-0.40)	0.143	252	6808	560	0.211	827	30839
96.4-100% (0.40-401)	1.42	264	1142	5010	1.63	5838	31981

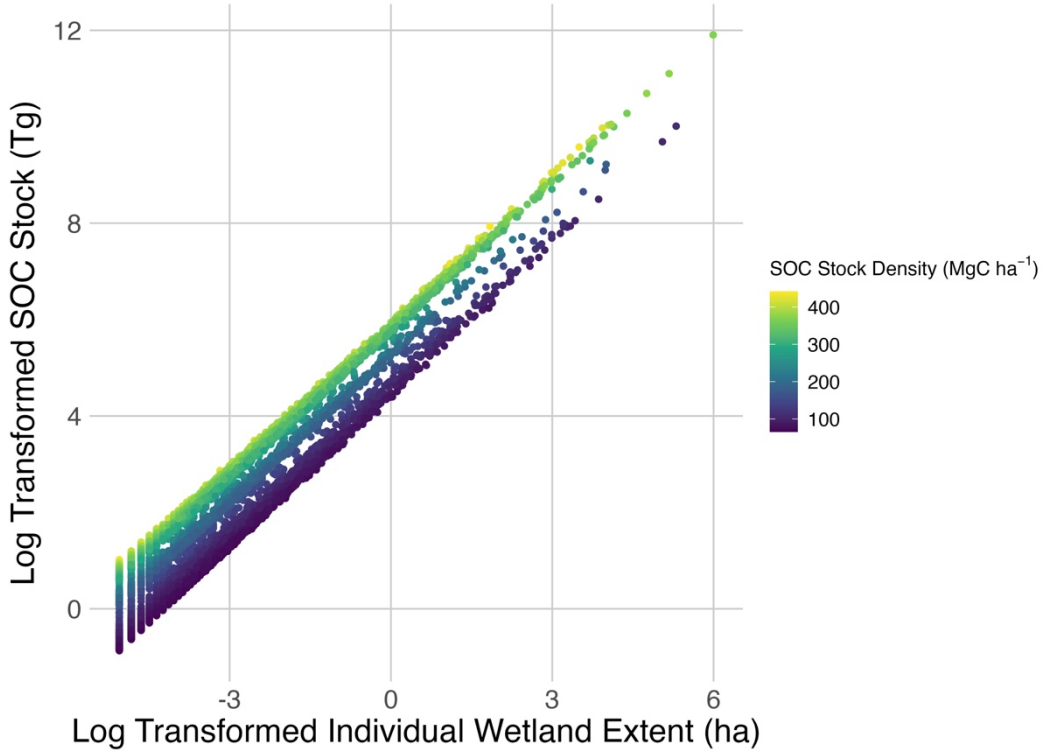

Supplemental Figure 1.8 Log transformed extent for individual wetlands in relation to log transform soil organic carbon (SOC) stock for individual wetlands. Points are colored by mean SOC stock density in each wetland.

Supplementary Table 1.4. Comparison of total soil organic carbon (SOC) stock for the entire Hoh River Watershed HRW between the Wetland Intrinsic Potential (WIP) SOC model and global map products. Global map products include the SoilGrids 2.0(Poggio et al., 2021) model and the United Nations Food and Agriculture Organization (UN FAO) Global Soil Organic Carbon (GSOC) 1.5 map (FAO, 2018). The ± indicates the standard deviation of the bootstrapped model predictions for the WIP derived estimates and published uncertainty ranges for SoilGrids and UN FAO GSOC. It should be noted that GSOC uncertainty maps contained incomplete data for the HRW, covering only 2996 ha. Therefore, mean SOC stock uncertainty was extrapolated to the full HRW area for a total GSOC SOC stock uncertainty.

Source	Surface Area	30cm Depth	
		Mean SOC Stock	Total SOC Stock
	(ha)	(MgC ha^{-1})	(TgC)
WIP	68,145	72.9 ± 12.5	5.0 ± 0.9
SoilGrids 2.0	68,145	115 ± 15.8	7.8 ± 1.1
UN FAO GSOC 1.5	68,145	56.9 ± 50.2	3.9 ± 3.4

Chapter 2: Advancing soil organic carbon mapping by incorporating inland freshwater wetland probability as a predictor

Author List

Anthony J Stewart[1]
Meghan Halabisky[1]
David V. D'Amore[2]
Diogo Spinola[3]
Chad Babcock[4]
L. Monika Moskal[1]
David Butman[1]

Affiliations

[1]School of Environmental and Forest Sciences, University of Washington, Seattle
[2]Pacific Northwest Research Station, U.S. Department of Agriculture Forest Service
[3]University of Northern British Columbia, Prince George, British Columbia
[4]Department of Forest Resources, University of Minnesota, St Paul

Abstract

Despite wetlands occupying only 6-8% of terrestrial land area while containing approximately 30% of global SOC, they remain underrepresented in digital soil mapping (DSM) efforts, resulting in incomplete characterization of landscape-scale carbon distribution. We assess how a probabilistic map of wetland presence—the Wetland Intrinsic Potential (WIP) tool—performs as a spatial predictor of SOC stock and concentration (SOC%) when combined with traditional DSM predictors. Using soil samples collected in four watershed study areas across the Pacific Northwest, we used both linear mixed models and quantile random forest models to predict SOC stock distribution and mineral soil SOC%. Results show that SOC stock models incorporated WIP as a significant predictor, ranked between depth and climate (particularly potential evapotranspiration to mean annual precipitation ratio) in the order of significance. For mineral soil SOC%, models did not include WIP and edaphic factors including depth, pH, and clay content were primary drivers. Our watershed-scale SOC mapping identified higher SOC stocks in wetlands compared to uplands, with mean wetland SOC stocks of 114-243 Mg C ha-1 compared to mean upland SOC stocks of 99.5-162 Mg C ha-1 across study watersheds. Comparison with existing models indicates our approach better captures fine-scale SOC spatial heterogeneity related to wetlands while maintaining similar estimates of total landscape SOC. This study demonstrates the importance of representing wetlands in SOC mapping and emphasizes how landscape-scale hydrology drives carbon accumulation patterns. Incorporating probabilistic wetland mapping in SOC prediction models provides critical information climate mitigation strategies targeting areas with high carbon storage potential.

Introduction

Soil organic carbon (SOC) is the largest terrestrial carbon pool and a key dynamic reservoir in the carbon cycle, with uncertain responses to climate change (Scharlemann et al., 2014; Varney et

al., 2022). The immense size of the SOC pool has raised concern for the potential positive feedback of carbon released back to the atmosphere (Bradford et al., 2016) but also has promoted policy makers and scientists to consider SOC for climate change mitigation as a nature-based or natural climate solution (Bossio et al., 2020; Derrien et al., 2023) To reduce uncertainty in both cases, maps and models of the SOC spatial distribution must be improved to capture the spatial heterogeneity across landscape to regional and global scales (Wiesmeier et al., 2019). This improvement faces two challenges: first, the key measurements of SOC, the concentration (SOC% of the bulk soil) and stock (mass per area, calculated from SOC%, bulk density and depth interval) can respond differently to the same biophysical drivers and need individual characterization (Don et al., 2007; Schrumpf et al., 2011); and second, there are significant gaps in mapping carbon rich ecosystems such as inland freshwater wetlands (Stewart et al., 2024). New research to improve SOC mapping and modeling needs an approach that comprehensively captures the full SOC landscape continuum of SOC (Doetterl et al., 2025)

Digital soil mapping (DSM) is a modeling approach used to capture the distribution of soil characteristics across spatial extents (Minasny et al., 2013; Minasny & McBratney, 2016). DSM uses geospatial predictors as proxies for soil formation and development, often applying the "SCORPAN" (McBratney et al., 2003) approach which adapts the original soil formation equation from Jenny (1941) to model a soil property as a function of other soil characteristics (S), climate (C), organisms (O), topography (R), parent material (P), time/age (A), and spatial location (N). DSM has been a robust approach for SOC modeling to produce spatially resolved estimates of both SOC% and SOC stock across various scales (Khaledian & Miller, 2020; Poggio et al., 2021; Chen et al., 2022; Vitharana et al., 2024). The SCORPAN modeling approaches can also be used to examine soil properties down the soil profile, using depth as a predictor and incorporating additional soil characteristics that are not mapped such as pH and particle size (von Fromm et al., 2024) Further,

many soil property relationships with depth can be exploited to produce 3D SOC stock estimates with a continuous depth predictor (Arrouays et al., 2020; Sothe et al., 2022) which facilitates SOC% and SOC stock modeling since both decline as depth increases at variable rates (Jobbágy & Jackson, 2000).

Although DSM approaches for SOC and products have greatly improved spatial-explicit maps of SOC, they have been more implicit for inland freshwater wetlands**,** where high SOC% and large SOC stocks occur. Inland freshwater wetlands (hereafter shortened to "wetlands") are an ecosystem characterized by soil saturation sufficient to develop hydric features, notably organic matter accumulation (Vepraskas & Craft, 2016). Thus, wetlands maintain disproportionately high SOC stocks per unit area compared to uplands, accounting for approximately 30% of the global SOC pool while occupying only 6-8% of the terrestrial surface area (Jackson et al., 2017; Poulter et al., 2021). Estimating wetland extent encompasses a widely diverse set of approaches ranging from: field surveys and aerial photo interpretation (Dahl, 2011); direct measurement of wetland features such as remote sensing detection of inundation (Poggio et al., 2021; Zhang et al., 2021); and DSM approaches which incorporate SCORPAN predictors (Minasny et al., 2023). Altogether, wetland extent maps have greatly improved across scales but are not tightly integrated into upscaling approaches for SOC. Wetlands are often mapped with discrete boundaries which may or may not reflect the continuous properties in the underlying soil such as the SOC% or SOC stock (Dodds et al., 2019; Halabisky et al., 2023). Additionally, many contemporary wetland maps are still challenged with identifying small and forested wetlands which can have high SOC stocks (Davidson et al., 2022) but require more localized and higher resolution DSM approaches ((Maxwell & Warner, 2019; Li et al., 2020; Halabisky et al., 2023). Consequently, despite the advances in wetland mapping and demonstrated disproportionately large SOC storage, hidden wetlands are often mis-classified as

uplands or another non-wetland type which distorts SOC spatial patterns (Sjögersten et al., 2014; Wickham et al., 2021).

A growing approach to improve wetland spatial representation, especially under forest vegetation, is to model a land surface as a continuous probability corresponding to wetland presence or water inundation using fine-resolution topography data (Maxwell et al., 2016; Delancey et al., 2019; Zhang et al., 2021; Halabisky et al., 2023). Previous research has demonstrated that small wetlands need more inclusion with higher resolution approaches (Siewert, 2018; Goldman et al., 2020) and the continuous probabilistic approach effectively captures SOC stock spatial patterns in forested wetlands (Stewart et al., 2024). This probabilistic mapping approach potentially enhances two aspects of DSM with respect to wetlands: 1) expressing an area as a gradient of potential hydrologic conditions across xeric, mesic, and hydric soil moisture regimes, the latter indicates wetland development and SOC accumulation (Lidberg et al., 2020; Ågren et al., 2021); and 2) after setting a threshold (commonly 50% probability Halabisky et al. (2023)), can facilitate identifying new wetlands and produce improved wetland maps (Maxwell et al., 2016; Delancey et al., 2019). These two notions indicate that a probabilistic wetland identification should be evaluated in mapping and non-mapping contexts to validate if the model output captures catena and hillslope soil hydrology dynamics, key drivers of SOC accumulation (Lawrence et al., 2021).

In this research, we assess how a probabilistic map of wetland presence performs as a spatial predictor of SOC stock and SOC% in combination with other SCORPAN predictors within four landscapes across different climatic regions. We chose to model SOC stock using a DSM approach with soil depth as a predictor to evaluate predictor strength with depth and generate estimates of SOC stock at different depth intervals for a study area. In addition, we also chose to model SOC% in the mineral soil separately in a non-DSM model since additional soil parameters that were not

spatially mapped, such as soil particle size, were used as predictors but measured in the mineral soil and not the organic soil. This research addresses three questions: 1)How well do models predict SOC distribution and concentration when combining wetland probability and SCORPAN predictors for landscapes across different climates?; 2) Which predictors from SCORPAN and wetland probability act as drivers of SOC stock and concentration?; and 3) Are the estimates of landscape-level SOC stocks derived from these models comparable to larger scale SOC maps? We then address three hypotheses: 1) Models that incorporate wetland probability along with SCORPAN predictors will accurately predict SOC stocks and concentrations across landscapes in different climates; 2) We expect depth to strongly influence SOC stock and SOC% while climatic factors related to water availability and high wetland probability to be stronger predictors than temperature, vegetation productivity, or landform for overall SOC stocks with high SOC concentrations in wetlands; and 3) We expect our wetland-inclusive model to predict similar total SOC stocks compared to existing models, but with a greater proportion of SOC attributed to wetland areas delineated by the wetland probability.

Methods

Study Areas

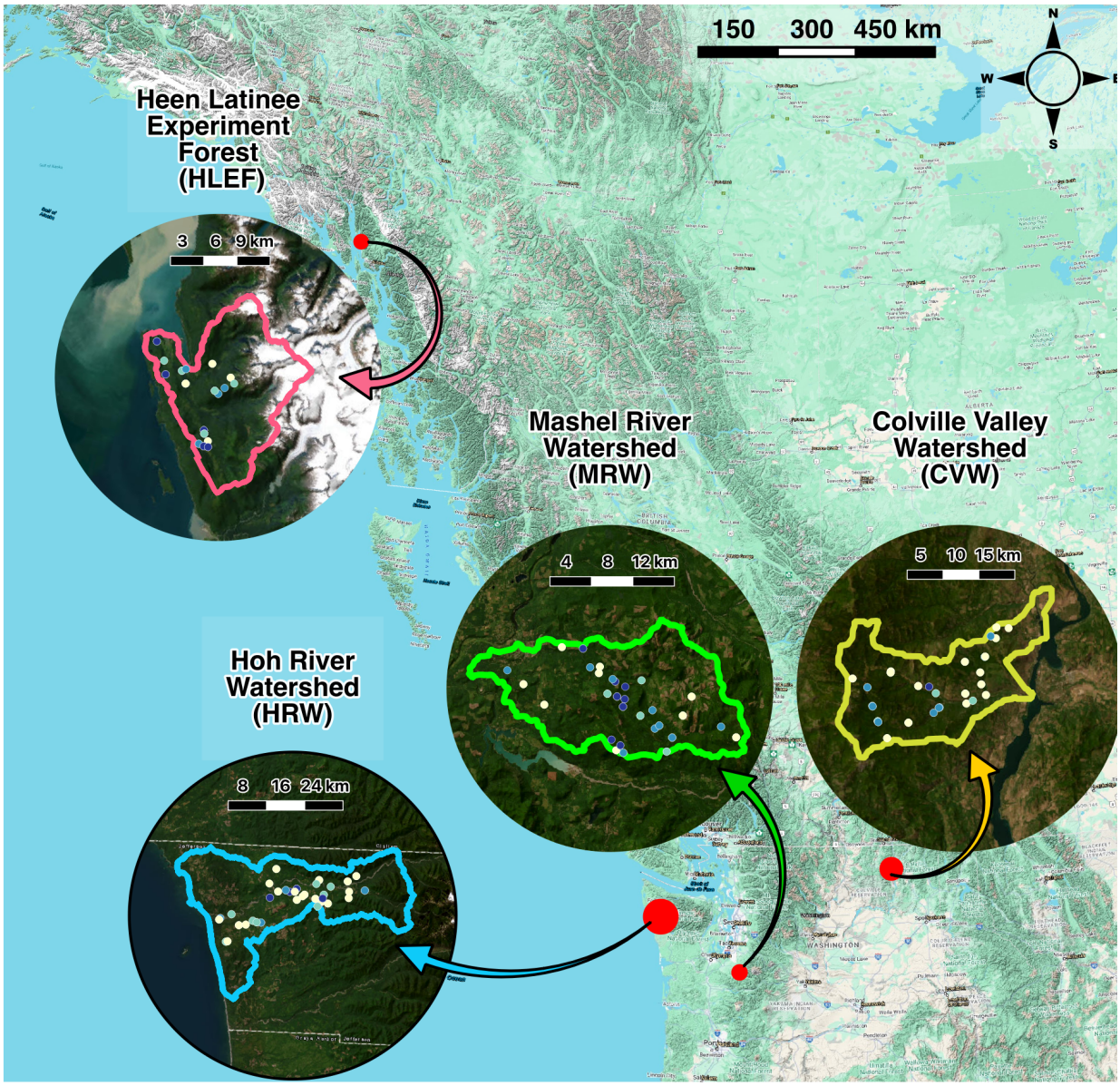

Figure 2.1: Map of study watersheds in the Pacific Northwest of North America. The Heen Latinee Experimental Forest (HLEF) is located in Southeast Alaska. The Hoh River Watershed (HRW), Mashel River Watershed (MRW), and Colville Valley Watershed (CVW) are located in Washington State. Basemap imagery provided by OpenStreetMap. Map lines delineate study areas and do not necessarily depict accepted national boundaries

We conducted field surveys, sample collection, and geospatial modeling across four study watersheds in the Pacific Northwest that stratify a climatic gradient (Figure 2.1). The Heen Latinee Experimental Forest (HLEF) is in Southeast Alaska near Juneau, AK with a mean annual

precipitation (MAP) of approximately 2284 mm and a mean annual temperature (MAT) of 4.3 °C. The Hoh River Watershed (HRW) is located on the west coast of the Olympic Peninsula where MAP is approximately 3061 mm and MAT is 10.0 °C. The Mashel River Watershed (MRW) is located on the western side of the Cascade Mountain Range near Tahoma (Mt. Rainier) and has a MAT of 8.4 °C and a MAP of approximately 1716 mm. The Colville Watershed (CVW) is located on the northeastern portion of the state and has a MAT of 6.5 °C and a MAP of 652 mm. The landscapes of the four study areas contain a range of landforms including mountains, hillslopes, alluvial floodplains, and glacial deposits. Geologic ages range from prominent recent Quaternary material from retreating glaciers in the HLEF and HRW, Oligocene-Eocene volcanic and sedimentary deposits in the MRW to Pre-Tertiary metamorphic rocks in the CRW. Vegetation is predominantly forested with the HLEF containing a mix of Western Hemlock (*Tsuga heterophylla*), and Sitka Spruce (*Picea sitchensis*) with small amounts of Yellow Cedar (*Cupressus nootkatensis*). The HRW forests contain Sitka Spruce (*Picea sitchensis*), Western Hemlock (*Tsuga heterophylla*), Western Red Cedar (*Thuja plicata*), and Bigleaf Maple (*Acer macrophyllum*). The MRW forests contain predominantly Douglas fir (*Pseudotsuga menziesii*), Western Hemlock (*Tsuga heterophylla*), and Red Alder (*Alnus rubra*). The CVW forests contain a mix of Ponderosa Pine (*Pinus ponderosa*), Douglas fir (*Pseudotsuga menziesii*), Lodgepole pine (*Pinus contorta*), Western Larch (*Larix occidentalis*), Western Hemlock (*Tsuga heterophylla*), and Western Red Cedar (*Thuja plicata*).

Wetland Identification with the Wetland Intrinsic Potential (WIP) Tool

We implemented the Wetland Intrinsic Potential (WIP) tool for each study watershed to model the gridded land surface in each study area as a continuous probability of wetland presence, with each grid pixel containing a value from 0-100%. The WIP tool is thoroughly described in Halabisky et al. (2023) and implemented for wetland identification in the HRW. Here, the WIP tool relies on multi-scale terrain metrics derived from DTMs as predictors of wetland presence on the

landscape which has been shown to improve wetland classification (Maxwell et al., 2016; Maxwell & Warner, 2019). These terrain metrics along with additional remote sensing metric representing wetland identifiers and formation factors were used in a Random Forest model (Breiman, 2001) with training data derived from the National Wetland Inventory and field-visit observations. The Random Forest model prediction then assigns grid pixels a probability value (0-1.0, revised to 0-100% for interpretability) based on a "wetland" or "upland" designation. We follow Halabisky et al. (2023) and others in using a probability threshold of ≥ 50% to define the cutoff for defining a wetland (≥50%) or upland (<50%). We utilized both the data and framework of the HRW WIP implementation to derive similar WIP models for the HLEF, MRW, and CRW study watersheds. More detailed methods describing the WIP implementation, including the variable importance for WIP (Supplementary Figure 2.1.) is in the Wetland Intrinsic Potential tool section of the Supplementary Materials.

Field sampling and laboratory analysis

Soil samples were collected over the course of two field summer field seasons in 2021-2022. Sample locations were pre-selected using a stratified random selection of points across the WIP probability for each study watershed to evaluate the full spread of the wetland-upland gradient. The WIP probability from 0-100% was stratified into 30 equal size bins and sample points were generated for those bins at random locations within each study watershed. Sample locations were then visited in the field as close to the sample point coordinates as possible and then updated with new GPS/GNSS location data. Overall, we collected samples from 114 pedon locations with 30 pedons each in the MRW and CVW, 36 pedons in the HRW, and 18 pedons in the HLEF. The HLEF also contained 3 legacy soil pedons sampled in 2019. Soil pedons were dug to at least 1 m depth unless there was a restrictive layer. Soil pedons were characterized according to NRCS field sampling guides (Soil Survey Staff, 2024) and soil samples for bulk density and bulk chemistry were

extracted by horizon and at the horizon center. Laboratory analysis started with drying samples to a constant weight at 70°C and sieving to 2 mm to remove coarse fragments. The mass of the < 2 mm fraction was then used to calculate bulk density and analyze carbon content, particle size distribution, and pH. Carbon content was measured using a Shimadzu Elemental Analyzer. Particle size distribution was measured using the hydrometer method. Soil pH was measured using 1:1 soil to water ratio, although a small number of soils required 1:1.5 or 1:2 soil to water ratios.

Geospatial data

Geospatial datasets were gathered to determine predictors for SOC stocks across the three study areas. We chose geospatial factors related to vegetation, climate, lithology and geology, and topography. For vegetation spectral indices, we used Google Earth Engine (Gorelick et al., 2017) to obtain satellite imagery for index calculation from the 5 year median of Sentinel-2 reflectance. For each study area, we calculated the enhanced vegetation index (EVI) (Huete et al., 2002) and normalized difference vegetation index (NDVI). Other metrics such as the soil adjusted vegetation index (SAVI) were also investigated but deemed too comparable to either NDVI or EVI to be included in the model. We also used a lidar derived canopy height model from the Washington Department of Natural Resources (WA DNR) which was measured as the elevation difference between the lidar DTM and the lidar DSM.

For climate predictors, we downloaded 800 m^2 gridded 30 year climate normals for mean annual precipitation (MAP) and mean annual temperature (MAT) from the Northwest Alliance for Computation Science and Engineering (PRISM Climate Group) for the three Washington study watersheds. We used ~1 km gridded historical climate data from WorldClim 2.1 (Fick & Hijmans, 2017) to extract MAP and MAT for the HLEF. In addition, we also downloaded Potential Evapotranspiration (PET) from the Version 3 of the Global Aridity Index and Potential

Evapotranspiration Database for all four study areas (Zomer et al., 2022). PET was divided by MAP to create an Aridity Index estimate of water availability. To capture finer scale effects of solar radiation and heat, we calculated a heat load index (HLI) from the lidar DTM (McCune & Keon, 2002).

Geology and lithology maps were downloaded from the Washington Department of Natural Resources at a 1:100,000 scale and from the USGS (Wilson et al., 2015). These maps contained a wide range of mapped geologic and lithologic categories, often combining with geomorphologic processes. We chose to consolidate them into six broad categories which would represent soil Parent Material (PM) and time since soil inception: Glacial Till and Drift, Glacial Outwash, Igneous, Metamorphic, Sedimentary, and Unconsolidated sediments. Both Alaska and Washington State are glacially influenced and we therefore modified glacial lithological categories into two categories corresponding to stratified (Glacial Outwash) and unstratified (Glacial Till and Drift). Glacial drift is a broad term referring to all types of glacial deposits and is difficult to assess stratification without more detailed examination of geomorphologic processes beyond the use of the available maps. Therefore, we chose to group Glacial Drift with Glacial Till as a broad "unstratified" category. More details regarding the reclassification of lithological categories are provided in the Parent Material section of the Supplementary Materials and Supplementary Table 2.1.

Modeling approach

Data structure

Our approach consisted of separating our data into two datasets: one for SOC stocks by equal depth intervals and another for SOC% using the original depth measurements. For the SOC stock dataset, we utilized a DSM approach to transform our SOC stock data into equal intervals of 25 cm using a mass preserving spline depth function (Chen et al., 2022; O'Brien, 2022). This approach is common in DSM and has been referred to as 3-D because it facilitates the prediction of

soil properties at any location within the study area at the designated depth intervals (Bishop et al., 1999; Malone et al., 2009; Helfenstein et al., 2024). The decision to use 25 cm intervals instead of the standardized intervals was to control the variability of SOC stock with depth interval thickness. We also chose this interval length to maintain a similar number of observations without exceeding the original dataset (Original: 573, Spline 499). We used the mass preserving spline function to calculate values of SOC%, Bulk Density, and Rock% down profile using a lambda = 0.7. These numbers were then used to calculate SOC stocks for each 25 cm depth interval by Equation 1:

$$Spline\ SOC_{g\ cm^{-2}} = SplineSOC_{\%} * SplineBD_{g\ cm^{-3}} * 25cm * (1 - SplineRock_{\%}) \qquad (2.1)$$

For the SOC% dataset, we removed observations that were heavily organic based on the organic soil definition of > 12% SOC (Soil Survey Staff, 2022). However, we also chose a more conservative threshold of >10% SOC to remove potential organic matter contamination in further analysis. The analyses for these samples consisted of measurements of Sand, Silt, Clay, and pH with distributions shown in Supplementary Figure 2.2. Measurements of Sand, Silt, Clay, and pH were not mapped and therefore, we did not use this dataset for digital soil mapping and therefore kept the original depth intervals from the field sampling. This dataset contained 426 observations compared to the 499 in the spline dataset and 573 in the original dataset.

Model Building and Selection

Linear Mixed Modeling

We chose to use two model types in our research to model SOC stock and SOC%: a linear mixed effects model (LMM) and a quantile random forest (RFM), creating four models in total. We chose to use a linear mixed effect modelling approach to test specific hypotheses about important predictors and examine predictor coefficients. To compare between models, both datasets for SOC

stock and SOC% were split into training and testing datasets using an 85:15 ratio. The same training and testing datasets would be used for all models to compare performance and accuracy.

In the LMMs, the sample location was chosen as a random effect and sample depth was specified as a random slope within the sample location. We chose to build several models that represented our a priori hypotheses with varying interactions between the predictors as well as eliminating predictors that were not significant down to a null model with no predictors. The final model was chosen using Akaike's information criterion (AIC) and parsimony then evaluated for violations of homogeneity of variance and linearity. Although some observations deviated slightly from the homoscedasticity assumption (Supplementary Figure 2.3 and 2.4), we deemed the model assumptions sufficiently met and therefore used to evaluate drivers and predict SOC stock and SOC%.

All data used to build models of SOC stock and SOC% were centered and scaled if they were continuous predictors. Correlated variables were removed if they had an $r > 0.6$. However, at this scale MAP and PET:MAP are highly correlated and thus we used separate models to assess the strength between the two predictors in our mixed model selection. The initial model selection process using maximum likelihood showed that models using PET:MAP instead of MAP were better fits to the data according to AIC.

For SOC stock, LMM selection using AIC comparisons removed models containing interactions among fixed effects, resulting in SOC stock modeled as a function of PET:MAP, WIP, Canopy Height (CHM), Heat Load Index (HLI), Parent Material, and Depth as fixed effects Equation 2 :

$$SOC\ stock_{ij} = \beta_0 + \beta_{ij} MAT + \beta_{ij} PET{:}MAP + \beta_{ij} WIP + \beta_{ij} CHM + \beta_{ij} ParentMaterial + \beta_{ij} Depth + b_{0_j} + b_{ij} Depth + \epsilon_{ij} \quad (2.2)$$

For SOC%, the LMM selection process was similar to SOC stock where fixed effects in separate models were removed depending on the AIC values. The best LMM at this stage contained depth, pH, Clay, and PET:MAP with interactions between the variables the latter three predictors. After this LMM was found, we also used the *dredge* function from the *MuMIn* R package to further identify if incorporated interactions between Clay% or Silt+Clay% and MAT outperformed the current LMM structure determined from earlier (Bartoń, 2023). The final LMM was chosen with the lowest AIC and/or fewest LMM parameters for parsimony with PET:MAP, pH, Clay% and Depth as fixed effects Equation 3 :

$$SOC\,\%_{ij} = \beta_0 + \beta_{ij} PET{:}\,MAP + \beta_{ij} Clay\% + \beta_{ij} pH + \beta_{ij} pH{:}\,(PET{:}\,MAP) + \beta_{ij} Depth + b_{0_j} + b_{ij} Depth + \epsilon_{ij} \quad (2.3)$$

All random effects in the LMM followed:

$$b_{0j} \sim N\left(0, \sigma^2_{b_0}\right) \quad (2.4)$$

$$b_{ij} Depth \sim N\left(0, \sigma^2_{b_{Depth}}\right) \quad (2.5)$$

$$\epsilon_{ij} \sim N(0, \sigma^2) \quad (2.6)$$

Where b_{0j} is the random intercept for the j-th group of each sample location and $b_{ij} Depth$ is the random slope of depth within the sample location. The final model was evaluated on the test dataset by measuring the R^2 and root mean square error (RMSE). Predictor variable importance was estimated using the 95% confidence intervals on the scaled coefficient estimates with important predictors having a confidence interval that did not cross 0.

We also examined SOC stock data and model residuals for spatial autocorrelation by examining semivariograms and the spatial autocorrelation within each study watershed expecting there to be minimal autocorrelation. There was some spatial pattern in the MRW but none in the

other three watersheds shown by the semivariograms within and across all study watersheds (Supplementary Figure 2.5). We concluded that our proposed model structure did not need to include a spatial autocorrelation random effect although this has been shown to be beneficial in mapping SOC (McKenzie & Ryan, 1999).

Random Forest Modeling

The Quantile Random Forest (RFM) was used to accommodate for potential non-linear relationships in our data as well as incorporate a more flexible approach to predictor selection. We used the *mlr3* package in *R* to implement the RFM from the *ranger* package (Wright & Ziegler, 2017; Lang et al., 2019). We used recursive feature elimination to narrow the number of predictors used in the model. Then, we tuned *num.trees*, *mtry*, and *max.depth* using repeated 10-fold cross validation on the training dataset. Out of bag (OOB) R^2 and RMSE were calculated from the model implemented on the training dataset. We R^2 and RMSE for the RFM on the test dataset similar to the LMM. Predictor variable importance was determined using SHAP (SHapley Additive exPlanations) values using a 200 observation subset of the training dataset as the rows to be explained and the full training dataset as the background (Lundberg et al., 2020) SHAP values were visualized using the *kernelshap* package (Mayer & Watson, 2024)We also investigated interactions between predictors in the RFM using the interpretable machine learning *iml* package and the *Interaction* function (Molnar et al., 2018).

SOC stock prediction and uncertainty

We chose to generate mapped predictions of SOC stock across all four study watersheds using the model with the best fit to the test dataset (R^2 and RMSE). The RFM was selected with these criteria and was used to generate SOC predictions for each depth interval (25 cm) and then combined to calculate a 1 m SOC stock. The RFM was built as a quantile random forest allowing the

prediction of the 97.5% and 2.5% quantiles of SOC stock. We used these quantiles as the 95% prediction interval and to show uncertainty ranges for our prediction.

We also used additional geospatial masks to remove surface water areas and urban zones. The Modified Normalized Difference Water Index (MNDWI) was used to remove surface water with a threshold of 0.3 (Xu, 2006). The National Land Cover Database (NLCD) was used to mask urban areas such as roads (Dewitz, 2021). Geospatial masks using the WIP threshold of 0.50 or 50% were used to estimate wetland and upland 1 m SOC stocks and were compared with 1 m SOC stock data from the National Wetland Condition Assessment (NWCA) which was upscaled using the National Land Cover Database (NLCD) in Uhran et al. (2021). We show these estimates using the term $NWCA_{NLCD}$.

We also extracted estimates of SOC stock from open data sources that have been used to model the spatial distribution of SOC at regional to global scales. For all study areas, we used an estimated mean 1 m SOC stock from an ensemble combination of global and regional models compiled and calculated by Jones & D'Amore (2024) for Alaska, British Columbia, Washington, Oregon, California, and Hawai'i. Additionally, a published map of 1 m SOC stocks was created specifically for the Pacific Coastal Temperate Rainforest by McNicol et al. (2019) which encompasses the HLEF.

Results

Wetland identification with the Wetland Intrinsic Potential (WIP) tool

Table 2.1: Wetland extent estimates from the Wetland Intrinsic Potential (WIP) Tool and the National Wetland Inventory (NWI). NWI estimates contain buffered streamlines from the National Hydrography Dataset. WIP wetland extents have removed surface water and NWI estimates have removed estuarine wetlands. A large polygon which was part of the Hoh River in the HRW was removed due to being surface water. Percent differences are calculated as the (WIP-NWI)/NWI.

Study Area	WIP Wetland Area (ha)	NWI Wetland Area (ha)	% Change (WIP-NWI)/NWI
HLEF	2,188	858	155.0
HRW	5,798	3,863	50.1
MRW	2,184	895	144.0
CVW	862	409	111.0

Wetland mapping conducted with the Wetland Intrinsic Potential (WIP) Tool (Halabisky et al., 2023) and setting the wetland classification threshold at ≥ 50% identified considerably more wetland area than the National Wetland Inventory (NWI) (Table 2.1 and Figure 2.2). Overall accuracy for the WIP models including both wetland and non-wetland identification was 87% in the HLEF, 92% in the HRW, 90% in the MRW, and 93% in the CVW. Wetland omission error was 15%, 14%, 12%, and 2% while wetland commission error was 10%, 11%, 6%, and 20% for the HLEF, HRW, MRW, and CVW, respectively. The HLEF had the largest relative wetland extent proportionally to the total watershed extent (20%) while the CVW had the lowest total and proportional wetland extent (2.7%). The largest percentage increase of wetland area identified occurred in the HLEF (155%) and the lowest occurred in the HRW (50.1%). The most important variables for these models included mostly terrain metrics such as gradient and deviation from mean elevation at various scales (See Methods for explanations on multiscale terrain metrics; Supplementary Figure 2.1).

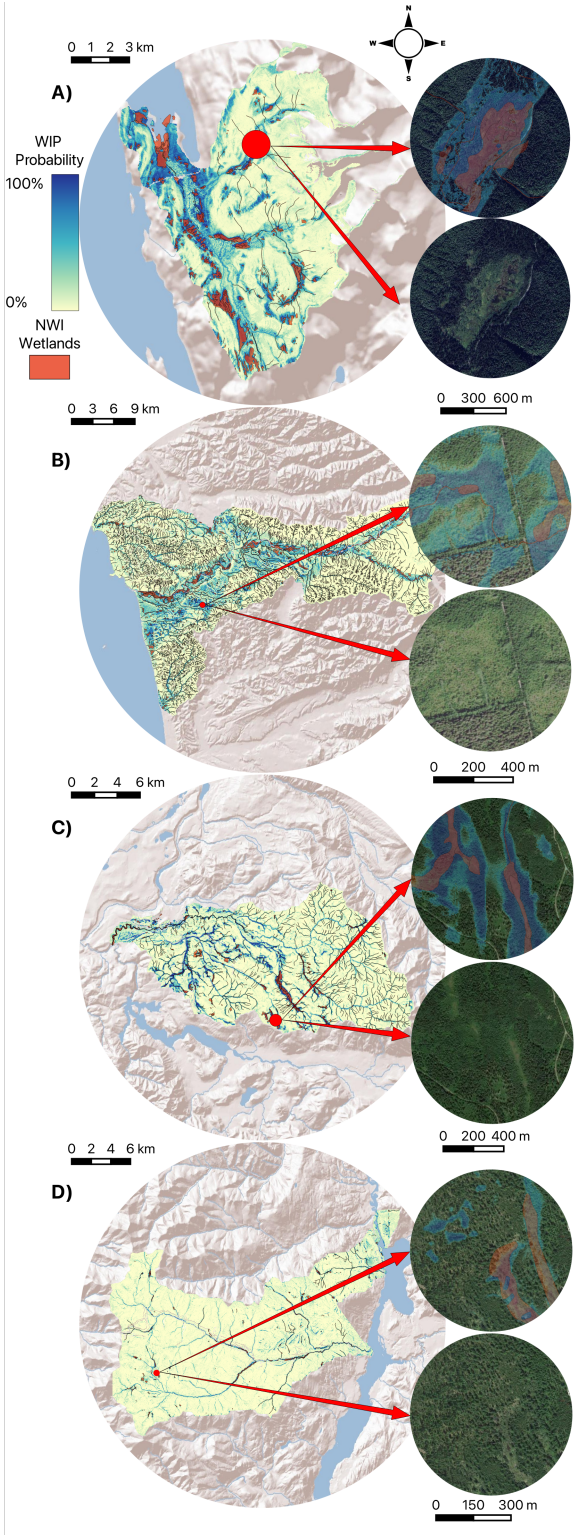

Figure 2.2. Wetland identification maps derived from the Wetland Intrinsic Potential (WIP) Tool (Halabisky et al., 2023). Insets show zoomed in sections with the WIP shading removed for uplands (WIP probability < 50%). Wetlands mapped by the National Wetland Inventory (NWI) are shown in orange polygons. Satellite imagery is provided by Google Satellite.

Variation across study areas along climatic gradient

Overall, SOC stocks were larger at shallow depths and smaller at deeper depths across the four study areas Table 2.2. We observed low SOC stocks in the CVW and high SOC stocks in the HLEF and HRW. The largest SOC stocks were mostly in the HLEF with proportionally more deep soil observation sampled in the HLEF (125-150 cm depth interval). Mineral SOC% was more evenly distributed across wetlands and uplands after applying 10% carbon concentration threshold to remove organic soil horizons from the original dataset (See Methods for mineral SOC% threshold explanation; Table 2.3). Overall mineral SOC% was highest in the HRW upland soils and was nearly twice as high compared to the HRW wetland soils. The next highest mineral SOC% were found more evenly distributed between wetlands and uplands in the MRW, HLEF, and CVW, respectively.

Table 2.2: SOC stock mean and variation across depth intervals within each watershed study area. Depth represents the bottom of the depth interval.

Study Area	Depth	Mean SOC Stock (g cm^{-2})	Std. Error SOC Stock (g cm^{-2})	n
All	25	0.90	0.04	114
	50	0.50	0.05	114
	75	0.33	0.04	105
	100	0.27	0.06	87
	125	0.22	0.04	56
	150	0.25	0.07	23
HLEF	25	1.24	0.12	18
	50	0.78	0.20	18
	75	0.57	0.17	15
	100	0.76	0.36	12
	125	0.46	0.17	10
	150	0.43	0.18	8
HRW	25	0.86	0.07	36
	50	0.59	0.08	36
	75	0.40	0.07	33
	100	0.26	0.06	29
	125	0.22	0.08	15
	150	0.12	0.00	2
MRW	25	0.96	0.08	30
	50	0.50	0.07	30
	75	0.31	0.07	28
	100	0.24	0.05	20
	125	0.21	0.05	14
	150	0.21	0.07	7
CVW	25	0.69	0.08	30
	50	0.23	0.05	30
	75	0.15	0.07	29
	100	0.07	0.01	26
	125	0.08	0.01	17
	150	0.10	0.01	6

Table 2.3: SOC stock mean and variation across depth intervals within each watershed study area

Study Area	Landscape Class	Mean SOC%	Std. Error SOC%	n
HLEF	Upland	2.89	0.40	34
	Wetland	2.46	0.39	25
HRW	Upland	4.25	0.31	89
	Wetland	2.75	0.56	25
MRW	Upland	3.38	0.31	52
	Wetland	3.31	0.38	54
CVW	Upland	1.39	0.17	94
	Wetland	1.48	0.27	53

Performance of models for SOC stock and mineral SOC%

The linear mixed model (LMM) for predicting SOC stocks accounted for 48% of the variability in the training dataset with a $R^2_{marginal}$ of 0.48 representing the fixed effects and $R^2_{conditional}$ of 0.91 including the random effects of sample location with depth Table 2.4. However, in the test dataset, the LMM accounted for a much lower proportion of the variation with an $R^2 = 0.28$ and had higher variability with an RMSE = 0.41 g cm^{-2} Figure 2.3. Separating the uplands and wetlands based on the ≥ 50% WIP threshold in the test dataset revealed the LMM had better prediction for the upland SOC stocks ($R^2 = 0.39$, RMSE = 0.30 g cm^{-2}) compared to the wetlands ($R^2 = 0.21$, RMSE = 0.51 g cm^{-2}). In contrast to the LMM, the quantile random forest model (RFM) had a lower $R^2 = 0.43$ and comparable RMSE = 0.41 g cm^{-2} when using the out of bag (OOB) data from the training dataset. The RFM outperformed the LMM on the test dataset with an $R^2 = 0.50$ and RMSE = 0.35 g cm^{-2}. The RFM also predicted the uplands test data ($R^2 = 0.54$, RMSE = 0.26 g cm^{-2}) better compared to the wetland test data ($R^2 = 0.45$, RMSE = 0.45 g cm^{-2}), with both predictions' better fits than the LMM. Both models can be characterized as underestimating high SOC stocks. Figure 2.3 A. & B. show the higher SOC stocks were largely in more wet and wetland soils which is consistent with the model performance in the wetland portion of the test dataset.

Table 2.4: Measurements of Linear Mixed Model (LMM) and Quantile Random Forest Model (RFM) fit on both the training and test datasets for SOC stock (g cm^{-2}) and mineral SOC%. the LMM fit to the training dataset is shown by the Marginal and Conditional R^2. The RFM fit to training dataset is shown by the out-of-bag R^2 and RMSE. The same test dataset was used for both models and compared R^2 and RMSE.

		LMM				RFM			
Model Prediction	Landscape Class	Marginal R^2	Conditional R^2	Test R^2	Test RMSE g cm^{-2}	OOB R^2	OOB RMSE g cm^{-2}	Test R^2	Test RMSE g cm^{-2}
SOC stock g cm^{-2}	Full	0.49	0.91	0.18	0.44	0.45	0.40	0.50	0.35
	Wetland	---	---	0.10	0.54	---	---	0.46	0.42
	Upland	---	---	0.25	0.34	---	---	0.52	0.27
SOC %	Full	0.59	0.83	0.56	1.36	0.50	1.86	0.64	1.23
	Wetland	---	---	0.03	2.05	---	---	0.60	1.32
	Upland	---	---	0.65	1.21	---	---	0.65	1.21

The LMM for predicting mineral SOC% showed a more robust fit to the training data than the LMM for SOC stocks with a $R^2_{marginal} = 0.59$ and $R^2_{conditional} = 0.83$ Table 2.4. The LMM fit to the test dataset showed better performance than the LMM for SOC stocks with a $R^2 = 0.56$ and RMSE = 1.36% (Figure 2.3). However, the fit to the wetland data in the test dataset was significantly poor with a negative $R^2 = 0.03$ and RMSE = 2.05%. The LMM was able to account for more variability in the uplands data with an $R^2 = 0.65$ and RMSE = 1.21%. The RFM for predicting mineral SOC% performed slightly lower compared to the LMM on the training dataset with a OOB $R^2 = 0.51$ and RMSE = 1.87 %. However, the RFM accounted for more variability across the entire test dataset compared to the LMM with an $R^2 = 0.64$ and RMSE = 1.24% . Further, the RFM appeared to capture the variability in the wetland subset of the test dataset in stark contrast to the LMM, with a $R^2 = 0.61$ and RMSE = 1.30%. The RFM also consistently accounted for variability in the upland subset of the test dataset ($R^2 = 0.64$, RMSE = 1.23%). Both models appeared able to constrain high mineral SOC% values in the test dataset which appeared to be more dispersed across wet and wetland soils (Figure 2.3).

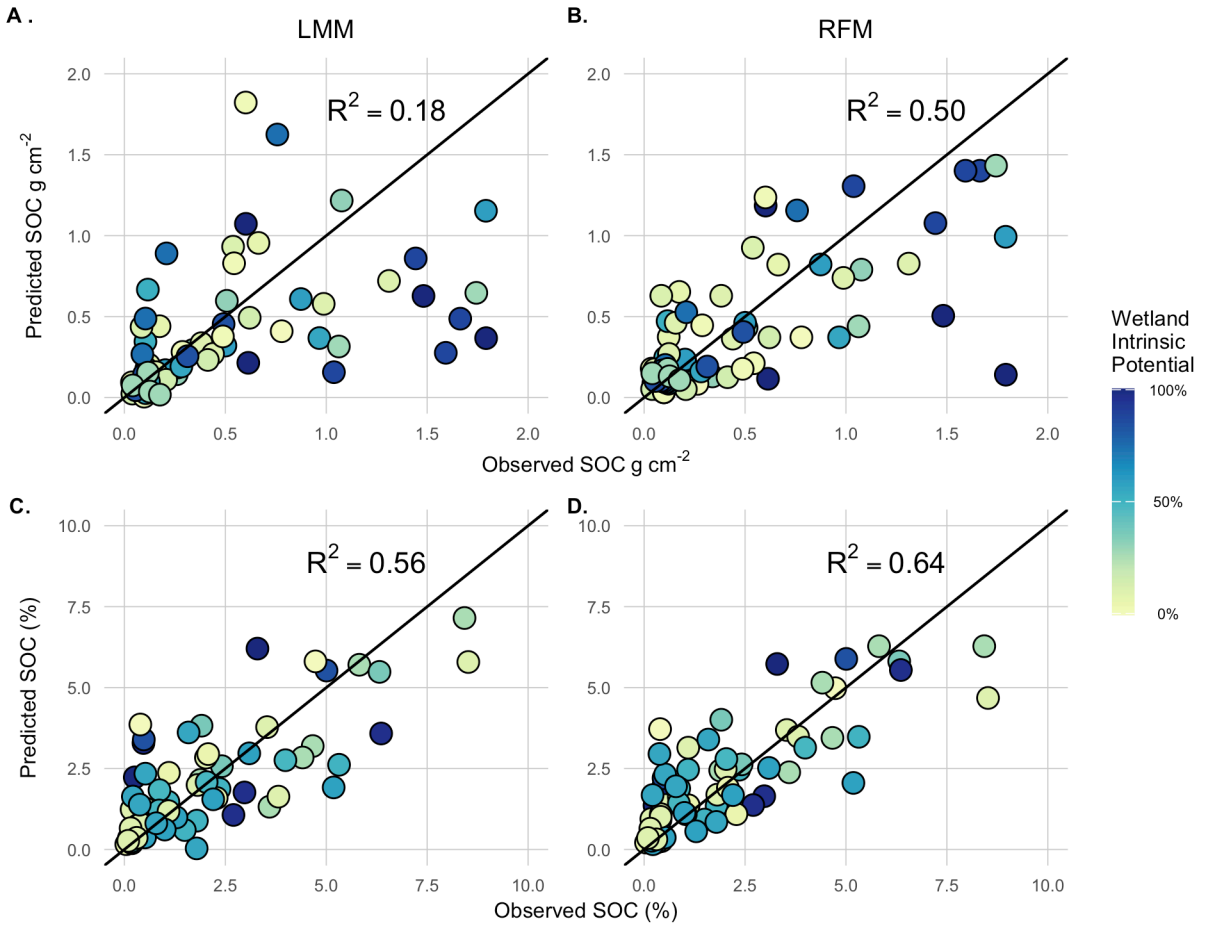

Figure 2.3: Predictions from the LMM and RFM models compared to observations in the test dataset colored by the wetland intrinsic potential probability shown as a 0-100% gradient from the four study watersheds. **A.)** Linear Mixed Model (LMM) SOC stock g cm^{-2} prediction vs. observations; **B.)** Quantile Random Forest Model (RFM) SOC stock g cm^{-2} prediction vs. observations; **C.)** LMM mineral SOC% prediction vs. observations; and D.) RFM mineral SOC% prediction vs. observations. Data in the LMM plots were back transformed from a $\log_{10}$ transformation.

Modeled drivers of SOC stock and mineral SOC%

Important predictors in the LMM and RFM predicting both SOC stock consistently included Depth (Figure 2.4 A.). Depth was the strongest predictor in the LMM with the largest absolute coefficient value and was negatively associated with SOC stock (scaled coefficient estimate = -0.43 95% CI: -0.49 - -0.38). The LMM for SOC stock also included an interaction between Depth and WIP (Figure 2.5 A), but this effect was not significant (scaled coefficient estimate = 0.05 95% CI: -0.01 - 0.11). Additionally, the LMM identified the PET:MAP climatic variable (scaled coefficient estimate = -0.21 95% CI: -0.28 - -0.14), Landforms, and Parent Material categories as the

next most important predictors. Landforms in the LMM which had significant negative associations with SOC stock were Flat (scaled coefficient estimate = -0.52 95% CI: -0.89 - -0.14) and Spur (scaled coefficient estimate = -0.33 95% CI: -0.64 - -0.03). The Parent Material categories of Sedimentary (scaled coefficient estimate = -0.48 95% CI: -0.71 - -0.25) and Unconsolidated (scaled coefficient estimate = -0.23 95% CI: -0.41 - -0.05) both had significant negative associations with SOC stock. The Wetland Intrinsic Potential (WIP), representing the upland-to-wetland gradient was a significant positive predictor in the model with a positive association (scaled coefficient estimate = 0.09 95% CI: 0 - 0.18) as well as Canopy Height (scaled coefficient estimate = 0.06 95% CI: 0 - 0.12).

In the RFM for SOC stocks, SHAP (SHapley Additive exPlanations) values were highest for Depth (Absolute Sum SHAP: 0.23) then followed by several variables within proximity to each other, indicating comparable variable importance after Depth (Figure 2.4). These included WIP with the second highest SHAP value (Absolute Sum SHAP: 0.07), PET:MAP as the third highest SHAP value (Absolute Sum SHAP: 0.05), and MAP as the fourth highest (Absolute Sum SHAP: 0.05). Predictors after MAP in terms of SHAP value were MAT, Elevation, Parent Material, and Canopy Height. According to the interaction strength measured by Friedman's H-statistic, WIP in the RFM for SOC stock showed high interaction values ($H_{statistic} \geq 0.2$) with PET:MAP, Landform, and the Enhanced Vegetation Index (EVI). PET:MAP in turn had a high interaction with WIP but also with the other climate variables, MAP and MAT. Depth was the largest individual predictor but showed little interaction strength ($H_{statistic} \leq 0.1$) with other variables compared to other predictors.

Further investigation into the top predictors for SOC stock using partial correlations to isolate predictors showed differences between wetlands and uplands for Depth, MAT, and WIP (Table 2.5). Depth and WIP had stronger negative and positive correlations, respectively, with

upland SOC stocks compared to wetlands. Wetlands had a stronger negative correlation with MAT compared to uplands. Smaller correlation difference between wetlands and uplands were noted in PET:MAP and Canopy Height.

Table 2.5: Partial correlations between important predictors and SOC Stocks and mineral SOC% between wetlands and uplands using the Wetland Intrinsic Potential threshold of 50%, above which are considered wetlands. Full datasets were used for calculating partial correlations and SOC Stock and mineral SOC% values were untransformed.

Predictor	SOC Stock (g cm^{-2}) Wetland (WIP ≥ 50%)	SOC Stock (g cm^{-2}) Upland (WIP < 50%)
Depth	-0.56	-0.70
PET:MAP	-0.41	-0.32
MAT	-0.18	-0.06
WIP	0.25	0.35
Canopy Height	-0.02	0.11
PM	-0.14	-0.20
Landform	0.17	-0.14
Predictor	**SOC% Wetland (WIP ≥ 50%)**	**SOC% Upland (WIP < 50%)**
Depth	-0.49	-0.54
PET:MAP	-0.02	-0.20
pH	-0.32	-0.17
Clay	0.51	0.21

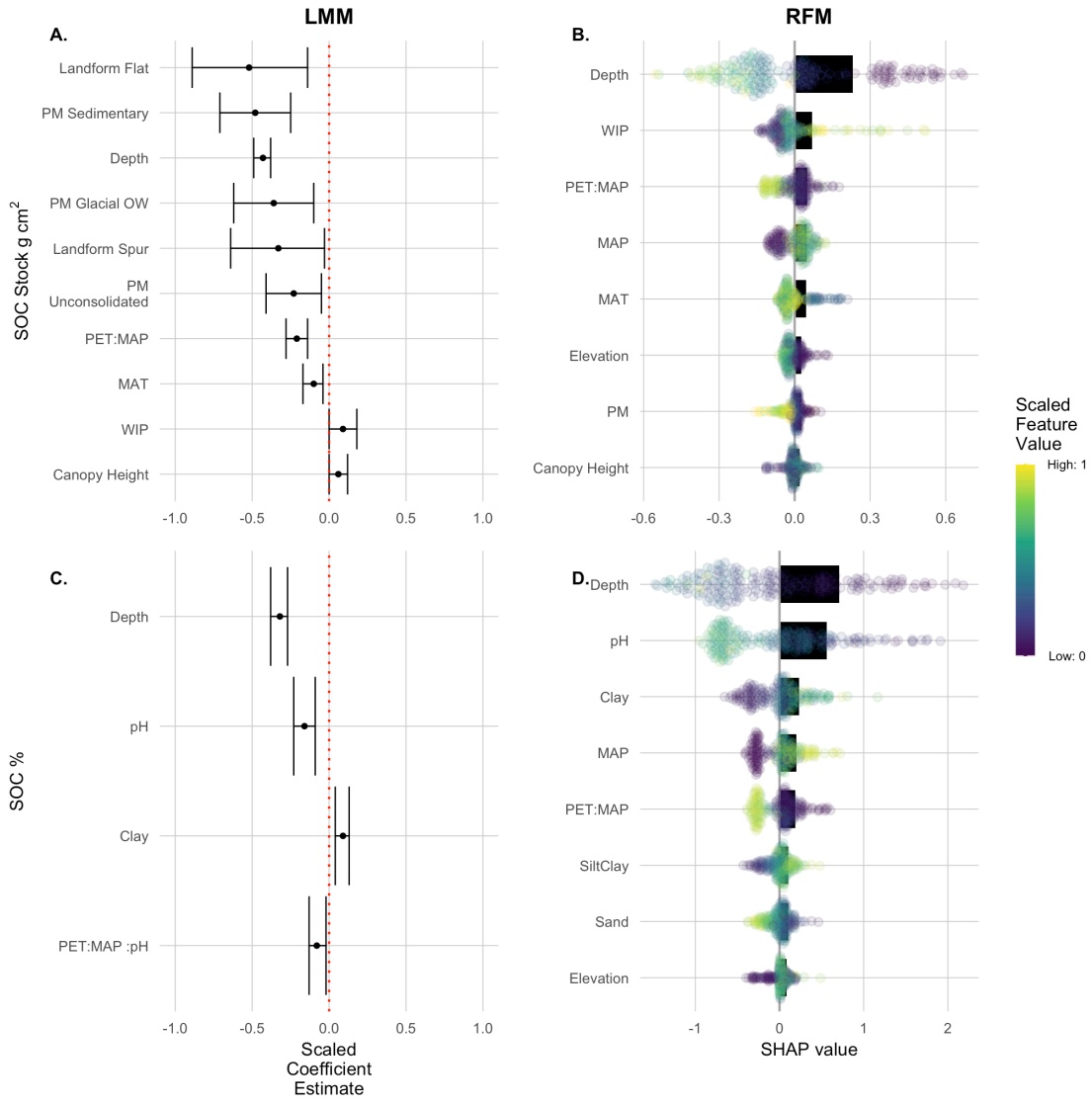

Figure 2.4: Variable importance for the Linear Mixed Model (LMM **A.** & **C.**) and Quantile Random Forest Model (RFM **B.** & **D.**). The scaled 95% confidence intervals for scaled LMM coefficients for SOC stocks and mineral SOC%, respectively. Note, individual Parent Material (PM) and Landform categories are shown but are considered a group under an overall PM and Landform categorical variable; Bar plots are the average absolute SHAP (SHapley Additive exPlanations) values for each feature in the RFM for SOC stock and mineral SOC%, respectively. Colored points on the bar plots are the min-max scaled SHAP feature values for each observation.

For mineral SOC%, Both the LMM and RFM had consistent agreement for important predictors, identifying Depth, pH, and Clay as the top three (Figure 2.4 C). Depth had the highest LMM coefficient and RFM SHAP value (scaled coefficient estimate = -0.32 95% CI: -0.38 - -0.27 & Absolute Sum SHAP: 0.71), consistent with the SOC stock models. pH showed a significant effect

on mineral SOC%, which decreased as mineral soil became more neutral indicated by the negative coefficient estimate in the LMM (0.56) and high SHAP value in the RFM (Absolute Sum SHAP: 0.56). Clay% had a positive coefficient in the LMM (scaled coefficient estimate = 0.09 95% CI: 0.04 - 0.13) and high SHAP value in the RFM (Absolute Sum SHAP: 0.24).

The LMM also identified a specific interaction between pH and the climate variable PET:MAP (scaled coefficient estimate = -0.08 95% CI: -0.13 - -0.02). Figure 2.5 B shows the decline in mineral SOC% as a function of pH but high PET:MAP increases the decline whereas low PET:MAP reduces the decline magnitude. Similar to the RFM for SOC stocks, Depth again had lower interaction values with other predictors except for pH (Figure 2.6; $H_{statistic} \leq 0.1$). Consistent with the LMM for mineral SOC%, the RFM also estimated that pH had a large interaction PET:MAP (Figure 2.6; $H_{statistic} \geq 0.2$). Clay% had stronger interactions overall compared to Depth and pH but with correlated variables such as Silt+Clay and Sand. The interaction between Clay and MAP and PET:MAP was also strong (Figure 2.6; $H_{statistic} \geq 0.2$).

Partial correlation strength for mineral SOC% differed between wetlands and uplands for PET:MAP, pH, and Clay (Table 2.5). Wetland mineral SOC% had a much smaller and almost 0 correlation with PET:MAP in contrast to a larger negative correlation in upland mineral SOC%. Wetland mineral SOC% also had a larger negative correlation with pH and a larger positive correlation with Clay compared to upland mineral SOC%. Depth appeared to have a marginal difference between wetlands and uplands.

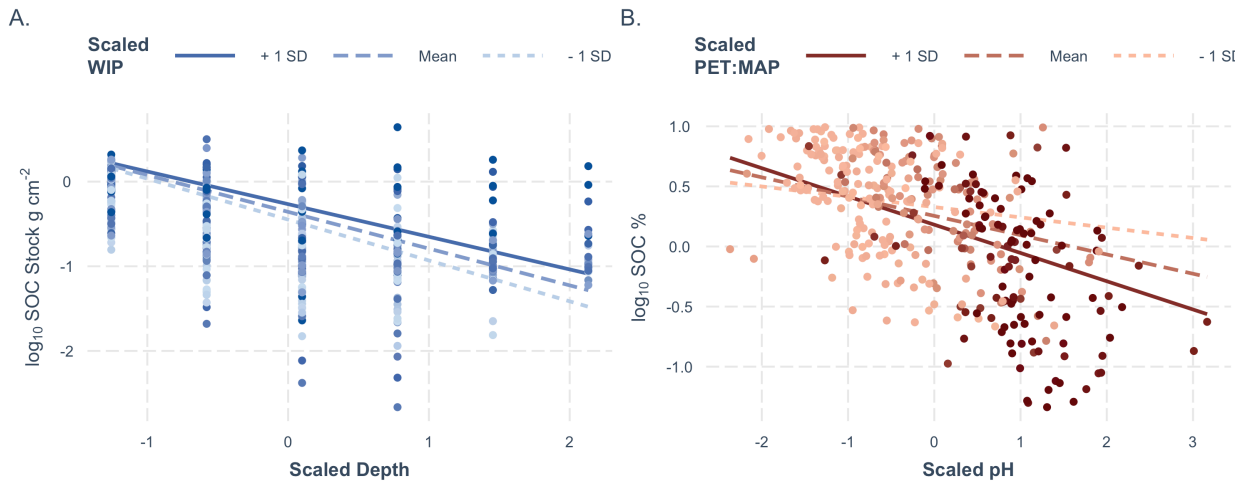

Figure 2.5: Variable interactions defined in the linear mixed models (LMMs). **A.)** The wetland intrinsic potential (WIP) and Depth interaction in the LMM for SOC stock. **B.)** The interaction between pH and PET:MAP in the LMM for mineral SOC%. The figure uses data points from the training dataset and contains the scaled predictors for both WIP, Depth, pH and PET:MAP. SOC stock (g cm^{-2}) and mineral SOC% are also log_{10} transformed as was in the original LMM.

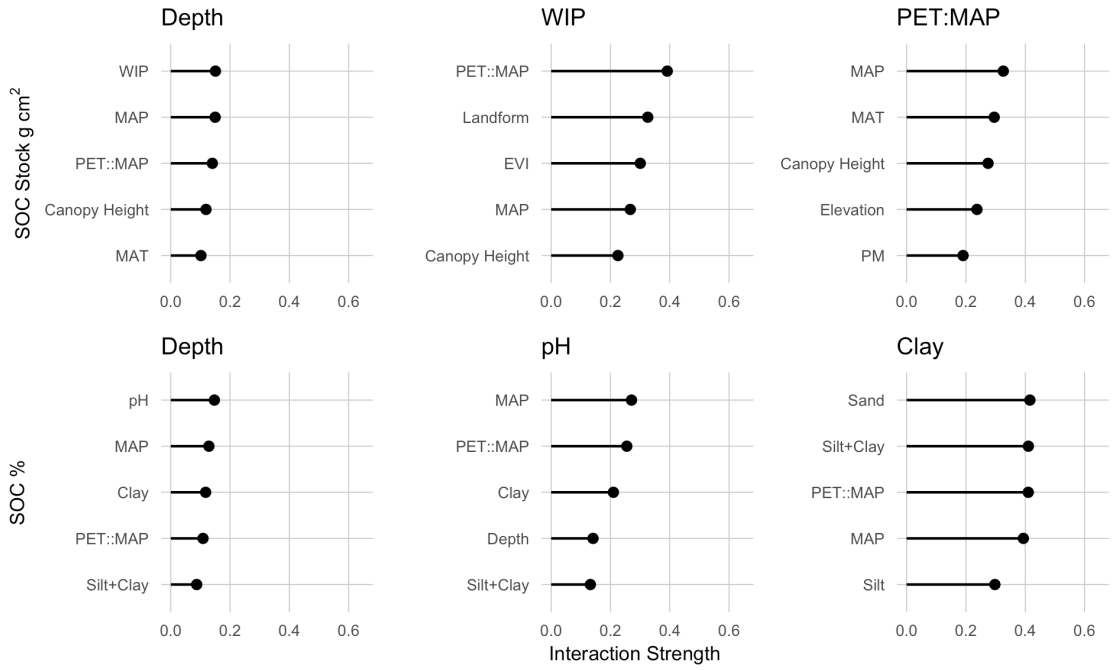

Figure 2.6: Interaction values for the largest three predictors by SHAP value in the RFM for SOC stock and mineral SOC%. Interaction values are derived by the H-Statistic.

Upscaling SOC stock estimates across watershed study areas

We chose to use the RFM for SOC stocks based on its fit to the test dataset to upscale the observations of SOC stocks to estimate 1 m SOC stocks across the full extent of the four study

watersheds (HLEF, HRW, MRW, and CVW) (Figure 2.7). The RFM also predicted uncertainty intervals using the 2.5th and 97.5th quantiles which were then summarized in Supplementary Table 2.2. We calculated that the HRW had the largest SOC stock of 8.68Tg due to its large areal extent compared to other watersheds (Table 2.6). The highest mean SOC stocks predicted by the RFM model were in the HLEF with a mean of 178 Mg ha^{-1}. We estimated the lowest total SOC stocks in the HLEF, which coincides with a small relative area compared to other watersheds. The lowest mean SOC stock was estimated in the CVW. Wetlands delineated by using the WIP probability threshold of greater than 50% showed consistently higher upscaled SOC stocks compared to the overall mean and non-wetland upland SOC stocks.

Table 2.6: Table of soil organic carbon (SOC) stocks derived from the mapping the RFM across the four study watersheds (HLEF, HRW, MRW, and CVW). Additional published estimates are added here for comparison. The mapped 1 m SOC stock from Jones and D'Amore, 2024 are derived from an ensemble of global models for the Pacific Northwest region and extracted for each study watershed. Wetland areas for Jones and D'Amore 2024 were derived by aggregating the WIP probability maps to 60 m resolution and considering the coverage of pixels with WIP values greater than 50% probability as wetlands. Currently available mapped estimates of wetland 1 m SOC stock for CONUS are provided by Uhran et al., (2021) using the data from the National Wetland Condition Assessment (NWCA) and the National Land Cover Database (NLCD).

Landscape Class	Study Area	Source	Total Area (ha)	Mean 1m SOC Stock (Mg ha^{-1})	Total 1m SOC Stock (Tg)
Total	HLEF	This Study	11,019	178.0	1.97
		Ensemble Model	11,764	195.0	2.29
	HRW	This Study	64,538	134.0	8.68
		Ensemble Model	70,009	205.0	14.30
	MRW	This Study	21,434	142.0	3.04
		Ensemble Model	22,310	169.0	3.76
	CVW	This Study	32,118	99.9	3.21
		Ensemble Model	33,761	124.0	4.17
Wetland	HLEF	This Study	2,188	243.0	0.53
		Ensemble Model	2,388	221.0	0.53
	HRW	This Study	5,798	194.0	1.12
		Ensemble Model	6,503	193.0	1.25
		Uhran et al., 2021	1,649	184.0	0.30
	MRW	This Study	2,184	162.0	0.35
		Ensemble Model	2,460	164.0	0.40
		Uhran et al., 2021	817	144.0	0.12
	CVW	This Study	862	114.0	0.10
		Ensemble Model	1,347	124.0	0.17
		Uhran et al., 2021	178	98.7	0.02
Upland	HLEF	This Study	8,831	162.0	1.43
		Ensemble Model	9,614	187.0	1.80
	HRW	This Study	58,739	129.0	7.56
		Ensemble Model	64,314	206.0	13.30
	MRW	This Study	19,250	140.0	2.69
		Ensemble Model	20,232	169.0	3.42
	CVW	This Study	31,256	99.5	3.11
		Ensemble Model	32,974	124.0	4.07

An ensemble mean of global and regional models for the PNW region (Jones & D'Amore, 2024) showed 1 m SOC stocks varied with broad similarly to our estimates across the four watersheds (Table 2.6). The ensemble combination of global models from Jones and D'Amore, 2024 had slightly higher but comparable estimates for total 1 m SOC stocks in the HLEF, MRW, and CVW with higher mean SOC stocks and larger areas. However, we estimated substantially less total

SOC in the HRW at 8.68TgC compared to 14.30TgC in Jones in D'Amore, 2024 Figure 2.7. We used the same WIP map with a threshold of 50% wetland probability to define wetlands in both the ensemble maps and our SOC maps. We saw small differences in wetland extent due to the differences in resolution (60 m in Jones and D'Amore 2024, 4-5 m in our maps). For wetlands defined by the WIP, our estimates of mean SOC stocks were slightly higher than Jones and D'Amore, 2024 for the HLEF and for the HRW but lower for wetlands in the MRW and CVW. Mean and total wetland SOC stock estimates from this study and Jones and D'Amore, 2024 were higher than upscaled mean and total wetland SOC estimates from the National Wetland Condition Assessment and the National Land Cover Database (NWCA) published by Uhran et al. (2021). However, estimated mean and total upland SOC stock from Jones and D'Amore, 2024 were much higher than our estimates. There is a notable difference for mean and total upland SOC stock for the HRW between our estimates and Jones and D'Amore, 2024.

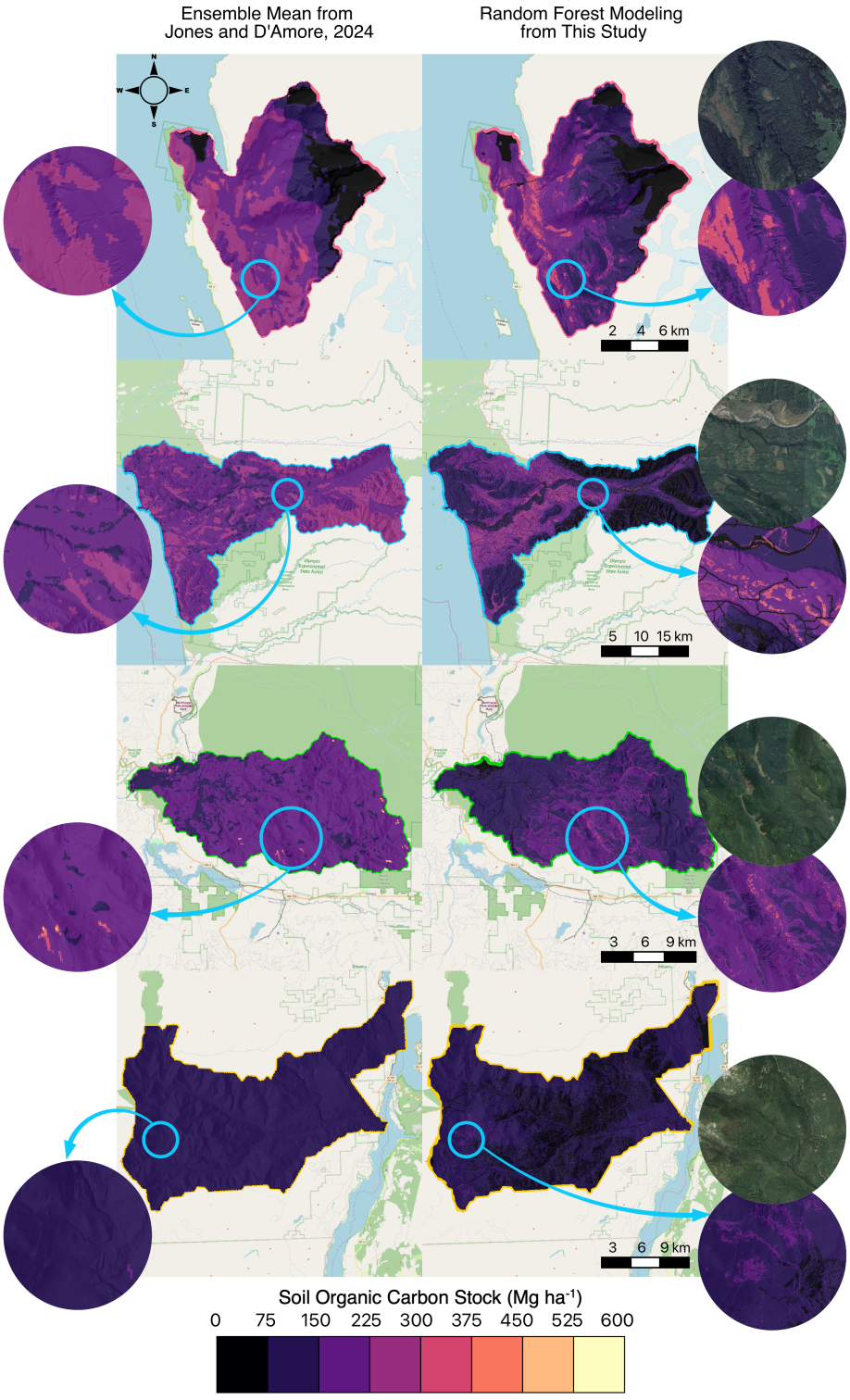

Figure 2.7: Comparison of mapped soil organic carbon (SOC) stocks between the ensemble of regional and global models from Jones and D'Amore, 2024 and the Random Forest Model (RFM). The ensemble model map has a resolution of 60 m compared to a resolution of 4 m for the RFM map.

Discussion

More accurate SOC mapping with the identification of wetlands is crucial for constraining estimates of carbon to the atmosphere and the implementation of natural climate solutions (Bradford et al., 2016; Bossio et al., 2020). The WIP tool approach implemented in each of the four watersheds showed large amounts of previously unmapped wetlands and enabled modeling of both wetland and upland SOC. We partially supported our first hypothesis with the inclusion of WIP in the RFM for SOC stocks that accounted for 50% of the test dataset variability and integrated other SCORPAN predictors. However, we found that models generated robust predictions of mineral SOC% without the WIP predictor, instead relying on edaphic factors and climate. We found support for part of our second hypothesis when the RFM included Depth, WIP, and PET:MAP as significant drivers although the drivers of mineral soil SOC% were largely Depth, pH, and Clay. Finally, we supported our third hypothesis by distinguishing high SOC stocks in wetlands within our study areas using the RFM with a higher wetland:upland SOC stock ratio compared to an ensemble mean from global and regional models. With these findings, we emphasize that future work towards estimating and mapping SOC should treat landscapes as a continuum through comprehensively integrating wetland observations and extent maps.

Improved wetland representation in SOC maps

Wetland identification and mapping using remote sensing continues rapid growth with new sensors and better computing performance (Mahdavi et al., 2018; Campbell et al., 2022). However, forested wetlands and generally wetlands under perennial dense vegetation are still difficult to capture and require tailored approaches depending on ecosystem characteristics (Du et al., 2020; Mahdianpari et al., 2020). The WIP tool framework is designed for forested wetlands by leveraging lidar-derived multi-scale terrain indices lidar which capture hydrologic patterns and wetland morphology across multiple scales Lang & McCarty, 2009; Lang et al., 2012; Maxwell et al., 2016;

Halabisky et al., 2023). Furthermore, the continuous probability of wetland presence highlights the transition zones between wetland and non-wetland areas (Maxwell et al., 2016; Halabisky et al., 2023). Wetland depiction and representation have been improved using probabilistic approaches in complex landscapes, highlighting that these ecosystems often do not have rigid boundaries (Delancey et al., 2019; Lidberg et al., 2020). We note that our WIP approach trained a model separately in each study watershed to precisely hone in on wetland patterns intrinsic to each area. Halabisky et al. (2023) discuss that WIP accuracy can suffer if a model is applied to dissimilar areas, and it would be inadvisable to apply a WIP model in one area to a separate area. However, larger scale implementations of this framework that span multiple climatic zones and ecoregions could provide insight into cross-scale drivers of wetland formation. Future research should also continue to validate patterns and processes that are captured by data-derived probabilistic and continuous approaches.

The RFM for SOC stocks corroborates the nascent notion that these data-derived probability patterns, for wetland presence in this case, can capture SOC accumulation. The RFM appeared to use the WIP more effectively than the LMM and it was noticeable that higher SOC stocks in wetland observations were more accurately modeled compared to the LMM Figure 2.3. Although the WIP was not explicitly included in the Ensemble, using the WIP to delineate wetland areas identified marginally higher SOC stocks in the Ensemble SOC maps for HLEF and MRW Table 2.6. Nevertheless, our WIP-integrated DSM approach strongly suggests that wetland extent and wetland SOC are under-mapped in forested regions. Other DSMs for SOC stocks have often used national wetland inventories, land cover classification maps, and topographic derivatives to represent wetlands and wet areas with potential SOC accumulation (Lamichhane et al., 2019). Hengl et al. (2023) used topography-derived hydrologic variables and lithological maps to represent potential wetland and wet areas in a DSM approach in Alberta, Canada but found that wetland SOC

stocks were underestimated after examining land cover maps. Walden et al. (2023) used DSM for blue carbon and terrestrial carbon stocks incorporating a multi-resolution decomposition of topographic wetness index (TWI) to improve Australia's national carbon inventory but likely included inland freshwater wetland ecosystems under terrestrial categories. The DSM by Sothe et al. (2022) greatly improved Canada's carbon inventory by including archived SOC data from peatland samples, soil type maps, and remote sensing indices, especially synthetic aperture radar that were sensitive to wetland presence. Helfenstein et al. (2024) more directly used peatland occurrence maps as predictors for SOC and further developed dynamic peatland occurrence maps over time between 1953 and 2022 to more accurately estimate changes in SOC. Although not wetland-specific, Larson et al. (2023) used a similar approach to our WIP wetland probability by including a predictor variable from a separate machine learning model designed to capture soil moisture with a probabilistic output. The probabilistic soil moisture model was used to accurately map both SOC and tree biomass carbon.

There is a clear growing trend of using more continuous approaches towards DSM and landscape modeling wetlands and even wet areas. However, there a few limitations for our modeling approach. The WIP model captures the pattern and probability of inundation or saturation soils related to wetlands in the training data but does not distinguish different classes of wetlands (Halabisky et al., 2023). We instead relied on landform, Parent Material, and vegetation indices to model the different SOC stocks between potential wetland types. However, our approach could be improved by explicitly modeling the different wetland classes as continuous probabilities, similar to peatland probabilities in other previous research (Delancey et al., 2019; Helfenstein et al., 2024). Chizen & Bedard-Haughn (2025) found that wetland class explained the largest amount of variability in the Prairie Pothole region and Pearse et al. (2018) showed that SOC stock can vary widely between different wetland types and vegetation cover. Additionally, the WIP does not specify the

underlying hydrologic mechanism for the wetland presence on the landscape. But process-based models such as modified SWAT (Evenson et al., 2016) could be used to further improve the understanding of landscape hydrologic drivers of SOC stock (Pierson et al., 2022).

Drivers of SOC stocks across scales

Depth as the largest significant predictor in both models for SOC stock was largely expected since SOC stocks typically decline with depth (Jobbágy & Jackson, 2000) and there were no other spatially-explicit predictors that accounted for variation within the pedon. Using depth as a predictor in a DSM approach has been termed "3D" mapping (Poggio & Gimona, 2014; Sothe et al., 2022). But our approach differs slightly by applying a "2.5D" DSM method using the mass-preserving spline function to harmonize our dataset observations across 25 cm depth intervals (Malone et al., 2009; O'Brien, 2022). The advantages with our approach allowed us to maintain the original dataset variation without inflating observations. Additionally, we limited the influence of large depth intervals on SOC stocks and obtained a negative exponential decline of SOC stock with Depth. This allowed our approach to use Depth as an effective predictor similar to "3D" DSM but with the mass-preserving spline of "2.5D" DSM.

After Depth, many of the largest drivers of SOC stock in both the LMM and RFM included large scale climatic variables, primarily PET:MAP and MAT. Climatic variables are a significant large scale factor in the original soil formation equation (Jenny, 1941) and the SCORPAN framework (Minasny et al., 2013). Water availability climatic predictors such as PET:MAP and MAP have been shown to outweigh temperature predictors such as MAT on overall SOC stocks (Jobbágy & Jackson, 2000; Hobley et al., 2015; Fromm et al., 2024). However, temperature has been shown to have a greater effect on SOC held in organic layers or composed in particulate forms (Georgiou et al., 2024) and this can be pronounced in cooler climates such as the Pacific Northwest (McNicol et al.,

2019; Wiesmeier et al., 2019). This is especially consequential for wetland SOC stocks since SOC tends to accumulate in organic horizons near or at the surface. Our results with partial correlation show WIP wetland SOC is more negatively associated by MAT which corroborates previous research that higher temperatures can stimulate decomposition in wetland and peatland SOC (Fellman et al., 2017; Hribljan et al., 2023).

Our wetland mapping with the WIP established its ability to produce accurate wetland maps. Interestingly the LMM performed worse on the test dataset while discounting WIP while the RFM showed improved performance with large WIP SHAP values. We believe that the lower performance of the LMM was due to the interactions and non-linear relationships between SOC stock and WIP similar to the non-linear soil moisture model in Larson et al. (2023) that predicted SOC stocks. But the RFM was able to accommodate for these relationships and produce higher predictive performance Figure 2.2. Building the WIP model functions similarly to multivariate variable reduction, focusing predictors on an explicit wetland-presence mechanism for SOC stock modeling. The WIP predictor can be considered a part of both the Organism and Relief parts of the SCORPAN framework since it incorporates mostly terrain metrics but also those related to wetland vegetation (Halabisky et al., 2023). Conspicuously, both models discounted explicit vegetation parameters such as Canopy Height, or EVI, with early model iterations also excluding vegetation type classification. This is consistent with larger scale findings that biological drivers may lag bio-climatic and edaphic predictors (Yu et al., 2021; Wang et al., 2024). Yet, our results are not completely conclusive since we do not include more complex biological drivers such fungal associations and plant biodiversity that can drive SOC accumulation in mineral soil (Lang et al., 2023). Overall, our study results show SOC stocks can be modeled in a DSM approach across wetland and uplands using drivers shown in previous SOC research. Wetlands may be more

sensitive to climatic drivers than uplands and this underlines that these missing wetland SOC stocks should be included more explicitly in future research.

Drivers of mineral soil SOC%

Unexpectedly, both models were able to capture majority of the variability for mineral SOC% across both wetlands and uplands without WIP unlike the models for SOC stock. This could be attributed to the aggressive 10% carbon content cutoff to remove organic horizons to examine the mineral soil specifically along with additional non-spatial soil edaphic predictors. Our methods were used to gain insight into factors controlling SOC within areas of the soil that might be associated with minerals and protected (Georgiou et al., 2022). Although we did not thoroughly examine the diverse array of soil parameters that drive SOC%, the lack of WIP in the final LMM and RFM indicate climatic and edaphic drivers of mineral SOC% are more significant than landscape-scale variables across the different regions. In particular, the landscape-scale WIP predictor appears to be more sensitive to organic matter accumulation near the surface in our study area's wetlands. However, our models did not replicate previous research in mineral soil wetlands without organic horizons that show SOC% declines going from frequently saturated to rarely saturated mineral soils (Tangen & Bansal, 2020; Kottkamp et al., 2022). Furthermore, we did not incorporate the study design from both Kottkamp et al. (2022) and Tangen & Bansal (2020) that thoroughly examined individual wetlands with sampling along transects whereas our sample locations were spread across each watershed. Replicating this study design across the regional scale would have imparted a prohibitively large effort needed to gather numerous soil pedon observations that could potentially hinder DSM implementation. Although, we acknowledge that intra-wetland SOC variability can be large (Stewart et al., 2023) and forested wetlands need a robust evaluation which could utilize a study design similar to Tangen & Bansal (2020) where wetland-upland transect

sampling for SOC% and edaphic factors are replicated across multiple individual wetlands and climatic regions.

In our study, the main drivers of mineral SOC% were primarily Depth, PET:MAP, pH, and Clay. Consistent with SOC stock models and consistent with our expectations, there was a large effect of Depth on mineral SOC%. However, the Depth LMM coefficient and SHAP value was not markedly larger than pH, the next largest significant predictor. This is consistent with previous research across continental scales, where pH and Depth accounted for large proportions of the variability in SOC% (Yu et al., 2021). Nie et al. (2023) also showed that pH played a major role in wetland SOC stocks and influenced effects from vegetation and climate which corresponds with our partial correlation that showed that wetland SOC% was more sensitive than upland SOC% to pH and Clay%. Clay% was the next largest predictor in terms of coefficient and SHAP value which is also consistent with a long history of research showing that higher Clay% is associated with higher SOC% (Jobbágy & Jackson, 2000). However, the relationship is not as clear in wetland soils. Kottkamp et al. (2022) found bulk SOC% was not related to Clay% but instead found that macroaggregates promoted more SOC storage. More detailed analysis in wetland soils has indicated a diverse array of factors that drive SOC% including the presence of metals (Liu et al., 2024). Dong et al. (2022) found that Cation Exchange Capacity (CEC) and Bulk Density were the largest predictors of SOC%. However, both CEC and Bulk Density measurements are often functions of SOC% and it is misleading to interpret that it is driving SOC% (Ross et al., 2008). For this reason, we also did not consider Bulk Density in our study as a driver for mineral SOC% and focused on the particle size and pH, although it is often useful to use BD as proxy for SOC%.

We also found that climate predictors, namely MAP and PET:MAP were included as the top predictors. However, the LMM, was more conservative and only included PET:MAP as an

interaction term with pH. Interactions between climate and soil factors, particularly geochemistry, have been well studied in recent years, with strong evidence that both groups play significant roles in SOC% (Doetterl et al., 2015; Rasmussen et al., 2018; Yu et al., 2021). Measuring geochemical factors such as Fe and Al oxides would likely provide more nuance to controlling predictors in our study and should be considered in future SOC research. Moreover, contemporary soil science research has shifted focus towards on the mineral-associated vs. particulate fractions which illuminate potential responses to climate change (Heckman et al., 2021; Rocci et al., 2021). There are many uncertainties for the driving factors of mineral-associated and particulate SOC, but this research area should also include wetlands soils to more comprehensively understand the overall terrestrial carbon cycle.

Conclusions

Here, our research provides the critical point for which move towards better representation of wetland soils and soils overall in SOC research. We find that wetlands are consistently under-mapped across watersheds from different climate regions in the Pacific Northwest leading to gaps in locating large SOC stocks. We find that our approach to use a continuous probability model of wetland presence facilitated improvements on SOC stock prediction and mapping compared to an external ensemble model using regional and global SOC maps. We consider the WIP wetland probability as a driver of SOC accumulation particularly for organic matter accumulation, a key property of wetlands. The use of WIP provides clarity for drivers of SOC stock rather than using a wide array of topographic and remote sensing metrics which indirectly represent wetlands. However, WIP was not a predictor of mineral SOC% where drivers were a mix of edaphic and climate predictors. Our study is limited in examining all potential factors driving mineral soil SOC% beyond pH and particle size. But these results should motivate a more comprehensive SOC assessments across both wetlands and uplands to enhance our understanding of SOC dynamics in response to climate change.

Supplementary information for Chapter 2. Advancing soil organic carbon mapping by incorporating inland freshwater wetland probability as a predictor

Wetland Intrinsic Potential (WIP) tool

Data for the WIP tool included lidar-derived digital terrain models (DTMs), digital surface models, and imagery from the National Agricultural Imagery Program (NAIP). Lidar DTMs and digital surface models were downloaded from the WA Department of Natural Resources Lidar Portal and spanned a range of dates from 2008-2016 in the CVW and 2007-2011 in the MRW in order to create a continuous surface area of the study areas. We also used the earliest available NAIP imagery from 2017. No NAIP data were available for the HLEF, and we therefore utilized Sentinel 2 for vegetation indices. A Lidar DTM and digital surface models were also downloaded from the Alaska State Division of Geological and Geophysical Surveys Elevation portal and were collected in 2012.

We calculated terrain indices using the Surface Metrics Toolbox developed by Halabisky et al. (2023) and implemented in ArcGIS Pro 3.1. The multi-scale terrain indices included gradient (slope), planform curvature, profile curvature, and deviation from the mean elevation calculated at 50 m, 300 m, and 1000 m length scales. Additional terrain metrics included Topographic Wetness Index (TWI, Beven & Kirkby, 1979) Topographic Depth to Water, and Elevation. We also included the normalized difference vegetation index (NDVI) and the normalized difference water index (NDWI), and canopy height in addition to terrain metrics for the WIP model. NDVI and NDWI were derived from aerial imagery collected by NAIP. We then took these 18 geospatial metrics and

re-sampled them to a 4 m resolution to match the former WIP model in the HRW. The default resolution for the HLEF was 5 m and all HLEF data were resampled to this resolution.

We derived training data for wetlands and uplands (non-wetlands) using the geospatial dataset from the National Wetland Inventory (NWI) and the Wetland Mapper Tool ("National Wetlands Inventory," n.d.). We extracted 3000 total training points from NWI wetlands in the HLEF, MRW, and CVW study areas (6000 total points) with approximately 2/3 of the training points classified as "upland" and 1/3 classified as "wetland". The training points were then used to extract data from the geospatial metrics in each study area. A random forest model was then constructed using a 70:30 training and testing dataset partition and then used to generate a preliminary WIP model. From this preliminary model, we utilized a similar approach to Halabisky et al. (2023) and generated another training dataset and a validation dataset by conducting a stratified sampling of 600 points and 300 points, respectively across the gradient of the preliminary model. The points from this stratification were then verified as either wetland or upland by two analysts who conducted site visits and referenced points using aerial imagery, pre-existing NWI data, and lidar-derived hillshades. The new training and validation points were then used in another separate random forest model which generated the final mapped prediction of the WIP model. The most important variables from the Random Forest models in all four study watersheds are shown in Supplementary Figure 2.1.

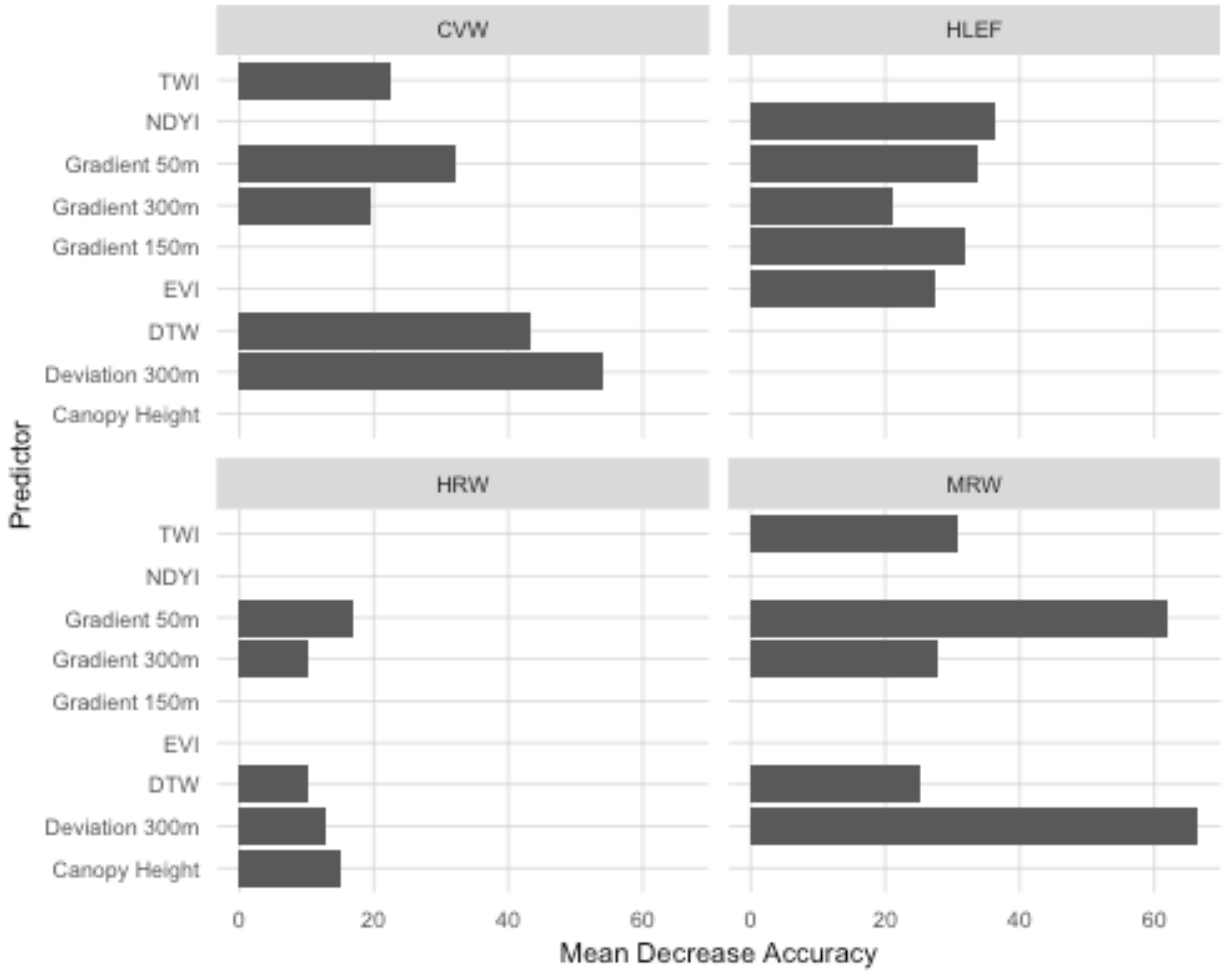

Supplementary Figure 2.1 Variable importance plots from the final WIP models in all four watersheds. Only the top 5 predictors were included from each watershed. We observed multiscale terrain metrics such as Gradient, and Deviation occurring frequently. Other terrain derived metrics such as depth to water (DTW), and topographic wetness index (TWI) were included in some but not all models. But we note that Canopy Height in the HRW and the normalized difference yellow index and enhanced vegetation index in the HLEF were vegetation indices which may have helped identify peat occurrence.

Parent Material

Table 2.1 Supplementary Table 1. The reclassification of original detailed geology and lithology categories into broader soil parent material categories

Site	Original Lithology	Reclassified Lithology
HLEF	Tonalite	metamorphic
	Metavolcanic	igneous
	TKts	
	Tcp	
	Slate	Slate
	Quaternary	Quaternary
	Glacier	NA
HRW	tectonic breccia	unconsolidated
	alluvium	
	mass-wasting deposits, mostly landslides	
	water	
	marine sedimentary rocks	sedimentary
	marine clastic rocks, dominantly thick-bedded lithic sandstone	
	alpine glacial drift, Fraser-age	glacial till and drift
	alpine glacial drift, pre-Fraser	
	alpine glacial till, pre-Fraser	
	alpine glacial drift, pre-Wisconsinan, older	
	alpine glacial drift, pre-Wisconsinan, younger	
	alpine glacial till, pre-Wisconsinan	
	alpine glacial till, Fraser-age	
	continental glacial and non-glacial deposits, Fraser-age	
	glacial outwash, alpine, Fraser-age	glacial outwash
	alpine glacial outwash, pre-Fraser	
	alpine glacial outwash, pre-Wisconsinan	
MRW	alluvium	unconsolidated
	continental sedimentary deposits or rocks	sedimentary
	volcaniclastic deposits or rocks	igneous
	intrusive andesite	
	basaltic andesite flows	
	tuffs and tuff breccias	
	alpine glacial drift, pre-Fraser	glacial till and drift
	continental glacial drift, Fraser-age	
	continental glacial drift, pre-Fraser	
	continental glacial till, Fraser-age	
	continental glacial outwash, Fraser-age	glacial outwash
CVW	alluvium	unconsolidated
	dune sand	
	water	
	marine metasedimentary rocks	sedimentary
	basic (mafic) intrusive rocks	metamorphic
	intrusive dacite	
	monzodiorite	
	metacarbonate	
	amphibolite	
	marble	

	migmatite	
	orthogneiss	
	orthogneiss, porphyritic	
	paragneiss	
	quartzite, high grade	
	schist, high grade	
	metavolcanic rocks	igneous
	glaciolacustrine deposits, Fraser-age	glacial till and drift
	continental glacial till, Fraser-age	
	continental glacial outwash, Fraser-age	glacial outwash

Soil particle size and pH

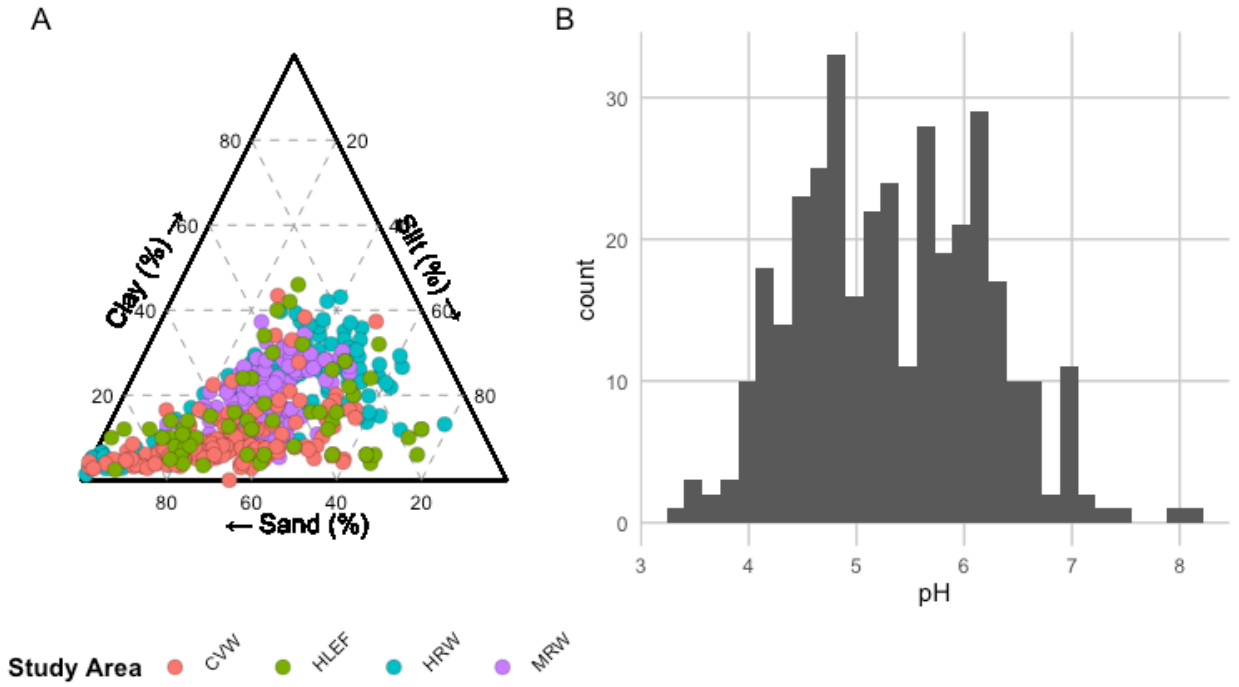

Supplementary Figure 2.2 A.) Soil texture triangle showing the sand, silt, and clay composition of all soil samples and **B.)** A histogram of pH values in the mineral soil subset dataset.

LMM assumptions check

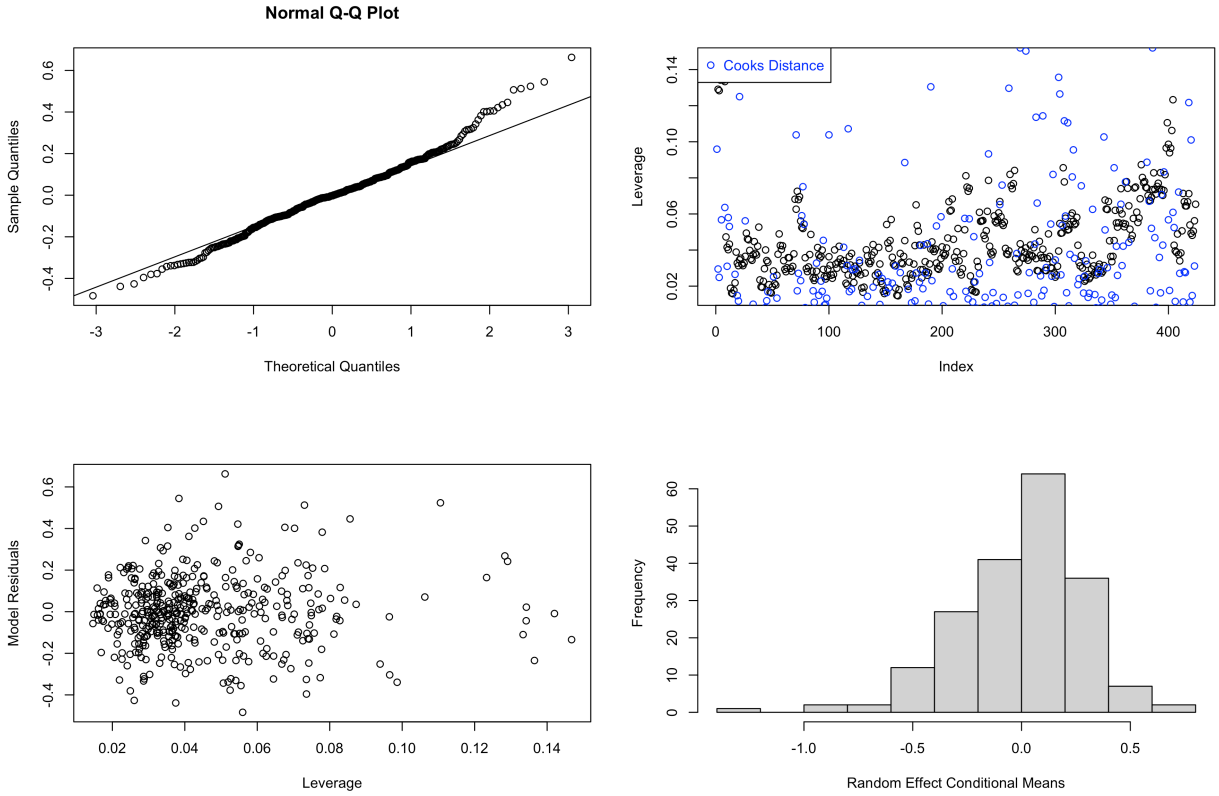

Supplementary Figure 2.3 Normal Quantile-Quantile plot used to evaluate if the distribution of the residuals and sample observations are similar for the LMM for SOC Stock. We note there are some observations that deviate from the 1:1 line but deemed it overall sufficient to proceed with the model.

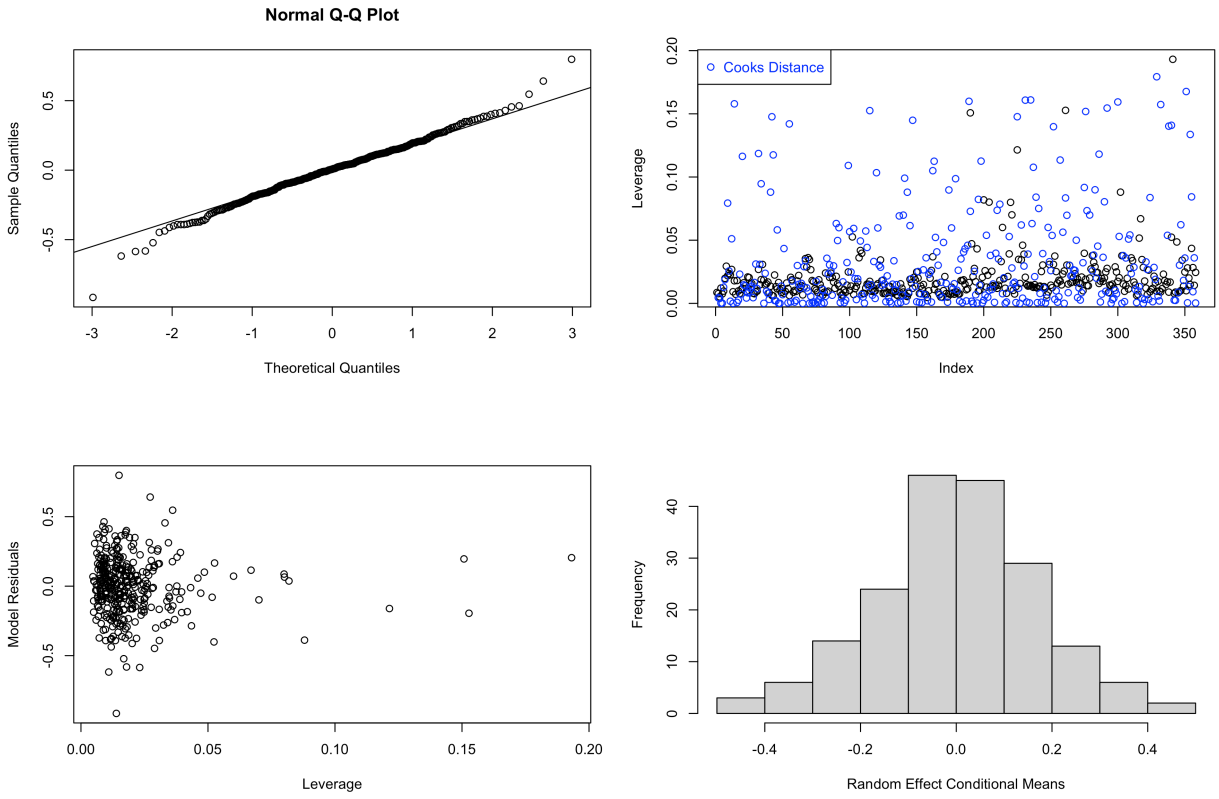

Supplementary Figure 2.4 Normal Quantile-Quantile plot used to evaluate if the distribution of the residuals and sample observations are similar for the LMM for SOC%. Fewer observations deviated from the 1:1 line than the SOC stock and were deemed sufficient to proceed with the model.

Spatial autocorrelation

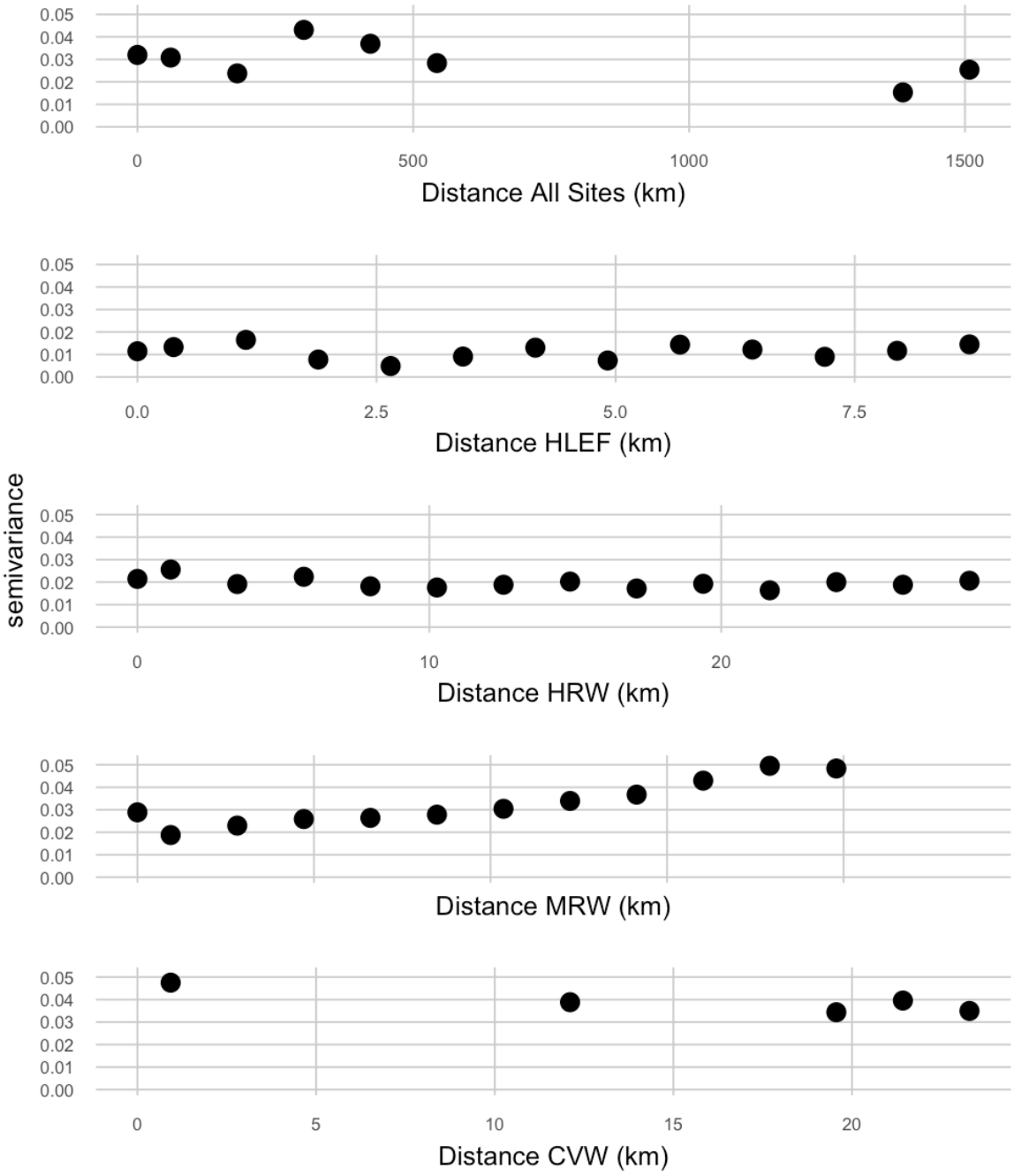

Supplementary Figure 2.5 Semivariograms showing the semivariance of location pairs across all study watersheds, the HRW, the MRW, and the CVW. We interpreted these semivariograms as showing little to no spatial structure within the dataset.

Mapped uncertainty

Supplementary Table 2.2 95% Prediction interval ranges for mapped SOC stocks. Prediction intervals were calculated using the quantile random forest prediction for the 2.5th and 97.5th quantiles.

Landscape Class	Study Area	Total Area (ha)	95% Prediction Interval Mean 1m SOC Stock Mg ha^{-1}	95% Prediction Interval Total 1m SOC Stock (Tg)
Total	HLEF	11,356	31.4 - 786	0.36 - 8.92
	HRW	68,525	29.4 - 567	2.02 - 38.9
	MRW	21,924	30 - 604	0.66 - 13.2
	CVW	32,827	24.8 - 572	0.81 - 18.8
Wetland	HLEF	2,205	32.8 - 1004	0.07 - 2.21
	HRW	6,748	30.3 - 719	0.2 - 4.85
	MRW	2,318	33 - 638	0.08 - 1.48
	CVW	1,097	26.4 - 558	0.03 - 0.61
Upland	HLEF	9,151	31.1 - 733	0.28 - 6.71
	HRW	61,778	29.3 - 551	1.81 - 34
	MRW	19,606	29.6 - 600	0.58 - 11.8
	CVW	31,731	24.7 - 573	0.78 - 18.2

Chapter 3: Older mineral-associated organic matter carbon found in forested wetlands compared to uplands in a coastal temperate rainforest

Author List
Anthony J Stewart[1]
Diogo Spinola[2]
Keith Morrison[2]
Karis McFarlane[2]
Meghan Halabisky[1]
L. Monika Moskal[1]
David Butman[1]
David V. D'Amore[3]
Katerina Georgiou[2,4]

Affiliations
1School of Environmental and Forest Sciences, University of Washington, Seattle
2Lawrence Livermore National Laboratory, Livermore, CA
3Pacific Northwest Research Station, U.S. Department of Agriculture Forest Service
4University of Northern British Columbia, Prince George, British Columbia

Abstract

Over the last few decades soil science research has examined the soil organic carbon (SOC) in mineral associated organic matter (MAOM-C) which has been shown to be persistent in soils by measuring the radiocarbon content ($\Delta^{14}C$). However, these measurements have seldom been conducted in inland freshwater forested wetlands, which are often excluded from inventories of SOC stocks as well as research evaluating SOC persistence. Therefore, there is a research gap examining the abundance and persistence of MAOM-C in forested wetlands compared to other landscape classes. We measure the MAOM-C and MAOM-$\Delta^{14}C$ across different hydropedologic units (HPUs): forested wetlands (FWL), dry uplands (DUP), wet uplands (WUP), and alluvial (ALV) soils and show that FWL have deeper mineral soils, contain similar bulk SOC content, and lower Fe content than other HPUs. These measurements are consistent with a lower MAOM-C and potentially lower MAOM-C saturation in FWL. However, we also find significantly older MAOM-$\Delta^{14}C$ in forested wetlands compared to all other HPUs. Modeling shows that, Depth, pH, and total Fe content drive the older MAOM-$\Delta^{14}C$. Further research should investigate the potential MAOM-C composition difference among wetlands and uplands to discern the makeup of a particularly persistent SOC pool.

Introduction

Inland freshwater wetlands store 30% of the global soil organic carbon (SOC) in only 6-8% of the terrestrial land surface, making them targets for monitoring potential terrestrial carbon transfers to the atmosphere (Scharlemann et al. 2014). The anoxic conditions in wetlands due to prolonged water inundation and saturation inhibit aerobic oxidation of soil organic matter (SOM) and leads to SOC accumulation (Mitsch and Gosselink 2015). The wetland SOC pool can shift from a carbon sink to a source due to changing environmental conditions such as reduced precipitation and increased temperature which alter the patterns of wetland hydrology and reduce soil inundation and saturation (Fellman et al. 2017; Miao et al. 2017). While seasonally saturated wetlands without prolonged inundation still hold significant SOC stocks (Tangen and Bansal 2020; Davidson et al. 2022; Stewart et al. 2024), it is uncertain how persistent or vulnerable these SOC stocks are to further impending climate changes.

SOM persistence is governed by a combination of physical inaccessibility, association with minerals and metals, abiotic environmental factors, biochemical diversity, and microbial diversity (Schmidt et al. 2011; Kleber et al. 2015; Lehmann and Kleber 2015). Mineral associated organic matter (MAOM) is more persistent than particulate organic matter (POM) due to the stabilizing effect of binding to soil minerals and metals which offers protection from microbial decomposition (Torn et al. 1997; Kögel-Knabner et al. 2008; Lavallee et al. 2020; Heckman et al. 2021). MAOM and POM have been operationally defined by Lavallee et al. (2020) where MAOM is defined as SOM associated with minerals, with a size smaller than 50-53 μm, and a density greater than 1.65-1.85 g cm^{-3}. POM on the other hand, has a size greater than 50-63 μm and a density lower than of a 1.65-1.85 g cm^{-3}. POM is often considered "less microbially processed" and derived from larger structural components of plant tissues, whereas MAOM is "more microbially processed" composed of small, plant and microbially-derived compounds sorbed directly to mineral surfaces (Lehmann

and Kleber 2015; Cotrufo et al. 2022; Rocci et al. 2024). The lack of mineral associations for POM contributes to its short persistence and vulnerability to microbial decomposition (Heckman et al. 2021; Rocci et al. 2021).

For inland freshwater wetlands, the majority of SOM and the SOC stock can be mostly composed of POM which accumulates on top of the mineral soils (Kayranli et al., 2010). The dominance of POM differentiates wetlands from uplands where MAOM often contains most of the SOC stock (Lavallee et al. 2020). Therefore, the SOC within MAOM or MAOM-C is likely to be more persistent in uplands whereas the larger proportion of SOC held in the POM fraction for wetland SOC stocks may indicate more vulnerability to decomposition (Fellman et al. 2017). However, mineral soil wetlands and the mineral soils under organic horizons in wetlands can still contain substantial amounts of SOC (Davidson et al. 2022) which has the potential to form MAOM and MAOM-C and can constitute a large percentage of the SOC stock (Wang et al., 2014). But the persistence of MAOM-C in wetlands soils is only recently explored in soil science persistence research, and measures of the carbon persistence for wetland MAOM-C are rare (Mirabito and Chambers 2023).

The persistence of this MAOM-C, as measured by radiocarbon dating (MAOM-$\Delta^{14}C$), can vary depending on soil factors such as pH, mineral type, oxygen availability, and moisture (Heckman et al. 2021; Rocci et al. 2024). In upland soils, it has been well established that smaller organic compounds along with fine soil particles (i.e. clay and silt) and Fe and Al oxides combine to constitute a significant proportion of the MAOM-C pool (Kögel-Knabner et al. 2008; Kleber et al. 2015; Lehmann and Kleber 2015). Particularly, the presence of short-range order and poorly crystalline Fe minerals can greatly contribute to MAOM formation (Kleber et al., 2005; Kögel-Knabner et al. 2008). However, fluctuating redox conditions in humid tropical upland soils have

been shown to alter MAOM formation where Fe in reducing conditions acts as a prominent electron acceptor facilitating anaerobic metabolism in Fe and SOC rich soils (Bhattacharyya et al. 2018; Anthony and Silver 2020; Huang et al. 2020). The reduced form of Fe (Fe(II)) is also water soluble and mobile in saturated soils compared to the oxidized Fe(III), a process which could potentially destabilize MAOM in wetland soils by facilitating anaerobic decomposition (Chen et al. 2020). These processes have mostly been evaluated in upland soils in humid climates or with induced anoxic conditions (Huang et al. 2020; Lacroix et al. 2022) but they have implications for MAOM-C and MAOM-Δ^{14}C in the wetland mineral soil matrix. Research evaluating both MAOM-C and MAOM-Δ^{14}C and their drivers in wetlands is very fragmented and often contains measurements of MAOM-C content only. Moreover, there are fewer which contrast wetland observations with uplands. Hence, there is a clear need to evaluate both MAOM-C abundance MAOM-Δ^{14}C in wetland soils with comparisons to upland soils to evaluate changes in drivers.

Our aim with this study is to evaluate how MAOM-C varies across soils in a hydrologic gradient in a forested landscape going across Dry Uplands, Wet Uplands, Forested Wetlands, and Alluvium soils. Each landscape class corresponds to distinct hydropedological units which have different hydrologic regimes that influence their soil development. We will evaluate the variation in MAOM-C and MAOM-Δ^{14}C across these classes and identify the significant drivers. Our hypotheses include: 1) MAOM-C content and MAOM-Δ^{14}C should be lower and younger, respectively, in Forested Wetlands compared to other hydropedological classes, especially dry uplands; 2) We expect poorly crystalline Fe, depth, and clay content to be the strongest drivers of MAOM-C abundance with depth and poorly crystalline Fe to be the strongest drivers of MAOM-C persistence.

Methods

Study Area

We conducted field sample collection in the Heen Latinee Experimental Forest (HLEF) (Figure 3.1) located in Southeast Alaska near the city of Juneau. The HLEF has a mean annual precipitation of approximately 2284 mm and a mean annual temperature of 4.3°C. Topography and geomorphology of the watershed contains hillslopes, valleys, alluvial floodplains, and glacial deposits. The elevation stretches from a river outlet into the ocean to mountainous glaciers, spanning approximately 0-1800 m. Spinola et al. (2022) described the lithology containing slate, metavolcanic, phyllite, and tonalite. Forest vegetation comprises of a mix of Western Hemlock (*Tsuga heterophylla*), and Sitka Spruce (*Picea sitchensis*) with small amounts of Yellow Cedar (*Cupressus nootkatensis*). The watershed is mostly upland forest but also contains numerous wetlands with fens, bogs, riparian, and freshwater forested wetlands.

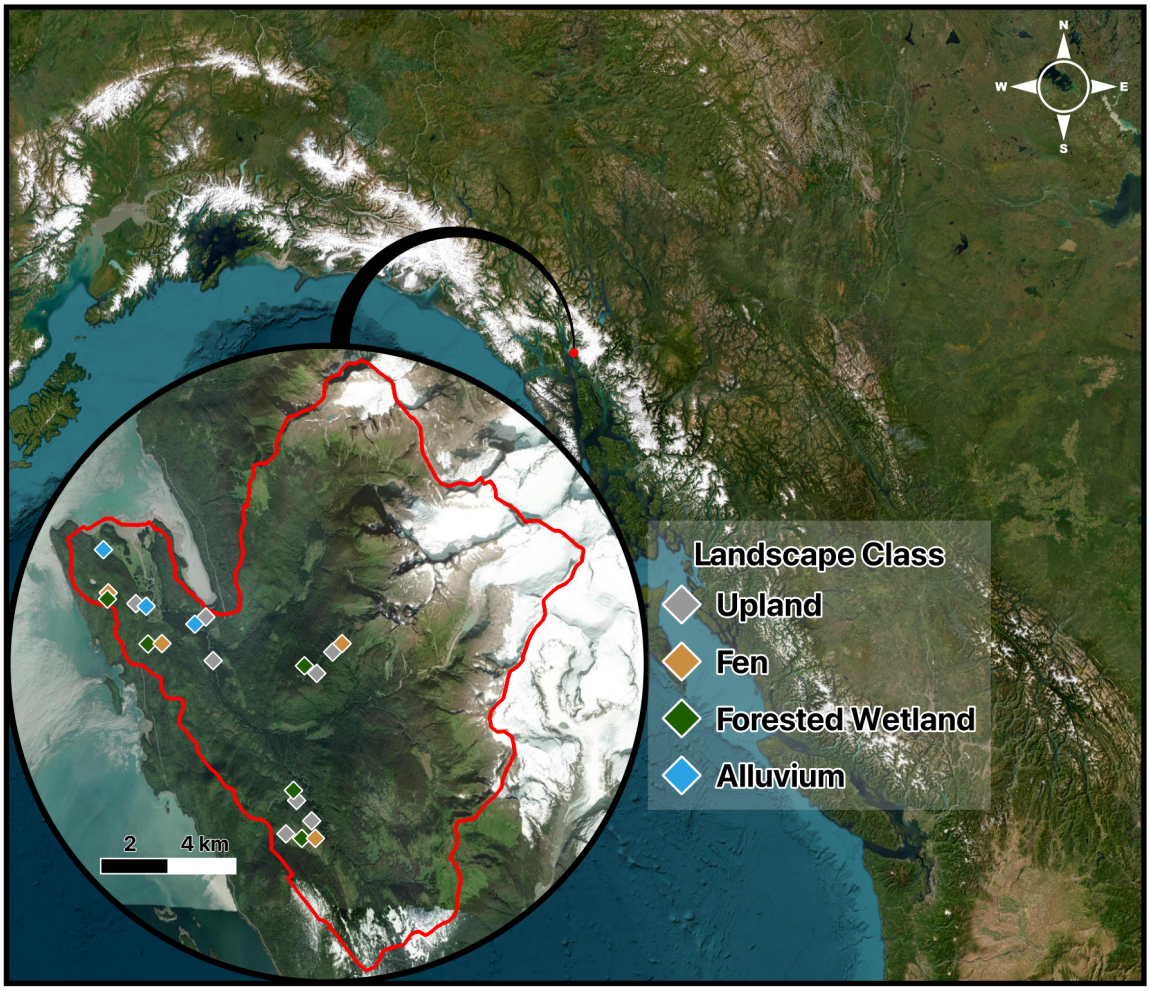

Figure 3.1 The Heen Latinee Experimental Forest (HLEF) study watershed located in the Pacific Northwest of North America in Southeast Alaska. Diamond symbols represent sample pedon locations and colors show the different landscape classes sampled.

Field Sample Collection

Field sampling occurred during the summer of 2022. We stratified the sample pedon locations across a soil wetness gradient within the HLEF (Figure 3.1). Sample pedon locations were classified in the field and post-hoc using information gathered on landform, soil hydric properties, vegetation, and hydrology. We adopted the hydropedology definition from Gannon et al. (2014) where hydropedological units are defined as "a grouping of variations in soil morphology that directly relate influence of water table regime, flow paths, and saturation to soil development." We then adapted this definition and the classification used by D'Amore et al. (2015a) to create four high

level hydropedological classes: Dry Upland (DUP), Wet Upland (WUP), Forested Wetland (FWL), Fen (FEN), and Alluvium (ALV). The FEN, FWL, and ALL represent different wetland types according to the hydropedological approach informed by D'Amore et al. (2015a), as well as the United States Department of Agriculture Natural Resources Conservation Service Field Indicators for Hydric Soils (United States Department of Agriculture, Natural Resources Conservation Service 2018). ALV soils were classified based on the location within a floodplain and the presence of several stratified soil horizon layers with low soil color values and chroma (value ≤3, chroma ≤1). FWL and FEN were both classified based on Histosol features with organic horizons ≥40 cm at the surface. FEN were classified based on the presence of peat/fibric organic matter instead of the muck/sapric material in FWL. The classification of an upland soil pedon as either dry or wet was based on soil features that indicated the drainage class as either "somewhat poorly drained" or "poorly drained", respectively, as the HLEF is situated in a persistent rainfall climate. DUP exhibited signs of somewhat poorly drained with nearly continuous rainfall and free water occurring in shallow soil horizons. WUP showed signs of poorly drained soils with a much higher water table than DUP indicated by the presence of redoximorphic features in the B horizons as well as a moderately thick organic layer that was below the threshold for histosols (40 cm) but larger than the typical DUP (approximately 10 cm). For wetlands, we emphasize that jurisdictional definitions of wetlands may differ than the classification applied here, and we are not classifying these locations as jurisdictional wetlands.

Pedons were dug to at least 1 m or more depending on restricting layers such as rock or hard till. We characterized soil pedon horizon morphology, soil color, root and coarse fragment composition, and noted redoximorphic features. We then extracted samples in each pedon by horizon, sampling from the center of the depth interval going down to the deepest depth. We collected samples from both organic and mineral soil horizons. Bulk density samples were collected

via a circular polyvinyl chloride corer to extract samples in a set volume. Extra care was taken to not compress soil bulk density samples, especially for more organic layers. We collected bulk soil samples separately from bulk density to be used in further laboratory analysis.

Laboratory Analysis

Bulk Soil

We processed bulk soil samples by drying to a constant weight at 40°C then sieving through a 2 mm mesh removing coarse fragments, roots, and organic debris. We then sent samples of the <2 mm fraction for both mineral and organic samples to be analyzed for carbon concentration (SOC mg g^{-1}), nitrogen concentration (N%), pH, and particle size (Clay%, Silt%, and Sand%) at the Oregon State University Soil Health Laboratory. In one sample, soil N% was measured as 0% and was replaced with a 0.005, which was the detection limit of 50 ppm in the Elementar Vario Macro Cube.

We conducted dithionate-citrate and ammonium-oxalate extractions on the bulk soil to analyze for concentrations of Fe and Al using inductively coupled plasma mass spectrometry (ICP-MS) at Lawrence Livermore National Laboratory. The dithionate-citrate extraction for Fe (Fe_{DC}) extracts both crystalline and poorly crystalline, or total pedogenic Fe oxides and for Al (Al_{DC}) it extracts Al substituted in Fe oxides. Ammonium-oxalate extractions for Fe (Fe_{AO}) extracts poorly crystalline Fe from aluminosilicates as well as total pedogenic Al (Al_{AO}) (Kleber et al., 2005; Spinola et al., 2022). In brief, the dithionate-citrate extraction was conducted using a 0.75 g bulk soil sample submerged and shaken in a solution of 0.57 M sodium citrate solution with an added 0.40 g of sodium dithionate powder. The ammonium-oxalate extraction used a 0.50 g bulk soil sample that was submerged in a 0.2 M ammonium-oxalate solution which was adjusted to a pH of 3.0 ± 0.05 using oxalic acid. The ammonium-oxalate extraction process was conducted using 50 mL conical tubes covered in aluminum foil to block any light from interfering with the extraction. Both extracts

were filtered using a 0.45 μm glass microfiber syringe filter. A 100 μm aliquot of extract was then subjected to a 1:1 treatment with H_2O_2 and then diluted to a 1:150 solution using 14.8 mL of 0.1 N HNO_3 with 0.002% HF before analysis on the ICP-MS. The ppm measurement from the ICP-MS was then converted to mg g^{-1} for analysis.

Density and Size Fractions

We conducted density and size fractionation on the mineral soil samples at the University of Washington to determine the amount of free particulate organic matter (fPOM), occluded particulate organic matter (oPOM), and MAOM (Sollins et al. 2009). A 15 g sample of the <2 mm fraction was submerged and shaken within a 1.65 g cm^{-3} solution of sodium polytungstate (SPT) to separate the floating fPOM from the rest of the sample. After the fPOM was collected, we subjected the remaining soil sample in SPT to sonication for 2 min and 30 sec at 100% power with a 3 sec pulse on and 5 sec pulse off. The sonication was performed in an ice-filled beaker and these sonicator settings ensured the sample reached at least 75-100 J/mL after which we collected the oPOM which floated to the top of the SPT solution. The remaining soil sample after fPOM and oPOM collection was subjected to wet sieving with a 0.53 μm sieve. The fine material collected after sieving was considered MAOM and was rinsed thoroughly to remove remaining SPT then dried to a constant mass.

The MAOM soil fraction was then transported to Lawerence Livermore National Laboratory for subsequent analysis which included analysis for MAOM C% and N% using a Vario Elemental Analyzer. $\Delta^{14}C$ measurements on the MAOM fraction were conducted at the Center for Accelerator Mass Spectrometry as per McFarlane et al. (2013) procedures. The $\Delta^{14}C$ was adjusted using measured $\partial^{13}C$ values for mass-dependent fractionation and corrected to the year of measurement (2022). We present the analysis for the MAOM fraction only and did not analyze the POM or oPOM fractions due to limited sample mass during the extractions.

Statistical analysis

Our initial statistical analysis examined bulk soil measurements and metal extract concentration differences between HPU classes using generalized linear mixed models and a Tukey Honest Significant Difference (HSD) test using the *lme4* (Bates et al. 2015), *car* (Fox and Weisberg 2019), and *emmeans* (Lenth 2024) packages in R version 4.3.3 Angel Food Cake. Models were evaluated for linearity, constant variance, and normal error distributions. The generalized linear mixed models used a Gamma family distribution and a *log* link function after examining all response variables fit the log-transformed normal distribution. A Gaussian distribution with identity link was used for MAOM-Δ^{14}C. The sample location as a random effect to account for the multiple profile observations. All models were examined for conforming to assumptions of homogeneity of variance, linearity of the response, and normality of the random effects. We also tested for significant outliers using Cooks Distance and leverage, but deemed all observations sufficient to be kept in the model datasets. Significant differences between HPU classes were determined by $p < 0.05$ from the *emmeans* Tukey HSD test.

We next tested the effect of HPU, bulk soil measurements, and metal extracts on the MAOM-C content and MAOM-Δ^{14}C age using generalized linear mixed models with a similar structure: Gamma family distribution with a *log* link for MAOM-C and Gaussian family distribution with identify link for MAOM-Δ^{14}C, which is a normal linear mixed model. Sample location was also designated as a random effect. Each bulk soil measurement and metal extract concentration was tested in a separate model as an interaction term with HPU and significant predictors were indicated using Type III Wald Chi-Square tests.

Partial correlation analysis was conducted using the *ppcor* package (Kim 2015) and compared to the zero-order correlation for changes in the correlation coefficient after controlling for a set of

variables. We tested if MAOM-C and MAOM-$\Delta^{14}C$ correlations with bulk soil measurements changed after controlling for soil metal extracts and vice-versa. While we note the significance of a correlation with a p-value <0.05, we also consider changes in the correlation coefficient to be significant if they differed by an absolute value of 0.2.

A final pair of linear mixed models were composed for predicting MAOM-C and MAOM-$\Delta^{14}C$ with a combination of bulk soil measurements and soil metal extracts. Similar to previous linear models, a generalized linear mixed model with a Gamma distributed log-link was used for MAOM-C, and a normal linear mixed effect model was used for MAOM-$\Delta^{14}C$. Both models underwent parsimonious predictor selection, with final model selection based on achieving the lowest Akaike's Information Criterion (AIC) while using the fewest predictors. Predictor importance was assessed using a Type III Wald chi-square test. Model prediction strength was assessed through marginal and conditional R^2 where the marginal R^2 represents the variation accounted for in the fixed effects and the conditional R^2 represents the variation accounted for in the random effects.

Results

Bulk soil and metal extract variation among hydropedological units (HPUs)

Bulk soil measurements were largely similar across the different HPUs, except for SOC content and Depth (Figure 3.2). For bulk soil SOC content, ALV soil was significantly lower than DUP soil, with intermediate SOC content for WUP and FWL, according to the pairwise comparisons in a post-hoc Tukey-HSD test ($p < 0.05$; Figure 3.2). The distribution of mineral soil horizon depths within soil pedons were deepest on average in FWL and ALV HPUs compared to DUP (Figure 3.2). There were no significant differences between the means for both Clay% and pH where ALV had a slightly lower Clay% and FWL had a slightly higher pH compared to other HPUs (Figure 3.2).

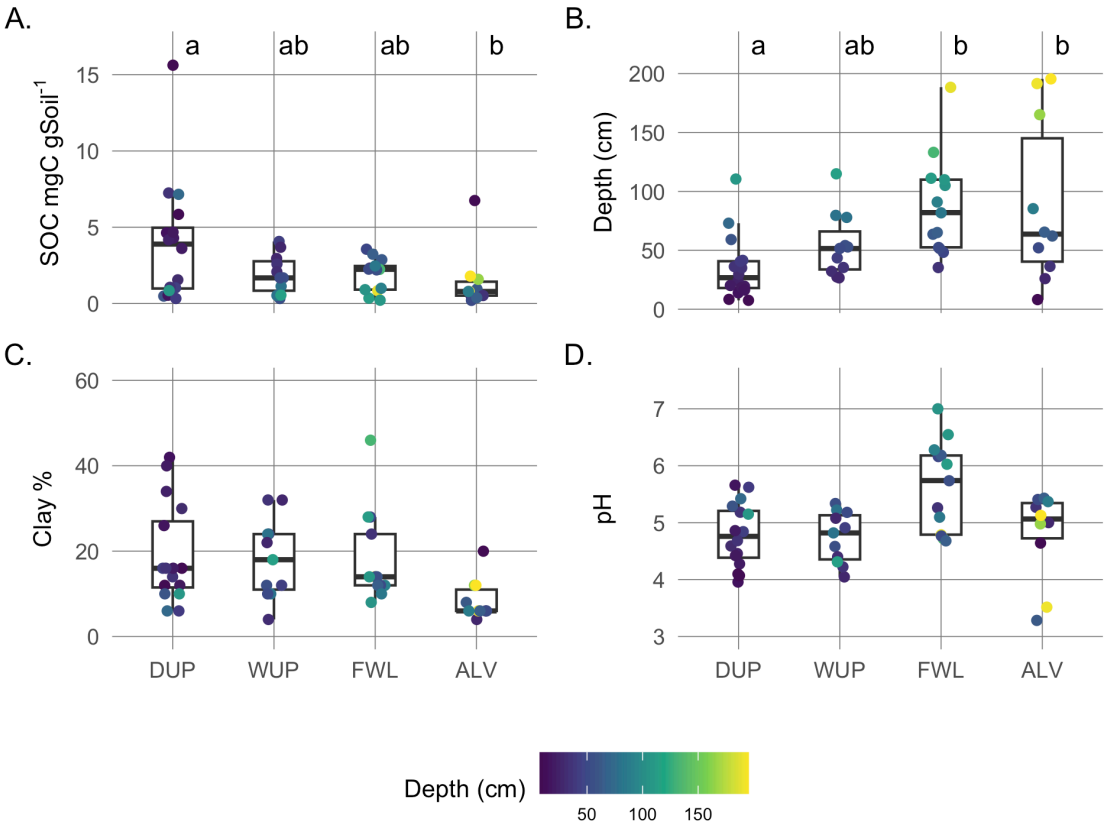

Figure 3.2 Differences between hydropedological units (HPUs): DUP = Dry Upland, WUP = Wet Upland, FWL = Forested Wetland, and ALV = Alluvium for bulk soil properties **A.)** Soil organic carbon (SOC) content, **B.)** Depth of sample, **C.)** Clay% content, and **D.)** soil pH. Lowercase letters denote significance between HPU groups in a linear mixed model using a Tukey HSD test with pairwise comparisons for each bulk soil measurement (on the y-axis). Similar letters within each measurement indicate statistical similarity ($p>0.05$). Different letters indicate statistical difference ($p<0.05$) No lettering means no significant effects between HPU groups. Points are colored by soil sampling depth

Measurements of both Fe_{DC} and Fe_{AO} showed more variability than the Al_{DC} and Al_{AO} between HPUs (Figure 3.3). An ANOVA with a Type II Wald Chi-square test showed HPU was a significant effect on Fe_{DC} and Fe_{AO} ($p <0.05$) with Tukey HSD pairwise comparisons identifying significantly lower Fe in the FWL compared to other HPUs, except for Fe_{AO} between FWL and ALV (Figure 3.3). Fe_{DC} was higher than Fe_{AO} in DUP and WUP soils but lower or approximately equal in FWL and ALV, respectively. For Al, HPU was a significant factor for Al_{DC} but not for Al_{AO} (Figure 3.3) and a Tukey HSD test only identified significantly lower Al_{DC} in ALV compared to DUP. Overall, Al_{AO} was higher than Al_{DC} for all HPUs.

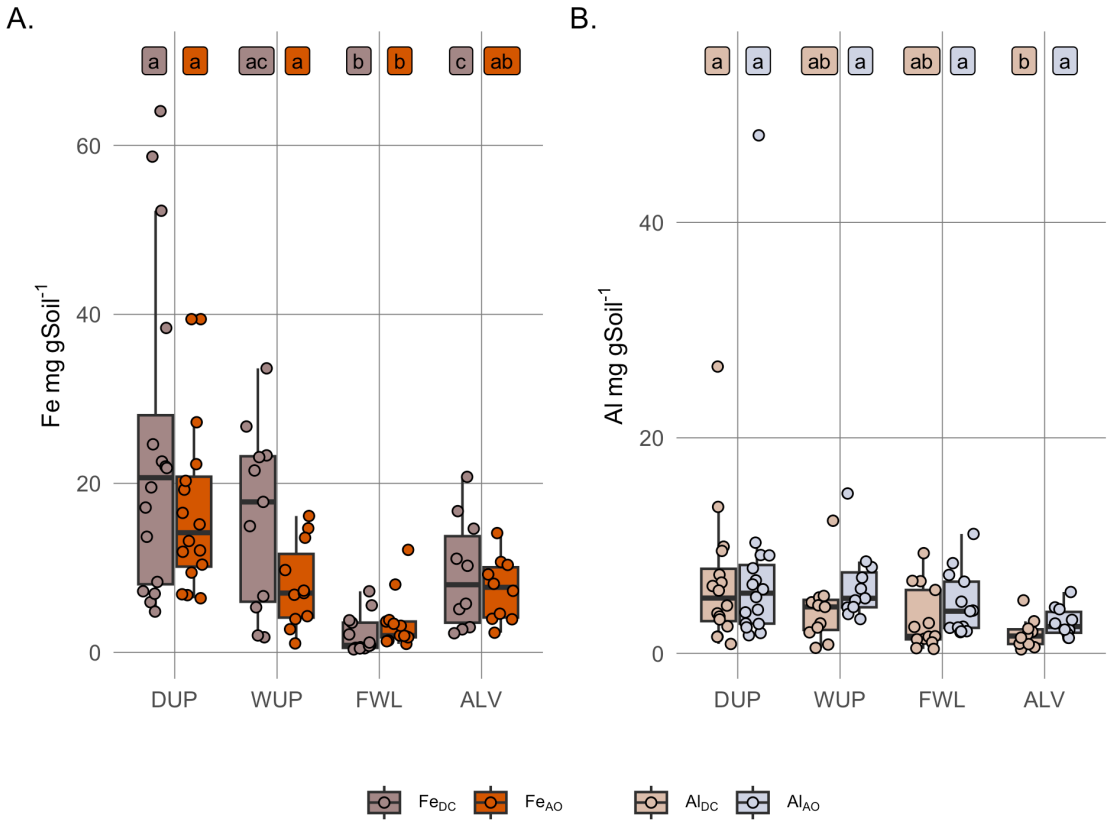

Figure 3.3 Differences between hydropedological units (HPUs): DUP = Dry Upland, WUP = Wet Upland, FWL = Forested Wetland, and ALV = Alluvium for dithionate-citrate (DC) and ammonium-oxalate (AO) extractable metals. **A.)** Iron (Fe) content and **B.)** Aluminum (Al) content. Lowercase letters denote significance between HPU groups in a linear mixed model using a Tukey HSD test with pairwise comparisons for each soil metal extract type. Only similar metals and similar extracts were compared. For example Fe_{DC} was compared to other HPU Fe_{DC}. Similar letters within each measurement indicate statistical similarity ($p>0.05$). Different letters indicate statistical difference ($p<0.05$) No lettering means no significant effects between HPU groups.

MAOM-C content and MAOM-Δ^{14}C variation across HPUs

MAOM-C content varied by HPU type and Depth (Figure 3.4). The FWL HPU had significantly lower MAOM-C content compared to the DUP but was similar to both the WUP and ALV (Figure 3.4). The HPU effect on MAOM-C was also influenced by Depth which was indicated by a significant interaction term in the ANOVA test. The interaction between Depth and HPU showed that FWL and ALV had flat slope relationships with Depth and MAOM-C compared to strong negative slopes for DUP and WUP (Figure 3.4). Overall, MAOM-C content decreased with depth in all HPUs except for ALV.

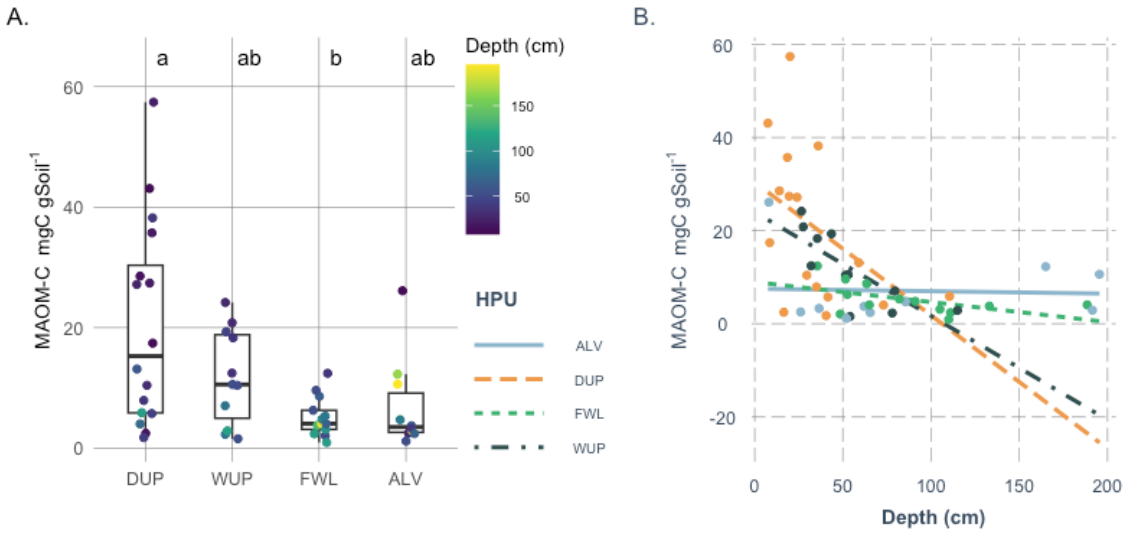

Figure 3.4 Boxplot **A.)** of MAOM-C content between different hydropedological units (HPUs): DUP = Dry Upland, WUP = Wet Upland, FWL = Forested Wetland, and ALV = Alluvium. **B.)** MAOM-C content as a function of depth and with an interaction of HPU.

While MAOM-C content was lower in FWL, MAOM-Δ^{14}C was significantly older in the FWL compared to all other HPUs indicated by a significantly more negative Δ^{14}C value (Figure 3.5). The mean MAOM-Δ^{14}C age of the DUP, WUP, and ALV was approximately 2,500 years old while the mean MAOM-Δ^{14}C age of the FWL was 8,300 years old. Two observations were over 20,000 years old in both FWL and DUP. HPU and Depth also had a significant interaction when predicting MAOM-Δ^{14}C (Figure 3.5). Depth had the strongest effect on MAOM-Δ^{14}C in the WUP and FWL compared to the other HPU classes where age increased with greater depth.

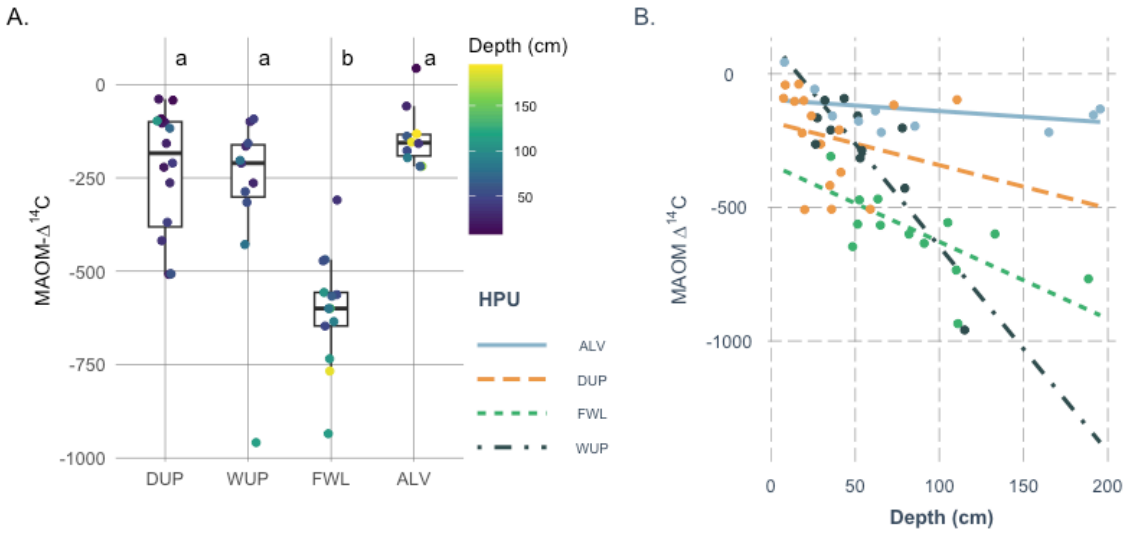

Figure 3.5 A.) Boxplot measurements of MAOM-$\Delta^{14}C$ between different hydropedological units (HPUs): DUP = Dry Upland, WUP = Wet Upland, FWL = Forested Wetland, and ALV = Alluvium. Lowercase letters denote significance in a linear mixed model with HPU as an additional effect. No lettering means no significant effects. **B.)** MAOM-$\Delta^{14}C$ as a function of depth and with an interaction of HPU.

The ratio of whole profile SOC stocks to MAOM-C stocks by HPU showed that FWL had the lowest MAOM-C:SOC stock ratio compared to the other HPUs (Figure 3.6). Both ALV and DUP were similar to each other both statistically and in the range of variation. However, there are only 2-4 observations per HPU since all samples in pedons were summed to estimate full pedon MAOM and SOC stocks. Therefore, significant differences should be interpreted carefully. Consistent with the patterns shown in Figure 3.4 and Figure 3.5, MAOM-C content was significantly related to MAOM-$\Delta^{14}C$ with a weak positive relationship (Figure 3.6; $p = 0.036$). The MAOM-C to bulk SOC content ratio was not significantly related to MAOM-$\Delta^{14}C$ (Figure 3.6C). For both MAOM-C and the MAOM-C to bulk SOC content ratio, the FWL was uniquely clustered in the graph space compared to other HPUs.

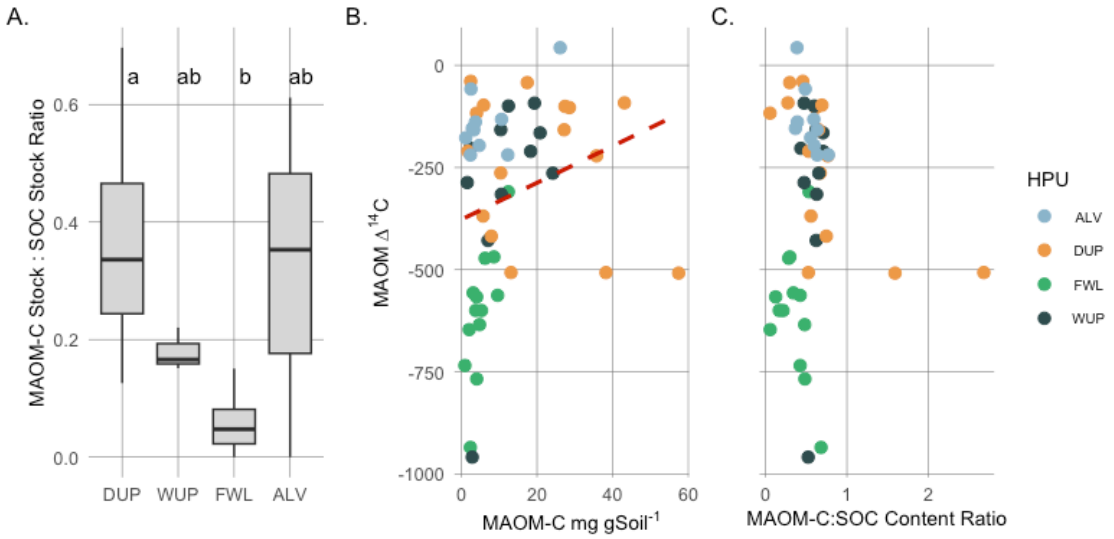

Figure 3.6 A.) Boxplot showing MAOM-C stock to SOC stock ratio within the different hydropedological units (HPUs): DUP = Dry Upland, WUP = Wet Upland, FWL = Forested Wetland, and ALV = Alluvium. Letters denote significant differences calculated from pairwise comparisons using a Tukey HSD test. **B.)** Scatter plot of MAOM-$\Delta^{14}C$ vs. MAOM-C content in mg $gSoil^{-1}$ colored by different HPUs. **C.)** Scatter plot of MAOM-$\Delta^{14}C$ vs. the MAOM-C content to SOC content ratio colored by different HPUs.

MAOM-C content as a function of Silt+Clay in the HLEF shows many of the observed soils may be below the potential saturation threshold for "High" and "Low" mineral activity derived from the 95th quantile response between MAOM-C and Silt+Clay across global soils (Georgiou et al. 2022) (Figure 3.7). In particular, FWL soils appear to have a much weaker relationship with Silt+Clay compared to other HPUs, but especially DUP. MAOM-C content in the DUP HPU sometimes exceeded the 95th quantile calculated for HLEF soils as well as the "High" activity minerals in the global relationship. MAOM-C content in WUP and ALV had intermediate positive slopes in the relationship with Silt+Clay.

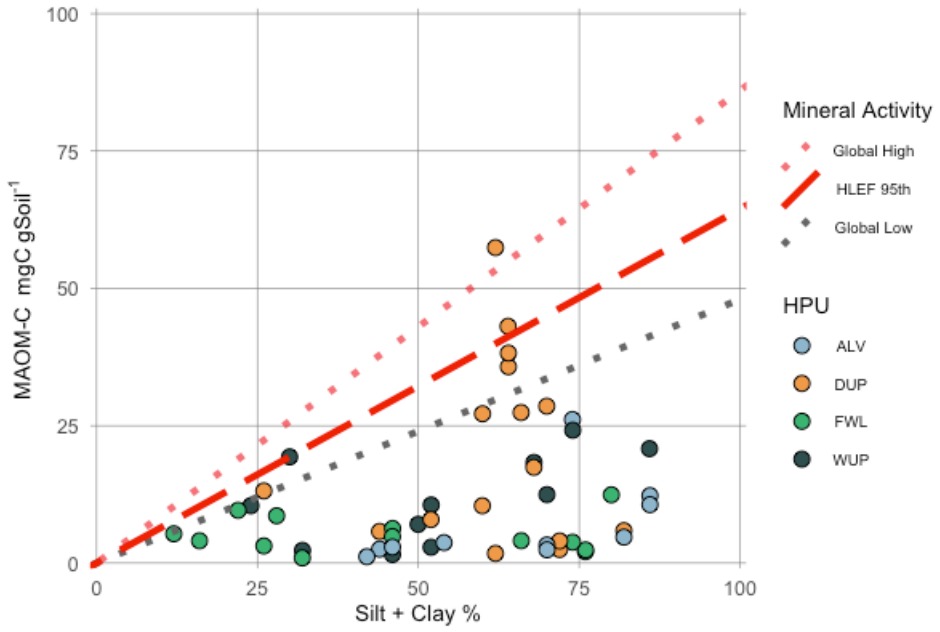

Figure 3.7 Estimated MAOM-C saturation using the 95th quantile linear relationship between Silt+Clay and MAOM-C content. High and Low mineral activity is derived from Georgiou et al., 2022.

Drivers of MAOM-C and MAOM-$\Delta^{14}C$

Relationships between bulk soil measurements and MAOM-C content showed a strong effect of bulk SOC content followed by Depth (Figure 3.8). Bulk SOC content had a strong positive correlation with MAOM-C while Depth had a negative correlation and accounted for less variability than SOC content. pH and Clay% followed Depth as the next strongest predictors with negative and positive correlations, respectively.

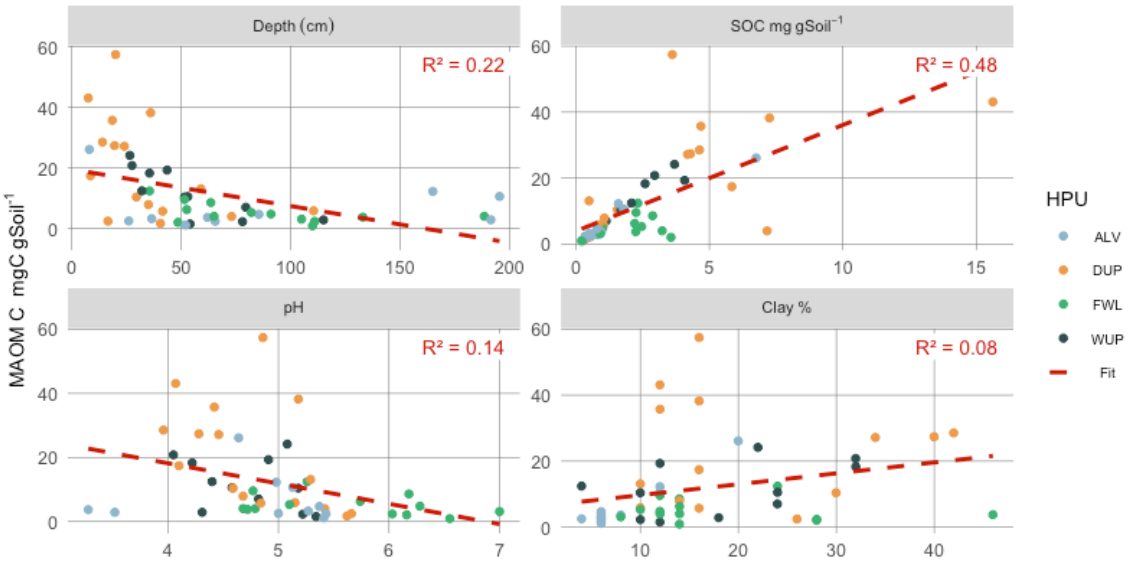

Figure 3.8: MAOM-C content relationships with bulk soil properties. Colors indicate HPU class. R^2 represents the fit in a univariate model between MAOM-C and the bulk soil measurement and is shown by the dashed red line

The relationships between extracted soil metals and MAOM-C content showed that both forms of Fe, Fe_{AO} and Fe_{DC}, had significant effects compared to both forms of Al (Figure 3.9). Al_{DC} accounted for a much lower amount of variation compared to Al_{AO}, both of which had positive correlations with MAOM-C content. $Fe_{AO,}$ accounted for similar variation compared to Fe_{DC}. Similar to Al, both forms of Fe had positive relationships with MAOM-C except for Fe_{AO} which was more strongly positively correlated with MAOM-C Al_{AO}. No extracted metal accounted for more variability than the bulk SOC content shown in Figure 3.8.

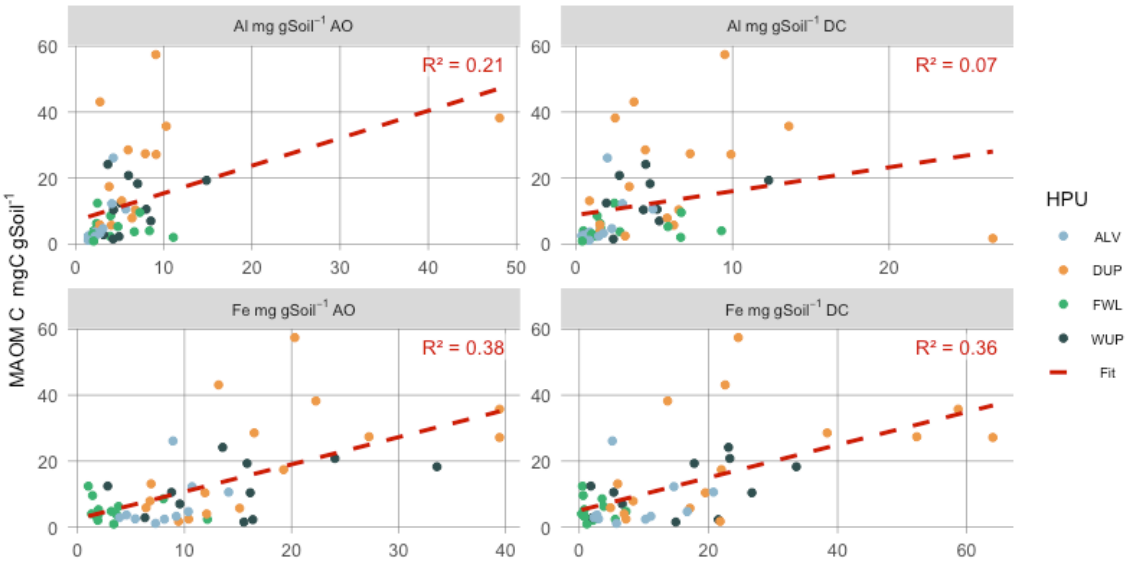

Figure 3.9: MAOM-C content relationships with extracted metals with Ammonium Oxalate (AO) and Dithionate Citrate (DC). Colors indicate HPU class. R^2 represents the fit in a univariate model between MAOM-C and the extracted metal and is shown by the dashed red line

Zero order correlations between MAOM-C content and single variables from bulk soil measurements and soil metal extracts showed that SOC content, pH, Fe_{DC}, and Fe_{AO} had some of the strongest correlation coefficients, all of which were positive. Partial correlations between MAOM-C and bulk soil measurements showed both ammonium-oxalate and dithionate-citrate extractions of Fe and Al greatly reduced the correlation strength and significance (Table 3.1). Controlling for both total (Fe_{DC} & Al_{AO}) and poorly crystalline (Al_{DC} & Fe_{AO}) significantly affected the correlations of Depth and Clay with MAOM-C, reducing the correlation strengths by approximately 50%. Correlations between MAOM-C and both forms of Fe and Al also appeared to be reduced by bulk soil properties, although changes in correlation strength significance were not as large proportionally. However, both the Fe extract correlations (Fe_{DC} & Fe_{AO}) were reduced by nearly 40% after controlling for bulk soil properties. Specifically controlling for Depth and pH contributed to most of the correlation strength decline.

Table 3.1: Zero order and partial correlation estimates between predictors and MAOM-C. Zero order correlation coefficients and p-values are Pearson correlation coefficients between MAOM-C and Predictor only. The partial correlation estimates are calculated as between the Predictor and MAOM-C while controlling for the Controlled Variables. Zero-Order and Partial-Correlation shows how much effect the Controlled variables have on the Predictor-MAOM-C relationship.

	Predictor	Zero Order Correlation Coef.	Zero Order P-value	Controlled Variables	Partial Correlation Coef.	Partial Correlation P-value
MAOM-C mg gSoil^{-1}	Depth	-0.42	0.002	Fe_{DC} mg gSoil^{-1}, Al_{AO} mg gSoil^{-1}	-0.24	0.104
	SOC mg gSoil^{-1}	0.64	0.000		0.54	0.000
	pH	-0.47	0.001		-0.39	0.007
	Clay%	0.33	0.019		0.13	0.387
	Depth	-0.42	0.002	Fe_{AO} mg gSoil^{-1}, Al_{DC} mg gSoil^{-1}	-0.30	0.041
	SOC mg gSoil^{-1}	0.64	0.000		0.56	0.000
	pH	-0.47	0.001		-0.41	0.004
	Clay%	0.33	0.019		0.21	0.146
	Fe_{DC} mg gSoil^{-1}	0.57	0.000	Depth, SOC mg gSoil^{-1}, pH, Clay%	0.36	0.013
	Al_{AO} mg gSoil^{-1}	0.41	0.003		0.30	0.044
	Fe_{AO} mg gSoil^{-1}	0.56	0.000		0.38	0.010
	Al_{DC} mg gSoil^{-1}	0.22	0.132		0.12	0.417

Fe_{DC} mg gSoil^{-1} and Al_{AO} mg gSoil^{-1} represent the total soil extracted metals while Fe_{AO} mg gSoil^{-1} and Al_{DC} mg gSoil^{-1} represent the poorly crystalline metals.

Relationships between MAOM-Δ^{14}C, bulk soil measurements, and soil metal extracts showed larger variability than the MAOM-C content (Figure 3.10). Depth and pH accounted for the most variability in MAOM-Δ^{14}C while SOC and Clay% did not account for much variation. Depth and pH both had negative correlations with MAOM-Δ^{14}C showing that older MAOM-C was found at deeper depths and at higher pH. Bulk SOC content had a weak positive correlation with MAOM-Δ^{14}C and there was almost no apparent slope in the Clay% and MAOM-Δ^{14}C relationship.

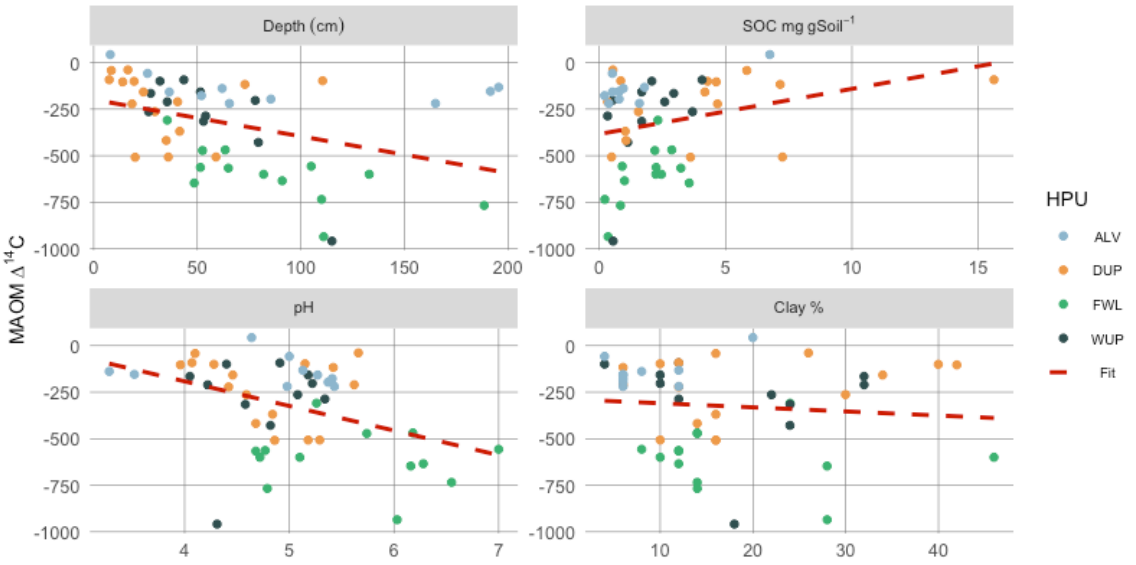

Figure 3.10: MAOM-Δ^{14}C relationship with bulk soil measurements. Colors indicate HPU class. R^2 represents the fit in a univariate model between MAOM-C and the bulk soil measurement and is shown by the dashed red line

Variability was similarly large for MAOM-Δ^{14}C with extracted metals (Figure 3.11). Both Al_{DC} and Al_{AO} did not account for any significant variability and had minimal slopes, indicating weak if any correlation direction. Conversely Fe_{DC} and Fe_{AO} accounted for moderate variability, with Fe_{DC} having a slightly higher R^2 and both having positive correlations with MAOM-Δ^{14}C.

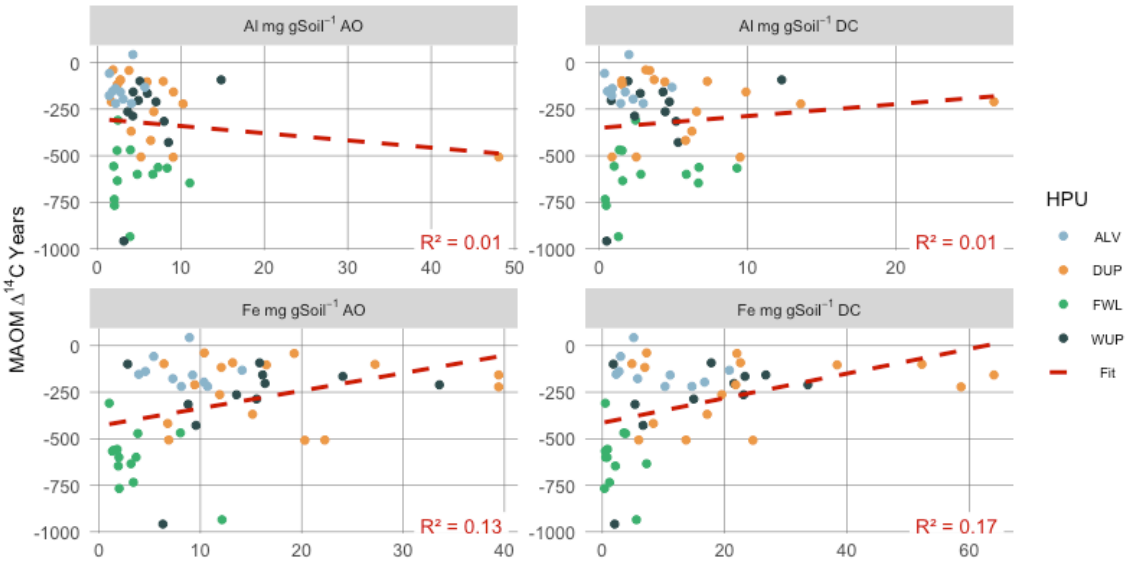

Figure 3.11: MAOM-Δ^{14}C relationship with Ammonium Oxalate (AO) and Dithionate-Citrate (DC) soil metal extracts. Colors indicate HPU class. R^2 represents the fit in a univariate model between MAOM-C and the soil extract and is shown by the dashed red line

The zero order correlations between MAOM-Δ^{14}C and single variables showed Fe_{DC}, pH, Depth, and Fe_{AO} had the higher correlation coefficients (Table 3.2). Partial correlation between MAOM-Δ^{14}C age and bulk soil measurements while controlling for the concentrations of extracted metals showed small decreases in correlation coefficients compared with the zero order correlation coefficient in Depth, SOC content pH and Clay% (Table 3.2). However, unlike MAOM-C content, partial correlations increased after controlling for the metal extract concentrations for Clay%, although the partial correlation coefficients were not significant. Examining the partial correlations of MAOM-Δ^{14}C age and metal extract concentrations showed Fe and Al were moderated by bulk soil measurements. Interestingly, Fe_{DC}, Fe_{AO}, and Al_{DC} correlations decreased while Al_{AO} correlation increased once bulk soil properties were controlled.

Table 3.2: Zero order and partial correlation estimates between predictors and MAOM-$\Delta^{14}C$ age. Zero order correlation coefficients and p-values are Pearson correlation coefficients between MAOM-$\Delta^{14}C$and Predictor only. Comparing the difference between the Zero-Order and Partial-Correlation shows how much effect the Controlled variables have on the Predictor-MAOM-$\Delta^{14}C$ relationship.

	Predictor	Zero Order Correlation Coef.	Zero Order P-value	Controlled Variables	Partial Correlation Coef.	Partial Correlation P-value
MAOM-$\Delta^{14}C$	Depth	-0.39	0.005	Fe_{DC} mg gSoil^{-1}, Al_{AO} mg gSoil^{-1}	-0.31	0.034
	SOC mg gSoil^{-1}	0.27	0.060		0.23	0.114
	pH	-0.40	0.004		-0.32	0.028
	Clay%	-0.09	0.516		-0.27	0.061
	Depth	-0.39	0.005	Fe_{AO} mg gSoil^{-1}, Al_{DC} mg gSoil^{-1}	-0.32	0.026
	SOC mg gSoil^{-1}	0.27	0.060		0.18	0.229
	pH	-0.40	0.004		-0.35	0.014
	Clay%	-0.09	0.516		-0.20	0.172
	Fe_{DC} mg gSoil^{-1}	0.41	0.003	Depth, SOC mg gSoil^{-1}, pH, Clay%	0.32	0.031
	Al_{AO} mg gSoil^{-1}	-0.11	0.455		-0.22	0.134
	Fe_{AO} mg gSoil^{-1}	0.30	0.031		0.20	0.190
	Al_{DC} mg gSoil^{-1}	0.12	0.411		-0.01	0.960

Fe_{DC} mg gSoil^{-1} and Al_{AO} mg gSoil^{-1} represent the total soil extracted metals while Fe_{AO} mg gSoil^{-1} and Al_{DC} mg gSoil^{-1} represent the poorly crystalline metals.

Feature selection during prediction model building for both MAOM-C and MAOM-$\Delta^{14}C$ identified Fe_{DC} as a significant predictor (Table 3.3). MAOM-C content was largely driven by SOC content and included pH as the smallest significant predictor. For MAOM-$\Delta^{14}C$, Depth was the largest significant predictor after feature selection during model building followed by pH, and Fe_{DC}. Clay was included in the final model but was not significant ($p > 0.05$). Fe_{DC} was selected over Fe_{AO} during feature selection, as models with Fe_{DC} performed better than models with Fe_{AO}. This was also true for the ratio of Fe_{AO}:Fe_{DC}.

Table 3.3: Table of linear mixed model predictors used to predict MAOM-C content and MAOM-$\Delta^{14}C$ age.

	Marginal R^2	Conditional R^2	Predictor	Chi-square Value	P-value
MAOM-C mg $gSoil^{-1}$	0.607	0.684	SOC mg $gSoil^{-1}$	18.094	0*
			Fe_{DC} mg $gSoil^{-1}$	6.995	0.008*
			pH	4.574	0.032*
MAOM-$\Delta^{14}C$	0.41	0.645	Depth	12.614	0*
			pH	6.400	0.011*
			Fe_{DC} mg $gSoil^{-1}$	4.967	0.026*
			Clay%	3.182	0.074

'*' denotes significance with a type III ANOVA chi-square test.

Discussion

FWL soils hold significant amounts of SOC (Stewart et al. 2024). However, much of this SOC is stored in the POM fraction of SOM, which is potentially more vulnerable to enhanced microbial decomposition from temperature and moisture changes (Fellman et al. 2017). Therefore, characterizing the MAOM fraction of FWL soils and comparing it to other soil types, in this case HPUs, provides insight into how wetland soils may respond to increased microbial decomposition (Heckman et al. 2021).

Controls on MAOM-C content across hydropedological units

We expected to find the significantly lower MAOM-C content along with lower abundance of both total and poorly crystalline Fe in FWL compared to DUP. Generally, upland forest soils accumulate SOC in subsurface mineral horizons (Rumpel and Kögel-Knabner 2011; Harrison et al. 2011) which leads to MAOM formation by sorption, ligand exchange, and co-precipitation with the prevalent Fe and Al oxides (von Lützow et al. 2006). Fe oxides are especially abundant in Southeast Alaska Spodosols/Podzols, where organic acids from surface horizons enhance weathering and facilitate the transport and accumulation of Fe and Al oxides in lower soil horizons (Burt and Alexander 1996). The high amount of Fe and Al in Southeast Alaska Spodosols contributes to the larger SOC stocks compared to Spodosols in other regions although, counterintuitively, overall SOC stock does not seem to vary amongst these soils by Fe and Al content or by the underlying Lithology (Fedenko et al. 2024). We show support for notions put forth by Fedenko et al. (2024) that MAOM-C content rather than bulk SOC is indeed driven by overall Fe content and more weakly driven by overall Al and clay content. This result is consistent with evidence that MAOM-C content increases with increasing poorly crystalline Fe (Torn et al. 1997; Kögel-Knabner et al. 2008; Kleber et al. 2005).

However, we have some Fe_{AO}:Fe_{DC} ratios that exceed 1.0 such that the extracted poorly crystalline Fe appears to be higher than the "total pedogenic" Fe. This is unexpected in our data and may point towards incomplete reduction of all Fe in soil samples during the Fe_{DC} extraction process. However, some observations in larger datasets have shown Fe_{AO}:Fe_{DC} above 1.0 albeit some of ours exceed 2.0 (Hall and Thompson, 2022). We could gain more insight and a more comprehensive evaluation of the Fe in these soil samples by including a pyrophosphate extraction that would extract Fe associated with SOM (Kleber et al., 2005). This would provide potential insight if a significant pool of the Fe is held in SOM associations which could be present in the ammonium-oxalate extraction but not the dithionate-citrate extraction. Although both Fe_{DC} and Fe_{AO} are well correlated and show similar patterns among the HPUs, we must proceed with caution in interpreting specific mechanisms of stability and persistence ascribed to Fe in this chapter.

Interestingly, we found that many of the MAOM-C observations were under potential saturation, indicated as a function of Silt+Clay. Spinola et al. (2022) postulated that Southeast Alaska Spodosols would be under-saturated due in part to the formation of organometallic complexes with Fe leading to more crystalline Fe forms. Our samples indicated a high proportion of poorly crystalline Fe in wetter HPUs, FWL and ALV. In the FWL, the low MAOM-C, Fe_{DC}, and Fe_{AO} but high proportion of poorly crystalline Fe suggests that these mineral soils may be nearer towards MAOM-C saturation than drier soils in DUP or WUP. As soil development and weathering is rapid in this region, increased Fe supply could support growing capacity for SOC and MAOM-C (Spinola et al. 2024). However, observations from other upland Spodosol soils sampled in the HLEF spanning non-aquic, well drained to aquic, poorly drained Spodosol morphologies which show Fe content decreasing with increasing soil water saturation (D'Amore et al. 2015b).

Soil moisture is one of the dominant controls on MAOM formation and can directly influence microbial decomposition and geochemistry through redox changes (Kleber et al. 2015). In upland soils, periods of brief water saturation can facilitate Fe(III) reduction to Fe(II) and can release SOM that was previously bound to Fe(III) (Zhao et al. 2017). Even brief soil water saturation events on the scale of minutes can cause the reduction of Fe(III) to Fe(II) in upland soils and Fe-reducing microbes can also contribute to high rates of CO_2 production under these oscillating redox conditions (Bhattacharyya et al. 2018). Under prolonged soil water saturation, such as those in wetlands, prolonged anoxic conditions can more thoroughly reduce Fe(III) to Fe(II), which disconnects Fe from SOM and potentially leads to more vulnerable SOC (Wang et al. 2017; Chen et al. 2020). Soils sampled in FWL and ALV exhibited prolonged water saturation or recent water movement that appeared to further facilitate reductive dissolution of Fe(III) to Fe(II), which can more easily dissolve into water and be transported to other locations (Buettner et al. 2014). This mechanism would explain the lower overall Fe in FWL and ALV compared to the other upland HPUs and its correlation with MAOM-C content.

Controls on MAOM-Δ^{14}C across hydropedological units

Although we found support for part of our first hypothesis, surprisingly, we did not support the part of hypothesis that MAOM-Δ^{14}C age would be younger in FWL. Instead, we found significantly older MAOM-Δ^{14}C compared to the other HPU classes. Most research examining the potential MAOM protections in wetland soils has passively assumed the longer residence time of MAOM-C, which is well supported in the current soil science literature (Lavallee et al. 2020; Heckman et al. 2021; Chizen et al., 2024). However, MAOM-Δ^{14}C can vary considerably across different biomes and ecosystems (Schmidt et al. 2011; Fromm et al. 2024). A consistent control on soil Δ^{14}C across biomes and ecosystems is Depth, where older MAOM-C is found at lower depths (Shi et al. 2020). Depth as a predictor variable for MAOM-Δ^{14}C aggregates a variety of soil processes

including weathering time, microbial substrate availability, and changes in soil mineral compositions (Heckman et al. 2021). The MAOM from FWL soils were extracted from samples below the thicker organic horizons which translated to deeper overall depths for FWL compared to other HPUs. However, it is unclear if depths represent the effects of soil processes that affect $\Delta^{14}C$ equally across HPUs. For instance, organic material may accumulate more quickly on the FWL soil surface than soils develop on DUP or WUP. Soil development is rapid in the Southeast Alaska region with climatic conditions that lead to high rates of weathering which could supply necessary minerals for MAOM formation (Spinola et al. 2024).

In humid climates where mean annual precipitation is greater than potential evapotranspiration, there is a tight link between MAOM-C content and MAOM-$\Delta^{14}C$ where as MAOM-C increases, MAOM-$\Delta^{14}C$ also increases or becomes younger (Heckman et al. 2023). Higher precipitation and soil moisture can also drive a loss of Fe through reductive dissolution leading to faster turnover of bulk SOC at younger $\Delta^{14}C$ age (Grant et al. 2022). Further, Grant et al. (2022) postulated that Fe and SOC loss, rather than the inability to sequester SOC, contributed to the younger SOC ages. Our results differ from these finding by examining the MAOM in wetter FWL mineral soils which had low MAOM-C content but old MAOM-$\Delta^{14}C$ age. Further, we also found FWL had both low Fe_{DC} and Fe_{AO}, but a high poorly crystalline proportion of Fe. The results corroborate that Fe is required to maintain older SOC but only in a small proportion within the MAOM-C pool. However, these results also bring up more questions about whether this small but persistent MAOM-C pool is present in all landscape and HPU classes and of if it is unique to FWL? Moreover, is the older MAOM-$\Delta^{14}C$ in FWL the product of SOC sequestration during a previous landscape class before FWL development contributed to MAOM-C loss or was FWL always present but able to retain older MAOM-$\Delta^{14}C$? These questions can be partially addressed by examining the

compounds that preserved in MAOM-C between the HPUs which would give insight into what compounds and SOC sources are being preserved.

Comparisons of MAOM-$\Delta^{14}C$ are needed between non-wetland and wetland soils to examine the potential differences in MAOM-C stabilization. Only a few studies have conducted $\Delta^{14}C$ measurements in wetlands with respect to SOM turnover and persistence. Radiocarbon measurements in streams draining wetlands have shown that wetlands export primarily young DOC to streams, which may indicate some retention of older SOC (Raymond et al. 2004). This is supported by observations that peatlands retain older SOC while exporting younger DIC, DOC, and CH_4 (Wilson et al. 2016). However, $\Delta^{14}C$ for mineral soil wetlands or mineral soils beneath the organic horizons of wetlands are rare. Daugherty et al. (2019) measured bulk soil $\Delta^{14}C$ age in depression and slope wetlands and found older, ~3,000-4,000 years old SOC in slope wetlands and attributed this to large proportions of aliphatic C compounds as well as more fine soil textures. However, MAOM-C fractions were not explicitly measured. Wang et al. (2023) also measured $\Delta^{14}C$ in the bulk wetland soil and showed SOC dated back to 7,300 years with accumulation rates peaking nearly 1,000 years ago. Again, the fractions of MAOM-C were not measured. In recently published work from Ma et al. (2025) metal-bound-SOC and metal-bound-$\Delta^{14}C$ were measured explicitly in one of the first large scale studies in this research area. Their analysis showed that wetland soils contained older metal-bound-SOC indicated by $\Delta^{14}C$ and that metal-bound-$\Delta^{14}C$ decreased with increasing reactive minerals in wetlands, contrasting with the conventional assumption that uplands contain more persistent SOC than wetlands.

Our results largely agree with Ma et al. (2025) with the exception that we found significantly lower MAOM-C content in wetland mineral soils than upland mineral soils which does not reflect the significantly higher metal-bound-SOC found in their study. One potential reason for this

difference was that our sites were mostly in a cool, wet, and forested watershed vs. the more arid-to-temperate samples from grasslands and forests for Ma et al. (2025) study sites. Forest soils have been shown to have lower microbial necromass and much higher POM compared to other biomes (Cotrufo et al. 2019; Angst et al. 2021) and combined with the perhumid climate would leave only larger plant-derived compounds for potential MAOM-C formation. Small organic molecules and compounds are the products of continual microbial decomposition of plant inputs and have a higher likelihood of sorbing to mineral surfaces and creating persistent MAOM-C (Lehmann and Kleber 2015). For our study, we suggest that water saturation inhibits decomposition activity which produces only small amounts of SOM that then sorbs to mineral surfaces and persist much longer in an anoxic environment. Incoming data from Pyrolysis-Gas Chromatography-Mass Spectrometry (pyGC-MS) characterizes the chemical composition and structure of samples that will soon shed light on if this hypothesis is supported.

Conclusions

Our research provides a unique insight into the magnitude and drivers of both MAOM-C content and MAOM-$\Delta^{14}C$ persistence in different landscape units. The HPU classification of our study sites was a differentiator for both MAOM-C and MAOM-$\Delta^{14}C$ even when factoring in sampling depth. This supports the notion that SOM dynamics are unique within FWL, where consistent anoxic conditions reduce the overall MAOM-C content but leave behind a very stable source of MAOM. The insights from drivers evaluated here support that the presence of Fe and especially a high proportion of poorly crystalline metals can contribute to this persistence in FWL soils. Yet, more research and data are needed to evaluate the other drivers of persistence, particularly the biodegradability of inputs, biochemical reactivity of SOM sorbed to minerals, and microbial physiology within forested wetlands.

Conclusions

Assessing and monitoring the SOC pool is critical due to its substantial size which impacts modeling the global carbon cycle and its response to global change (Scharlemann et al., 2014). Long held knowledge that an inordinate amount of SOC is contained in inland freshwater wetlands has given impetus towards study more wetland SOC and include its dynamics in global climate models (Köchy et al., 2015; Luo et al., 2016; Malhotra et al., 2019). This dissertation supports this notion of more wetland inclusion and that wetlands are not well represented spatially, both in extent and SOC estimates. Moreover, it is not enough to measure wetlands separately from non-wetlands, but to integrate its characterization comprehensively with the rest of the soil landscape. These notions apply to examining wetland soils under the newer soil science paradigms of SOC persistence and overall promote more comprehensive perspectives to SOC research.

The findings of the first chapter show that improvements to inland freshwater wetlands extent maps using continuous wetland probability models can improve estimates of wetland SOC stocks and reveal new patterns of SOC distribution within forested landscapes. The second chapter expands on the notion that modeling SOC with the explicit inclusion of wetlands and wetland presence enhances maps of SOC stock by modeling both wetland probability and then SOC across a range of climate regimes. This chapter presents the perspective that including the potential of a wetland approximates the hydrologic SOC accumulation driver occurring on the land surface which has significant effects in a model of SOC with climate and depth. However, the lack of large difference in mineral SOC% between wetlands and uplands is intriguing since this goes against conventional assumptions about wetland vs. upland SOC. Yet, water saturation could alter the physiochemical characteristics that were not measured or characterized in the second chapter

analysis. The third chapter capitalized on this notion by separating the MAOM and POM soil fractions in both upland and wetland soils to show that forested wetland indeed contain differences in finer scale aspects of SOC composition. Finding that forested wetlands and dry uplands were similar in many soil characteristics but different in both MAOM-C and MAOM-Δ^{14}C, shows that MAOM-C is affected by the wetland characteristics. However, further data measuring the poorly crystalline Fe with ammonium-oxalate extractions would help elucidate the other driving factors of MAOM-C and MAOM-Δ^{14}C.

Implications

An overarching finding throughout this dissertation is that omitting, excluding, or mis-classifying wetlands in SOC and land mapping research has limited the understanding of the terrestrial environment composition and its potential SOC pools. Consistently this research shows that a large amount of wetland extent and SOC needs to be mapped to provide a full account of the landscape SOC. It is not necessarily that there are vast stores of SOC added onto the current estimates, but rather, more of the landscape SOC is contained in wetlands and wet soils which are unmapped. The results presented here have more direct implications for SOC mapping at the landscape scale but there are further implications for larger scale SOC research.

SOC has been a scientific area of inquiry for well over a century following the earliest soil scientists such as Vasily Dokuchaev in the mid-1800s who examined soil for ways to increase agricultural productivity but also recognized soil as a dynamic system (Rusakova et al., 2022). Much later towards the mid-1900s and into the 1970s, more attention was drawn to estimating the total amount of SOC in the earth system (Rubey, 1951; Bolin, 1970; Bohn, 1976; Schlesinger, 1977). Into the 1980s and 1990s there was convergence towards a 1 m depth SOC stock of approximately 1500 PgC in global soils, excluding permafrost and that estimate has persisted towards the present day

with subsequent studies (Batjes, 1996, 2016; Scharlemann et al., 2014; Jackson et al., 2017). However, more recent estimates from spatially explicit models using remote sensing in addition to other data such as the SoilGrids or GSOC Map (FAO, 2018; Poggio et al., 2021) have estimated the total global SOC amount to approximately 2500-3400 PgC. There are many reasons for this wide range of global 1 m SOC estimates including uncertainties with bulk density measurements (Köchy et al., 2015) and the distribution of observations (Poggio et al., 2021). But a large source of uncertainty is the challenge with accurately depicting wetlands and peatlands (Tifafi et al., 2018).

Both the first and second chapters of this dissertation support the approach that models SOC over the entire landscape or area with a wetland explicit indicator. In this approach, complex models can be used to estimate SOC stocks across heterogeneous landscapes and represent both smooth and dramatic transitions between high and low SOC areas. Many of the current approaches with digital soil mapping lack a wetland explicit parameter or lack wetland observations. Indeed, while there are many soil profile observations and SOC measurements spread throughout the globe, there is still room to grow these datasets and include wetland observations within them. For instance, Sothe et al., (2022) sought to explicitly include peatland measurements from a legacy dataset which helped identify the large peatland SOC stocks within the Canadian Shield and produced a continuous wall-to-wall map of SOC stocks for Canada. Probabilistic wetland mapping also has room to improve but substantial efforts to map inundation potential (a continuous probability variable) for CH_4 could be an area that could be integrated to help model overall SOC stocks (Zhang et al., 2021). One aspect for improving these global wetland models regarding SOC modeling is to integrate terrain metrics instead of relying specifically on observed inundation which is hindered by the canopy (Maxwell et al., 2016; Delancey et al., 2019). At a global scale this could help achieve more robust mapping in forested regions overall, especially in areas where peatlands may still be underestimated such as tropical and temperate areas (Gumbricht et al., 2017; Poulter et

al., 2021). Furthermore, wetland specific SOC accounting is not disadvantaged using this approach as shown in both the first and second chapters and improvements can be made for wetland specific SOC maps.

Estimating the total global wetland SOC stock has lagged behind the estimates of the overall total global SOC stock for the last few decades in terms of number of efforts and comprehensive evaluation. Gorham, (1991) provided a first estimate of peatland SOC with 455 PgC based on inventories of soils at that point. Batjes, (1996) followed this estimate by using histosol coverage from the FAO-UNESCO soil map to estimate histosol SOC at 330 PgC. Bridgham et al., (2006) later again used multiple soil inventory sources to estimate 513 PgC in peatlands and 46 PgC in freshwater mineral wetlands. The estimate of total wetland and peatland SOC was scrutinized further by (Köchy et al., 2015) who noted that bulk density was likely overestimated for histosols and peat as well as inconsistent definitions for wetlands leading to dramatic revisions downward for the overall to 82-158 PgC with 32.3 PgC in freshwater marshes and 13.2 in freshwater swamps. Finally, the most recent research using both current and past data resources by Poulter et al., (2021) estimated between 498.6-680 PgC for all wetlands with 27-3-38.1 PgC in temperate non-peatland wetlands. However, all estimates thus far have lacked spatial explicit representation across the global scale.

An interesting realization is that global scale products for overall SOC poorly represent wetland areas while global scale wetland SOC estimates lack spatial characterization. Ideally, the spatially-explicit global scale SOC map would improve wetland representation, but it is difficult to imagine how current products are integrated into the digital soil mapping approaches used by SoilGrids 2.0, for example. This dissertation provides a rectification for wetland inclusion in SOC in both observations and an explicit model predictor for a more comprehensive landscape

representation, but it is limited to direct application at the landscape to regional scale, far from the continental and global scales of other past efforts. Nevertheless, the dissertation results suggest that the most straightforward improvement to global SOC maps would be integrating enhanced global wetland maps that correspond to soil saturation and inundation patterns. Already, global wetlands are being mapped by researchers improving bottom-up estimates of CH_4 (Zhang et al., 2021) and these products could be integrated with SOC observations to improve both wetland and overall global SOC stocks. In addition, machine learning along with remote sensing data continue to improve which can be leveraged to generate more accurate global wetland SOC estimates at finer resolutions which could reveal more realistic SOC patterns (Poggio et al., 2021; Sothe et al., 2022).

Improving the wetland area representation has implications for modeling Earth's climate using large scale Earth System Models (ESMs). Early dynamic global vegetation model evaluation found that integrating peatland extent was a significant model factor in determining northern latitude respiration (Wania et al., 2009) and later facilitated wetland and peatland CH_4 modeling (Wania et al., 2010). Since then, there has been a persistent challenge to constrain the differences between top-down and bottom-up approaches to global wetland CH_4 fluxes which differ by as much as 150 $TgCH_4\ yr^{-1}$ (Zhang et al., 2017; Saunois et al., 2020; Chang et al., 2023). Many of the land surface models (LSMs) which are integrated into ESMs struggle with representing wetlands spatially, but also temporally. Currently, no LSMs distinguish different classes of wetlands, and few can represent the changes in soil conditions with hydrology (Forbrich et al., 2024). These same challenges have arisen from the results of this dissertation with the WIP approach to representing wetlands. Integrating results from larger scale WIP modeling would likely increase the estimated wetland extent which would have significant effects on calculating bottom-up CH_4 fluxes especially using finer resolution data (Zhang et al., 2021). Providing a baseline SOC stock map for wetlands could also enhance modeled estimates of greenhouse gas and CH_4 fluxes (Hugelius et al., 2020;

Davidson et al., 2022). However, developing the WIP to identify different wetland classes and be a temporally sensitive model with changing hydrology would facilitate better LSM integration to directly address enhancing CH_4 flux estimation. This work comes at a time when there is also growing research integrating wetland representation with satellite remote sensing observations into larger earth system models (Luo et al., 2016). More satellite observatories will be coming online soon that are anticipated to enhance global wetland monitoring and detection, particularly synthetic aperture radar and NISAR (Adeli et al., 2021).

While this dissertation has generally applied to the spatial distribution of SOC stocks across landscapes to regional scales, the third chapter provides insight to intrinsic soil property differences between wetlands and uplands at the scale of the individual pedon. The inspiration for this chapter was driven by questioning the persistence of some of the large wetland SOC stocks measured in previous chapters. Finding a small but persistent pool of MAOM-C in forested wetlands raises some larger questions about wetlands and mineral protections. Poorly crystalline Fe (Fe_{AO}) abundance or was significant but outweighed by freely available Fe (Fe_{DC}) for MAOM-C abundance and MAOM-$\Delta^{14}C$. This has corroborated understanding that Fe still plays a significant role in MAOM-C and MAOM-$\Delta^{14}C$ and poorly crystalline Fe was still significantly related to both as it can adsorb to organic molecules due to the high specific surface area (Kleber et al., 2015). There is a significant question on how well saturated the mineral surfaces are with MAOM-C. The Clay+Silt relationship with MAOM-C has been examined and used to model a saturation limit for MAOM-C due to the maximum surface space of fine minerals (Georgiou et al., 2022). This approach was applied to the HLEF soils and qualitatively found they are undersaturated. However, this does not evaluate the more specific MAOM-C saturation of Fe. If the forested wetland soils of the HLEF are undersaturated, there may be an exciting opportunity to explore increases to the small but persistent MAOM-C in forested wetlands through currently developing management strategies which include

POM management (Angst et al., 2023). More research is especially needed for wetland specific management strategies since they will have to account for more potent greenhouse gas effects from CH_4 emissions compared to CO_2. It would be interesting as well to examine the relative ages of CH_4 and CO_2 compared to the MAOM-$\Delta^{14}C$ in the soil. There are few if any studies that relate MAOM-$\Delta^{14}C$ to the ages of CH_4 and CO_2 but studies that have examined CH_4 ages from wetlands and peatlands note that it appears to be older (Miller, 2011; Taillardat et al., 2025) and aged DOC and DOM appear to be exported from wetlands as well (Schefuß et al., 2016).

Broader Implications

Much of the research in this dissertation depended on the publicly available data, university and federal research facilities, and a diverse network of scientists. It is uncertain whether the funding that develops satellite and other remote sensing tools will be available in the future in the U.S. Broadly speaking the whole of the scientific research engine in the U.S. is under threat and it would be neglectful to avoid discussion of the state of federal funding which supported most of this dissertation research (Moskal et al., 2022). The priorities established by the current administration create an environment unconducive to the success of this of research which heavily depended on national scale datasets such as the NWI and NLCD which are provided by the U.S. Fish and Wildlife Service and U.S. Geological Survey. The outlook for federal agencies such as these providing rich data sources is very uncertain and grim. Currently the federal executive branch is seeking to handicap vital climate science research at the U.S. National Oceanic and Atmospheric Agency (NOAA) which has worked closely with NASA to develop remote sensing products (Witze et al., 2025). The Department of Energy which supported the work in Chapter 3. also faces grave uncertainty with cuts to the indirect rate (Palmer, 2025).

References

Abatzoglou, John T., Solomon Z. Dobrowski, Sean A. Parks, and Katherine C. Hegewisch. "TerraClimate, a High-Resolution Global Dataset of Monthly Climate and Climatic Water Balance from 1958–2015." *Scientific Data* 5, no. 1 (January 9, 2018): 170191. https://doi.org/10.1038/sdata.2017.191.

Abramoff, Rose Z., Bertrand Guenet, Haicheng Zhang, Katerina Georgiou, Xiaofeng Xu, Raphael A. Viscarra Rossel, Wenping Yuan, and Philippe Ciais. "Improved Global-Scale Predictions of Soil Carbon Stocks with Millennial Version 2." *Soil Biology & Biochemistry* 164 (January 1, 2022): 108466. https://doi.org/10.1016/j.soilbio.2021.108466.

Abril, Gwenael, Jean-Michel Martinez, L. Felipe Artigas, Patricia Moreira-Turcq, Marc F. Benedetti, Luciana Vidal, Tarik Meziane, et al. "Amazon River Carbon Dioxide Outgassing Fuelled by Wetlands." *Nature* 505, no. 7483 (2014): 395. https://doi.org/10.1038/nature12797.

Adeli, Sarina, Bahram Salehi, Masoud Mahdianpari, Lindi J. Quackenbush, Brian Brisco, Haifa Tamiminia, and Stephen Shaw. "Wetland Monitoring Using SAR Data: A Meta-Analysis and Comprehensive Review." *Remote Sensing* 12, no. 14 (January 2020): 2190. https://doi.org/10.3390/rs12142190.

Adeli, Sarina, Bahram Salehi, Masoud Mahdianpari, Lindi J. Quackenbush, and Bruce Chapman. "Moving toward L-Band NASA-ISRO SAR Mission (NISAR) Dense Time Series: Multipolarization Object-Based Classification of Wetlands Using Two Machine Learning Algorithms." *Earth and Space Science* 8, no. 11 (2021): e2021EA001742. https://doi.org/10.1029/2021EA001742.

Ågren, A. M., W. Lidberg, M. Strömgren, J. Ogilvie, and P. A. Arp. "Evaluating Digital Terrain Indices for Soil Wetness Mapping – a Swedish Case Study." *Hydrology and Earth System Sciences* 18, no. 9 (September 12, 2014): 3623–34. https://doi.org/10.5194/hess-18-3623-2014.

Ågren, Anneli M., Johannes Larson, Siddhartho Shekhar Paul, Hjalmar Laudon, and William Lidberg. "Use of Multiple LIDAR-Derived Digital Terrain Indices and Machine Learning for High-Resolution National-Scale Soil Moisture Mapping of the Swedish Forest Landscape." *Geoderma* 404 (December 15, 2021): 115280. https://doi.org/10.1016/j.geoderma.2021.115280.

Anderegg, William R. L., Anna T. Trugman, Grayson Badgley, Christa M. Anderson, Ann Bartuska, Philippe Ciais, Danny Cullenward, et al. "Climate-Driven Risks to the Climate Mitigation Potential of Forests." *Science* 368, no. 6497 (June 19, 2020): eaaz7005. https://doi.org/10.1126/science.aaz7005.

Angst, Gerrit, Kevin E. Mueller, Michael J. Castellano, Cordula Vogel, Martin Wiesmeier, and Carsten W. Mueller. "Unlocking Complex Soil Systems as Carbon Sinks: Multi-Pool Management as the Key." *Nature Communications* 14, no. 1 (June 15, 2023): 2967. https://doi.org/10.1038/s41467-023-38700-5.

Angst, Gerrit, Kevin E. Mueller, Klaas G. J. Nierop, and Myrna J. Simpson. "Plant- or Microbial-Derived? A Review on the Molecular Composition of Stabilized Soil Organic Matter." *Soil Biology & Biochemistry* 156 (May 1, 2021): 108189. https://doi.org/10.1016/j.soilbio.2021.108189.

Anthony, Tyler L., and Whendee L. Silver. "Mineralogical Associations with Soil Carbon in Managed Wetland Soils." *Global Change Biology* 26, no. 11 (2020): 6555–67. https://doi.org/10.1111/gcb.15309.

Arrouays, Dominique, Laura Poggio, Osvaldo A. Salazar Guerrero, and Vera Laetitia Mulder. "Digital Soil Mapping and *GlobalSoilMap*. Main Advances and Ways Forward." *Geoderma Regional* 21 (June 1, 2020): e00265. https://doi.org/10.1016/j.geodrs.2020.e00265.

Bailey, Scott W., Patricia A. Brousseau, Kevin J. McGuire, and Donald S. Ross. "Influence of Landscape Position and Transient Water Table on Soil Development and Carbon Distribution in a Steep, Headwater Catchment." *Geoderma* 226–227 (August 1, 2014): 279–89. https://doi.org/10.1016/J.GEODERMA.2014.02.017.

Bartoń, Kamil. "MuMIn: Multi-Model Inference," 2023. https://CRAN.R-project.org/package=MuMIn.

Bates, Douglas, Martin Mächler, Ben Bolker, and Steve Walker. "Fitting Linear Mixed-Effects Models Using Lme4." *Journal of Statistical Software* 67, no. 1 (2015): 1–48. https://doi.org/10.18637/jss.v067.i01.

Batjes, N. H. "Harmonized Soil Property Values for Broad-Scale Modelling (WISE30sec) with Estimates of Global Soil Carbon Stocks." *Geoderma* 269 (May 1, 2016): 61–68. https://doi.org/10.1016/j.geoderma.2016.01.034.

Batjes, N. H. "Total Carbon and Nitrogen in the Soils of the World." *European Journal of Soil Science* 65, no. 1 (1996): 10–21. https://doi.org/10.1111/ejss.12114_2.

Batjes, Niels H., Eloi Ribeiro, and Ad van Oostrum. "Standardised Soil Profile Data to Support Global Mapping and Modelling (WoSIS Snapshot 2019)." *Earth System Science Data* 12, no. 1 (February 10, 2020): 299–320. https://doi.org/10.5194/essd-12-299-2020.

Bernal, Blanca, and William J. Mitsch. "Comparing Carbon Sequestration in Temperate Freshwater Wetland Communities." *Global Change Biology* 18, no. 5 (May 2012): 1636–47. https://doi.org/10.1111/j.1365-2486.2011.02619.x.

Bernhardt, Emily S., Joanna R. Blaszczak, Cari D. Ficken, Megan L. Fork, Kendra E. Kaiser, and Erin C. Seybold. "Control Points in Ecosystems: Moving beyond the Hot Spot Hot Moment Concept." *Ecosystems* 20, no. 4 (June 1, 2017): 665–82. https://doi.org/10.1007/s10021-016-0103-y.

Beven, K. J., and M. J. Kirkby. "A Physically Based, Variable Contributing Area Model of Basin Hydrology / Un Modèle à Base Physique de Zone d'appel Variable de l'hydrologie Du Bassin Versant." *Hydrological Sciences Bulletin* 24, no. 1 (1979): 43–69. https://doi.org/10.1080/02626667909491834.

Bhattacharyya, Amrita, Ashley N. Campbell, Malak M. Tfaily, Yang Lin, Ravi K. Kukkadapu, Whendee L. Silver, Peter S. Nico, and Jennifer Pett-Ridge. "Redox Fluctuations Control the Coupled Cycling of Iron and Carbon in Tropical Forest Soils." *Environmental Science & Technology* 52, no. 24 (December 18, 2018): 14129–39. https://doi.org/10.1021/acs.est.8b03408.

Bidlack, Allison L, Sarah M Bisbing, Brian J Buma, Heida L Diefenderfer, Jason B Fellman, William C Floyd, Ian Giesbrecht, et al. "Climate-Mediated Changes to Linked Terrestrial and Marine Ecosystems across the Northeast Pacific Coastal Temperate Rainforest Margin." *Bioscience* 71, no. 6 (June 1, 2021): 581–95. https://doi.org/10.1093/biosci/biaa171.

Bishop, T. F. A., A. B. McBratney, and G. M. Laslett. "Modelling Soil Attribute Depth Functions with Equal-Area Quadratic Smoothing Splines." *Geoderma* 91, no. 1 (August 1, 1999): 27–45. https://doi.org/10.1016/S0016-7061(99)00003-8.

Bogard, Matthew J., Brian A. Bergamaschi, David E. Butman, Frank Anderson, Sara H. Knox, and Lisamarie Windham-Myers. "Hydrologic Export Is a Major Component of Coastal Wetland Carbon Budgets." *Global Biogeochemical Cycles* 34, no. 8 (2020): e2019GB006430. https://doi.org/10.1029/2019GB006430.

Bohn, Hinrich L. "Estimate of Organic Carbon in World Soils." *Soil Science Society of America Journal* 40, no. 3 (1976): 468–70. https://doi.org/10.2136/sssaj1976.03615995004000030045x.

Bolin, Bert. "The Carbon Cycle," September 1, 1970. https://www.scientificamerican.com/article/the-carbon-cycle/.

Bossio, D. A., S. C. Cook-Patton, P. W. Ellis, J. Fargione, J. Sanderman, P. Smith, S. Wood, et al. "The Role of Soil Carbon in Natural Climate Solutions." *Nature Sustainability* 3, no. 5 (May 2020): 391–98. https://doi.org/10.1038/s41893-020-0491-z.

Bradford, Mark A., William R. Wieder, Gordon B. Bonan, Noah Fierer, Peter A. Raymond, and Thomas W. Crowther. "Managing Uncertainty in Soil Carbon Feedbacks to Climate Change." *Nature Climate Change* 6, no. 8 (August 2016): 751–58. https://doi.org/10.1038/nclimate3071.

Breiman, Leo. "Random Forests." *Machine Learning* 45, no. 1 (October 1, 2001): 5–32. https://doi.org/10.1023/A:1010933404324.

Bridgham, Scott D., J. Patrick Megonigal, Jason K. Keller, Norman B. Bliss, and Carl Trettin. "The Carbon Balance of North American Wetlands." *Wetlands* 26, no. 4 (December 2006): 889–916. https://doi.org/10.1672/0277-5212(2006)26[889:TCBONA]2.0.CO;2.

Brinson, Mark M. "A Hydrogeomorphic Classification for Wetlands." In *A Hydrogeomorphic Classification for Wetlands*, 103. US Army Corps of Engineers Waterways Experiment Station, 1993.

Brogniez, D. de, C. Ballabio, A. Stevens, R. J. A. Jones, L. Montanarella, and B. van Wesemael. "A Map of the Topsoil Organic Carbon Content of Europe Generated by a Generalized Additive Model." *European Journal of Soil Science* 66, no. 1 (2015): 121–34. https://doi.org/10.1111/ejss.12193.

Buettner, Shea W., Marc G. Kramer, Oliver A. Chadwick, and Aaron Thompson. "Mobilization of Colloidal Carbon during Iron Reduction in Basaltic Soils." *Geoderma* 221–222 (June 2014): 139–45. https://doi.org/10.1016/j.geoderma.2014.01.012.

Buffam, Ishi, Monica G. Turner, Ankur R. Desai, Paul C. Hanson, James A. Rusak, Noah R. Lottig, Emily H. Stanley, and Stephen R. Carpenter. "Integrating Aquatic and Terrestrial Components to Construct a Complete Carbon Budget for a North Temperate Lake District." *Global Change Biology* 17, no. 2 (February 2011): 1193–1211. https://doi.org/10.1111/j.1365-2486.2010.02313.x.

Bui, Elisabeth N. "Data-Driven Critical Zone Science: A New Paradigm." *Science of the Total Environment* 568 (October 15, 2016): 587–93. https://doi.org/10.1016/j.scitotenv.2016.01.202.

Burt, R., and E.B. Alexander. "Soil Development on Moraines of Mendenhall Glacier, Southeast Alaska. 2. Chemical Transformations and Soil Micromorphology." *Geoderma* 72, no. 1–2 (July 1996): 19–36. https://doi.org/10.1016/0016-7061(96)00022-5.

Byun, Eunji, Sarah A. Finkelstein, Sharon A. Cowling, and Pascal Badiou. "Potential Carbon Loss Associated with Post-Settlement Wetland Conversion in Southern Ontario, Canada." *Carbon Balance and Management* 13, no. 1 (April 20, 2018): 6. https://doi.org/10.1186/s13021-018-0094-4.

Campbell, Anthony D, Temilola Fatoyinbo, Sean P Charles, Laura L Bourgeau-Chavez, Joaquim Goes, Helga Gomes, Meghan Halabisky, et al. "A Review of Carbon Monitoring in Wet Carbon Systems Using Remote Sensing." *Environmental Research Letters* 17, no. 2 (February 1, 2022): 25009. https://doi.org/10.1088/1748-9326/ac4d4d.

Cao, Baijing, Grant M. Domke, Matthew B. Russell, and Brian F. Walters. "Spatial Modeling of Litter and Soil Carbon Stocks on Forest Land in the Conterminous United States." *Science of*

the Total Environment 654 (March 1, 2019): 94–106. https://doi.org/10.1016/j.scitotenv.2018.10.359.

Carpenter, Dunbar N., James G. Bockheim, and Paul F. Reich. "Soils of Temperate Rainforests of the North American Pacific Coast." *Geoderma* 230–231 (October 1, 2014): 250–64. https://doi.org/10.1016/j.geoderma.2014.04.023.

Carter, Trevor A, and Brian Buma. "The Distribution of Tree Biomass Carbon within the Pacific Coastal Temperate Rainforest, a Disproportionally Carbon Dense Forest." *Canadian Journal of Forest Research*, April 19, 2024. https://doi.org/10.1139/cjfr-2024-0015.

Carvalhais, Nuno, Matthias Forkel, Myroslava Khomik, Jessica Bellarby, Martin Jung, Mirco Migliavacca, Mingquan Mu, et al. "Global Covariation of Carbon Turnover Times with Climate in Terrestrial Ecosystems." *Nature* 514, no. 7521 (October 2014): 213–17. https://doi.org/10.1038/nature13731.

Chang, Kuang-Yu, William J. Riley, Nathan Collier, Gavin McNicol, Etienne Fluet-Chouinard, Sara H. Knox, Kyle B. Delwiche, et al. "Observational Constraints Reduce Model Spread but Not Uncertainty in Global Wetland Methane Emission Estimates." *Global Change Biology* 29, no. 15 (2023): 4298–4312. https://doi.org/10.1111/gcb.16755.

Chen, Chunmei, Steven J. Hall, Elizabeth Coward, and Aaron Thompson. "Iron-Mediated Organic Matter Decomposition in Humid Soils Can Counteract Protection." *Nature Communications* 11, no. 1 (May 7, 2020): 2255. https://doi.org/10.1038/s41467-020-16071-5.

Chen, Songchao, Dominique Arrouays, V.L. Mulder, Laura Poggio, Budiman Minasny, Pierre Roudier, Zamir Libohova, et al. "Digital Mapping of GlobalSoilMap Soil Properties at a Broad Scale: A Review." *Geoderma*, 2022. https://doi.org/10.1016/j.geoderma.2021.115567.

Chizen, Chantel J., and Angela K. Bedard-Haughn. "Drivers of Soil Carbon Variability in North America's Prairie Pothole Wetlands: A Review." *Wetlands* 45, no. 1 (January 30, 2025): 18. https://doi.org/10.1007/s13157-025-01898-9.

Chizen, Chantel J., Bobbi L. Helgason, Blake Weiseth, Gurbir Singh Dhillon, Helen M. Baulch, Jeff J. Schoenau, and Angela K. Bedard-Haughn. "Soil Carbon Dynamics in Drained Prairie Pothole Wetlands." *Frontiers in Environmental Science* 12 (March 15, 2024). https://doi.org/10.3389/fenvs.2024.1353802.

Christensen, Jay R., Heather E. Golden, Laurie C. Alexander, Brian R. Pickard, Ken M. Fritz, Charles R. Lane, Marc H. Weber, Rose M. Kwok, and Madeline N. Keefer. "Headwater Streams and Inland Wetlands: Status and Advancements of Geospatial Datasets and Maps across the United States." *Earth-Science Reviews* 235 (December 1, 2022): 104230. https://doi.org/10.1016/j.earscirev.2022.104230.

Cook-Patton, Susan C., Sara M. Leavitt, David Gibbs, Nancy L. Harris, Kristine Lister, Kristina J. Anderson-Teixeira, Russell D. Briggs, et al. "Mapping Carbon Accumulation Potential from Global Natural Forest Regrowth." *Nature* 585, no. 7826 (September 2020): 545–50. https://doi.org/10.1038/s41586-020-2686-x.

Cotrufo, M. Francesca, Michelle L. Haddix, Marie E. Kroeger, and Catherine E. Stewart. "The Role of Plant Input Physical-Chemical Properties, and Microbial and Soil Chemical Diversity on the Formation of Particulate and Mineral-Associated Organic Matter." *Soil Biology & Biochemistry* 168 (May 1, 2022): 108648. https://doi.org/10.1016/j.soilbio.2022.108648.

Cotrufo, M. Francesca, Maria Giovanna Ranalli, Michelle L. Haddix, Johan Six, and Emanuele Lugato. "Soil Carbon Storage Informed by Particulate and Mineral-Associated Organic Matter." *Nature Geoscience* 12, no. 12 (December 2019): 989–94. https://doi.org/10.1038/s41561-019-0484-6.

Creed, I. F., S. E. Sanford, F. D. Beall, L. A. Molot, and P. J. Dillon. "Cryptic Wetlands: Integrating Hidden Wetlands in Regression Models of the Export of Dissolved Organic Carbon from

Forested Landscapes." *Hydrological Processes* 17 (2003): 3629–48. https://doi.org/10.1002/HYP.1357.

Creed, Irena, Pascal Badiou, Eric Enanga, David Lobb, John Pattison-Williams, Patrick Lloyd-Smith, and Mark Gloutney. "Can Restoration of Freshwater Mineral Soil Wetlands Deliver Nature-Based Climate Solutions to Agricultural Landscapes?" *Frontiers in Ecology and Evolution* 10 (July 1, 2022): 932415. https://doi.org/10.3389/fevo.2022.932415.

Dahl, T E. *Status and Trends of Wetlands in the Conterminous United States 2004 to 2009*. US Department of the Interior; Fish and Wildlife Service, 2011.

D'Amore, David V., Rick T. Edwards, and Frances E. Biles. "Biophysical Controls on Dissolved Organic Carbon Concentrations of Alaskan Coastal Temperate Rainforest Streams." *Aquatic Sciences* 78, no. 2 (April 1, 2016): 381–93. https://doi.org/10.1007/s00027-015-0441-4.

D'Amore, David V., Rick T. Edwards, Paul A. Herendeen, Eran Hood, and Jason B. Fellman. "Dissolved Organic Carbon Fluxes from Hydropedologic Units in Alaskan Coastal Temperate Rainforest Watersheds." *Soil Science Society of America Journal* 79, no. 2 (2015a): 378–88. https://doi.org/10.2136/sssaj2014.09.0380.

D'Amore, David V., Chien-Lu Ping, and Paul A. Herendeen. "Hydromorphic Soil Development in the Coastal Temperate Rainforest of Alaska." *Soil Science Society of America Journal* 79, no. 2 (2015b): 698–709. https://doi.org/10.2136/sssaj2014.08.0322.

Daugherty, Ellen E., Georgina A. McKee, Robert Bergstrom, Sarah Burton, Céline Pallud, Robert M. Hubbard, Eugene F. Kelly, Charles C. Rhoades, and Thomas Borch. "Hydrogeomorphic Controls on Soil Carbon Composition in Two Classes of Subalpine Wetlands." *Biogeochemistry* 145, no. 1 (October 1, 2019): 161–75. https://doi.org/10.1007/s10533-019-00597-y.

Davidson, Eric A., and Ivan A. Janssens. "Temperature Sensitivity of Soil Carbon Decomposition and Feedbacks to Climate Change." *Nature* 440, no. 7081 (March 2006): 165–73. https://doi.org/10.1038/nature04514.

Davidson, Scott J., Emily Dazé, Eunji Byun, Dean Hiler, Markus Kangur, Julie Talbot, Sarah A. Finkelstein, and Maria Strack. "The Unrecognized Importance of Carbon Stocks and Fluxes from Swamps in Canada and the USA." *Environmental Research Letters* 17, no. 5 (April 2022): 53003. https://doi.org/10.1088/1748-9326/ac63d5.

Dazé, Emily, Eunji Byun, and Sarah A. Finkelstein. "Long-Term Carbon Accumulation in Temperate Swamp Soils: A Case Study from Greenock Swamp, Ontario, Canada." *Wetlands* 42, no. 8 (December 3, 2022): 121. https://doi.org/10.1007/s13157-022-01641-8.

DeLancey, Evan R., John F. Simms, Masoud Mahdianpari, Brian Brisco, Craig Mahoney, and Jahan Kariyeva. "Comparing Deep Learning and Shallow Learning for Large-Scale Wetland Classification in Alberta, Canada." *Remote Sensing* 12, no. 1 (January 2020): 2. https://doi.org/10.3390/rs12010002.

Delancey, Evan Ross, Jahan Kariyeva, Jason T. Bried, and Jennifer N. Hird. "Large-Scale Probabilistic Identification of Boreal Peatlands Using Google Earth Engine, Open-Access Satellite Data, and Machine Learning." *PLOS One* 14, no. 6 (2019). https://doi.org/10.1371/journal.pone.0218165.

DellaSala, Dominick A., Paul Alaback, Toby Spribille, Henrik von Wehrden, and Richard S. Nauman. "Just What Are Temperate and Boreal Rainforests?" edited by Dominick A. DellaSala, 1–41. Washington, DC: Island Press, 2011. https://doi.org/10.5822/978-1-61091-008-8_1.

Deluca, T. H., and C. Boisvenue. "Boreal Forest Soil Carbon: Distribution, Function and Modelling." *Forestry* 85, no. 2 (April 1, 2012): 161–84. https://doi.org/10.1093/forestry/cps003.

Derrien, Delphine, Pierre Barré, Isabelle Basile-Doelsch, Lauric Cécillon, Abad Chabbi, Alexandra Crème, Sébastien Fontaine, et al. "Current Controversies on Mechanisms Controlling Soil Carbon Storage: Implications for Interactions with Practitioners and Policy-Makers. A Review." *Agronomy for Sustainable Development* 43, no. 1 (February 6, 2023): 21. https://doi.org/10.1007/s13593-023-00876-x.

Dewitz, Jon. "National Land Cover Database (NLCD) 2019 Products," 2021. https://doi.org/10.5066/P9KZCM54.

Dodds, Walter K., Lindsey Bruckerhoff, Darold Batzer, Anne Schechner, Casey Pennock, Elizabeth Renner, Flavia Tromboni, Kari Bigham, and Samantha Grieger. "The Freshwater Biome Gradient Framework: Predicting Macroscale Properties Based on Latitude, Altitude, and Precipitation." *Ecosphere (Washington, D.C)* 10, no. 7 (2019): e02786. https://doi.org/10.1002/ecs2.2786.

Doetterl, Sebastian, Asmeret Asefaw Berhe, Katherine Heckman, Corey Lawrence, Jörg Schnecker, Rodrigo Vargas, Cordula Vogel, and Rota Wagai. "A Landscape-Scale View of Soil Organic Matter Dynamics." *Nature Reviews Earth and Environment* 6, no. 1 (January 2025): 67–81. https://doi.org/10.1038/s43017-024-00621-2.

Doetterl, Sebastian, Antoine Stevens, Johan Six, Roel Merckx, Kristof Van Oost, Manuel Casanova Pinto, Angélica Casanova-Katny, et al. "Soil Carbon Storage Controlled by Interactions between Geochemistry and Climate." *Nature Geoscience* 8, no. 10 (October 2015): 780–83. https://doi.org/10.1038/ngeo2516.

Don, Axel, Jens Schumacher, Michael Scherer-Lorenzen, Thomas Scholten, and Ernst-Detlef Schulze. "Spatial and Vertical Variation of Soil Carbon at Two Grassland Sites — Implications for Measuring Soil Carbon Stocks." *Geoderma* 141, no. 3 (October 15, 2007): 272–82. https://doi.org/10.1016/j.geoderma.2007.06.003.

Dong, Junyu, Lifei Wang, Quan Quan, Jianguo Zhang, Xin Li, Di Zhao, Jiaohui Fang, Qingqing Cao, and Jian Liu. "Factors Controlling Soil Organic Carbon Content in Wetlands at Multiple Scales and Assessment of the Universality of Estimation Equations: A Mega-Data Study." *Science of the Total Environment* 827 (June 25, 2022): 154380. https://doi.org/10.1016/j.scitotenv.2022.154380.

Dronova, Iryna, and Sophie Taddeo. "Remote Sensing of Phenology: Towards the Comprehensive Indicators of Plant Community Dynamics from Species to Regional Scales." *Journal of Ecology* 110, no. 7 (2022): 1460–84. https://doi.org/10.1111/1365-2745.13897.

Du, Ling, Gregory W. McCarty, Xin Zhang, Megan W. Lang, Xia Li, Chengquan Huang, Sangchul Lee, and Zhenhua Zou. "Mapping Forested Wetland Inundation in the Delmarva Peninsula, USA Using Deep Convolutional Neural Networks." *Remote Sensing* 12, no. 4 (February 15, 2020): 644. https://doi.org/10.3390/rs12040644.

Durden, E. H. "On the Application of Peat and Its Products, to Manufacturing, Agricultural, and Sanitary Purposes." *Proceedings of the Yorkshire Geological Society* 3, no. 1 (January 1849): 339–66. https://doi.org/10.1144/pygs.3.339a.

Edmonds, Robert L., Roger D. Blew, James L. Marra, Judy Blew, Amy K Barg, Georgia Murray, and Ted B. Thomas. "Vegetation Patterns, Hydrology, and Water Chemistry in Small Watersheds in the Hoh River Valley, Olympic National Park." National Park Service, 1998.

Ellis, Peter Woods, Aaron Marr Page, Stephen Wood, Joseph Fargione, Yuta J. Masuda, Vanessa Carrasco Denney, Campbell Moore, et al. "The Principles of Natural Climate Solutions." *Nature Communications* 15, no. 11 (January 2024): 547. https://doi.org/10.1038/s41467-023-44425-2.

Evenson, Grey R., Heather E. Golden, Charles R. Lane, and Ellen D'Amico. "An Improved Representation of Geographically Isolated Wetlands in a Watershed-Scale Hydrologic Model." *Hydrological Processes* 30, no. 22 (2016): 4168–84. https://doi.org/10.1002/hyp.10930.

Fao. *Global Soil Organic Carbon Map (GSOCmap): Technical Report*. Rome, Italy: FAO, 2018. https://www.fao.org/documents/card/en/c/I8891EN.

Fedenko, Jennifer, David D'Amore, Diogo Spinola, Raquel Portes, Ashlee Dere, and Rebecca A. Lybrand. "Spodosol Development and Soil Organic Carbon Distribution along a Lithosequence in Perhumid Coastal Temperate Rainforest." *Soil Science Society of America Journal* n/a, no. n/a (March 27, 2024). https://doi.org/10.1002/saj2.20695.

Fedenko, Jennifer M. *Soil Development and Organic Carbon Stocks across a Lithosequence in the Perhumid Coastal Temperate Rainforests of Southeast Alaska*. Oregon State University, 2021.

Fellman, Jason B., David V. D'Amore, Eran Hood, and Pat Cunningham. "Vulnerability of Wetland Soil Carbon Stocks to Climate Warming in the Perhumid Coastal Temperate Rainforest." *Biogeochemistry* 133, no. 2 (April 1, 2017): 165–79. https://doi.org/10.1007/s10533-017-0324-y.

Fleiner, Julia H. "Lithologic Controls on Soil Carbon Partitioning in the Alaskan Coastal Temperate Rainforest," 2021. https://ir.library.oregonstate.edu/concern/graduate_thesis_or_dissertations/cr56n792p?locale=en.

Fluet-Chouinard, Etienne, Bernhard Lehner, Lisa-Maria Rebelo, Fabrice Papa, and Stephen K. Hamilton. "Development of a Global Inundation Map at High Spatial Resolution from Topographic Downscaling of Coarse-Scale Remote Sensing Data." *Remote Sensing of Environment* 158 (March 1, 2015): 348–61. https://doi.org/10.1016/j.rse.2014.10.015.

Fluet-Chouinard, Etienne, Benjamin D. Stocker, Zhen Zhang, Avni Malhotra, Joe R. Melton, Benjamin Poulter, Jed O. Kaplan, et al. "Extensive Global Wetland Loss over the Past Three Centuries." *Nature* 614, no. 7947 (February 9, 2023): 281–86. https://doi.org/10.1038/s41586-022-05572-6.

Foley, Jonathan A., Ruth DeFries, Gregory P. Asner, Carol Barford, Gordon Bonan, Stephen R. Carpenter, F. Stuart Chapin, et al. "Global Consequences of Land Use." *Science* 309, no. 5734 (July 22, 2005): 570–74. https://doi.org/10.1126/science.1111772.

Forbrich, Inke, Theresia Yazbeck, Benjamin Sulman, Timothy H. Morin, Angela Che Ing Tang, and Gil Bohrer. "Three Decades of Wetland Methane Surface Flux Modeling by Earth System Models-Advances, Applications, and Challenges." *Journal of Geophysical Research: Biogeosciences* 129, no. 3 (2024): e2023JG007915. https://doi.org/10.1029/2023JG007915.

Fox, John, and Sanford Weisberg. *An R Companion to Applied Regression*. 3rd ed. Thousand Oaks CA: Sage, 2019. https://www.john-fox.ca/Companion/.

Friedlingstein, Pierre, Michael O'Sullivan, Matthew W. Jones, Robbie M. Andrew, Luke Gregor, Judith Hauck, Corinne Le Quéré, et al. "Global Carbon Budget 2022." *Earth System Science Data* 14, no. 11 (November 11, 2022): 4811–4900. https://doi.org/10.5194/essd-14-4811-2022.

Friedlingstein, Pierre, Michael O'Sullivan, Matthew W. Jones, Robbie M. Andrew, Judith Hauck, Peter Landschützer, Corinne Le Quéré, et al. "Global Carbon Budget 2024." *Earth System Science Data Discussions*, November 13, 2024, 1–133. https://doi.org/10.5194/essd-2024-519.

Fromm, Sophie F. von, Alison M. Hoyt, Markus Lange, Gifty E. Acquah, Ermias Aynekulu, Asmeret Asefaw Berhe, Stephan M. Haefele, et al. "Continental-Scale Controls on Soil Organic Carbon across Sub-Saharan Africa." *Soil* 7, no. 1 (June 29, 2021): 305–32. https://doi.org/10.5194/soil-7-305-2021.

Fromm, Sophie F. von, Alison M. Hoyt, Carlos A. Sierra, Katerina Georgiou, Sebastian Doetterl, and Susan E. Trumbore. "Controls and Relationships of Soil Organic Carbon Abundance and Persistence Vary across Pedo-Climatic Regions." *Global Change Biology* 30, no. 5 (2024): e17320. https://doi.org/10.1111/gcb.17320.

Gannon, John P., Scott W. Bailey, and Kevin J. McGuire. "Organizing Groundwater Regimes and Response Thresholds by Soils: A Framework for Understanding Runoff Generation in a Headwater Catchment." *Water Resources Research* 50, no. 11 (2014): 8403–19. https://doi.org/10.1002/2014WR015498.

Gavin, Daniel G, David M Fisher, Erin M Herring, Ariana White, and Linda B Brubaker. "Paleoenvironmental Change on the Olympic Peninsula, Washington: Forests and Climate from the Last Glaciation to the Present." FINAL REPORT TO OLYMPIC NATIONAL PARK. National Park Service, March 13, 2013.

Genet, Hélène, Yujie He, Zhou Lyu, A. David McGuire, Qianlai Zhuang, Joy Clein, David D'Amore, et al. "The Role of Driving Factors in Historical and Projected Carbon Dynamics of Upland Ecosystems in Alaska." *Ecological Applications* 28, no. 1 (2018): 5–27. https://doi.org/10.1002/eap.1641.

Georgiou, Katerina, Robert B. Jackson, Olga Vindušková, Rose Z. Abramoff, Anders Ahlström, Wenting Feng, Jennifer W. Harden, et al. "Global Stocks and Capacity of Mineral-Associated Soil Organic Carbon." *Nature Communications* 13, no. 1 (July 1, 2022): 3797. https://doi.org/10.1038/s41467-022-31540-9.

Georgiou, Katerina, Charles D. Koven, William R. Wieder, Melannie D. Hartman, William J. Riley, Jennifer Pett-Ridge, Nicholas J. Bouskill, et al. "Emergent Temperature Sensitivity of Soil Organic Carbon Driven by Mineral Associations." *Nature Geoscience*, February 20, 2024, 1–8. https://doi.org/10.1038/s41561-024-01384-7.

Georgiou, Katerina, Avni Malhotra, William R. Wieder, Jacqueline H. Ennis, Melannie D. Hartman, Benjamin N. Sulman, Asmeret Asefaw Berhe, et al. "Divergent Controls of Soil Organic Carbon between Observations and Process-Based Models." *Biogeochemistry* 156, no. 1 (October 1, 2021): 5–17. https://doi.org/10.1007/s10533-021-00819-2.

Gessler, P. E., O. A. Chadwick, F. Chamran, L. Althouse, and K. Holmes. "Modeling Soil–Landscape and Ecosystem Properties Using Terrain Attributes." *Soil Science Society of America Journal* 64, no. 6 (2000): 2046–56. https://doi.org/10.2136/sssaj2000.6462046x.

Goldman, Margaret A., Brian A. Needelman, Martin C. Rabenhorst, Megan W. Lang, Gregory W. McCarty, and Phillip King. "Digital Soil Mapping in a Low-Relief Landscape to Support Wetland Restoration Decisions." *Geoderma* 373 (August 15, 2020): 114420. https://doi.org/10.1016/j.geoderma.2020.114420.

Gorelick, Noel, Matt Hancher, Mike Dixon, Simon Ilyushchenko, David Thau, and Rebecca Moore. "Google Earth Engine: Planetary-Scale Geospatial Analysis for Everyone." *Remote Sensing of Environment*, Big remotely sensed data: tools, applications and experiences, 202 (December 1, 2017): 18–27. https://doi.org/10.1016/j.rse.2017.06.031.

Gorham, Eville. "Northern Peatlands: Role in the Carbon Cycle and Probable Responses to Climatic Warming." *Ecological Applications* 1, no. 2 (1991): 182–95. https://doi.org/10.2307/1941811.

Grant, Katherine E., Valier V. Galy, Negar Haghipour, Timothy I. Eglinton, and Louis A. Derry. "Persistence of Old Soil Carbon under Changing Climate: The Role of Mineral-Organic Matter Interactions." *Chemical Geology* 587 (January 5, 2022): 120629. https://doi.org/10.1016/j.chemgeo.2021.120629.

Gray, Jonathan M., Thomas F.A. Bishop, and Brian R. Wilson. "Factors Controlling Soil Organic Carbon Stocks with Depth in Eastern Australia." *Soil Science Society of America Journal* 79, no. 6 (2015): 1741–51. https://doi.org/10.2136/sssaj2015.06.0224.

Griscom, Bronson W., Justin Adams, Peter W. Ellis, Richard A. Houghton, Guy Lomax, Daniela A. Miteva, William H. Schlesinger, et al. "Natural Climate Solutions." *Proceedings of the National Academy of Sciences* 114, no. 44 (October 31, 2017): 11645–50. https://doi.org/10.1073/pnas.1710465114.

Group, PRISM Climate. "30 Year Normals," February 4, 2014.

Grybos, Malgorzata, Mélanie Davranche, Gérard Gruau, Patrice Petitjean, and Mathieu Pédrot. "Increasing pH Drives Organic Matter Solubilization from Wetland Soils under Reducing Conditions." *Geoderma* 154, no. 1 (December 15, 2009): 13–19. https://doi.org/10.1016/j.geoderma.2009.09.001.

Guevara, Mario, Guillermo Federico Olmedo, Emma Stell, Yusuf Yigini, Yameli Aguilar Duarte, Carlos Arellano Hernández, Gloria E. Arévalo, et al. "No Silver Bullet for Digital Soil Mapping: Country-Specific Soil Organic Carbon Estimates across Latin America." *Soil* 4, no. 3 (August 1, 2018): 173–93. https://doi.org/10.5194/soil-4-173-2018.

Gumbricht, Thomas, Rosa Maria Roman-Cuesta, Louis Verchot, Martin Herold, Florian Wittmann, Ethan Householder, Nadine Herold, and Daniel Murdiyarso. "An Expert System Model for Mapping Tropical Wetlands and Peatlands Reveals South America as the Largest Contributor." *Global Change Biology* 23, no. 9 (2017): 3581–99. https://doi.org/10.1111/gcb.13689.

Halabisky, Meghan, Dan Miller, Anthony J. Stewart, Amy Yahnke, Daniel Lorigan, Tate Brasel, and Ludmila Monika Moskal. "The Wetland Intrinsic Potential Tool: Mapping Wetland Intrinsic Potential through Machine Learning of Multi-Scale Remote Sensing Proxies of Wetland Indicators." *Hydrology and Earth System Sciences* 27, no. 20 (October 20, 2023): 3687–99. https://doi.org/10.5194/hess-27-3687-2023.

Hall, Steven J., and Whendee L. Silver. "Reducing Conditions, Reactive Metals, and Their Interactions Can Explain Spatial Patterns of Surface Soil Carbon in a Humid Tropical Forest." *Biogeochemistry* 125, no. 2 (September 1, 2015): 149–65. https://doi.org/10.1007/s10533-015-0120-5.

Hall, Steven J., and Aaron Thompson. "What Do Relationships between Extractable Metals and Soil Organic Carbon Concentrations Mean?" *Soil Science Society of America Journal* 86, no. 2 (2022): 195–208. https://doi.org/10.1002/saj2.20343.

Hancock, G. R., D. Murphy, and K. G. Evans. "Hillslope and Catchment Scale Soil Organic Carbon Concentration: An Assessment of the Role of Geomorphology and Soil Erosion in an Undisturbed Environment." *Geoderma* 155, no. 1 (February 15, 2010): 36–45. https://doi.org/10.1016/j.geoderma.2009.11.021.

Hansen, Paige M., Rebecca Even, Alison E. King, Jocelyn Lavallee, Meagan Schipanski, and M. Francesca Cotrufo. "Distinct, Direct and Climate-Mediated Environmental Controls on Global Particulate and Mineral-Associated Organic Carbon Storage." *Global Change Biology* 30, no. 1 (2024): e17080. https://doi.org/10.1111/gcb.17080.

Harrison, Robert B., Paul W. Footen, and Brian D. Strahm. "Deep Soil Horizons: Contribution and Importance to Soil Carbon Pools and in Assessing Whole-Ecosystem Response to Management and Global Change." *Forest Science* 57, no. 1 (February 1, 2011): 67–76. https://doi.org/10.1093/forestscience/57.1.67.

Harrison, Xavier A., Lynda Donaldson, Maria Eugenia Correa-Cano, Julian Evans, David N. Fisher, Cecily E. D. Goodwin, Beth S. Robinson, David J. Hodgson, and Richard Inger. "A Brief Introduction to Mixed Effects Modelling and Multi-Model Inference in Ecology." *PeerJ* 6 (May 23, 2018): e4794. https://doi.org/10.7717/peerj.4794.

Heckman, Katherine A., Angela R. Possinger, Brian D. Badgley, Maggie M. Bowman, Adrian C. Gallo, Jeff A. Hatten, Lucas E. Nave, et al. "Moisture-Driven Divergence in Mineral-

Associated Soil Carbon Persistence." *Proceedings of the National Academy of Sciences* 120, no. 7 (February 14, 2023): e2210044120. https://doi.org/10.1073/pnas.2210044120.

Heckman, Katherine, Caitlin E. Hicks Pries, Corey R. Lawrence, Craig Rasmussen, Susan E. Crow, Alison M. Hoyt, Sophie F. von Fromm, et al. "Beyond Bulk: Density Fractions Explain Heterogeneity in Global Soil Carbon Abundance and Persistence." *Global Change Biology* 28, no. 3 (2021): 1178–96. https://doi.org/10.1111/gcb.16023.

Helfenstein, Anatol, Vera L. Mulder, Gerard B. M. Heuvelink, and Mirjam J. D. Hack-ten Broeke. "Three-Dimensional Space and Time Mapping Reveals Soil Organic Matter Decreases across Anthropogenic Landscapes in the Netherlands." *Communications Earth & Environment* 5, no. 1 (March 15, 2024): 1–16. https://doi.org/10.1038/s43247-024-01293-y.

Hengl, Tomislav, Jorge Mendes de Jesus, Gerard B. M. Heuvelink, Maria Ruiperez Gonzalez, Milan Kilibarda, Aleksandar Blagotić, Wei Shangguan, et al. "SoilGrids250m: Global Gridded Soil Information Based on Machine Learning." *PLOS One* 12, no. 2 (February 16, 2017): e0169748. https://doi.org/10.1371/journal.pone.0169748.

Hengl, Tomislav, Preston Sorenson, Leandro Parente, Kimberly Cornish, Jeffrey Battigelli, Carmelo Bonannella, Monika Gorzelak, and Kris Nichols. "Assessment of Soil Organic Carbon Stocks in Alberta Using 2-Scale Sampling and 3D Predictive Soil Mapping." *Facets* 8 (January 2023): 1–17. https://doi.org/10.1139/facets-2023-0040.

Hicks Pries, Caitlin E., C. Castanha, R. C. Porras, and M. S. Torn. "The Whole-Soil Carbon Flux in Response to Warming." *Science* 355, no. 6332 (March 31, 2017): 1420–23. https://doi.org/10.1126/science.aal1319.

Hicks Pries, Caitlin, Rebecca Ryals, Biao Zhu, Kyungjin Min, Alexia Cooper, Sarah Goldsmith, Jennifer Pett-Ridge, Margaret Torn, and Asmeret Asefaw Berhe. "The Deep Soil Organic Carbon Response to Global Change." *Annual Review of Ecology, Evolution, and Systematics* 54, no. 1 (2023): null. https://doi.org/10.1146/annurev-ecolsys-102320-085332.

Hijmans, R. "Terra Spatial Data Analysis," 2023. <https://CRAN.R-project.org/package=terra>.

Hobley, Eleanor, Brian Wilson, Arjan Wilkie, Jonathan Gray, and Terry Koen. "Drivers of Soil Organic Carbon Storage and Vertical Distribution in Eastern Australia." *Plant and Soil* 390, no. 1 (May 1, 2015): 111–27. https://doi.org/10.1007/s11104-015-2380-1.

Houghton, R. A., J. I. House, J. Pongratz, G. R. van der Werf, R. S. DeFries, M. C. Hansen, C. Le Quéré, and N. Ramankutty. "Carbon Emissions from Land Use and Land-Cover Change." *Biogeosciences* 9, no. 12 (December 13, 2012): 5125–42. https://doi.org/10.5194/bg-9-5125-2012.

Hribljan, John A., Moira Hough, Erik A. Lilleskov, Esteban Suarez, Katherine Heckman, Ana Maria Planas-Clarke, and Rodney A. Chimner. "Elevation and Temperature Are Strong Predictors of Long-Term Carbon Accumulation across Tropical Andean Mountain Peatlands." *Mitigation and Adaptation Strategies for Global Change* 29, no. 1 (December 30, 2023): 1. https://doi.org/10.1007/s11027-023-10089-y.

Hribljan, John A., Esteban Suarez, Laura Bourgeau-Chavez, Sarah Endres, Erik A. Lilleskov, Segundo Chimbolema, Craig Wayson, Eleanor Serocki, and Rodney A. Chimner. "Multidate, Multisensor Remote Sensing Reveals High Density of Carbon-Rich Mountain Peatlands in the Páramo of Ecuador." *Global Change Biology* 23, no. 12 (2017): 5412–25. https://doi.org/10.1111/gcb.13807.

Huang, Wenjuan, Chenglong Ye, William C. Hockaday, and Steven J. Hall. "Trade-Offs in Soil Carbon Protection Mechanisms under Aerobic and Anaerobic Conditions." *Global Change Biology* 26, no. 6 (2020): 3726–37. https://doi.org/10.1111/gcb.15100.

Huete, A, K Didan, T Miura, E. P Rodriguez, X Gao, and L. G Ferreira. "Overview of the Radiometric and Biophysical Performance of the MODIS Vegetation Indices." *Remote Sensing*

of Environment, The moderate resolution imaging spectroradiometer (MODIS): a new generation of land surface monitoring, 83, no. 1 (November 1, 2002): 195–213. https://doi.org/10.1016/S0034-4257(02)00096-2.

Hugelius, Gustaf. "Spatial Upscaling Using Thematic Maps: An Analysis of Uncertainties in Permafrost Soil Carbon Estimates." *Global Biogeochemical Cycles* 26, no. 2 (2012). https://doi.org/10.1029/2011GB004154.

Hugelius, Gustaf, Julie Loisel, Sarah Chadburn, Robert B. Jackson, Miriam Jones, Glen MacDonald, Maija Marushchak, et al. "Large Stocks of Peatland Carbon and Nitrogen Are Vulnerable to Permafrost Thaw." *Proceedings of the National Academy of Sciences of the United States of America* 117, no. 34 (August 25, 2020): 20438–46. https://doi.org/10.1073/pnas.1916387117.

Intergovernmental Panel On Climate Change. *Climate Change and Land: IPCC Special Report on Climate Change, Desertification, Land Degradation, Sustainable Land Management, Food Security, and Greenhouse Gas Fluxes in Terrestrial Ecosystems*. 1st ed. Cambridge University Press, 2022. https://www.cambridge.org/core/product/identifier/9781009157988/type/book.

Jackson, Robert B., Kate Lajtha, Susan E. Crow, Gustaf Hugelius, Marc G. Kramer, and Gervasio Piñeiro. "The Ecology of Soil Carbon: Pools, Vulnerabilities, and Biotic and Abiotic Controls." *Annual Review of Ecology, Evolution, and Systematics* 48, no. 1 (November 2, 2017): 419–45. https://doi.org/10.1146/annurev-ecolsys-112414-054234.

Janisch, Jack E., Alex D. Foster, and William J. Ehinger. "Characteristics of Small Headwater Wetlands in Second-Growth Forests of Washington, USA." *Forest Ecology and Management* 261, no. 7 (April 1, 2011): 1265–74. https://doi.org/10.1016/j.foreco.2011.01.005.

Jenny, Hans. "Factors of Soil Formation." *Soil Science* 52, no. 5 (1941). https://journals.lww.com/soilsci/fulltext/1941/11000/factors_of_soil_formation.9.aspx.

———. *Factors of Soil Formation: A System of Quantitative Pedology*. New York: Dover, 1994.

Jin, Suming, Collin Homer, Limin Yang, Patrick Danielson, Jon Dewitz, Congcong Li, Zhe Zhu, George Xian, and Danny Howard. "Overall Methodology Design for the United States National Land Cover Database 2016 Products." *Remote Sensing* 11, no. 24 (January 2019): 2971. https://doi.org/10.3390/rs11242971.

Jobbágy, Esteban G., and Robert B. Jackson. "The Vertical Distribution of Soil Organic Carbon and Its Relation to Climate and Vegetation." *Ecological Applications* 10, no. 2 (2000): 423–36. https://doi.org/10.1890/1051-0761(2000)010[0423:TVDOSO]2.0.CO;2.

Jones, Dryw, and David V. D'Amore. "Ensemble Model and Input Model Rasters for Soil Organic Carbon Stock Mean and Uncertainties for Alaska, British Columbia, Washington, Oregon, California, and Hawai'i," 2024. https://doi.org/doi.org/10.2737/RDS-2024-0009.

Joosten, Hans. *The Global Peatland CO2 Picture - Peatland Status and Drainage Related Emissions in All Countries of the World*. Wetland International, Ede, The Netherlands, 2010.

Jungkunst, Hermann F., Jan Göpel, Thomas Horvath, Simone Ott, and Melanie Brunn. "Global Soil Organic Carbon–Climate Interactions: Why Scales Matter." *WIREs Climate Change* 13, no. 4 (2022): e780. https://doi.org/10.1002/wcc.780.

Kayranli, Birol, Miklas Scholz, Atif Mustafa, and Åsa Hedmark. "Carbon Storage and Fluxes within Freshwater Wetlands: A Critical Review." *Wetlands* 30, no. 1 (February 2010): 111–24. https://doi.org/10.1007/s13157-009-0003-4.

Khaledian, Yones, and Bradley A. Miller. "Selecting Appropriate Machine Learning Methods for Digital Soil Mapping." *Applied Mathematical Modelling* 81 (May 1, 2020): 401–18. https://doi.org/10.1016/j.apm.2019.12.016.

Kim, Seongho. "Ppcor: An R Package for a Fast Calculation to Semi-Partial Correlation Coefficients." *Communications for Statistical Applications and Methods* 22, no. 6 (November 2015): 665–74. https://doi.org/10.5351/CSAM.2015.22.6.665.

Kleber, M., R. Mikutta, M. S. Torn, and R. Jahn. "Poorly Crystalline Mineral Phases Protect Organic Matter in Acid Subsoil Horizons." *European Journal of Soil Science* 56, no. 6 (2005): 717–25. https://doi.org/10.1111/j.1365-2389.2005.00706.x.

Kleber, Markus, Karin Eusterhues, Marco Keiluweit, Christian Mikutta, Robert Mikutta, and Peter S. Nico. "Chapter One - Mineral–Organic Associations: Formation, Properties, and Relevance in Soil Environments." edited by Donald L. Sparks, 130:1–140. Academic Press, 2015. https://doi.org/10.1016/bs.agron.2014.10.005.

Knowles, J.E., and C. Frederick. "merTools: Tools for Analyzing Mixed Effect Regression Models," 2023. https://CRAN.R-project.org/package=merTools.

Köchy, M., A. Don, M. K. van der Molen, and A. Freibauer. "Global Distribution of Soil Organic Carbon – Part 2: Certainty of Changes Related to Land Use and Climate." *Soil* 1, no. 1 (April 16, 2015): 367–80. https://doi.org/10.5194/soil-1-367-2015.

Köchy, M., R. Hiederer, and A. Freibauer. "Global Distribution of Soil Organic Carbon – Part 1: Masses and Frequency Distributions of SOC Stocks for the Tropics, Permafrost Regions, Wetlands, and the World." *Soil* 1, no. 1 (April 16, 2015): 351–65. https://doi.org/10.5194/soil-1-351-2015.

Kögel-Knabner, Ingrid, Georg Guggenberger, Markus Kleber, Ellen Kandeler, Karsten Kalbitz, Stefan Scheu, Karin Eusterhues, and Peter Leinweber. "Organo-Mineral Associations in Temperate Soils: Integrating Biology, Mineralogy, and Organic Matter Chemistry." *Journal of Plant Nutrition and Soil Science* 171, no. 1 (February 2008): 61–82. https://doi.org/10.1002/jpln.200700048.

Kolka, R., C. Trettin, W. Tang, K. Krauss, S. Bansal, J. Drexler, K. Wickland, et al. "Chapter 13: Terrestrial Wetlands." In *Second State of the Carbon Cycle Report (SOCCR2): A Sustained Assessment Report*, edited by N. Cavallaro, G. Shrestha, R. Birdsey, M. A. Mayes, R. G. Najjar, S. C. Reed, P. Romero-Lankao, and Z. Zhu, 507–67. U.S. Global Change Research Program, 2018. doi:10.7930/SOCCR2.2018.Ch13.

Kottkamp, Anna I., C. Nathan Jones, Margaret A. Palmer, and Katherine L. Tully. "Physical Protection in Aggregates and Organo-Mineral Associations Contribute to Carbon Stabilization at the Transition Zone of Seasonally Saturated Wetlands." *Wetlands* 42, no. 5 (May 11, 2022): 40. https://doi.org/10.1007/s13157-022-01557-3.

Lacroix, E. M., Y. Masue-Slowey, G. A. Dlott, M. Keiluweit, O. A. Chadwick, and S. Fendorf. "Mineral Protection and Resource Limitations Combine to Explain Profile-Scale Soil Carbon Persistence." *Journal of Geophysical Research: Biogeosciences* 127, no. 4 (2022): e2021JG006674. https://doi.org/10.1029/2021JG006674.

Lajtha, K., V. Bailey, K. McFarlane, K. Paustian, D. Bachelet, R. Abramoff, D. Angers, et al. "Chapter 12: Soils." In *Second State of the Carbon Cycle Report (SOCCR2): A Sustained Assessment Report*, edited by N. Cavallaro, G. Shrestha, R. Birdsey, M. A. Mayes, R. Najjar, S. Reed, P. Romero-Lankao, and Z. Zhu, 469–506. U.S. Global Change Research Program, 2018. https://doi.org/10.7930/SOCCR2.2018.Ch12.

Lal, Rattan. "Carbon Sequestration." *Philosophical Transactions of the Royal Society B: Biological Sciences* 363, no. 1492 (February 27, 2008): 815–30. https://doi.org/10.1098/rstb.2007.2185.

Lamichhane, Sushil, Lalit Kumar, and Brian Wilson. "Digital Soil Mapping Algorithms and Covariates for Soil Organic Carbon Mapping and Their Implications: A Review." *Geoderma* 352 (October 15, 2019): 395–413. https://doi.org/10.1016/j.geoderma.2019.05.031.

Lane, Charles R., Ellen D'Amico, Jay R. Christensen, Heather E. Golden, Qiusheng Wu, and Adnan Rajib. "Mapping Global Non-Floodplain Wetlands." *Earth System Science Data* 15, no. 7 (July 11, 2023): 2927–55. https://doi.org/10.5194/essd-15-2927-2023.

Lang, Ashley, Jennifer Pett-Ridge, Karis Mcfarlane, and Richard Phillips. "Climate, Soil Mineralogy, and Mycorrhizal Fungi Influence Soil Organic Matter Fractions in Eastern US Temperate Forests." *Journal of Ecology* 111 (March 13, 2023). https://doi.org/10.1111/1365-2745.14094.

Lang, Megan, Owen McDonough, Greg McCarty, Robert Oesterling, and Bill Wilen. "Enhanced Detection of Wetland-Stream Connectivity Using LiDAR." *Wetlands* 32, no. 3 (June 2012): 461–73. https://doi.org/10.1007/s13157-012-0279-7.

Lang, Megan W., J.C. Ingebritsen, and R.K. Griffin. "Status and Trends of Wetlands in the Conterminous United States 2009 to 2019." Washington, D.C., 2024.

Lang, Megan W., and Greg W. McCarty. "Lidar Intensity for Improved Detection of Inundation below the Forest Canopy." *Wetlands* 29, no. 4 (December 2009): 1166–78. https://doi.org/10.1672/08-197.1.

Lang, Michel, Martin Binder, Jakob Richter, Patrick Schratz, Florian Pfisterer, Stefan Coors, Quay Au, Giuseppe Casalicchio, Lars Kotthoff, and Bernd Bischl. "A Modern Object-Oriented Machine Learning Framework in R." *Journal of Open Source Software*, December 2019. https://doi.org/10.21105/joss.01903.

Lange, Markus, Nico Eisenhauer, Hongmei Chen, and Gerd Gleixner. "Increased Soil Carbon Storage through Plant Diversity Strengthens with Time and Extends into the Subsoil." *Global Change Biology* 29, no. 9 (2023): 2627–39. https://doi.org/10.1111/gcb.16641.

Larson, Johannes, Jörgen Wallerman, Matthias Peichl, and Hjalmar Laudon. "Soil Moisture Controls the Partitioning of Carbon Stocks across a Managed Boreal Forest Landscape." *Scientific Reports* 13, no. 1 (September 9, 2023): 14909. https://doi.org/10.1038/s41598-023-42091-4.

Laudon, H., M. Berggren, A. Ågren, I. Buffam, K. Bishop, T. Grabs, M. Jansson, and S. Köhler. "Patterns and Dynamics of Dissolved Organic Carbon (DOC) in Boreal Streams: The Role of Processes, Connectivity, and Scaling." *Ecosystems* 14 (2011): 880–93. https://doi.org/10.1007/s10021-011-9452-8.

Lavallee, Jocelyn M., Jennifer L. Soong, and M. Francesca Cotrufo. "Conceptualizing Soil Organic Matter into Particulate and Mineral-Associated Forms to Address Global Change in the 21st Century." *Global Change Biology* 26, no. 1 (2020): 261–73. https://doi.org/10.1111/gcb.14859.

Lawrence, Corey R., Marjorie S. Schulz, Caroline A. Masiello, Oliver A. Chadwick, and Jennifer W. Harden. "The Trajectory of Soil Development and Its Relationship to Soil Carbon Dynamics." *Geoderma* 403 (December 1, 2021): 115378. https://doi.org/10.1016/j.geoderma.2021.115378.

Lehmann, Johannes, and Markus Kleber. "The Contentious Nature of Soil Organic Matter." *Nature* 528, no. 7580 (December 2015): 60–68. https://doi.org/10.1038/nature16069.

Leibowitz, Scott G., Parker J. Wigington Jr., Kate A. Schofield, Laurie C. Alexander, Melanie K. Vanderhoof, and Heather E. Golden. "Connectivity of Streams and Wetlands to Downstream Waters: An Integrated Systems Framework." *JAWRA Journal of the American Water Resources Association* 54, no. 2 (2018): 298–322. https://doi.org/10.1111/1752-1688.12631.

Lenth, Russell V. "Emmeans: Estimated Marginal Means, Aka Least-Squares Means," 2024. https://CRAN.R-project.org/package=emmeans.

Li, Zhan, Hao Chen, Joanne C. White, Michael A. Wulder, and Txomin Hermosilla. "Discriminating Treed and Non-Treed Wetlands in Boreal Ecosystems Using Time Series Sentinel-1 Data." *International Journal of Applied Earth Observation and Geoinformation* 85 (March 1, 2020): 102007. https://doi.org/10.1016/j.jag.2019.102007.

Liaw, Andy, and Matthew Wiener. "ClassifiCation and Regression by randomForest," n.d.

Lidberg, William, Mats Nilsson, and Anneli Ågren. "Using Machine Learning to Generate High-Resolution Wet Area Maps for Planning Forest Management: A Study in a Boreal Forest

Landscape." *Ambio* 49, no. 2 (February 1, 2020): 475–86. https://doi.org/10.1007/s13280-019-01196-9.

Liu, Chengzhu, Yunpeng Zhao, Lixiao Ma, Guoqing Zhai, Xingqi Li, Chris Freeman, and Xiaojuan Feng. "Metallic Protection of Soil Carbon: Divergent Drainage Effects in *Sphagnum* vs. Non-*Sphagnum* Wetlands." *National Science Review* 11, no. 11 (October 21, 2024): nwae178. https://doi.org/10.1093/nsr/nwae178.

Lu, Mingzhi, Yuanchun Zou, Qilei Xun, Zicheng Yu, Ming Jiang, Lianxi Sheng, Xianguo Lu, and Deli Wang. "Anthropogenic Disturbances Caused Declines in the Wetland Area and Carbon Pool in China during the Last Four Decades." *Global Change Biology* 27, no. 16 (2021): 3837–45. https://doi.org/10.1111/gcb.15671.

Lundberg, Scott M, and Su-In Lee. "A Unified Approach to Interpreting Model Predictions," Vol. 30. Curran Associates, Inc., 2017. https://proceedings.neurips.cc/paper/2017/hash/8a20a8621978632d76c43dfd28b67767-Abstract.html.

Luo, Yiqi, Anders Ahlström, Steven D. Allison, Niels H. Batjes, Victor Brovkin, Nuno Carvalhais, Adrian Chappell, et al. "Toward More Realistic Projections of Soil Carbon Dynamics by Earth System Models." *Global Biogeochemical Cycles* 30, no. 1 (2016): 40–56. https://doi.org/10.1002/2015GB005239.

Luo, Zhongkui, Guocheng Wang, and Enli Wang. "Global Subsoil Organic Carbon Turnover Times Dominantly Controlled by Soil Properties Rather than Climate." *Nature Communications* 10, no. 1 (August 15, 2019): 3688. https://doi.org/10.1038/s41467-019-11597-9.

Lützow, M. von, I. Kögel-Knabner, K. Ekschmitt, E. Matzner, G. Guggenberger, B. Marschner, and H. Flessa. "Stabilization of Organic Matter in Temperate Soils: Mechanisms and Their Relevance under Different Soil Conditions – a Review." *European Journal of Soil Science* 57, no. 4 (2006): 426–45. https://doi.org/10.1111/j.1365-2389.2006.00809.x.

Lützow, Margit von, and Ingrid Kögel-Knabner. "Temperature Sensitivity of Soil Organic Matter Decomposition—What Do We Know?" *Biology and Fertility of Soils* 46, no. 1 (November 1, 2009): 1–15. https://doi.org/10.1007/s00374-009-0413-8.

Ma, Lei, Gaofeng Zhu, Bolong Chen, Kun Zhang, Shuli Niu, Jinsong Wang, Phillipe Ciais, and Hongchao Zuo. "A Globally Robust Relationship between Water Table Decline, Subsidence Rate, and Carbon Release from Peatlands." *Communications Earth & Environment* 3, no. 1 (October 29, 2022): 1–14. https://doi.org/10.1038/s43247-022-00590-8.

Ma, Tian, Yiyun Wang, Guohua Dai, Juan Jia, Zongguang Liu, Yufu Jia, Simin Wang, et al. "Prolonged Storage of Bound Organic Carbon in Wetland but Not Upland Soils: A 13C and 14C Perspective." *Geophysical Research Letters* 52, no. 1 (2025): e2024GL112491. https://doi.org/10.1029/2024GL112491.

Ma, Yuxin, Budiman Minasny, Brendan P. Malone, and Alex B. Mcbratney. "Pedology and Digital Soil Mapping (DSM)." *European Journal of Soil Science* 70, no. 2 (2019): 216–35. https://doi.org/10.1111/ejss.12790.

Ma, Yuxin, Budiman Minasny, Alex McBratney, Laura Poggio, and Mario Fajardo. "Predicting Soil Properties in 3D: Should Depth Be a Covariate?" *Geoderma* 383 (February 1, 2021): 114794. https://doi.org/10.1016/j.geoderma.2020.114794.

Mahdavi, Sahel, Bahram Salehi, Jean Granger, Meisam Amani, Brian Brisco, and Weimin Huang. "Remote Sensing for Wetland Classification: A Comprehensive Review." *GIScience & Remote Sensing* 55, no. 5 (September 3, 2018): 623–58. https://doi.org/10.1080/15481603.2017.1419602.

Mahdianpari, Masoud, Jean Elizabeth Granger, Fariba Mohammadimanesh, Bahram Salehi, Brian Brisco, Saeid Homayouni, Eric Gill, Brian Huberty, and Megan Lang. "Meta-Analysis of

Wetland Classification Using Remote Sensing: A Systematic Review of a 40-Year Trend in North America." *Remote Sensing* 12, no. 11 (January 2020): 1882. https://doi.org/10.3390/rs12111882.

Malhotra, Avni, Katherine Todd-Brown, Lucas E Nave, Niels H Batjes, James R Holmquist, Alison M Hoyt, Colleen M Iversen, et al. "The Landscape of Soil Carbon Data: Emerging Questions, Synergies and Databases." *Progress in Physical Geography: Earth and Environment* 43, no. 5 (October 1, 2019): 707–19. https://doi.org/10.1177/0309133319873309.

Malone, B. P., A. B. McBratney, B. Minasny, and G. M. Laslett. "Mapping Continuous Depth Functions of Soil Carbon Storage and Available Water Capacity." *Geoderma* 154, no. 1 (December 15, 2009): 138–52. https://doi.org/10.1016/j.geoderma.2009.10.007.

Matthews, Jeffrey W., Dennis Skultety, Bradley Zercher, Michael P. Ward, and Thomas J. Benson. "Field Verification of Original and Updated National Wetlands Inventory Maps in Three Metropolitan Areas in Illinois, USA." *Wetlands* 36, no. 6 (December 1, 2016): 1155–65. https://doi.org/10.1007/s13157-016-0836-6.

Maxwell, Aaron E., and Timothy A. Warner. "Is High Spatial Resolution DEM Data Necessary for Mapping Palustrine Wetlands?" *International Journal of Remote Sensing* 40, no. 1 (January 2, 2019): 118–37. https://doi.org/10.1080/01431161.2018.1506184.

Maxwell, Aaron E., Timothy A. Warner, and Michael P. Strager. "Predicting Palustrine Wetland Probability Using Random Forest Machine Learning and Digital Elevation Data-Derived Terrain Variables." *Photogrammetric Engineering and Remote Sensing* 82, no. 6 (June 2016): 437–47. https://doi.org/10.14358/PERS.82.6.437.

Mayer, Mathias, Cindy E. Prescott, Wafa E. A. Abaker, Laurent Augusto, Lauric Cécillon, Gabriel W. D. Ferreira, Jason James, et al. "Tamm Review: Influence of Forest Management Activities on Soil Organic Carbon Stocks: A Knowledge Synthesis." *Forest Ecology and Management* 466 (June 15, 2020): 118127. https://doi.org/10.1016/j.foreco.2020.118127.

Mayer, Michael, and David Watson. "Kernelshap: Kernel SHAP," 2024. https://github.com/ModelOriented/kernelshap.

McBratney, A. B, M. L Mendonça Santos, and B Minasny. "On Digital Soil Mapping." *Geoderma* 117, no. 1 (November 1, 2003): 3–52. https://doi.org/10.1016/S0016-7061(03)00223-4.

McClain, Michael E., Elizabeth W. Boyer, C. Lisa Dent, Sarah E. Gergel, Nancy B. Grimm, Peter M. Groffman, Stephen C. Hart, et al. "Biogeochemical Hot Spots and Hot Moments at the Interface of Terrestrial and Aquatic Ecosystems." *Ecosystems* 6, no. 4 (June 1, 2003): 301–12. https://doi.org/10.1007/s10021-003-0161-9.

McCune, Bruce, and Dylan Keon. "Equations for Potential Annual Direct Incident Radiation and Heat Load." *Journal of Vegetation Science* 13, no. 4 (August 2002): 603–6. https://doi.org/10.1111/j.1654-1103.2002.tb02087.x.

McFarlane, Karis J., Margaret S. Torn, Paul J. Hanson, Rachel C. Porras, Christopher W. Swanston, Mac A. Callaham, and Thomas P. Guilderson. "Comparison of Soil Organic Matter Dynamics at Five Temperate Deciduous Forests with Physical Fractionation and Radiocarbon Measurements." *Biogeochemistry* 112, no. 1 (March 1, 2013): 457–76. https://doi.org/10.1007/s10533-012-9740-1.

McKenzie, Neil J., and Philip J. Ryan. "Spatial Prediction of Soil Properties Using Environmental Correlation." *Geoderma* 89, no. 1–2 (April 1999): 67–94. https://doi.org/10.1016/S0016-7061(98)00137-2.

McNicol, Gavin, Chuck Bulmer, David D'Amore, Paul Sanborn, Sari Saunders, Ian Giesbrecht, Santiago Gonzalez Arriola, Allison Bidlack, David Butman, and Brian Buma. "Large, Climate-Sensitive Soil Carbon Stocks Mapped with Pedology-Informed Machine Learning in

the North Pacific Coastal Temperate Rainforest." *Environmental Research Letters* 14, no. 1 (January 3, 2019): 14004. https://doi.org/10.1088/1748-9326/aaed52.

Miao, Guofang, Asko Noormets, Jean-Christophe Domec, Montserrat Fuentes, Carl C. Trettin, Ge Sun, Steve G. McNulty, and John S. King. "Hydrology and Microtopography Control Carbon Dynamics in Wetlands: Implications in Partitioning Ecosystem Respiration in a Coastal Plain Forested Wetland." *Agricultural and Forest Meteorology* 247 (December 15, 2017): 343–55. https://doi.org/10.1016/j.agrformet.2017.08.022.

Miller, Robin L. "Carbon Gas Fluxes in Re-Established Wetlands on Organic Soils Differ Relative to Plant Community and Hydrology." *Wetlands* 31, no. 6 (December 1, 2011): 1055–66. https://doi.org/10.1007/s13157-011-0215-2.

Milner, Alice, Andy Baird, Scott Davidson, Emily Lines, Dan Abrahams, Crystal Ahiable, Nadia Barsoum, et al. "The Forgotten Forests: Incorporating Temperate Peat-Forming Wet Woodlands as Nature-Based Solutions into Policy and Practice." *Ecological Solutions and Evidence* 5 (June 16, 2024). https://doi.org/10.1002/2688-8319.12346.

Minasny, Budiman, Brendan Malone, Alex Mcbratney, Denis Angers, Dominique Arrouays, Adam Chambers, Vincent Chaplot, et al. "Soil Carbon 4 per Mille." *Geoderma* 292 (April 1, 2017): 59–86. https://doi.org/10.1016/j.geoderma.2017.01.002.

Minasny, Budiman, and Alex. B. McBratney. "Digital Soil Mapping: A Brief History and Some Lessons." *Geoderma*, Soil mapping, classification, and modelling: history and future directions, 264 (February 15, 2016): 301–11. https://doi.org/10.1016/j.geoderma.2015.07.017.

Minasny, Budiman, Alex B. McBratney, Brendan P. Malone, and Ichsani Wheeler. "Chapter One - Digital Mapping of Soil Carbon." edited by Donald L. Sparks, 118:1–47. Advances in Agronomy. Academic Press, 2013. https://doi.org/10.1016/B978-0-12-405942-9.00001-3.

Minasny, Budiman, Jose Padarian, Laura Poggio, Alexandre ten Caten, Daniel Thompson, Clint Tuve, and Wirastuti Widyatmanti. "Digital Mapping of Peatlands - a Critical Review." *Earth-Science Reviews* 196, no. Journal Article (2019). https://doi.org/10.1016/j.earscirev.2019.05.014.

Mirabito, Anthony J., and Lisa G. Chambers. "Quantifying Mineral-Associated Organic Matter in Wetlands as an Indicator of the Degree of Soil Carbon Protection." *Geoderma* 430 (February 1, 2023): 116327. https://doi.org/10.1016/j.geoderma.2023.116327.

Mishra, U., and W. J. Riley. "Alaskan Soil Carbon Stocks: Spatial Variability and Dependence on Environmental Factors." *Biogeosciences (Online)* 9, no. 9 (September 20, 2012): 3637–45. https://doi.org/10.5194/bg-9-3637-2012.

Mitsch, William, and James Gosselink. *Wetlands, 5th Edition*, 2015.

Molnar, Christoph, Giuseppe Casalicchio, and Bernd Bischl. "Iml: An R Package for Interpretable Machine Learning." *Journal of Open Source Software* 3, no. 26 (2018): 786.

Moore, Sam, Chris D. Evans, Susan E. Page, Mark H. Garnett, Tim G. Jones, Chris Freeman, Aljosja Hooijer, Andrew J. Wiltshire, Suwido H. Limin, and Vincent Gauci. "Deep Instability of Deforested Tropical Peatlands Revealed by Fluvial Organic Carbon Fluxes." *Nature* 493, no. 7434 (January 2013): 660–63. https://doi.org/10.1038/nature11818.

Moskal, L. M., Meghan Halabisky, Anthony J. Stewart, David E. Butman, Chad Babcock, and David V. D'Amore. "Teal Carbon – Stakeholder-Driven Monitoring of Forested Wetland Carbon" 2022 (December 1, 2022): INV32B-13.

Nahlik, A. M., and M. S. Fennessy. "Carbon Storage in US Wetlands." *Nature Communications* 7, no. 1 (December 2016): 13835. https://doi.org/10.1038/ncomms13835.

"National Wetlands Inventory," n.d. https://fwsprimary.wim.usgs.gov/wetlands/apps/wetlands-mapper/.

Neubauer, Scott C., and J. Patrick Megonigal. "Biogeochemistry of Wetland Carbon Preservation and Flux," 33–71. American Geophysical Union (AGU), 2021. https://doi.org/10.1002/9781119639305.ch3.

Nie, Xiuqing, Dong Wang, Lining Ren, Yangong Du, and Guoying Zhou. "Storage and Controlling Factors of Soil Organic Carbon in Alpine Wetlands and Meadow across the Tibetan Plateau." *European Journal of Soil Science* 74, no. 3 (2023): e13383. https://doi.org/10.1111/ejss.13383.

NOAA National Centers for Environmental Information. "Climate at a Glance: County Mapping," 2023. https://www.ncei.noaa.gov/access/monitoring/climate-at-a-glance/county/mapping.

Noon, Monica L., Allie Goldstein, Juan Carlos Ledezma, Patrick R. Roehrdanz, Susan C. Cook-Patton, Seth A. Spawn-Lee, Timothy Maxwell Wright, et al. "Mapping the Irrecoverable Carbon in Earth's Ecosystems." *Nature Sustainability* 5, no. 1 (January 2022): 37–46. https://doi.org/10.1038/s41893-021-00803-6.

Novick, Kimberly A., Trevor F. Keenan, William R. L. Anderegg, Caroline P. Normile, Benjamin R. K. Runkle, Emily E. Oldfield, Gyami Shrestha, et al. "We Need a Solid Scientific Basis for Nature-Based Climate Solutions in the United States." *Proceedings of the National Academy of Sciences* 121, no. 14 (April 2, 2024): e2318505121. https://doi.org/10.1073/pnas.2318505121.

Novick, Kimberly A., Stefan Metzger, William R. L. Anderegg, Mallory Barnes, Daniela S. Cala, Kaiyu Guan, Kyle S. Hemes, et al. "Informing Nature-Based Climate Solutions for the United States with the Best-Available Science." *Global Change Biology* 28, no. 12 (2022): 3778–94. https://doi.org/10.1111/gcb.16156.

O'Brien, Lauren. "Mpspline2: Mass-Preserving Spline Functions for Soil Data," 2022. https://CRAN.R-project.org/package=mpspline2.

Osland, Michael J., Christopher A. Gabler, James B. Grace, Richard H. Day, Meagan L. McCoy, Jennie L. McLeod, Andrew S. From, et al. "Climate and Plant Controls on Soil Organic Matter in Coastal Wetlands." *Global Change Biology* 24, no. 11 (2018): 5361–79. https://doi.org/10.1111/gcb.14376.

Palmer, Kathryn. "Department of Energy Caps Universities' Indirect Research Costs at 15%," 2025. https://www.insidehighered.com/news/government/science-research-policy/2025/04/14/doe-puts-15-cap-universities-indirect-research.

Pangala, Sunitha R., Alex Enrich-Prast, Luana S. Basso, Roberta Bittencourt Peixoto, David Bastviken, Edward R. C. Hornibrook, Luciana V. Gatti, et al. "Large Emissions from Floodplain Trees Close the Amazon Methane Budget." *Nature* 552, no. 7684 (2017): 230. https://doi.org/10.1038/nature24639.

Patton, Nicholas R., Kathleen A. Lohse, Mark S. Seyfried, Sarah E. Godsey, and Susan B. Parsons. "Topographic Controls of Soil Organic Carbon on Soil-Mantled Landscapes." *Scientific Reports* 9, no. 1 (April 23, 2019): 6390. https://doi.org/10.1038/s41598-019-42556-5.

Pearse, Alex L., Jan L. Barton, Rebecca E. Lester, Atun Zawadzki, and Peter I. Macreadie. "Soil Organic Carbon Variability in Australian Temperate Freshwater Wetlands." *Limnology and Oceanography* 63, no. S1 (2018): S254–66. https://doi.org/10.1002/lno.10735.

Pebesma, Edzer. "Simple Features for R: Standardized Support for Spatial Vector Data." *R Journal* 10, no. 1 (2018): 439. https://doi.org/10.32614/RJ-2018-009.

Pierson, Derek, Kathleen A. Lohse, William R. Wieder, Nicholas R. Patton, Jeremy Facer, Marie-Anne de Graaff, Katerina Georgiou, Mark S. Seyfried, Gerald Flerchinger, and Ryan Will. "Optimizing Process-Based Models to Predict Current and Future Soil Organic Carbon Stocks at High-Resolution." *Scientific Reports* 12, no. 1 (June 25, 2022): 10824. https://doi.org/10.1038/s41598-022-14224-8.

Poggio, L., R. Artz, and A. Gimona. "Digital Soil Mapping for Northern Peatlands: Examples of Mapping Peats and Their Characteristics in Scotland," 1st ed., 6. London, UK: Taylor & Francis Group, 2020.

Poggio, Laura, and Alessandro Gimona. "National Scale 3D Modelling of Soil Organic Carbon Stocks with Uncertainty Propagation — an Example from Scotland." *Geoderma* 232–234 (November 1, 2014): 284–99. https://doi.org/10.1016/j.geoderma.2014.05.004.

Poggio, Laura, Luis M. de Sousa, Niels H. Batjes, Gerard B. M. Heuvelink, Bas Kempen, Eloi Ribeiro, and David Rossiter. "SoilGrids 2.0: Producing Soil Information for the Globe with Quantified Spatial Uncertainty." *Soil* 7, no. 1 (June 14, 2021): 217–40. https://doi.org/10.5194/soil-7-217-2021.

Poulter, Benjamin, Etienne Fluet-Chouinard, Gustaf Hugelius, Charlie Koven, Lola Fatoyinbo, Susan E. Page, Judith A. Rosentreter, et al. "A Review of Global Wetland Carbon Stocks and Management Challenges," 1–20. American Geophysical Union (AGU), 2021. https://doi.org/10.1002/9781119639305.ch1.

Pugh, Thomas A. M., Almut Arneth, Markus Kautz, Benjamin Poulter, and Benjamin Smith. "Important Role of Forest Disturbances in the Global Biomass Turnover and Carbon Sinks." *Nature Geoscience* 12, no. 9 (September 2019): 730–35. https://doi.org/10.1038/s41561-019-0427-2.

Qiu, Chunjing, Philippe Ciais, Dan Zhu, Bertrand Guenet, Shushi Peng, Ana Maria Roxana Petrescu, Ronny Lauerwald, et al. "Large Historical Carbon Emissions from Cultivated Northern Peatlands." *Science Advances* 7, no. 23 (June 4, 2021): eabf1332. https://doi.org/10.1126/sciadv.abf1332.

Rasmussen, Craig, Katherine Heckman, William R. Wieder, Marco Keiluweit, Corey R. Lawrence, Asmeret Asefaw Berhe, Joseph C. Blankinship, et al. "Beyond Clay: Towards an Improved Set of Variables for Predicting Soil Organic Matter Content." *Biogeochemistry* 137, no. 3 (February 1, 2018): 297–306. https://doi.org/10.1007/s10533-018-0424-3.

Raymond, Peter A., James E. Bauer, Nina F. Caraco, Jonathan J. Cole, Brett Longworth, and Steven T. Petsch. "Controls on the Variability of Organic Matter and Dissolved Inorganic Carbon Ages in Northeast US Rivers." *Marine Chemistry* 92, no. 1–4 (December 2004): 353–66. https://doi.org/10.1016/j.marchem.2004.06.036.

Reis, Vanessa, Virgilio Hermoso, Stephen K. Hamilton, Douglas Ward, Etienne Fluet-Chouinard, Bernhard Lehner, and Simon Linke. "A Global Assessment of Inland Wetland Conservation Status." *Bioscience* 67, no. 6 (June 1, 2017): 523–33. https://doi.org/10.1093/biosci/bix045.

Riedel, Jon, Sharon Sarrantonio, and Stephen Dorsch. "Geomorphology of Coastal Olympic National Park," June 2021. https://doi.org/10.36967/nrr-2286564.

Robertson, G. Philip, Stephen K. Hamilton, Keith Paustian, and Pete Smith. "Land-Based Climate Solutions for the United States." *Global Change Biology* 28, no. 16 (2022): 4912–19. https://doi.org/10.1111/gcb.16267.

Rocci, Katherine S., M. Francesca Cotrufo, Jessica Ernakovich, Erika Foster, Serita Frey, Katerina Georgiou, A. Stuart Grandy, et al. "Bridging 20 Years of Soil Organic Matter Frameworks: Empirical Support, Model Representation, and next Steps." *Journal of Geophysical Research: Biogeosciences* 129, no. 6 (2024): e2023JG007964. https://doi.org/10.1029/2023JG007964.

Rocci, Katherine S., Jocelyn M. Lavallee, Catherine E. Stewart, and M. Francesca Cotrufo. "Soil Organic Carbon Response to Global Environmental Change Depends on Its Distribution between Mineral-Associated and Particulate Organic Matter: A Meta-Analysis." *Science of the Total Environment* 793 (November 1, 2021): 148569. https://doi.org/10.1016/j.scitotenv.2021.148569.

Román Dobarco, Mercedes, Alexandre M. J.-C. Wadoux, Brendan Malone, Budiman Minasny, Alex B. McBratney, and Ross Searle. "Mapping Soil Organic Carbon Fractions for Australia, Their Stocks, and Uncertainty." *Biogeosciences (Online)* 20, no. 8 (April 19, 2023): 1559–86. https://doi.org/10.5194/bg-20-1559-2023.

Ross, D. S., G. Matschonat, and U. Skyllberg. "Cation Exchange in Forest Soils: The Need for a New Perspective." *European Journal of Soil Science* 59, no. 6 (2008): 1141–59. https://doi.org/10.1111/j.1365-2389.2008.01069.x.

Rubey, William W. "Geologic History of Sea Water: An Attempt to State the Problem." *Geological Society of America Bulletin* 62, no. 9 (1951): 1111–48. https://doi.org/10.1130/0016-7606(1951)62[1111:GHOSW]2.0.CO;2.

Ruehr, Sophie, Trevor F. Keenan, Christopher Williams, Yu Zhou, Xinchen Lu, Ana Bastos, Josep G. Canadell, Iain Colin Prentice, Stephen Sitch, and César Terrer. "Evidence and Attribution of the Enhanced Land Carbon Sink." *Nature Reviews Earth and Environment*, July 25, 2023, 1–17. https://doi.org/10.1038/s43017-023-00456-3.

Rumpel, Cornelia, and Ingrid Kögel-Knabner. "Deep Soil Organic Matter—a Key but Poorly Understood Component of Terrestrial C Cycle." *Plant and Soil* 338, no. 1 (January 1, 2011): 143–58. https://doi.org/10.1007/s11104-010-0391-5.

Rusakova, Elena, Elena Sukhacheva, and Alfred E. Hartemink. "Vasiliy Dokuchaev – a Biographical Sketch on the Occasion of His 175th Birthday." *Geoderma* 412 (April 15, 2022): 115718. https://doi.org/10.1016/j.geoderma.2022.115718.

Salimi, Shokoufeh, Suhad A. A. A. N. Almuktar, and Miklas Scholz. "Impact of Climate Change on Wetland Ecosystems: A Critical Review of Experimental Wetlands." *Journal of Environmental Management* 286 (May 15, 2021): 112160. https://doi.org/10.1016/j.jenvman.2021.112160.

Sanderman, Jonathan, Jeffrey A. Baldock, and Ronald Amundson. "Dissolved Organic Carbon Chemistry and Dynamics in Contrasting Forest and Grassland Soils." *Biogeochemistry* 89, no. 2 (June 1, 2008): 181–98. https://doi.org/10.1007/s10533-008-9211-x.

Sanderman, Jonathan, Tomislav Hengl, and Gregory J. Fiske. "Soil Carbon Debt of 12,000 Years of Human Land Use." *Proceedings of the National Academy of Sciences* 114, no. 36 (September 5, 2017): 9575–80. https://doi.org/10.1073/pnas.1706103114.

Saunois, Marielle, Ann R. Stavert, Ben Poulter, Philippe Bousquet, Josep G. Canadell, Robert B. Jackson, Peter A. Raymond, et al. "The Global Methane Budget 2000–2017." *Earth System Science Data* 12, no. 3 (July 15, 2020): 1561–1623. https://doi.org/10.5194/essd-12-1561-2020.

Scharlemann, Jörn PW, Edmund VJ Tanner, Roland Hiederer, and Valerie Kapos. "Global Soil Carbon: Understanding and Managing the Largest Terrestrial Carbon Pool." *Carbon Management* 5, no. 1 (February 2014): 81–91. https://doi.org/10.4155/cmt.13.77.

Schefuß, Enno, Timothy I. Eglinton, Charlotte L. Spencer-Jones, Jürgen Rullkötter, Ricardo De Pol-Holz, Helen M. Talbot, Pieter M. Grootes, and Ralph R. Schneider. "Hydrologic Control of Carbon Cycling and Aged Carbon Discharge in the Congo River Basin." *Nature Geoscience* 9, no. 9 (September 2016): 687–90. https://doi.org/10.1038/ngeo2778.

Schimel, David S., B. H. Braswell, Elisabeth A. Holland, Rebecca McKeown, D. S. Ojima, Thomas H. Painter, William J. Parton, and Alan R. Townsend. "Climatic, Edaphic, and Biotic Controls over Storage and Turnover of Carbon in Soils." *Global Biogeochemical Cycles* 8, no. 3 (1994): 279–93. https://doi.org/10.1029/94GB00993.

Schlesinger, William H. "Carbon Balance in Terrestrial Detritus." *Annual Review of Ecology and Systematics* 8, no. 1 (1977): 51–81. https://doi.org/10.1146/annurev.es.08.110177.000411.

Schmidt, Michael W. I., Margaret S. Torn, Samuel Abiven, Thorsten Dittmar, Georg Guggenberger, Ivan A. Janssens, Markus Kleber, et al. "Persistence of Soil Organic Matter as an Ecosystem

Property." *Nature* 478, no. 7367 (October 2011): 49–56. https://doi.org/10.1038/nature10386.
Schrumpf, M., E. D. Schulze, K. Kaiser, and J. Schumacher. "How Accurately Can Soil Organic Carbon Stocks and Stock Changes Be Quantified by Soil Inventories?" *Biogeosciences (Online)* 8, no. 5 (May 18, 2011): 1193–1212. https://doi.org/10.5194/bg-8-1193-2011.
Schwertmann, U., and R. M. Taylor. "Iron Oxides," 2nd ed., 1:379–438. SSSA Book Series. Soil Science Society of America, 1989. https://acsess.onlinelibrary.wiley.com/doi/10.2136/sssabookser1.2ed.c8.
Sexton, Joseph O., Xiao-Peng Song, Min Feng, Praveen Noojipady, Anupam Anand, Chengquan Huang, Do-Hyung Kim, et al. "Global, 30-m Resolution Continuous Fields of Tree Cover: Landsat-Based Rescaling of MODIS Vegetation Continuous Fields with Lidar-Based Estimates of Error." *International Journal of Digital Earth* 6, no. 5 (September 1, 2013): 427–48. https://doi.org/10.1080/17538947.2013.786146.
Shanley, Colin S., Rose A. Graves, C. Ronnie Drever, Michael Schindel, James C. Robertson, Michael J. Case, and Tanushree Biswas. "Mapping Forest-Based Natural Climate Solutions." *Communications Earth & Environment* 5, no. 1 (September 12, 2024): 1–12. https://doi.org/10.1038/s43247-024-01678-z.
Shanley, Colin S., Sanjay Pyare, Michael I. Goldstein, Paul B. Alaback, David M. Albert, Colin M. Beier, Todd J. Brinkman, et al. "Climate Change Implications in the Northern Coastal Temperate Rainforest of North America." *Climatic Change* 130, no. 2 (May 1, 2015): 155–70. https://doi.org/10.1007/s10584-015-1355-9.
Shi, Zheng, Steven D. Allison, Yujie He, Paul A. Levine, Alison M. Hoyt, Jeffrey Beem-Miller, Qing Zhu, William R. Wieder, Susan Trumbore, and James T. Randerson. "The Age Distribution of Global Soil Carbon Inferred from Radiocarbon Measurements." *Nature Geoscience* 13, no. 8 (August 2020): 555–59. https://doi.org/10.1038/s41561-020-0596-z.
Shukla, P. R., Jim Skea, Andreas Reinhard Reisinger, and IPCC, eds. *Climate Change 2022: Mitigation of Climate Change*. Geneva: IPCC, 2022.
Siewert, Matthias B. "High-Resolution Digital Mapping of Soil Organic Carbon in Permafrost Terrain Using Machine Learning: A Case Study in a Sub-Arctic Peatland Environment." *Biogeosciences (Online)* 15, no. 6 (March 21, 2018): 1663–82. https://doi.org/10.5194/bg-15-1663-2018.
Six, J., R. T. Conant, E. A. Paul, and K. Paustian. "Stabilization Mechanisms of Soil Organic Matter: Implications for C-Saturation of Soils." *Plant and Soil* 241, no. 2 (April 1, 2002): 155–76. https://doi.org/10.1023/A:1016125726789.
Sjögersten, Sofie, Colin R. Black, Stephanie Evers, Jorge Hoyos-Santillan, Emma L. Wright, and Benjamin L. Turner. "Tropical Wetlands: A Missing Link in the Global Carbon Cycle?" *Global Biogeochemical Cycles* 28, no. 12 (December 2014): 1371–86. https://doi.org/10.1002/2014GB004844.
Slaets, Johanna I. F., Runa S. Boeddinghaus, and Hans-Peter Piepho. "Linear Mixed Models and Geostatistics for Designed Experiments in Soil Science: Two Entirely Different Methods or Two Sides of the Same Coin?" *European Journal of Soil Science* 72, no. 1 (2021): 47–68. https://doi.org/10.1111/ejss.12976.
Smith, Pete, Joanna I. House, Mercedes Bustamante, Jaroslava Sobocká, Richard Harper, Genxing Pan, Paul C. West, et al. "Global Change Pressures on Soils from Land Use and Management." *Global Change Biology* 22, no. 3 (2016): 1008–28. https://doi.org/10.1111/gcb.13068.
Smith, Pete, Jean-Francois Soussana, Denis Angers, Louis Schipper, Claire Chenu, Daniel P. Rasse, Niels H. Batjes, et al. "How to Measure, Report and Verify Soil Carbon Change to Realize

the Potential of Soil Carbon Sequestration for Atmospheric Greenhouse Gas Removal." *Global Change Biology* 26, no. 1 (2020): 219–41. https://doi.org/10.1111/gcb.14815.
Soil Science Division Staff. *Soil Survey Manual*. U.S. Department of Agriculture, 2017.
Soil Survey Staff. *Field Book for Describing and Sampling Soils, Version 4.0*. Natural Resources Conservation Service. U.S. Government Printing Office, 2024.
Soil Survey Staff. *Keys to Soil Taxonomy*. 13th ed. USDA Natural Resources Conservation Service, 2022.
Soil Survey Staff, and Terrance Loecke. In *Rapid Carbon Assessment: Methodology, Sampling, and Summary*, edited by Skye Willis, 1–24. U.S. Department of Agriculture, Natural Resources Conservation Service, 2016. https://www.nrcs.usda.gov/Internet/FSE_DOCUMENTS/nrcs142p2_052841.pdf.
Sollins, Phillip, Marc G. Kramer, Christopher Swanston, Kate Lajtha, Timothy Filley, Anthony K. Aufdenkampe, Rota Wagai, and Richard D. Bowden. "Sequential Density Fractionation across Soils of Contrasting Mineralogy: Evidence for Both Microbial- and Mineral-Controlled Soil Organic Matter Stabilization." *Biogeochemistry* 96, no. 1 (December 1, 2009): 209–31. https://doi.org/10.1007/s10533-009-9359-z.
Solomon, Susan, Gian-Kasper Plattner, Reto Knutti, and Pierre Friedlingstein. "Irreversible Climate Change Due to Carbon Dioxide Emissions." *Proceedings of the National Academy of Sciences* 106, no. 6 (February 10, 2009): 1704–9. https://doi.org/10.1073/pnas.0812721106.
Sothe, Camile, Alemu Gonsamo, Joyce Arabian, and James Snider. "Large Scale Mapping of Soil Organic Carbon Concentration with 3D Machine Learning and Satellite Observations." *Geoderma* 405 (January 2022): 115402. https://doi.org/10.1016/j.geoderma.2021.115402.
Spinola, Diogo, Alana Margerum, Yakun Zhang, Randy Hesser, David D'Amore, and Raquel Portes. "Rapid Soil Formation and Carbon Accumulation along a Little Ice Age Soil Chronosequence in Southeast Alaska." *Catena* 246 (November 1, 2024): 108460. https://doi.org/10.1016/j.catena.2024.108460.
Spinola, Diogo, Raquel Portes, Jennifer Fedenko, Rebecca Lybrand, Ashlee Dere, Frances Biles, Thomas Trainor, Mark E. Bowden, and David D'Amore. "Lithological Controls on Soil Geochemistry and Clay Mineralogy across Spodosols in the Coastal Temperate Rainforest of Southeast Alaska." *Geoderma* 428 (December 15, 2022): 116211. https://doi.org/10.1016/j.geoderma.2022.116211.
Stewart, Anthony J., Meghan Halabisky, Chad Babcock, David E. Butman, David V. D'Amore, and L. Monika Moskal. "Revealing the Hidden Carbon in Forested Wetland Soils." *Nature Communications* 15, no. 11 (January 2024): 726. https://doi.org/10.1038/s41467-024-44888-x.
Stewart, Graham A., Anna I. Kottkamp, Michael R. Williams, and Margaret A. Palmer. "Setting a Reference for Wetland Carbon: The Importance of Accounting for Hydrology, Topography, and Natural Variability." *Environmental Research Letters* 18, no. 6 (May 2023): 64014. https://doi.org/10.1088/1748-9326/acd26a.
Strack, Maria, Scott J. Davidson, Takashi Hirano, and Christian Dunn. "The Potential of Peatlands as Nature-Based Climate Solutions." *Current Climate Change Reports* 8, no. 3 (September 1, 2022): 71–82. https://doi.org/10.1007/s40641-022-00183-9.
Sulla-Menashe, Damien, Josh M. Gray, S. Parker Abercrombie, and Mark A. Friedl. "Hierarchical Mapping of Annual Global Land Cover 2001 to Present: The MODIS Collection 6 Land Cover Product." *Remote Sensing of Environment* 222 (March 1, 2019): 183–94. https://doi.org/10.1016/j.rse.2018.12.013.
Sun, Jingjing, Angela Gallego-Sala, and Zicheng Yu. "Topographic and Climatic Controls of Peatland Distribution on the Tibetan Plateau." *Scientific Reports* 13, no. 1 (September 8, 2023): 14811. https://doi.org/10.1038/s41598-023-39699-x.

Taillardat, Pierre, Jared Moore, Sigit Sasmito, Chris D. Evans, Tiara Alfina, Sophie Lok, Aditya Bandla, et al. "Methane and Carbon Dioxide Production and Emission Pathways in the Belowground and Draining Water Bodies of a Tropical Peatland Plantation Forest." *Geophysical Research Letters* 52, no. 4 (February 28, 2025): e2024GL112903. https://doi.org/10.1029/2024GL112903.

Taillardat, Pierre, Benjamin S. Thompson, Michelle Garneau, Karelle Trottier, and Daniel A. Friess. "Climate Change Mitigation Potential of Wetlands and the Cost-Effectiveness of Their Restoration." *Interface Focus* 10, no. 5 (October 6, 2020): 20190129. https://doi.org/10.1098/rsfs.2019.0129.

Tangen, Brian, and Sheel Bansal. "Soil Organic Carbon Stocks and Sequestration Rates of Inland, Freshwater Wetlands: Sources of Variability and Uncertainty." *Science of the Total Environment* 749 (August 1, 2020): 141444. https://doi.org/10.1016/j.scitotenv.2020.141444.

Thorslund, Josefin, Jerker Jarsjo, Fernando Jaramillo, James W. Jawitz, Stefano Manzoni, Nandita B. Basu, Sergey R. Chalov, et al. "Wetlands as Large-Scale Nature-Based Solutions: Status and Challenges for Research, Engineering and Management." *Ecological Engineering*, Ecological engineering of sustainable landscapes, 108 (November 1, 2017): 489–97. https://doi.org/10.1016/j.ecoleng.2017.07.012.

Tifafi, Marwa, Bertrand Guenet, and Christine Hatté. "Large Differences in Global and Regional Total Soil Carbon Stock Estimates Based on SoilGrids, HWSD, and NCSCD: Intercomparison and Evaluation Based on Field Data from USA, England, Wales, and France." *Global Biogeochemical Cycles* 32, no. 1 (2018): 42–56. https://doi.org/10.1002/2017GB005678.

Todd-Brown, K. E. O., J. T. Randerson, W. M. Post, F. M. Hoffman, C. Tarnocai, E. a. G. Schuur, and S. D. Allison. "Causes of Variation in Soil Carbon Simulations from CMIP5 Earth System Models and Comparison with Observations." *Biogeosciences* 10, no. 3 (March 13, 2013): 1717–36. https://doi.org/10.5194/bg-10-1717-2013.

Torn, Margaret, Susan Trumbore, Oliver Chadwick, Peter Vitousek, and David Hendricks. "Mineral Control of Soil Organic Carbon Storage and Turnover." *Nature* 389 (September 11, 1997): 170–73. https://doi.org/10.1038/38260.

Trettin, C. C., M. Davidian, M. F. Jurgensen, and R. Lea. "Organic Matter Decomposition Following Harvesting and Site Preparation of a Forested Wetland." *Soil Science Society of America Journal* 60, no. 6 (1996): 1994–2003. https://doi.org/10.2136/sssaj1996.03615995006000060053x.

Trettin, Carl, M.F. Jurgensen, Margaret Gale, and James McLaughlin. "Recovery of Carbon and Nutrient Pools in a Northern Forested Wetland 11 Years after Harvesting and Site Preparation." *Fuel and Energy Abstracts* 262 (November 1, 2011): 1826–33. https://doi.org/10.1016/j.foreco.2011.07.031.

Trumbore, Susan. "Radiocarbon and Soil Carbon Dynamics." *Annual Review of Earth and Planetary Sciences* 37, no. 1 (May 1, 2009): 47–66. https://doi.org/10.1146/annurev.earth.36.031207.124300.

Uhran, Bergit, Lisamarie Windham-Myers, Norman Bliss, Amanda M. Nahlik, Eric T. Sundquist, and Camille L. Stagg. "Improved Wetland Soil Organic Carbon Stocks of the Conterminous U.S. through Data Harmonization." *Frontiers in Soil Science* 1 (2021). https://www.frontiersin.org/articles/10.3389/fsoil.2021.706701.

United States Department of Agriculture, Natural Resources Conservation Service. "Field Indicators of Hydric Soils in the United States; a Guide for Identifying and Delineating Hydric Soils," 2018.

U.S. Supreme Court. Sackett ET UX. v. Environmental Protection Agency et al., 598 Rebecca A. Womeldorf (The Supreme Court 2023).

Vanderhoof, Melanie K., Laurie Alexander, Jay Christensen, Kylen Solvik, Peter Nieuwlandt, and Mallory Sagehorn. "High-Frequency Time Series Comparison of Sentinel-1 and Sentinel-2 Satellites for Mapping Open and Vegetated Water across the United States (2017–2021)." *Remote Sensing of Environment* 288 (April 1, 2023): 113498. https://doi.org/10.1016/j.rse.2023.113498.

Varney, Rebecca M., Sarah E. Chadburn, Eleanor J. Burke, and Peter M. Cox. "Evaluation of Soil Carbon Simulation in CMIP6 Earth System Models." *Biogeosciences (Online)* 19, no. 19 (October 5, 2022): 4671–4704. https://doi.org/10.5194/bg-19-4671-2022.

Vepraskas, Michael J., and Christopher B. Craft. *Wetland Soils: Genesis, Hydrology, Landscapes, and Classification, Second Edition*. CRC Press, 2016.

Vitharana, U. W. A., Nora J. Casson, Darshani Kumaragamage, Umakant Mishra, and Karl Friesen-Hughes. "Factors Controlling the Spatial Heterogeneity of Soil Organic Carbon Concentrations and Stocks in a Boreal Forest." *Geoderma Regional* 36 (March 1, 2024): e00749. https://doi.org/10.1016/j.geodrs.2023.e00749.

Wadoux, Alexandre M. J. -C., Budiman Minasny, and Alex B. McBratney. "Machine Learning for Digital Soil Mapping: Applications, Challenges and Suggested Solutions." *Earth-Science Reviews* 210 (November 1, 2020): 103359. https://doi.org/10.1016/j.earscirev.2020.103359.

Walden, Lewis, Oscar Serrano, Mingxi Zhang, Zefang Shen, James Sippo, Lauren Bennett, Damien Maher, et al. "Multi-Scale Mapping of Australia's Terrestrial and Blue Carbon Stocks and Their Continental and Bioregional Drivers." *Communications Earth & Environment* 4 (June 1, 2023). https://doi.org/10.1038/s43247-023-00838-x.

Wang, Qing-Feng, Hui-Jun Jin, Cui-Cui Mu, Xiao-Dong Wu, Lin Zhao, and Qing-Bai Wu. "Non-Climate Environmental Factors Matter to Holocene Dynamics of Soil Organic Carbon and Nitrogen in an Alpine Permafrost Wetland, Qinghai–tibet Plateau." *Advances in Climate Change Research*, Special issue on changing boreal-arctic permafrost and snow-cover and their impacts, 14, no. 2 (April 1, 2023): 213–25. https://doi.org/10.1016/j.accre.2023.04.001.

Wang, Yiyun, Hao Wang, Jin-Sheng He, and Xiaojuan Feng. "Iron-Mediated Soil Carbon Response to Water-Table Decline in an Alpine Wetland." *Nature Communications* 8, no. 1 (June 26, 2017): 15972. https://doi.org/10.1038/ncomms15972.

Wang, Zhuonan, Jitendra Kumar, Samantha R. Weintraub-Leff, Katherine Todd-Brown, Umakant Mishra, and Debjani Sihi. "Upscaling Soil Organic Carbon Measurements at the Continental Scale Using Multivariate Clustering Analysis and Machine Learning." *Journal of Geophysical Research: Biogeosciences* 129, no. 2 (2024): e2023JG007702. https://doi.org/10.1029/2023JG007702.

Wania, R., I. Ross, and I. C. Prentice. "Implementation and Evaluation of a New Methane Model within a Dynamic Global Vegetation Model: LPJ-WHyMe v1.3.1." *Geoscientific Model Development* 3, no. 2 (October 27, 2010): 565–84. https://doi.org/10.5194/gmd-3-565-2010.

———. "Integrating Peatlands and Permafrost into a Dynamic Global Vegetation Model: 2. Evaluation and Sensitivity of Vegetation and Carbon Cycle Processes." *Global Biogeochemical Cycles* 23, no. 3 (September 1, 2009). https://doi.org/10.1029/2008GB003413.

Wickham, James, Stephen V. Stehman, Daniel G. Sorenson, Leila Gass, and Jon A. Dewitz. "Thematic Accuracy Assessment of the NLCD 2016 Land Cover for the Conterminous United States." *Remote Sensing of Environment* 257 (May 1, 2021): 112357. https://doi.org/10.1016/j.rse.2021.112357.

Wiesmeier, Martin, Livia Urbanski, Eleanor Hobley, Birgit Lang, Margit von Lützow, Erika Marin-Spiotta, Bas van Wesemael, et al. "Soil Organic Carbon Storage as a Key Function of Soils -

a Review of Drivers and Indicators at Various Scales." *Geoderma* 333 (January 1, 2019): 149–62. https://doi.org/10.1016/j.geoderma.2018.07.026.

Wilson, F.H., C.P. Hults, C.G. Mull, and S.M. Karl. "Geologic Map of Alaska: U.S. Geological Survey Scientific Investigations Map 3340," 2015. https://pubs.usgs.gov/publication/sim3340.

Wilson, R. M., A. M. Hopple, M. M. Tfaily, S. D. Sebestyen, C. W. Schadt, L. Pfeifer-Meister, C. Medvedeff, et al. "Stability of Peatland Carbon to Rising Temperatures." *Nature Communications* 7, no. 1 (December 13, 2016): 13723. https://doi.org/10.1038/ncomms13723.

Witze, Alexandra, Dan Garisto, and Jeff Tollefson. "Five Key Climate and Space Projects on Trump's Chopping Block." *Nature*, April 14, 2025. https://doi.org/10.1038/d41586-025-01217-6.

Wright, Marvin N., and Andreas Ziegler. "Ranger: A Fast Implementation of Random Forests for High Dimensional Data in C++ and R." *Journal of Statistical Software* 77 (March 31, 2017): 1–17. https://doi.org/10.18637/jss.v077.i01.

Wynn, Jonathan G., Michael I. Bird, Lins Vellen, Emilie Grand-Clement, John Carter, and Sandra L. Berry. "Continental-Scale Measurement of the Soil Organic Carbon Pool with Climatic, Edaphic, and Biotic Controls." *Global Biogeochemical Cycles* 20, no. 1 (2006). https://doi.org/10.1029/2005GB002576.

Xia, Jianyang, Jing Wang, and Shuli Niu. "Research Challenges and Opportunities for Using Big Data in Global Change Biology." *Global Change Biology* 26, no. 11 (2020): 6040–61. https://doi.org/10.1111/gcb.15317.

Xiao, Jingfeng, Frederic Chevallier, Cecile Gomez, Luis Guanter, Jeffrey A. Hicke, Alfredo R. Huete, Kazuhito Ichii, et al. "Remote Sensing of the Terrestrial Carbon Cycle: A Review of Advances over 50 Years." *Remote Sensing of Environment* 233 (November 1, 2019): 111383. https://doi.org/10.1016/j.rse.2019.111383.

Xu, Hanqiu. "Modification of Normalised Difference Water Index (NDWI) to Enhance Open Water Features in Remotely Sensed Imagery." *International Journal of Remote Sensing* 27, no. 14 (July 20, 2006): 3025–33. https://doi.org/10.1080/01431160600589179.

Xu, Shan, Junjian Wang, Emma J. Sayer, Shu Kee Lam, and Derrick Y. F. Lai. "Precipitation Change Affects Forest Soil Carbon Inputs and Pools: A Global Meta-Analysis." *Science of the Total Environment* 908 (January 15, 2024): 168171. https://doi.org/10.1016/j.scitotenv.2023.168171.

Xu, Xibao, Minkun Chen, Guishan Yang, Bo Jiang, and Ji Zhang. "Wetland Ecosystem Services Research: A Critical Review." *Global Ecology and Conservation* 22 (June 1, 2020): e01027. https://doi.org/10.1016/j.gecco.2020.e01027.

Ye, Chenglong, Wenjuan Huang, Steven J. Hall, and Shuijin Hu. "Association of Organic Carbon with Reactive Iron Oxides Driven by Soil pH at the Global Scale." *Global Biogeochemical Cycles* 36, no. 1 (2022): e2021GB007128. https://doi.org/10.1029/2021GB007128.

Yu, Wenjuan, Samantha R. Weintraub, and Steven J. Hall. "Climatic and Geochemical Controls on Soil Carbon at the Continental Scale: Interactions and Thresholds." *Global Biogeochemical Cycles* 35, no. 3 (2021): e2020GB006781. https://doi.org/10.1029/2020GB006781.

Zhang, Bowen, Hanqin Tian, Chaoqun Lu, Guangsheng Chen, Shufen Pan, Christopher Anderson, and Benjamin Poulter. "Methane Emissions from Global Wetlands: An Assessment of the Uncertainty Associated with Various Wetland Extent Data Sets." *Atmospheric Environment* 165 (September 2017): 310–21. https://doi.org/10.1016/j.atmosenv.2017.07.001.

Zhang, Yuxue, Xiaowei Guo, Longxue Chen, Yakov Kuzyakov, Ruzhen Wang, Haiyang Zhang, Xingguo Han, Yong Jiang, and Osbert Jianxin Sun. "Global Pattern of Organic Carbon

Pools in Forest Soils." *Global Change Biology* 30, no. 6 (2024): e17386. https://doi.org/10.1111/gcb.17386.

Zhang, Zhen, Etienne Fluet-Chouinard, Katherine Jensen, Kyle McDonald, Gustaf Hugelius, Thomas Gumbricht, Mark Carroll, Catherine Prigent, Annett Bartsch, and Benjamin Poulter. "Development of the Global Dataset of Wetland Area and Dynamics for Methane Modeling (WAD2M)." *Earth System Science Data* 13, no. 5 (May 11, 2021): 2001–23. https://doi.org/10.5194/essd-13-2001-2021.

Zhao, Qian, Dinesh Adhikari, Rixiang Huang, Aman Patel, Xilong Wang, Yuanzhi Tang, Daniel Obrist, Eric E. Roden, and Yu Yang. "Coupled Dynamics of Iron and Iron-Bound Organic Carbon in Forest Soils during Anaerobic Reduction." *Chemical Geology*, Adsorption of metals by geomedia III: Fundamentals and implications of metal adsorption, 464 (August 5, 2017): 118–26. https://doi.org/10.1016/j.chemgeo.2016.12.014.

Zhao, Qian, Simon R. Poulson, Daniel Obrist, Samira Sumaila, James J. Dynes, Joyce M. McBeth, and Yu Yang. "Iron-Bound Organic Carbon in Forest Soils: Quantification and Characterization." *Biogeosciences (Online)* 13, no. 16 (August 24, 2016): 4777–88. https://doi.org/10.5194/bg-13-4777-2016.

Zhao, Yunpeng, Chengzhu Liu, Xingqi Li, Lixiao Ma, Guoqing Zhai, and Xiaojuan Feng. "Sphagnum Increases Soil's Sequestration Capacity of Mineral-Associated Organic Carbon via Activating Metal Oxides." *Nature Communications* 14, no. 1 (August 19, 2023): 5052. https://doi.org/10.1038/s41467-023-40863-0.

Zhu, Erxiong, Zongguang Liu, Simin Wang, Yiyun Wang, Ting Liu, and Xiaojuan Feng. "Organic Carbon and Lignin Protection by Metal Oxides versus Silicate Clay: Comparative Study Based on Wetland and Upland Soils." *Journal of Geophysical Research: Biogeosciences* 128, no. 7 (2023): e2023JG007474. https://doi.org/10.1029/2023JG007474.

Zomer, Robert J., Jianchu Xu, and Antonio Trabucco. "Version 3 of the Global Aridity Index and Potential Evapotranspiration Database." *Scientific Data* 9, no. 1 (July 15, 2022): 409. https://doi.org/10.1038/s41597-022-01493-1.